Biochemical characterization of the PARP domain-containing proteins AtRCD1 and TaSRO1

Inaugural-Dissertation

to obtain the academic degree

Doctor rerum naturalium (Dr. rer. nat.)

submitted to the Department of Biology, Chemistry, Pharmacy
of Freie Universität Berlin

by

Raffaella De Masi

2022

I hereby declare that I have completed the submitted dissertation independently and without the use of sources and aids other than those indicated. I have marked as such all statements that are taken literally or in content from other writings. This dissertation has not yet been presented to any other examination authority in the same or a similar form and has not yet been published.

The investigations for the present work were carried out from March 2017 to February 2020 at the Freie Universität Berlin, Institute for Biology, Department of Plant Biochemistry under the guidance of Dr. Lennart Wirthmüller.

Date of defense: March 31st, 2022

1st reviewer: Dr. Lennart Wirthmüller

2nd reviewer: Prof. Dr. Daniel Schubert

Parts of this work have been published in the following publications:

Vainonen, J.P, Shapiguzov, A., Krasensky-Wrzaczek, J., Gossens, R., De Masi, R., Danciu, I., Battchikova, N., Jonak, C., Wirthmueller. L, Wrzaczek, M., Kangasjärvi, J. "Arabidopsis Poly(ADP-ribose)-binding protein RCD1 interacts with Photoregulatory Protein Kinases in nuclear bodies". Manuscript pre-print https://doi.org/10.1101/2020.07.02.184937

Vogt, S., Feijs, K., Hosch, S., De Masi, R., Lintermann, R., Loll, B., Wirthmueller, L. "The superior salinity tolerance of wheat cultivar Shanrong No. 3 cannot be attributed to elevated Ta-sro1 poly(ADP-ribose) polymerase activity". Manuscript pre-print https://doi.org/10.1101/2021.10.20.465099

List of contents

Zusammenfassung

Eine schnelle und fein abgestimmte Reaktion auf die verschiedenen abiotischen Belastungen ist ein wesentliches Merkmal für das Überleben von Pflanzen als sessile Organismen. Die Signalwege, die maßgeschneiderte Reaktionen auf zellulärer und systemischer Ebene bestimmen, müssen streng reguliert und koordiniert werden, um eine schnelle Aktivierung der Abwehr- bzw. Stresstoleranzmechanismen zu ermöglichen. Eine zentrale Rolle bei der Integration und Regulation verschiedener molekularer Signalwege spielen Proteine, die als „zelluläre Hubs" bezeichnet werden. Ein Beispiel für diese Hub-Proteine ist *A. thaliana* RADICAL-INDUCED CELL DEATH1 (RCD1), das am besten charakterisierten Mitglied der pflanzenspezifischen SIMILAR TO RCD1 (SRO) -Proteinfamilie. Es wurde beschrieben, dass RCD1 an der apoplastischen ROS-Toleranz und Pflanzenentwicklung sowie an der Reaktion auf Hitze und chloroplastischen ROS-Stress durch Wechselwirkung mit verschiedenen Transkriptionsfaktoren über seine RST-Domäne beteiligt ist.

In dieser Arbeit wurde die biochemische Charakterisierung der Funktion der WWE-Domäne am N-Terminus von RCD1 durchgeführt, um ihre Funktionen in der Regulation der RCD1-Aktivität in der Pflanzenzellkern aufzuklären. Die mit verschiedenen Versionen von RCD1 durchgeführte Lokalisierungsstudie zeigte, dass die WWE-Domäne einen großen Einfluss auf die charakteristische subnukleare Lokalisierung von RCD1 in membranlosen Kompartimenten hat, die in Größe und Anzahl variieren. Co-Immunpräzipitationsversuche bestätigten die Rolle des N-Terminus von RCD1 und seines nächsten Homologs, SIMILAR TO RCD1 1 (SRO1), einschließlich der WWE-Domäne, im Oligomerisierungsprozess, der an der Bildung der membranlosen Kompartimente beteiligt sein könnte. Zuvor identifizierte Phophorylierungsstellen am N-terminalen Teil von RCD1 wurde mutiert, um zu testen, ob der Phosphorylierungszustand der betrachteten Aminosäuren eine Rolle bei der Regulation der RCD1-Aktivität in der Pflanzenzelle spielen könnte. In dieser Arbeit wurde gezeigt, dass Mutationen von phosphorylierten Resten sowohl auf makroskopischer als auch auf molekularer Ebene nachweisbare Auswirkungen auf die RCD1 Proteinaktivität haben.

Zusätzlich wurde in dieser Arbeit ein weiteres Mitglied der SRO-Proteinfamilie, die allelische SR3-Variante von *Triticum aestivum* SRO1, in Bezug auf die zuvor beschriebene katalytische Aktivität seiner Poly (ADP) -Ribose-Polymerase (PARP) -Domäne untersucht. TaSRO1 ist bisher das einzige bekannte Mitglied der SRO-Familie, dass eine enzymatische PARP-Aktivität aufweist. Mit den in dieser Arbeit durchgeführten Versuchen konnten die zuvor veröffentlichten Ergebnisse jedoch nicht bestätigt werden.

Summary

Quick and finely tuned response to the different abiotic stresses are an essential feature for the survival of of plants as sessile organisms. The signalling pathways that determine tailored responses at cellular and systemic level need to be strictly regulated, as well as coordinated, in order to allow a fast rise of defensive mechanisms. A pivotal role in the integration and regulation of different molecular pathways is played by proteins defined as "cellular hubs": an example of these proteins is *A. thaliana* RADICAL-INDUCED CELL DEATH1 (RCD1), the best characterized member of the plant-specific SIMILAR TO RCD1 (SRO) protein family. It was first described to be involved in apoplastic ROS tolerance and development, as well as in response to heat and chloroplastic ROS stress, *via* interaction with different transcription factors through its RST domain.

However, the mechanism, by which the interaction between RCD1 and its targets is regulated, has not been uncovered yet. In this work, the biochemical characterization of the function of the WWE domain, located at the N-terminus of RCD1, was carried out, in order to uncover its functions in the regulation of RCD1 activity in the plant cell nucleus. The localization study performed with different RCD1 constructs showed how the WWE domain has a major influence on the characteristic subnuclear localization of RCD1 in nuclear bodies, present in different sizes and number. The Co-immunoprecipitation assays confirmed the role of the N-terminus of RCD1 and its closest homologue, SIMILAR TO RCD1 1 (SRO1), including the WWE domain, in the oligomerisation process, that could be involved in the formation of the nuclear bodies. Alteration of previously identified phophosites on the N-terminal portion of RCD1 were generated to test whether the phosphorylation state of the considered phosphorylatable residues might play a role in the regulation of RCD1's activity in the plant cell. In this work it was shown that mutations on phosphosites produced noticeable effects both on the macroscopic and on the molecular level.

Additionally, in this work another member of the SRO protein family, the SR3 allelic variant of *Triticum aestivum* SRO1 was studied, in relation to the previously described catalytic activity of its Poly(ADP)-ribose Polymerase (PARP) domain, that would make this the only known member of the SRO family to present PARP enzymatic activity. However, with the assays performed in this work, the previously published findings could not be confirmed.

List of figures

List of tables

List of abbreviations

Abbreviation	Description
µg	Microgram
µm	Micrometre
µl	Microliter
µM	Micromolar
35S	Cauliflower mosaic virus (CaMV) Promotor 35S
A	Alanine
allA	RCD1 construct with residues S27, T33, S36, T204 S230, S231, T239, S242, S244, T257, S263 mutated to Alanine
allD	RCD1 construct with residues S27, T33, S36, T204 S230, S231, T239, S242, S244, T257, S263 mutated to Aspartate
APS	Ammonium peroxodisulphate
A. thaliana/*At*	*Arabidopsis thaliana*
ATP	Adenosine Triphosphate
A. tumefaciens	*Agrobacterium tumefaciens*
bp	Base pair(s)
CA	RCD1 construct with residues S230, S231, T239, S242, S244, T257, S263 mutated to Alanine
CA.2	RCD1 construct with residues T204, S230, S231, T239, S242, S244, T257, S263 mutated to Alanine
ca.	Circa
CD	RCD1 constructs with residues S230, S231, T239, S242, S244, T257, S263 mutated to Aspartate
CDS	Coding sequence
cDNA	Complementary DNA
cm	Centimetre
Col-0	*Arabidopsis thaliana* Ecotype Col-0

Continues on the next page

Abbreviation	Description
C-terminus	Carboxy-terminus
D	Aspartate
dpi	Days post-infection
DNA	Deoxyribonucleic acid
DNAse	Deoxyribonuclease
dNTP	Deoxynucleoside triphosphate
DTT	Dithiothreitol
E. coli	*Escherichia coli*
EDTA	Ethylenediaminetetraacetic acid
e.g.	*exempli gratia* – For example
ETI	Effector-triggered immunity
et al.	*and others*
fw, F	Forward
g	Gram
h	Hour(s)
HA	Hemagglutinin
HRP	Horseradish peroxidase
IPTG	Isopropyl β-d-1-thiogalactopyranoside
kb	Kilobase
kDa	Molecular weight, Kilodalton
M	Molar
MES	2-(N-Morpholino)ethanesulfonic acid
mg	Milligram(s)
min	Minute(s)

Continues on the next page

Abbreviation	Description
ml	Millilitre(s)
mM	Millimolar
NA	RCD1 construct with residues S27, T33, S36, T204 mutated to Alanine
NAD	Nicotinamide adenine dinucleotide
ND	RCD1 construct with residues S27, T33, S36, T204 mutated to Aspartate
ng	Nanogram
N. benthamiana	*Nicotiana benthamiana*
nm	Nanometre
N-terminus	Amino-terminus
OD_{600}	Optical density measured at a wavelength of 600 nm
PAGE	Polyacrylamide gel electrophoresis
PARP	Poly (ADP-ribose) polymerase
PCR	Polymerase chain reaction
PEG	Polyethylene glycol
PTI	PAMP-triggered Immunity
qRT-PCR	Quantitative Real-Time PCR
RNA	Ribonucleic acid
RST	RCD1-SRO-TAF4 domain (PF12174)
RNAse	Ribonuclease
rpm	Revolutions per minute
RT	Room temperature
rv, R	Reverse
s	Second(s)

Continues on the next page

Abbreviation	Description
SDS	Sodium dodecyl sulfate
Ser	Serine
TBS	Tris-buffered saline
TBS-T	TBS buffer + Tween
TEMED	N, N, N′, N′-Tetramethylethane-1,2-diamine
T. aestivum / *Ta*	*Triticum aestivum*
Tris	Tris(hydroxymethyl)aminomethane
v	Volume
V	Volt
w	Weight
WT	Wild type
WWE	Tryptophan(W)- Tryptophan(W)-Glutamate(E) domain (Aravind, 2000)

1 Introduction

The ability to perceive, recognize and respond to different external stimuli is essential to any living organism in order to survive. The variations in the surrounding environment can be various: the uprising of a new predator species, adverse weather conditions, alterations in nutrients availability represent only a few of the challenges to the survival of living organisms.

Plants make no exception: in fact, their sessile lifestyle determines the inability to act on external conditions, e.g., moving to a more favourable environment, as other non-sessile organisms do. Hence, plants have developed, throughout their evolutive pathway, several and complex mechanisms to cope with external stimuli, being either biotic stresses, deriving from the action of other living beings on the plant, or abiotic stresses, deriving from chemical and physical agents, e.g., drought stress, heat stress, osmotic stress (**Figure 1.1**).

1.1 Basic principles of immune responses to biotic stresses in plants

The considerable variety of stressors that can affect the internal homeostasis of plants determined the development of just as many mechanisms to sense and cope with stresses. The immune responses of higher plants against biotic stresses consist of two strategies: the first one in line of defence in case of pathogen attack is the pattern-triggered immunity (PTI) (Jones & Dangl, 2006), which starts with the recognition of microbe- or damage-associated molecular pattern (MAMPs or DAMPs) by specific receptors, such as pattern recognition receptors (PRRs) (Zipfel, 2014). Once the receptors bind their ligand, the formation of complexes with coreceptor or adapter kinases triggers protein phosphorylation cascades, ultimately resulting in transcriptional, translational and metabolic reprogramming of the cell (Zhang *et al.*, 2010; Tena *et al.*, 2011). Although PTI responses are alone able to prevent the vast majority of microbial infections, they do not prove to be adequate for all of those pathogenic microorganisms that acquired the ability to synthesize effectors, molecules whose primary function is to manipulate host immunity via interacting with specific target components of the PTI, determining an effector-triggered susceptibility (Abramovitch *et al.*, 2006). Therefore, plants evolved a plethora of intracellular effector-binding proteins, called resistance proteins (R proteins), each of which

recognizes a specific effector, hence implementing the immune response called effector-triggered immunity (ETI) (Jones & Dangl, 2006).

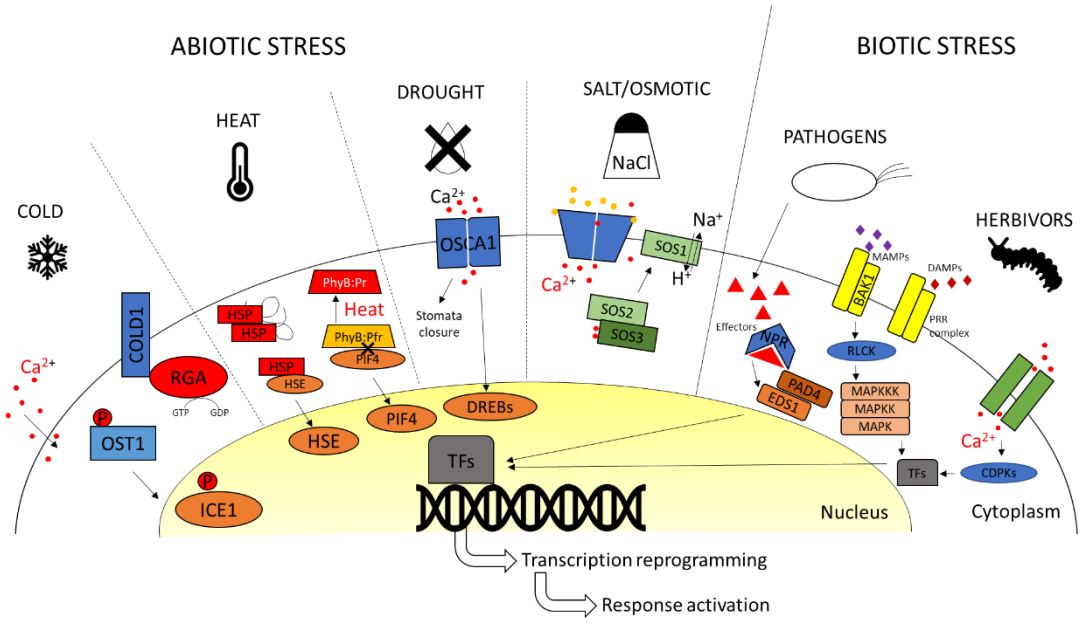

Figure 1.1: Schematic representation of abiotic and biotic stress sensing and signalling, down to transcriptional reprogramming in plant cells. The perception of stress stimuli may be at the cell membrane level, via membrane receptors, or in the cytoplasm, via intracellular receptors. The signalling cascades, via different mechanisms according to each signalling pathway, ultimately lead to the transcription reprogramming and the appropriate response activation.

1.2 Basic principles of responses to abiotic stresses in plants

A different response to the one triggered by PTI and ETI is induced in plant cells under abiotic stress (Zhu, 2016). Although the sensing mechanisms have not yet been identified for each of the different stressing stimuli, the signalling pathways at cytoplasmic levels that terminate in the reprogramming of transcriptional activity in cell nuclei were uncovered in the past decades and are singularly described in the following sections.

1.2.1 Heat stress

Variations in external temperature influence several processes in the plant life cycle, such as circadian clock and vernalization. Hence, a correct perception of these alterations and the downstream signalling are essential for the rapid adjustment of cell and plant metabolism. External temperature affects the physical properties of all cellular molecules, altering protein folding and binding, membrane fluidity and enzymatic

kinetics. In plants, these alterations were found for both mild and drastic increases in external temperature. Slight increases in ambient temperature provoke the physical shift from Pfr (far-red light) active state to Pr (red light) inactive state in PHYB, a phytochrome functioning both as light and as temperature sensor (Legris *et al.*, 2016; Jung *et al.*, 2016), via thermal reversion. This process leads to the accumulation of PHYTOCHROME INTERACTING FACTOR4 (PIF4), a central regulator in the convergence of light and temperature signalling pathways (Delker *et al.*, 2014) that promotes cell elongation at warm temperatures (Casal and Balasubramanian, 2019).

When plants experience high temperatures, HEAT SHOCK PROTEINS (HSPs), a protein family of molecular chaperones highly conserved throughout the evolution of living organisms (Schlesinger, 1990), senses the protein denaturation by binding exposed hydrophobic regions, hence releasing the HEAT SHOCK FACTORS (HSFs). HSFs are transcription factors that become available to activate heat stress responses (Scharf *et al.*, 2012). Under normal conditions, HEAT SHOCK PROTEIN 70 (HSP70) and HEAT SHOCK PROTEIN 90 (HSP90) interact with HEAT SHOCK TRANSCRIPTION FACTOR A1 (HSFA1) and repress its activity and nuclear localization, whereas, upon heat stress, HSFA1 is released (Hahn *et al.*, 2011; Yamada *et al.*, 2007). HSFA1s has been described as the "master regulator" of thermotolerance (Liu *et al.*, 2011; Nishizawa-Yokoi *et al.*, 2011; Yoshida *et al.*, 2011): it activates the expression of heat stress-responsive genes, amongst which *HSFA7a*, *HSFBs* and *DREB2A*, modulating the synthesis of chaperones and enzymes involved in the degradation of unfolded protein, as well as in ROS scavenging (Ohama *et al.*, 2017; Yoshida *et al.*, 2011).

Emerging evidence was reported of an additional heat-stress response pathway that acts independently of HSFA1: an example is the transcription factor bZIP28, which under normal conditions is bound to BIP3, hence being retained at the membrane level of the endoplasmic reticulum (ER). Upon heat stress stimulus, the induction of proteolytic cleavage of bZIP28 allows the latter to move to the nucleus and start the induction of genes involved in heat-stress response (Gao *et al.*, 2008). Other HSFA transcription factors, including HSFA5, HSFA4 and HSFA9, modulate the expression of heat stress-responsive genes in an HSFA1-independent manner (Baniwal *et al.*, 2007; Kotak *et al.*, 2007b; von Koskull-Döring *et al.*, 2007).

1.2.2 Cold stress

Lowering of external temperature is involved in the delay of developmental processes and growth in plants and, when reaching freezing temperatures, determines permanent damage to cells due to ice crystal formation. Two main signalling pathways have been

identified so far for the induction of cold-stress responsive genes. The signalling pathway activated upon cold stress perception in *A. thaliana* is mainly attributed to OPEN STOMATA 1 (OST1), a member of SNF1-RELATED PROTEIN KINASES 2 (SNRK2) family and already known for its role in ABA-dependent response to osmotic stress and stomatal closure (Mustilli *et al.*, 2002; Ding *et al.*, 2015). At low temperatures, decreased levels in myristoylation of clade-E GROWTH-REGULATING 2 (EGR2) result in a decrease of its binding ability; this impedes EGR2 interaction with OST1, which is released and activated (Ding *et al.*, 2019). The targets of OST1 kinase activity are INDUCER OF CBF EXPRESSION 1 (ICE1) and BASIC TRANSCRIPTION FACTOR 3 (BTF3), two transcription factors that regulate the induction of cold-regulated (*COR*) genes expression (Ding *et al.*, 2015; Ding *et al.*, 2018).

In *Oryza sativa*, transmembrane protein COLD1 interacts with G-PROTEIN α SUBUNIT 1 (RGA1), enhancing GTPase activity and Ca^{2+} influx in the cell, ultimately leading to the activation of the cold tolerance response (Ma *et al.*, 2015). Two orthologs of COLD1 in *A. thaliana*, GTG1 and GTG2, were identified as plasma membrane-localized G protein-coupled receptors and described to play a role in plant development (Jaffé *et al.*, 2012), but their involvement in cold sensing or tolerance has not been described.

The transcription of cold-regulated (*COR*) genes is orchestrated by a network of master transcription factors. For example, the C-REPEAT BINDING FACTOR/DEHYDRATION-RESPONSIVE ELEMENT BINDING FACTOR 1 (CBF/DREB1) pathway is a well-studied cold regulatory pathway. CBFs are *AP2/ERF* transcriptional activators, which bind to *CRT/DRE* sequences in the promoters of *COR* genes (Stockinger *et al.*, 1997). At low temperature, INDUCER OF CBF EXPRESSION 1 (ICE1) interacts with MYB15, member of MYB family of transcriptional repressors (Agarwal *et al.*, 2006), activating the transcription of *CBF3* (Chinnusamy *et al.*, 2003) and other *CBF* genes by binding to Myb recognition sequences on the respective promoters (Agarwal *et al.*, 2006). Furthermore, recent evidence indicated that not only CALMODULIN BINDING TRANSCRIPTION ACTIVATORS (CAMTAs) function as positive regulators of *CBFs* (Doherty *et al.*, 2009), but also phytohormones interact with the CBF pathways to regulate cold stress responses (Shi *et al.*,2015). While CBF1 reduces bioactive gibberellin levels, enhancing freezing tolerance (Achard *et al.*, 2008), brassinosteroids (BR) regulate the activity of BR-regulated transcription factors BRZ1, BES1 and CESTA, which in turn activate the expression of *CBFs* and downstream *COR* genes (Eremina *et al.*, 2016). Additionally, auxin is involved in cold-related damage control in the roots, where columella stem cell daughters are sacrificed to allow the whole root to withstand the chilling stress and recover growth (Hong *et al.*, 2017). It

should be noticed that, although the CBFs are the most well-known regulators of *COR* gene expression, only about 15% of the *COR* genes are regulated by CBFs. Other master regulators intervene in the cold-stress response, like SALT-INDUCIBLE ZINC FINGER 2 (SZF2), RESPONSIVE TO HIGH LIGHT 41 (RHL41), and HEAT SHOCK TRANSCRIPTION FACTOR C1 (HSFC1) (Jia *et al.*, 2016; Park *et al.*, 2015; Zhao *et al.*, 2016). Along with the abovementioned transcription factors, in recent years, the role of chromatin structure remodelling in response to cold stress has been addressed (Kim *et al.*, 2015), particularly the role of epigenetic regulators, such as histone deacetylases. An example is the histone deacetylase HDA6 in *A. thaliana*, which plays a central role in cold response activation, as well as in freezing tolerance (To *et al.*, 2011), whereas the histone deacetylase complex (HDAC) is involved in cold responses regulation (Kim *et al.*, 2004). Although several findings prove the involvement of epigenetic regulation in cold stress responses, for the most part, the molecular details are yet to be defined (Kong *et al.*, 2020).

1.2.3 Salt stress

Changes in the soil composition, such as the increase in salt concentration, expose plants to experiencing two different kinds of stress at the same time: the osmotic stress due to the decreased water potential in the soil and the accumulation of toxic ions in plant cells (Munns and Tester, 2008), mainly Na^+ ions. The latter, known as ion toxicity, determines several changes in plant physiology, such as reduced photosynthetic capacity while requiring changes in plant development to ensure plant survival (Julkowska and Testerink, 2015). The sensing mechanisms of alterations in ion concentrations have not been unravelled yet. In 2019 Jiang *et al.* identified MOCA1, a glucuronosyltransferase involved in the induction of Ca^{2+} spikes initiated by monovalent cations (Na^+, Li^+, K^+) that activates specific responses. In experimental conditions, upon administration of sodium ions, Ca^{2+} spikes are observable within 10 seconds leading to the activation of Na^+ exclusion operated by the SALT OVERLY SENSITIVE (SOS) pathway. The SOS pathway involves three main steps: Ca^{2+} sensing by SOS3 and SCABP8 sensors, the activation of protein kinases SOS2 and SOS2-like, e.g. PKB5, and the phosphorylation of Na^+/H^+ antiporter SOS1 (Liu and Zhu, 1997; Shi *et al.*, 2002; Yang *et al.*, 2019). Immediately after Ca^{2+} spikes, SOS3, in the roots, and SCABP8, in the shoots (Quan *et al.*, 2007) are activated and SOS2 dissociates from its inhibitors, 14-3-3 proteins (Zhou *et al.*, 2014). The phosphorylation of SOS1, operated by SOS2 (Liu *et al.*, 2000; Quintero *et al.*, 2002), leads to the activation of the Na^+ exclusion process via the SOS1 plasma membrane Na^+/H^+ antiporter activity (Shi *et al.*, 2000, 2002 and 2003), within 20 seconds from sodium ions application (Martínez-Atienza *et al.*, 2007). In *A. thaliana,* SOS1 presents a 700 amino acid long cytosolic C-terminal region (Shi *et al.*, 2000): in

this portion of the antiporter there are an autoinhibitory domain and a cNMP-binding domain that inhibits the Na^+ extrusion under unstressed conditions. Furthermore, the C-terminus of SOS1, like its mammalian counterpart NHE1, interacts with putative regulatory proteins, such as RADICAL-INDUCED CELL DEATH 1 (RCD1) (Katiyar-Agarwal *et al.*, 2006), which was identified as the coordinating hub of plant responses to abiotic stresses (Kragelund *et al.*,2012).

The primary function of the SOS pathway is to regulate the ion homeostasis in plant cells. Other than the activation of the SOS1 antiporter, the activation of the SOS pathway in *A. thaliana* leads to the inactivation of the HKT1 membrane transporter, which is involved in Na^+ ions entering the cell. Although the mechanism of the inactivation of AtHKT1 by the SOS pathway has not yet been uncovered, it was shown that loss-of-function of *AtHKT1* led to suppression of hypersensitivity to salt in *sos1, sos2 and sos3* mutants (Rus *et al.,* 2001 and 2004).

Nevertheless, the increased cytoplasmic concentration of Na^+ must be dealt with using several concomitant strategies: the most immediate one is the re-localization of the Na^+ ions in the vacuole through Na^+/H^+ exchangers (Blumwald and Poole, 1985; Ismail and Horie 2017). This mechanism in the root cells allows the accumulation of Na^+ in the vacuoles, hence preventing the ions from entering the root xylem, through which those could reach the shoots, especially leaves cells, where essential processes, such as photosynthesis, occur. In this process, the tonoplast-localized NHX-type Na^+/ H^+ antiporters play a preeminent role, particularly NHX1 (Na^+/H^+ EXCHANGER 1) in *A. thaliana,* whose overexpression enhances salt tolerance (Zhang and Shi, 2013).

1.2.4 Drought stress

Water availability in the surrounding soil influences many critical aspects of plant physiology and, in extreme cases, threatens its survival. Hence, the sensing and responding mechanisms to the lack of water, commonly referred to as drought stress, have a fundamental role: amongst these, reduction in turgor pressure and photosynthetic reaction rate results in reduced growth and, hence, in decreased crop yield (Farooq *et al.*, 2012). The sensors of internal water deficit are also known as osmosensors since this unfavourable condition results in a decrease of the osmotic potential of the extracellular environment, e.g. the soil, in comparison to the intracellular water potential. Due to the complexity of the responses during drought stress and its correlation with osmotic stress responses, several sensing mechanisms have been hypothesized. Still, a coherent model is yet to be proved. In 2014, Yuan *et al.* isolated OSCA1, a Ca^{2+}-permeable ion channel, part of a protein family presenting fifteen calcium-channel homologues (Liu *et al.*, 2018). Decreased water levels result in

increased extracellular osmotic potential and physical tensions at the plasma membrane, determining the opening of OSCA1 pore and the rapid increase in cytosolic [Ca^{2+}].

The sensing mechanism of water deficit in the soil is yet to be uncovered; however, it has been determined that plants use a root redirecting strategy to survive drought, known as hydrotropism. This mechanism generates cytosolic Ca^{2+} signalling along the phloem upon water gradient perception, possibly inducing the bending of the roots to avoid proceeding in the direction of lower water potential (Shkolnik *et al.*, 2018). Furthermore, after drought perception at the root level, the signal is transmitted to the shoots via long-distance messengers, such as abscisic acid (ABA), H^+ ions (pH), Ca^{2+} and small peptides. Amongst the latter, the recently identified small peptide CLE25 (CLAVATA3/ENDOSPERM SURROUNDING REGION-RELATED 25) was found to be increasingly expressed in root vascular tissues upon dehydration (Takahashi *et al.*, 2018). Once in the leaves, it binds the receptors BAM1 and BAM3, thus promoting *NCED3* expression and ABA biosynthesis. ABA is also transported from roots to shoots in consequence of water deficit perception, and here, interacts with its receptors PYR/PYL/RCAR (PYRABACTIN RESISTANCE (PYR)/PYR1-LIKE (PYL)/REGULATORY COMPONENTS OF ABA RECEPTOR (RCAR) proteins (Ma *et al.*, 2009; Park *et al.*, 2009). The ABA/PYR/PYL/RCAR complex binds to PROTEIN PHOSPHATASE 2Cs (PP2Cs), acting as co-receptor, thus releasing SNF1-RELATED PROTEIN KINASES 2 (SNRK2s), in particular SNRK2.2, SNRK2.3 and OPEN STOMATA 1 (OST1). Once released of the inhibiting component PP2Cs, SNRK2s activate the downstream ABA signalling pathway (Cutler *et al.*, 2010; Raghavendra *et al.*, 2010; Zhu, 2016; Qi *et al.*, 2018), which leads to transcription of ABA-dependent drought-responsive genes via phosphorylation of several ABA-RESPONSIVE ELEMENT (ABRE) TRANSCRIPTION FACTORS (ABFs) (Yoshida *et al.*, 2015). At the same time, the stomatal closure is initiated, via simultaneous ABA-dependent ion influx channel (such as KAT1) closure and efflux channel (such as SLAC1) opening, leading to decreased osmotic potential and cell turgor in guard cells, determining stomata closure.

It is worth noticing that up to 30% of total genes undergoes modulation of expression upon drought stress through regulation of transcriptional factor activity (Maruyama *et al.*, 2014). Among those, a relevant portion is activated upon drought stress, but independently of ABA perception. For example, the APETALA2/ETHYLENE RESPONSE FACTORS (AP2/ERFs) family includes several TFs that recognize the dehydration responsive element (*DRE*) in the promoter region of many drought-responsive genes, hence being named DEHYDRATION RESPONSIVE ELEMENT-BINDING PROTEINS (DREBs). DREBs are involved in response to several abiotic

stresses: DREB1s are involved in cold stress response (Liu *et al.*, 1998; Guo *et al.*, 2018), whereas DREB2s are involved in drought stress response (Sakuma *et al.*, 2006). In particular, DREB2A regulates the transcription of ABA-independent drought-responsive genes, and its activity is regulated by 26S proteasome-mediated proteolysis as well as through its interaction with the abiotic stress response protein hub RCD1, which was suggested to regulate DREB2A function by inhibiting it via protein binding (Vainonen *et al.*, 2012).

1.3 Abscisic acid (ABA) functions as a regulator of abiotic stress response and physiological processes

Abscisic acid is a ubiquitous plant hormone that plays a prominent role in plant development, such as seed dormancy, maturation and germination, (Finkelstein *et al.*, 2002; Cutler *et al.*, 2010; Liu *et al.*, 2016), as well as in response to various abiotic stresses, such as cold, high salinity and drought (Zhu, 2016). One of the rate-limiting steps of ABA biosynthesis is the 9-*cis*-epoxycarotenoid dioxygenase NCED3, which produces xanthoxin, a precursor of abscisic acid that is converted to active ABA via two consecutive oxidising reactions performed in the cytoplasm (González-Guzmán *et al.*, 2002). The conjugation of free active ABA with glucosyl ester (GE) produces ABA-GE, which is physiologically inactive and is stored in vacuoles. Upon increased accumulation of β-glucosidases BG1 and BG2, e.g., upon dehydration sensing, the inactive ABA-GE is quickly hydrolysed (Lee *et al.*, 2006) and the free ABA can act in the drought response activation.

As mentioned above, ABA plays an essential role in response activation to dehydration and cold stresses, e.g., stomata closure and transcriptional reprogramming (Zhu, 2002). On the other hand, under unstressed conditions, ABA perception and downstream signalling pathways are necessary for several physiological mechanisms in plants, such as seed development and dormancy and adult leaf senescence (Lee *et al.*, 2015; Gao *et al.*, 2016). For example, the already mentioned ABRE-BINDING PROTEINS (AREBs) or FACTORS (ABFs) are a subfamily of the BASIC LEUCINE ZIPPER (bZIP) family, presenting nine members in *A. thaliana*. Four of the ABFs family members, ABF1, ABF2, ABF3, and ABF4, were identified as the regulating TFs of ABA-dependent drought-responsive gene expression (Yoshida *et al.*, 2010; Yoshida *et al.*,2015). Other ABA-dependent transcription factors are the NAC factors, such as ANAC019/055/072 and ANAC096, that recognize and bind the *NAC* sequence in the promoter region of drought-responsive genes (Tran *et al.*, 2004; Xu *et al.*,2013).

1.4 Transcription factors play a pivotal role in abiotic and biotic stress response activation

Living organisms regularly face stress stimuli, both of biotic and abiotic kind, and, while non-sessile organisms can either "fight or flight", plants can only fight. Hence, several diversified response strategies for counteracting external stimuli were developed during evolution, especially by higher plants. The core of all these coping mechanisms is the transcriptional regulation: differential expression of genes upon different circumstances is the key to fine-tuning molecular and physiological homeostatic processes.

The modulation, either by activation or inhibition, of gene expression is achieved via different molecular mechanisms. Amongst those, chromatin state regulation via epigenetic modifications induces conformational changes of chromatin. Various modifications have different and opposite effects on the chromatin state, hence affecting gene transcription: the mono-, di- and trimethylation of Lysine 4 (K4) on histone 3 (H3) (H3K4me1, H3K4me2 and H3K4me3) are epigenetic modifications only present in chromatin regions encoding genes and promoters, hence marking the active chromatin (Zhang *et al.*, 2009). Whilst the H3K4me3 is correlated with active gene transcription, the trimethylation of the Lysine 27 (K27) on histone 3 (H3) (H3K27me3) is the most well-known marker of gene silencing, which only occurs in the euchromatic regions (Schubert *et al.*, 2006). In contrast, the heterochromatic regions, tightly packed and inaccessible to the transcriptional machinery, are characterized by the distinctive marker H3K9me2 (Fuchs *et al.*, 2006).

A central role in transcriptional regulation of stress-responsive genes is played by the activation mechanisms of transcription factors (TF). To ensure a prompt response to external inputs, most of the TFs are present at any time in an "inactive state", which prevents the binding to the DNA binding site present in the promoter regions of the target genes. The inactivity of a TF might depend on different circumstances: it can be influenced by its phosphorylation or redox state and the lack or the presence of TF-binding proteins, which may have either an activating or inhibiting effect.

Many TF-binding proteins have already been characterized for their relevant role in regulating transcriptional mechanisms, especially regarding the activation of defence responses against biotic and abiotic stresses. For example, several members of the bZIP TF family have been reported to interact with other proteins that regulate the localization and the activity of these transcription factors: amongst these TF interacting proteins, also known as transcriptional regulators, it is worth mentioning NON-EXPRESSER OF PATHOGEN-RELATED (PR) GENES (NPR1), whose

monomerization (Rochon *et al.*, 2006) and translocation to the nucleus via nuclear pore complex, upon salicylic acid (SA) perception, allows it to bind to the TGA transcription factors (group D of the *A. thaliana* bZIP family), hence activating transcription of genes involved in biotic stress responses (Despres *et al.,* 2000).

However, the mechanism of action of TF binding proteins is not limited to the activation of the TFs. On the contrary, it can also be involved in the inhibition of the transcriptional activation by binding to the target TF, which, in turn, is no longer able to bind the *cis*-elements of the genes whose transcription it is meant to initialize. For example, in *A. thaliana,* the TF MYELOBLASTOSIS RELATED 30 (MYB30) is involved in the activation of genes involved in the synthesis of very-long-chain fatty acid (VLCFA) in response to biotic stress (Raffaele *et al.*, 2008). Under normal conditions, MYB30 binds to MIEL1 (MYB30-INTERACTING E3 LIGASE1) in the nucleus, and through this interaction, it is ubiquitinated and consequently degraded via 26S proteasome. However, upon the perception of bacterial infection, the expression of MIEL1 is ceased, hence enabling the increase of MYB30 concentration and determining the activation of transcription of its target genes (Marino *et al.,* 2013).

Furthermore, the regulation of the TFs activity does not entirely depend on plant molecular mechanisms. In fact, some pathogenic species of bacteria and viruses can interfere with the regular functioning of specific TFs to impede the activation of host defence response via transcription reprogramming. Indeed, this has been reported in *A. thaliana* during infection by *Xanthomonas campestris* pathovar *campestris* (*Xcc*B100), whose XopD effector targets MYB30, hence inhibiting the transcriptional activation of the defence responses associated with VLCFAs synthesis (Canonne J. *et al.,* 2012).

1.5 Post-translational phosphorylation modulates protein activity in different ways

Another effective mechanism for a rapid and finely tuned regulation of protein activity, especially for initiating fast responses to external stimuli, is the modification of target proteins on specific residues after the protein synthesis to influence their biochemical features and, thus, their activation state. The study of post-translational modifications (PTMs) has identified several types of these that occur either on amino acid side chains or on the N- or C-terminus of proteins. The classification of these modifications is based on their chemical features: the addition can involve one or more moieties of chemical groups, such as methyl or phosphate, resulting in methylation or phosphorylation of the modified protein; the addition of complex groups, such as glycans or mono- or poly-ADP-ribose moieties, results in glycosylation or MAR- or PARylation. Finally, the

addition of peptides, such as ubiquitin or SUMO moieties, or their cleavage, via proteolysis, completes the scenario of the possible modifications that can be operated on proteins, at the same or different times in the protein lifetime on different residues, often with opposite effects on protein activity.

In plants, the most frequently occurring and best characterized PTM yet is the phosphorylation (Millar *et al.*, 2019) and it was estimated that one-third of the eukaryotic proteome carries at least one phosphorylation modification (Schwenke, 1997). It can occur as singular or multiple additions of a phosphate group (80 Da) to the side chain of either a Serine (80-85%), a Threonine (10-15%) or a Tyrosine (0-5%), and rarely on Histidine, Aspartate and Arginine (Besant & Atwood, 2009; Lohrmann, & Harter, 2002; Trentini *et al.*, 2014). In addition, the occurrence of post-translational phosphorylation has been widely studied to generate predictive algorithms that would help identify new phosphorylation sites *in silico* (Christian *et* al., 2012; Luo *et al.*, 2019). Interestingly, the analysis of empirically discovered phosphorylated residues has highlighted that the distribution of phosphorylation sites along with the protein sequences often correlates with intrinsically disordered regions that possibly undergo a disorder-to-order conformational transition (Iakoucheva *et al.,* 2004).

The study of post-translational phosphorylation in proteins has uncovered several effects of this PTM, which vary from structural changes due to biochemical changes in one or more regions of the target protein to regulate protein activity and variation in subcellular localization. For example, phosphorylation at specific residue (Thr^{947}) induces conformational changes in plasma membrane H^+-ATPase AtAHA2, which causes the autoinhibitory domain of AHA2 to be displaced (Fuglsang *et al.*, 2003). Interestingly, the phosphorylation of two other residues, Ser^{899} and Ser^{944}, on the same protein results in the inhibition of the proton pump of AHA2 (Fuglsang *et al.*, 2007). A similar case of inhibition determined by phosphorylation is the NONEXPRESSOR OF PATHOGENESIS-RELATED (PR) GENES 1 (NPR1), a SA-responsive plant immune regulator in *A. thaliana*: phosphorylated Ser^{55} and Ser^{59} prevent NPR1 SUMOylation while promoting its interaction with the TF WRKY70, hence repressing *PR1* gene transcription (Saleh *et al.*, 2015) and maintaining the regulator in a stable, inactive state. On the other hand, a secondary event of phosphorylation on Ser^{11} and Ser^{15} is catalysed upon dephosphorylation or Ser^{55} and Ser^{59} and SUMOylation, further enhancing NPR1-SUMO3 interaction and ultimately activating the transcription of *PR1* defence genes, as well as leading to NPR1 degradation (Saleh *et al.*, 2015). In addition, it has also been described that the phosphorylation of the residue Thr^{373} of NPR1 by SNF1-RELATED KINASE 2.8 (SNRK2.8) is necessary to the translocation of the monomeric form of

NPR1 from the cytosol to the nucleus, where it plays its function in establishing Systemic Acquired Resistance (SAR) upon pathogen attack (Lee *et al.*, 2015).

As already mentioned, the post-translational modification of proteins by adding phosphate groups might interest one or more residues along the protein sequence. In the first case, the addition of a single phosphate group act as a "switch" that might result in the activation of the enzymatic activity of the target protein or conformational rearrangements. On the other hand, the occurrence of multiple phosphorylations at different residues on the target protein act as a signal integrating mechanism and a molecular tool for fine-tuning protein activity. As an example, the transcription factor AtPIF3 presents several phosphorylation sites, whose modification by the PHOTOREGULATORY PROTEIN KINASES (PPK1, PPK2, PPK3 and PPK4; formerly called MUT9-LIKE KINASES (MLK4, MLK1, MLK2, MLK3) induces degradation of PIF3 itself to allow the activation of light-dependent growth pathways (Ni *et al.*, 2017).

Overall, post-translational phosphorylation of proteins has been proved to be a versatile biochemical tool by which proteins are regulated in their activity under many aspects. For example, a single phosphorylation can result in the activation or deactivation of a specific enzyme, while multiple phosphorylation sites can play a primary role in the modulation of protein activity or its targeting towards the degradation pathway.

1.6 *A. thaliana* RADICAL-INDUCED CELL DEATH1 (AtRCD1) is involved in stress response regulation via TF binding

Among the several transcriptional regulation mechanisms, the protein-protein interaction of master regulator proteins with TFs is one of the most well studied. One of the TF-binding proteins, *Arabidopsis thaliana* RADICAL-INDUCED CELL DEATH1 (RCD1), was initially known for its susceptibility to apoplastic ROS production upon ozone treatments (Overmyer *et al.*, 2000). Recently, RCD1 has been found to play a primary role in regulating plant stress responses and plant development (Jaspers *et al.*, 2009; Teotia and Lamb, 2009). RCD1 is the best-characterized member of the plant-specific SIMILAR TO RCD1 (SRO) protein family, consisting of five SRO proteins (AtSRO1, AtSRO2, AtSRO3, AtSRO4 and AtSRO5), plus RCD1 itself. All the members of the SRO family share common structural features, such as the core domain of poly(ADP-ribose) polymerase (PARP domain, PS51059), as well as an RCD1-SRO-TAF4 (RST, PF12174) domain at the C-terminus. Furthermore, RCD1 and SRO1 both present, at the N-terminus, a WWE domain, whose name derives from the three

specific conserved residues, two tryptophan (W) and one glutamate (E) residues (Aravind, 2001).

Due to the pleiotropic phenotype of the corresponding knockout mutant (Overmyer *et al.*, 2000; Jaspers *et al.*, 2009; Teotia and Lamb, 2009), RCD1 has been raising a particular interest over the years. By now, both the RST and the PARP domain of RCD1 have been structurally and functionally characterized. The RST domain presents a flexible structure that allows it to bind to intrinsically disordered regions of many transcription factors (Tossavainen *et al.*, 2017; Bugge *et al.,* 2018), hence being the domain that directly regulates the transcription pathways, in which RCD1 has been described to be involved. The variety of transcription factors interacting with the RCD1 RST domain has been attributed to the presence, along the aminoacidic sequence, of these different intrinsically disordered regions. Among the TFs that have been reported to interact with RCD1, the aforementioned DREB2A, ANAC013, ANAC017 and RAP2.4A are some of the most relevant. In 2012, Vainonen *et al*. demonstrated the interaction between RCD1 and DREB2A, the latter playing a pivotal role in the transcriptional reprogramming in response to drought and osmotic stress. This protein-protein interaction has been ascribed to the presence of a specific RIM motif (FDXXELLXXLN) of the DREB2A transcription factor. The product of a splice variant of *DREB2A* lacking the RIM motif, which accumulates during senescence and heat stress, did not show any interaction with the RCD1 RST domain. Hence, the interaction between RCD1 and DREB2A regulates the transcriptional reprogramming upon heat stress, during which RCD1 is degraded, while DREB2A.1 is stabilized, and the DREB2A.2 splice variant starts accumulating. The interaction between RCD1 and the transcription factors ANAC013 and ANAC017 was reported by Shapiguzov *et al*. (2019). These two TFs are transcriptional regulators of the *mitochondrial dysfunction stimulon* (*MDS*) genes and their interaction with the RCD1 RST domain has an inhibitory effect on the transcription of the MDS regulon. The *rcd1-1* knockout mutant shows increased tolerance to chloroplastic ROS due to the constant activation of AOX1A, the most abundant isoform of the MITOCHONDRIAL ALTERNATIVE OXIDASES (AOXs). Furthermore, the constitutive expression of MSD genes and the accumulation and enzymatic activity of their products were demonstrated to be the molecular basis of the enhanced chloroplastic ROS tolerance in the *rcd1* knockout mutant. Furthermore, it was observed that the interaction between RCD1 and RAP2.4A, a TF regulating the transcription of several genes encoding chloroplast antioxidant enzymes (e.g., *2CPA* (Baier *et al.,* 2004)), has a pivotal role in chloroplast antioxidant protection of *A. thaliana* in an age-dependent manner (Hiltscher *et l.*, 2014).

1.7 AtRCD1 Poly-(ADP-Ribosyl)-Polymerising (PARP) domain lacks catalytic activity

As aforementioned, there are different kinds of PTMs, whose effects on target proteins can affect their folding, localization and activity. Amongst these, Mono- and Poly(ADP-ribos)ylation (MARylation and PARylation) are reversible post-translational modifications, regulating plenty of molecular mechanisms in plant cells, including transcription reprogramming, chromatin remodelling and apoptosis, acting in conjunction with calcium signalling and phosphorylation cascades (Schreiber *et al.*, 2006; Chang *et al.*, 2009; Messner *et al.*, 2011). The addition of one or more ADP-ribose moieties is catalysed by mono (ADP-ribosyl) transferases (mARTs) or by poly-(ADP-ribosyl)-polymerases (PARPs), respectively via ART or PARP domain. Higher plants present two groups of proteins with PARP catalytic domain: one group is constituted by PAR-polymerases (PARPs), presenting a PARP regulatory domain and a PARP catalytic domain, and the other group is the aforementioned SRO family, whose member present PARP-like domains, in which the canonical catalytic triad (histidine, tyrosine and glutamate, H-Y-E) is not conserved (Vainonen *et al.*, 2016).

Regarding the differences between catalytically active and inactive PARP domains, the AtRCD1 PARP domain has been characterized to have a similar three-dimensional structure to the human PARP1 (HsPARP1). Substantial modification in the residues constituting the catalytic triad in the plant homologue of this domain has led to the conclusion that the RCD1 PARP domain possesses neither mono- nor poly-(ADP-ribosyl) catalytic activity, thus becoming named a "pseudo-PARP" domain (Wirthmüller *et al.,* 2018). Additionally, superimposing the crystal structure of RCD1 PARP domain (PDB code 5NGO) to HsPARP14 (PDB code 3SE2, by Wahlberg *et al.*, 2012), the three residues constituting the catalytic triad (H-Y-L) of HsPARP14, a mono (ADP-ribosyl) transferase, are not conserved in the PARP domain of RCD1, implying that the lack of these critical residues for NAD^+ binding would result in the absence of PARP catalytic activity in RCD1.

1.8 The WWE domain of AtRCD1 could be involved in the regulation of RCD1 activity

In *A. thaliana,* the subgroup Type A of the SRO protein family includes two members: RCD1 and SRO1, both distinguishable from the members of the Type B subgroup by the presence of the WWE domain at the N-terminal end of their amino acid sequences (**Figure 1.2**). This domain is the least well-characterized domain of RCD1 and its function in plants has not been clearly identified yet. It was first described as a potential

protein-protein interacting domain (Aravind, 2001), involved in binding protein targets of ubiquitin ligases and PARPs.

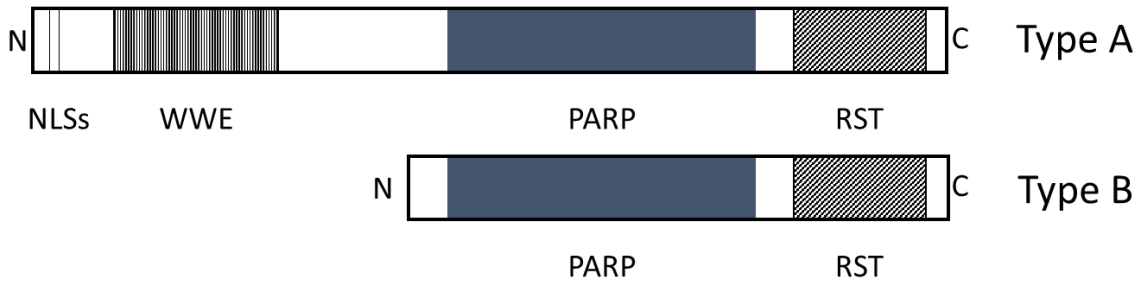

Figure 1.2: Schematic representation of SRO family and its two structural classes: Type A includes members presenting the WWE domain at the N-terminus (RCD1 and SRO1); Type B includes the remaining SRO family proteins (SRO2, SRO3, SRO4 and SRO5).

In *H. sapiens*, it has been demonstrated that the WWE of RNF146 binds to iso-ADP-ribose moieties, acting as a "reader" for PAR chains (Wang *et al.*, 2012), in conjunction with the RING domain of the same protein (DaRosa *et al.*, 2015). In *A. thaliana*, the PAR chains binding activity of the RCD1 WWE domain has been recently announced by Vainonen *et al.*, 2021, via plasma surface resonance and dot-blot assays.

Little else is known about the WWE domain function in AtRCD1 molecular and physiological role. Mass-spectrometry analysis and Yeast-2-Hybrid assay confirmed that this domain is involved in protein-protein interaction with a *Hyaloperonospora arabidopsidis* effector HaRxL106 and the *A. thaliana* MUT9-LIKE KINASES (MLK1, MLK2, MLK3, MLK4) (Wirthmüller *et al.,* 2018), later renamed respectively PPK2, PPK3, PPK4 and PPK1. The HaRxL106 effector was shown to affect the immune response in *A. thaliana* via its binding to the WWE domain and a linker region of AtRCD1, whereas the PPKs were found to interact with the same protein region (Wirthmüller *et al.,* 2018). Altogether, these findings suggest that the WWE domain could play a crucial role in regulating RCD1 function inside the plant cell, but this hypothesis is yet to be supported by data.

1.9 SIMILAR TO RCD1 (SRO1) in *Triticum aestivum* presents PAR polymerizing activity and enhances abiotic stress resistance.

The SIMILAR TO RCD1 (SRO) protein family is specific to plants and highly conserved amongst land plants (Jasper *et al.*, 2010). Many of the SRO family members are involved in abiotic stress response, as reported in the paragraphs above, but only one of the SRO family members has been found to have a PARylating catalytic activity so far. In 2014, Liu *et al.* described that *Triticum aestivum* TaSRO1, as well as the protein product of an allelic variant found in the cultivar Shanrong No. 3 (SR3), Ta-sro1, present PARP enzymatic activity. It was shown that the PARylating activity was increased in Ta-sro1 due to three point mutations on the CDS sequence of this allelic variant, resulting in two mutated residues (Gly^{250} and Ala^{343} in TaSRO1 to Val^{250} and Thr^{343} in Ta-sro1). It was reported that the considerably increased PARP activity of Ta-sro1, in respect to TaSRO1, was to be ascribed to the two amino acid substitutions (G250V and A343T), arguing that the first mutated residue resulted in an increased DNA binding capacity, while the A343T mutation favoured the interaction with the substrate (NAD^+), due to the presence of a methyl and a hydroxyl group of $Threonin^{343}$ on the surface of the catalytic site.

Additionally, it was observed that the canonical catalytic triad, conserved in many active PARP enzymes, consisting in Histidine, Tyrosine and Glutamate (Citarelli *et al.*, 2010) and forming a negatively charged pocket that binds NAD^+ molecules, was not conserved in neither of the two TaSRO1 variants. On the contrary, Liu *et al.* identified three different residues ($Leucine^{312}$-$Histidine^{344}$–$Histidine^{407}$) to form the catalytic triad in the two *Triticum aestivum* cultivars studied in their work. However, it should be noticed that the three amino acids described to be responsible for the PARP activity of TaSRO1 and Ta-sro1 do not share the same chemical features of the three conserved amino acids in canonical PARP enzymes.

Interestingly, the catalytic triad of TaSRO1 alleles presents a noticeable similarity to the AtRCD1 triad, $Leucine^{345}$ - $Histidine^{377}$ - $Asparagine^{440}$. This unorthodox triad does not include the tyrosine residue that, together with the histidine, is necessary to bind NAD^+ in all canonical ADP-ribosyl-transferases (Vyas *et al.,* 2014). A further investigation on the enzymatic activity of TaSRO1 could shed some light on this unique catalytic mechanism amongst the SRO family members, especially in respect of the close similarity of AtRCD1 inactive PARP catalytic triad to the ones described to be active in TaSRO1 and its allelic variant Ta-sro1 (Liu *et al.* 2014).

2 Materials and Methods

2.1 Materials

2.1.1 Plant material and growth conditions

All work and analysis in the present doctoral thesis were carried out using *Arabidopsis thaliana* plants of the ecotype Columbia-0 (Col-0). The *rcd1-1* line is an EMS homozygous knockout (KO) mutant line, courtesy of Prof. Dr. Jaakko Kangasjärvi (University of Helsinki). Table 2-1 lists the complemented homozygous lines carrying different versions of *AtRCD1* (AT1G32230): these lines were obtained via Agrobacterium-mediated transformation of *Arabidopsis thaliana rcd1-1* KO line, using the floral dip method as described in Logemann *et al.* (2006). *Nicotiana benthamiana* plants were used for transient expression of heterologous proteins for biochemical characterization.

Table 2-1 *Arabidopsis thaliana* lines used in this work

Name	Background	Line	Mutagen	Source/Reference
Wild type (WT) Columbia-0 (COL-0)	Col-0	-	-	J. Dangl (University of North Carolina, Chapel Hill, USA)
rcd1-1	Col-0	-	EMS	J. Kangasjärvi Lab (University of Helsinki, Helsinki, Finland)
rcd1-1 RCD1_NA	*rcd1-1*	#2.16 #2.4	-	Generated in this work *via A. tumefaciens*-mediated stable transformation of *A. thaliana rcd1-1* knockout mutant line.

Continues on the next page

Table 2-1: *Arabidopsis thaliana* lines used for this work

Name	Background	Line	Mutagen	Source/Reference
rcd1-1 RCD1_CD	*rcd1-1*	#3.1 #3.6 #4.8	-	Generated in this work *via A. tumefaciens*-mediated stable transformation of *A. thaliana rcd1-1* knockout mutant line.
rcd1-1 RCD1_CA	*rcd1-1*	#3.2 #12.11	-	

2.1.2 Bacterial strains used in this work

In Table 2-2, all the bacterial strains used in this work are listed with the corresponding genotypes.

Table 2-2 Bacterial strains used in this work

Species	Strain	Genotype	Purpose
Escherichia coli	DH10B	*E. coli* F- mcrA (mrr-hsdRMSmcrBC) φ80lacZ ΔM15 ΔlacX74 (Grant et al. 1990)	Amplification of cloning vectors
Escherichia coli	SHuffle	F- lac, pro, lacIQ/ Δ(ara-leu) 7697 araD139 fhuA2lacZ::T7 geneΔ (phoA)PvuII phoR ahpC* galE (or U) galK λatt::pNEB3-r1-cDsbC (SpecR,lacIq) Δtrx BrpsL150 (StrR) ΔgorΔ (malF)3 (Biolabs)	Protein expression in *E. coli*

Continues on the next page

Table 2-2 Bacterial strains used in this work

Species	Strain	Genotype	Purpose
Escherichia coli	BL21(DE3)	*E. coli* B F- dcm ompT hsdS (rB-mB-) gal λ (DE3) (Stratagen)	Protein expression in *E. coli*
	SoluBL21	*E.coli* F-ompT hsdSB (rB- mB-) gal dcm (DE3) (Gentlantis)	Protein expression in *E. coli*
Agrobacterium tumefaciens	GV3101:: pMP90	C58 (rifR) Ti pMP90 (pTiC58DT-DNA) (gentR) Nopaline.	Protein expression in *N. benthamiana*
Agrobacterium tumefaciens	C58C1:pCH32	C58C1, RifR, GmR (Voinnet *et al*. 2003)	Protein expression of P19 silencing inhibitor in *N. benthamiana*

2.1.3 Vectors

2.1.3.1 Destination vectors

Table 2-3 lists the destination vectors that were used in this work.

Table 2-3 Destination vectors used in this work

Vector	Features	Application
pOPIN-F (Berrow *et al*., 2007)	Amp^R, T7lacO, CMV enhancer and ββ-actin promoter, p10 promoter/ lef-2 and 1629 baculo elements.	*E. coli* expression vector for N-terminal HIS-tagged fusion proteins.

Continues on the next page

Table 2-3: Destination vectors used in this work

Vector	Features	Application
pK7FWG2 (Karimi *et al.*, 2002)	ori ColE1, ori RK2, CaMV p35S, pA35S, $Spec^R$, eGFP	Gateway-compatible binary vector for C-terminal GFP-fusion and overexpression *in planta* under CaMV 35S promoter.
pK7WGF2 (Karimi *et al.*, 2002)	$Spec^R$, ori ColE1, ori RK2, CaMV p35S, pA35S, eGFP	Gateway-compatible binary vector for N-terminal GFP-fusion and overexpression *in planta*, under CaMV 35S promoter.
pH7RWG2 (Karimi *et al.*, 2002)	$Spec^R$, ori ColE1, ori RK2, CaMV p35S, pA35S, RFP	Gateway-compatible binary vector for C-terminal RFP-fusion and overexpression *in planta*, under CaMV 35S promoter.
pGWB414 (Nakagawa *et al.*, 2007)	$Spec^R$, CaMV p35S, 3HA	Gateway-compatible binary vector for C-terminal 3-HA-fusion and overexpression *in planta*, under CaMV 35S promoter.
pXCSG-GW-mYFP-NLS (From PD Dr. M. Wiermer)	Amp^R , NLS from SV40	Gateway-compatible binary vector for C-terminal YFP-fusion, NLS and overexpression *in planta*, under CaMV 35S promoter.

2.1.3.2 Vectors used in this work

Table 2-4 lists the vectors generated and used in this work.

Table 2-4: Vectors used in this work

Vector	Description	Source / Reference
pENTRD_Topo_gRCD1 pENTRD_Topo_gRCD1_ND pENTRD_Topo_gRCD1_CD pENTRD_Topo_gRCD1_allD pENTRD_Topo_gRCD1_NA pENTRD_Topo_gRCD1_CA pENTRD_Topo_gRCD1_CA.2 pENTRD_Topo_gRCD1_allA	Cloning vector carrying the genomic sequence of RCD1 (WT or with various mutations at different amino acids in WWE domain and/or linker region).	Generated in this work, except for the vector carrying the WT version of RCD1, developed by Dr. Wirthmüller
pK7FWG2-RCD1_GFP pK7FWG2-RCD1_Nter_GFP pK7FWG2-RCD1_ND-GFP pK7FWG2-RCD1_NA-GFP pK7FWG2-RCD1_CD-GFP pK7FWG2-RCD1_allD-GFP pK7FWG2-RCD1_CA-GFP pK7FWG2-RCD1_CA.2-GFP pK7FWG2-RCD1_allA-GFP pK7FWG2-RCD1_PARP2-GFP	Binary expression vector carrying the genomic sequence of RCD1 (WT or with various mutations at different amino acids in WWE domain and/or linker region), GFP-labelled, under control of the CaMV 35S promoter.	Generated in this work, except for the vector carrying the WT version of RCD1, RCD1 N-terminus and PARP2, generated by Dr. Wirthmüller.
pGWB414-RCD1-3HA pGWB414-RCD1_ND-3HA pGWB414-RCD1_CD-3HA pGWB414-RCD1_allD-3HA pGWB414-RCD1_NA-3HA pGWB414-RCD1_CA-3HA pGWB414-RCD1_CA.2-3HA pGWB414-RCD1_allA-3HA pGWB414-RCD1_PPK1-3HA pGWB414-RCD1_PPK3-3HA pGWB414-RCD1_PPK4-3HA	Binary expression vector carrying the genomic sequence of RCD1 with various mutations at different amino acids in WWE domain and/or linker region, 3HA-labelled, under control of the CaMV 35S promoter.	Generated in this work, except for the vector carrying the WT version of PPK1, -3, -4, generated by Dr. Wirthmüller.

Continues on the next page

Table 2-4: Vectors used in this work

Vector	Description	Source / Reference
pXCSG-GW-RCD1ΔNterYFP:NLS pXCSG-GW-SRO1ΔNterYFP:NLS	Binary expression vector carrying the genomic sequence of RCD1 and SRO1 (lacking WWE domain and linker region), YFP-labelled, with heterologous NLS, under control of the CaMV 35S promoter.	Generated in this work.
pH7RWG2_RCD1_RFP pH7RWG2_SRO1_RFP pH7RWG2_RCD1_205_RFP pH7RWG2_SRO1_203_RFP pH7RWG2_RCD1_265_RFP pH7RWG2_SRO1_262_RFP pH7RWG2_PPK1_RFP pH7RWG2_PPK3_RFP pH7RWG2_PPK4_RFP	Binary expression vector carrying the genomic sequence of RCD1, SRO1 (full-length, only WWE domain or WWE+linker region), PPK1, PPK3, PPK4, RFP-labelled, under control of the CaMV 35S promoter.	Generated in this work.
pBm43GW- cRCD1-3V pBm43GW- cRCD1-3VΔWWE pBm43GW- cRCD1-3VΔPARP	Binary expression vector carrying the CDS of RCD1 (WT or versions lacking different regions of the protein) with a triple Venus tag, under control of CaMV 35S promoter.	J.Kangasjärvi Lab (University of Helsinki, Helsinki, Finland)
pUC57_RCD1_ND pUC57_RCD1_NA pUC57_RCD1_CD pUC57_RCD1_CA	Cloning vector carrying different modified versions of previously identified phospho-sites on RCD1.	Genereted by Biocat (Heideberg), carrying fragments designed by Dr. Wirthmüller.

Continues on the next page

Table 2-4: Vectors used in this work

Vector	Description	Source / Reference
pRT30_RFP_FLAG	Binary expression vector carrying the coding sequence of Red Fluorescent protein (RFP) coupled with a FLAG tag, under control of the CaMV 35S promoter	D.Schubert Lab (FU Berlin, Germany)
pCAMBIA_GW_YFP	Binary expression vector carrying the coding sequence of Yellow Fluorescent protein (YFP), under control of the CaMV 35S promoter	M Hülskamp Lab (University of Cologne, Germany)
popinF_TaSRO1_PARP-HIS	Vector for bacterial expression of PARP domain of *Triticum aestivum* SRO1 (246 to 453 aa), HIS6-labelled, under control of T7 promoter.	Generated by Dr. Wirthmüller.
popinF_TaSRO1_PARP-HIS_sv	Vector for bacterial expression of PARP domain of *Triticum aestivum* SRO1 (246 to 433 aa), HIS6-labelled, under control of T7 promoter.	Generated in this work.
pET24a_TaSRO1	Vector for bacterial expression of the full-length version of *Triticum aestivum* SRO1, HIS6-labelled, under control of T7 promoter.	Liu *et al.*, 2014
pOPIN-E_GFPnanobody	Vector for bacterial expression of GFP-nanobodies, carrying a Halo tag for production of anti-GFP magnetic beads.	Generated by Dr. Wirthmüller.

Continues on the next page

Table 2-4: Vectors used in this work

Vector	Description	Source / Reference
pET28_HsPARP1(L713F)	Vector for bacterial expression of PARP domain of HsPARP1, HIS6-labelled, under control of T7 promoter.	Langelier *et al.*, 2012

2.1.4 Chemicals

Unless otherwise stated, the chemical compounds used in this work were purchased from the following companies: AppliChem (Darmstadt), Biorad Laboratories (Munich), GE Healthcare (Freiburg), Invitrogen (Karlsruhe), Merck (Darmstadt), Roth (Karlsruhe), Sigma-Aldrich, now Merck (Steinheim). The generation of plasmids pUC57 carrying mutated fragments of *AtRCD1* (AT1G32230) was commissioned to Biocat (Heidelberg). Oligonucleotides were supplied by Sigma-Aldrich, now Merck (Steinheim). Macrogen EZ-Seq (Amsterdam) provided the sequencing service.

2.1.5 Enzymes, proteins, size standards and antibodies

Table 2-5 lists the enzymes, proteins, size standards and antibodies that were used in this work.

Table 2-5 List of enzymes, proteins, size standards and antibodies

Description	Manufacturer
5x DNA loading buffer	Bioline (Luckenwalde)
Anti-GFP (mouse)	Sigma-Aldrich, now Merck (Steinheim)
Anti-GFP pAb (rabbit)	Amsbio (Abingdon)
Anti-GST antibody	Thermo Scientific (USA)
Anti-mCherry antibody	Abcam (Cambridge)
Anti-Mouse IgG Peroxidase antibody from Goat	Sigma-Aldrich, now Merck (Steinheim)
Anti-PAR pAb (Rabbit)	Biozol (Eching)
BamHI Fast Digest Restriction enzyme	Thermo Scientific (USA)
BSA (Bovines Serum Albumin)	Sigma-Aldrich, now Merck (Steinheim)
DpnI	Fermentas (St. Leon-Rot)
FIREPol Master Mix	Solis Biodyne (Estland)
Gateway® LR Clonase® II Enzyme mix	Thermo Scientific (USA)
Gibson Assembly® Master Mix	New England Biolabs (Frankfurt am Main)
Goat Anti-Rat IgG Antibody, HRP conjugate	Sigma-Aldrich, now Merck (Steinheim)
GoScript Reverse Transcription System 100rxn	Promega (Mannheim)
GoTaq qPCR Master Mix	Promega (Mannheim)
HyperLadder I	Bioline (Luckenwalde)
Instant Blue stain	Sigma-Aldrich, now Merck (Steinheim)
Lysozyme	Sigma-Aldrich, now Merck (Steinheim)
Magne® HaloTag® Beads	Promega (Mannheim)
Methyl viologen dichloride hydrate	Sigma-Aldrich, now Merck (Steinheim)

Continues on the next page

Table 2-5: List of enzymes, proteins, size standards and antibodies

Description	Manufacturer
NcoI Fast Digest Restriction Enzyme	Thermo Scientific (USA)
NotI Fast Digest Restriction Enzyme	Thermo Scientific (USA)
PageRuler plus (Prestained Protein Ladder)	Fermentas (St. Leon-Rot)
Phusion High-Fidelity DNA Polymerase	Thermo Scientific (USA)
Protease inhibitor cocktail for plants (P9599)	Sigma-Aldrich, now Merck (Steinheim)
Protease inhibitor mix for *E. coli* (P8849)	Sigma-Aldrich, now Merck (Steinheim)
Seleno-L-methionine	Sigma-Aldrich, now Merck (Steinheim)
SuperSignal West Femto Maximum Sensitivity HRP Substrate	Thermo Scientific (USA)
Trisure	Bioline (Luckenwalde)
Water LC-MS grade	VWR (Darmstadt)
Western BLoT Ultra-Sensitive HRP Substrate	Takara Bio Europe (Saint-Germain-en-Laye)
XhoI Fast Digest Restriction Enzyme	Thermo Scientific (USA)
Z-Leu-Leu-Leu-al (MG132)	Sigma-Aldrich, now Merck (Steinheim)

2.1.6 Culture Media

Table 2-6 lists the culture media used in this work for different purposes, such as selection of transformed bacterial colonies, plant growth, resistant plant selection and allele segregation assays. For selection purposes, the media were added with the appropriate antibiotics after cooling to the temperature of about 55 °C. The corresponding working concentrations of the antibiotics are listed in the Table 2-7. The media were used either in liquid or solid form: the media for bacterial selection in plates were added with 1.5% w/v of Agar-Agar (Roth), while the medium for plant growth in plate were added with 0.8% w/v of Plant Agar (Duchefa).

Table 2-6 List of culture media

Medium	Composition
LB	25 g/l LB (Roth)
YEB	0.5% (w / v) meat extract, 0.5% (w / v) peptone, 0.5% (w / v) sucrose, 0.1% (w / v) yeast extract, 2 nM $MgSO_4$, pH 7.2 adjusted with 1 M NaOH
½ MS	2.2 g/l Murashige&Skoog-Salz (Duchefa), pH 5.7 adjusted with KOH

Table 2-7 List of antibiotics

Antibiotic	Concentration
Ampicillin	100 µg/ml
Carbenicillin	50 µg/ml for liquid media, 75 µg/ml for solid media
Gentamycin	15 µg/ml
Kanamycin	50 µg/ml
Rifampicin	50 µg/ml

2.1.7 Computer programs

Plasmid sequences and maps, as well sequencing data were collected and analyzed with the free online software Genome Compiler (Genome Compiler Corporation, Los Altos). The analysis of gene expression using quantitative real-time PCR (qPCR) was performed with the Bio-Rad CFX Manager 3.0 (Bio-Rad, Munich). The same software was used to analyze the thermal stability assay data. Statistic data analysis for qPCR data was performed using LinRegPCR software (Ruijter *et al.*, 2009) and GraphPad QuickCalcs Web site (GraphPad Software, San Diego, California USA).

2.2 Methods

2.2.1 Plant assays and growth condition

2.2.1.1 *Arabidopsis thaliana* seeds sterilization

To cultivate *A. thaliana* on soil, seeds were placed in the dark at 4 °C for 12 hours and then directly transferred to Jiffy7 soil. For cultivation of Arabidopsis plants on sterile plant medium, the sterilization was carried out by washing the seeds twice in 1 ml 100% (v/v) 2-propanol, followed by washing twice with 1 ml of sterile ddH_2O; seeds were then incubated at room temperature with a buffer containing 1.6% sodium hypochlorite and 0.001% SDS for 10 minutes. Afterwards, the seeds were washed thoroughly with sterile ddH_2O five times and sown on sterile plant medium.

2.2.1.2 Growth conditions of *Arabidopsis thaliana* and *Nicotiana benthamiana*

The cultivation of *A. thaliana* plants was carried out on mixed soil (42.42% (w/w) soil Type T, 42.42% (w/w) soil Type P and 15.16% (w/w) Perlite (Kausek, Mittenwalde)) under short-day conditions (SD, 8 hours of light/day) at 20 °C, light intensity of 100 µmol/(m^2s) and 55% air humidity. For seeds generation purposes, plants were moved under long-day condition (LD, 16 hours of light/day) at 22 °C and a light intensity of 150 µmol/(m^2s) and approx. 55% air humidity. For assay on MS medium, seeds were sown on solid medium and let overnight at 4 °C in the dark for stratification purposes. *Nicotiana benthamiana* plants were cultivated on Floratonerde (92% peat, 0.15% salinity, pH 5-6) in greenhouses with a 16 hours photoperiod, 22 °C and approximately 30% air humidity. For transient expression of heterologous proteins, 5-weeks-old (ca.) plants of *Nicotiana benthamiana* were used.

2.2.2 *A. thaliana* transgenic lines generation *via A. tumefaciens*

According to the method published by Logemann *et al.*, (2006), to generate transgenic lines of *A. thaliana* using transgenic *A. tumefaciens* strains, overnight cell culture of the Agrobacterium strain carrying the gene of interest was incubated at 28 °C, shaking at 180 rpm. The following day, plants were dipped for 15 seconds under gentle shaking in 120 ml of a solution (5% (w/v) sucrose, 0.03% (v/v) Silwet L-77) added with the Agrobacterium culture to an OD_{600} of 0.25. Dipped plants were laid horizontally in a tray, covered with a lid, sprayed with water to maintain high humidity and let rest overnight. The following day the plants were transferred to LD condition (16 hours of

light/day) in the greenhouses, until seeds maturation. Harvested and sterilized seeds were later sown on ½ MS plates added with the appropriate antibiotic to select resistant seedlings from which T3 homozygous lines were obtained by screening using segregation tests.

2.2.3 Tolerance assay to chloroplast oxidative stress in *A. thaliana*

To test plant tolerance to oxidative compound methyl viologen (Sigma-Aldrich), sterilized seeds of different genotypes were sown on solid ½ MS plates, added with methyl viologen to a final concentration of either 0.5 µM or 1 µM. The plates were transferred to a growth chamber under short-day (SD) conditions (10 h light/day, 55% air humidity) at 20 °C for 20 days. After this period, the number of true leaves per each genotype was scored and compared to the number of true leaves scored for the Col-0 wild type. The same experiment was performed under long-day (LD) conditions (16h light/day, 55% air humidity) at 22 °C, using three different methyl viologen concentrations in the ½ MS medium (0.5µM, 1 µM or 1.5 µM).

2.3 Microbiological methods

2.3.1 Bacterial growth

Escherichia coli cultures were grown in liquid LB culture medium, at 37 °C and 180 rpm for 16 hours or on solid LB culture medium (1.5% w/v agar) in the incubator at 37 °C. *Agrobacterium tumefaciens* cultures were grown in liquid YEB medium or on solid YEB medium (1.5% w/v agar) with the appropriate antibiotics (see Table 2-7) at 28 °C for 2-3 days, in liquid culture shaking at180 rpm for 48 hours (ca.) or on plates in an incubator.

2.3.2 Preparation of chemocompetent *E. coli* cells

To produce chemocompetent *E. coli* cells, 200 ml of liquid LB medium were incubated overnight at 37 °C and 180 rpm to reach an OD_{600} of ca. 0.5. The centrifugation was carried out at 2000 x *g* for 10 minutes and 4 °C. All the following steps were carried out on ice. The bacterial pellet was suspended in 60 ml of transformation buffer I (TB I: 30 nM Potassium acetate, 50 nM MnCl2, 100 nM RbCl2, 10 nM CaCl2, 15% (v/v) glycerol, pH 5.8) and centrifuged again. After resuspension of the bacterial pellet in 8 ml of transformation buffer II (TB II: 10 nM MOPS, 10 nM $RbCl_2$, 75 nM $CaCl_2$, 15% (v/v) glycerol, pH 6.5), 100 µL aliquots of competent cells were quick-frozen in liquid nitrogen and stored at -80 °C.

2.3.3 Preparation of electrocompetent *A. tumefaciens* cells

For the production of electrocompetent *A. tumefaciens* cells, 200 ml YEB without antibiotic were inoculated with two 5 ml overnight *A. tumefaciens* cultures (YEB liquid medium with appropriate antibiotics) and let grow to an OD_{600} of 0.6 at 28 °C and 180 rpm. After cooling for 5 minutes on ice, the bacterial suspension was centrifuged at 3500 x *g* for 20 minutes at 4 °C. All further steps were carried out on ice with pre-cooled solutions. The supernatant was discarded, and the cell pellet was carefully resuspended in 200 ml ddH_2O and, after re-centrifugation, was again resuspended in 100 ml cold ddH_2O. After further centrifugation, the pellet was washed in 8 ml of 10% cold glycerol and gently resuspended again in 8 ml of 10% cold glycerol. 50 µl aliquots were snap-frozen in liquid nitrogen and stored at -80 °C.

2.3.4 Heat shock transformation of chemocompetent *E. coli* cells

The transformation with recombinant plasmids was performed using 100 µl aliquots of chemocompetent *E. coli* cells and 50-100 ng plasmid DNA or 5 µl of a ligation batch. After 30 minutes of incubation on ice, cells were exposed to a heat shock at 42 °C for 1 minute. After adding 1 ml of LB medium and incubating in a shaker for 1 hour at 37 °C and 180 rpm, the cells were centrifuged at 3000 x *g* for 2 minutes, and the resuspended pellet was plated on LB plates (1.5 % agar (w/v)) with appropriate antibiotics.

2.3.5 Electroporation of *A. tumefaciens* cells

For the transformation of *A. tumefaciens* cells, 50 µl of electrocompetent cells with 100-150 ng of chosen plasmid DNA were mixed and incubated on ice for 5 minutes. The suspension was transferred to an electroporation cuvette and placed in the MicroPulser electroporator (BioRad, Munich). After the electroporation, 0.5 ml of sterile YEB liquid medium were added, and the suspension was incubated for 1 hour at 28 °C, shaking at 180 rpm. 5 µl of the transformation mixture were plated on YEB plates (1.5 % agar (w/v)) with the appropriate antibiotics and incubated for 2-3 days at 28 °C.

2.3.6 Production of bacterial permanent stocks

To obtain bacterial permanent stocks, 500 µl of bacterial cultures were mixed with 500 µl 50% (v/v) glycerol, in sterile screw-cap tubes and under sterile conditions. The stocks were stored at -80 °C.

2.4 Molecular biology methods

2.4.1 DNA isolation from *A. thaliana* according to Edwards *et al.* (1991)

Frozen leaf material was dissolved in 300 µl of Edwards buffer (200 mM Tris-HCl pH 7.5, 200 mM NaCl, 25 mM EDTA), homogenized in a mixer mill with two steel beads (3 mm Ø) per tube for 2 minutes at 25-30 Hz/s. After adding 10 µl of 10% (w/v) SDS solution and thorough mixing, the insoluble leaf components were centrifuged at 10000 x *g* for 5 minutes. Then, 150 µl of the supernatant was transferred to a clean reaction tube and extracted DNA material was precipitated by adding 150 µl of isopropanol (100% (v/v)). After incubating for 2 minutes at room temperature (RT), the precipitated DNA was centrifuged at 10000 x *g* for 10 minutes. The supernatant was removed, and the pellet was washed with 70% (v/v) ethanol. After centrifuging again at 10000 x *g* for 5 minutes, the pellet was air-dried under the fume hood and re-suspended in 100 µl of ddH_2O. 2 µL of DNA extract was used to set up a 20 µL PCR reaction.

2.4.2 *E. coli* plasmid DNA isolation

The isolation of plasmid DNA from *E. coli* on a small-scale was performed using the GenJet Plasmid Miniprep Kit (Thermo Scientific, USA) according to the manufacturer's instructions.

2.4.3 RNA isolation from *A. thaliana* according to Chomczynski and Sacchi (2006)

Homogenized frozen plant material from three leaves (ca. 200 mg) was placed in 2 ml reaction tubes and added with 1 ml Trisure (Bioline, Luckenwalde), thoroughly mixed and incubated at room temperature for 10 minutes. After centrifuging for 10 minutes at 12000 x *g* and 4 °C, the supernatant was transferred into a new 2 ml reaction tube containing 0.2 ml of chloroform (100% (v/v)) and mixed for 15 seconds. After incubating for 3 minutes at room temperature, samples were centrifuged at 12000 x *g* for 15 minutes at 4 °C for phase separation. The upper aqueous phase containing the RNA was transferred to a new 1.5 ml reaction tube. To precipitate the RNA, 0.5 ml of isopropanol (100% (v/v)) were added and incubated at room temperature for 10 minutes. After centrifuging at 12000 x *g* for 10 minutes at 4 °C, the extracted RNA was added with 1 ml of 70% (v/v) ethanol and centrifuged at 7500 x *g* for 5 minutes at 4 °C. After drying at room temperature, the RNA pellet was dissolved in 30 µl of RNase-free ddH_2O and then heated for 10 minutes at 50-60 °C. The determination of the RNA

concentration was performed as stated in section 2.4.10. For quality control, 1 µl of RNA was loaded on agarose (1% (w/v)) gel and gel electrophoresis was performed. RNA was snap-frozen in liquid nitrogen and stored at -80 °C. During further processing, RNA was always kept on ice.

2.4.4 DNase Treatment on RNA

1 µl of RNase-free DNase and 1x DNase buffer (New England Biolabs, Frankfurt am Main) were added to 20 µl of purified RNA and samples were incubated at 37 °C for one hour. The DNase was irreversibly inactivated by adding 2 µl of 50 mM EDTA and incubating for 10 minutes at 75 °C. Checking the RNA for possible residual contamination with genomic DNA was carried out with intron-specific oligonucleotides using real-time quantitative PCR described in section 2.4.11.

2.4.5 cDNA synthesis

The cDNA synthesis for quantitative Real-Time Polymerase Chain Reaction (RT-PCR) was carried out with the GoScript ReverseTranscription System (Promega, Mannheim). A 10 µl reaction was set up using 2 µg of RNA, 0.5 µg of oligo(dT) primers and 0.5 µg of random primers. After incubating for 5 minutes at 70 °C, 10 µl of transcription reaction mix was added (1 x GoScript™ reaction buffer, 1.5 mM $MgCl_2$, 0.5 nM dNTPs, 20 U RNasin® ribonuclease inhibitor, 1U GoScript™ reverse transcriptase) and the mix was incubated for 5 minutes at 25 °C. This step was followed by cDNA synthesis at 42 °C for one hour. The inactivation of the enzymes was performed heating up the samples at 70°C for 15 minutes. The cDNA was diluted 1:1 with RNase free water.

2.4.6 Polymerase Chain Reaction (PCR) according to Mullis *et al.* (1986)

DNA fragments were amplified by Polymerase Chain Reaction (PCR) from plant cDNA, genomic DNA or plasmid DNA template. DNA polymerases FIREPol (Solis Biodyne) or Phusion High-Fidelity (Thermo Scientific, USA) were used to perform the reactions, according to the purpose of the assay. The amplification of fragments in which mutations were introduced by overlap-extension PCR (OE-PCR) (Higuchi *et al.*, 1988) was performed according to the same method by Mullis *et al.,* (1986), using appropriate overlapping primers to introduce the intended mutations. The specificity of the binding between oligonucleotides and template was guaranteed by the length of the nucleotides (between 20 and 33 base pairs), which are listed in Table A.1 in the Appendix. The following Tables 2-8 to 2-10 list the composition of the PCR reaction mixtures and PCR programs of the PCR reactions performed.

Table 2-8: PCR reaction for FIREPOL polymerase

Component	Volume per reaction	Final concentration
5x FIREPol Master Mix ready to load 7.5 mM $MgCl_2$ + Polymerase	4 µl	1x
DNA Template	1 µl	50–200 ng
Forward Primer (100 µM)	0.5 µl	2.5 µM
Reverse Primer (100 µM)	0.5 µl	2.5 µM
ddH_2O	Up to 20 µl	

Table 2-9: PCR reaction for Phusion polymerase

Component	Volume per reaction	Final concentration
5x Phusion HF buffer 7.5 mM $MgCl_2$	4 µl	1x
DNA Template	1 µl	50–200 ng
dNTPs (10 µM)	0.4 µl	0.2 mM
Forward Primer (100 µM)	0.5 µl	2.5 µM
Reverse Primer (100 µM)	0.5 µl	2.5 µM
Polymerase Phusion (2U/µl)	0.4 µl	1U
ddH_2O	Up to 20 µl	

Table 2-10: PCR programs:

Step	Temperature	Time	No. of cycles
1. Starting denaturation	95 °C (FIREPol) 98 °C (Phusion)	3 min. (FIREPol) 5 min. (Phusion)	1
2.1 Denaturation	95 °C (FIREPol) 98 °C (Phusion)	30 sec. (FIREPol) 20 sec. (Phusion)	30 - 40
2.2 Annealing	T_A °C	30 sec. (FIREPol) 30 sec. (Phusion)	
2.3 Amplification	72 °C	1 min/1 kb FIREPol) 30 sec/1 kb (Phusion)	
3. Final Amplification	72 °C	10 min.	1

2.4.7 Site-direct mutagenesis by PCR according to Weiner *et al.* (1994)

In order to induce a point mutation on the vector pGWB414-RCD1_CA-3HA, to obtain the clone pGWB414-RCD1_CA.2-3HA, a site-direct mutagenesis was performed. The mutagenesis oligonucleotides are listed in the appendix in Table A.2. The mutagenesis primers were 32bp in length and the sequence template mismatch occurring was in the middle of the oligonucleotide sequence. Tables 2-11 and 2-12 below describe the composition of the PCR reaction mix and the PCR program for site-direct mutagenesis. The DNA product of the site-direct mutagenesis via PCR was subsequently treated with 10 U of the restriction enzyme DpnI, which recognizes and cuts only methylated DNA and incubated for 1 hour or overnight at 37 °C. 10 µl of the DpnI-treated PCR product were transformed into DH10B *E. coli* chemocompetent cells.

Table 2-11: PCR reaction for site-direct mutagenesis via PCR.

Component	Volume per reaction	Final concentration
5x Phusion HF buffer 7.5 mM $MgCl_2$	4 µl	1x
DNA Template	1 µl	50 ng
dNTPs (10 µM)	0.4 µl	0.2 mM
Forward Primer (100 µM)	0.5 µl	2.5 µM
Reverse Primer (100 µM)	0.5 µl	2.5 µM
Polymerase Phusion (2U/µl)	0.4 µl	1U
ddH_2O	Up to 20 µl	

Table 2-12: PCR program for site-direct mutagenesis via PCR.

Step	Temperature	Time	No. of cycles
1. Starting denaturation	98 °C	5 minutes	1
2.1 Denaturation	98 °C	30 seconds	18
2.2 Annealing	55 °C	30 seconds	
2.3 Amplification	72 °C	1 minute/1 kb	
3. Final Amplification	72 °C	10 minutes	1

2.4.8 Agarose gel electrophoresis

The gel electrophoretic separation of nucleic acid fragment (DNA and RNA) was carried out in 1-2% (w/v) agarose gels in TAE buffer (40 mM Tris-HCl, 0.1 mM EDTA with 28.55% (v/v) acetic acid, pH 8.5) with 50 ng/ml ethidium bromide. TAE was used as the electrophoresis buffer. For gel loading, 20 µl of the nucleic acids preparation were added with 5 µl of 5X DNA loading buffer (Bioline, Luckenwalde) and loaded on the agarose gel. As size standard, 5 µl of Hyperladder I (Bioline, Luckenwalde) were loaded on the first well of each row of gel loading wells. The applied voltage was between 80 and 150 V, according to the electrophoresis chamber used. After the electrophoresis, the separated DNA fragments were visualized with an UV transilluminator (254 nm).

2.4.9 DNA extraction from agarose gels

After ethidium bromide staining and size check, the DNA bands (from restriction approaches or PCR products for cloning) were excised from the agarose gel under UV light and purified according to the manufacturer's instructions with the NucleoSpin® Gel and PCR Cleanup (Macherey-Nagel). The elution of the purified DNA fragments was carried out in a volume of 20 µl.

2.4.10 DNA and RNA quantification

The spectrophotometer Nanodrop ND-100 (PEQLAB, Erlangen) was used for nucleic acid concentration and purity determination. The amount of nucleic acid was determined by the measurement of the extinction coefficient at a wavelength between 260 and 280 nm.

2.4.11 Quantitative real-time PCR (qRT-PCR)

The quantitative real-time PCR (qRT-PCR) was carried out in a 10 µl batch with 1 µl of diluted cDNA, 5 µl of GoTaq qPCR Master Mix (Promega, Mannheim) and 0.5 µM of each oligonucleotide. The PCR was performed with the thermocycler CFX 96 (Bio-Rad, Munich) (see Table 2-13). The quantification of the expression levels for each gene of interest was carried out with 1 µl of cDNA, as described above. The assay was performed with appropriate oligonucleotide pairs for each gene (see Table A.3 in the Appendix). Per each experiment, at least three biological replicates were tested, each with three technical replicates. The specificity of the PCR reaction was checked by analysis of the PCR product dissociation curves. The analysis of the results of the qRT-PCR assays was performed with the software LinRegPCR (Ruijter et al., 2009), using *NBLACK* (AT4G34270) as reference gene (Czechowski *et al.*, 2005).

Table 2-13: qRT-PCR program using Power SYBR Green.

Step	Temperature	Time	No. of cycles
1. Starting denaturation and heat activation of the polymerase	95°C	10 min.	1
2.1 Denaturation	95 °C	15 sec.	40
2.2 Annealing + Amplification	60 °C	50 sec.	
3. Dissociation curve	At intervals of 0.5° C	Every 2 sec.	1

2.4.12 Cloning methods

2.4.12.1 Gibson assembly®

To perform the Gibson assembly® (New England Biolabs, USA) accordingly to the manufacturer's instructions, 1 µl of entry clone was digested with the appropriate restriction enzymes as described in section 2.4.14, and purified from gel, after running the reaction product on an agarose gel, as described in section 2.4.8 and 2.4.9. The target sequence was amplified *via* PCR using Phusion High-Fidelity polymerase (Thermo Scientific, USA), as described in Table 2-9 and Table 2-10, and purified from agarose gel, after checking the size of the amplified fragment (sections 2.4.8 and 2.4.9). The Gibson assembly® reaction was set up as described below in Table 2-14 and the mix was incubated in a thermocycler at 50°C for 1 hour. 2 µl of the assembly reaction were retransformed in DH10b *E. coli* chemocompetent cells, as described in section 2.3.4.

Table 2-14: List of Gibson assembly® components

Component	Quantity
Gibson Assembly Master Mix (2X)	10 µl
Linearized vector	50-100 ng
PCR amplified fragment	100-200 ng
ddH_2O	Up to 20 µl

2.4.12.2 LR reaction for Gateway™ cloning system

To clone the gene of interest from the entry clone into the destination vector, LR reactions for Gateway™ cloning system (Thermo Scientific, USA) were performed accordingly to the manufacturer's instructions. The LR reaction was carried out in TE buffer (10 mM Tris, 1 mM EDTA, pH 8), and the set-up is described in Table 2.15. The reaction mix was prepared in a 1.5 ml tube incubated at room temperature overnight. 1 µl of the mix was retransformed in DH10b chemocompetent *E. coli* cells, as described section in 2.3.4.

Table 2-15: List of LR reaction components for Gateway™ cloning system

Component	Quantity
Entry clone	1–7 µl (50-150 ng)
Destination vector	1 µl (150 ng/µl)
LR Clonase ™ II enzyme mix	2 µl
TE buffer	Up to 10 µl

2.4.13 Vectors generated via different cloning methods

Tables 2-16, 2-17, 2-18, 2-19 and 2-20 show the vectors generated in this work, according to the different cloning strategies. Cloning and mutagenesis PCRs were performed either with cDNA, gDNA or already existing plasmids with appropriate CDS as template.

Table 2-16: List of entry clones obtained via Gibson® assembly isothermal cloning

Target sequence	Vector	Oligonucleotides F: Forward primer R: Reverse primer	Entry clone
gRCD1_Δ-Nter	pENTR4	F: TACAAAAAAGCAGGCTCCACATGG CCAAGCTTACGGGAAG R: GAAAGCTGGGTCTAGATATCTCGA GTTCAATCCACCTGCACCTTC	pENTR4_gRCD1_Δ-Nter
gSRO1_Δ-Nter	pENTR4	F: TACAAAAAAGCAGGCTCCACATGG CCAAGCTTACGGGAAG R: GAAAGCTGGGTCTAGATATCTCGA GTTACCCAAACTCCTTTGAAGG	pENTR4_gSRO1_Δ-Nter
TaSRO1	pENTR4	F: TACAAAAAAGCAGGCTCCACATGG AAAGGAAGACTGGAATGGTAC R: GAAAGCTGGGTCTAGATATCTCGA GTTGGAGGTGCTGCTCCCTCC	pENTR4_TaSRO1
TaSRO1_PARP_SV	pOPIN F	F: AAGTTCTGTTTCAGGGCCCGATTG GCCAACCTGTTG R: ATGGTCTAGAAAGCTTCAATTGGT CATGGAAGGTGCTTTG	pOPINF_TaSRO1_PARP_sv
RNF146_WWE_CDS	pENTR4	F: TACAAAAAAGCAGGCTCCACGGAA ATGGTGAATATGCATGG R: GAAAGCTGGGTCTAGATATCTCGA GTTTAGCCTAAGTCCAGCTACTCC	pENTR4_RNF146_WWE_CDS

Table 2-17: Entry clone obtained via site-direct mutagenesis

PCR template	Oligonucleotides F: Forward primer R: Reverse primer	Entry clone
pENTR_DTopo_ gRCD1_CA	F: TTAATGGTGGCGAGGCACCGAGGT- TAAATTTG R: AATTTAACCTCGGTGCCTCGCCA- CCATTAA	pENTR_DTopo_ gRCD1_CA.2

Table 2-18 List of entry clones generated *via* overlap-extension PCR (OE-PCR) combined with Gibson assembly® isothermal cloning

PCR template	Oligonucleotides F: Forward primer R: Reverse primer	Entry clone
pUC57_gRCD1_ND	F_1: CCGCGGCCGCCCCCTTCAC CATGGAAGCCAAGATCG R_1: ATCGTCCATCATATTATCA CCAG F_2: CTGGTGATAATATGATGGA CGATG R_2: CTGGTGATAATATGATGGA CGATG	pENTR_D Topo_gRCD1_ND
pUC57_gRCD1_ND pUC57_gRCD1_CD	F_1: CCGCGGCCGCCCCCTTCAC CATGGAAGCCAAGATCG R_1: ATCGTCCATCATATTATCA CCAG F_2: CTGGTGATAATATGATGGA CGATG R_2: CTGGTGATAATATGATGGA CGATG	pENTR_D Topo_gRCD1_allD
pUC57_gRCD1_NA pUC57_gRCD1_CA.2	F_1: CCGCGGCCGCCCCCTTCAC CATGGAAGCCAAGATCG R_1: ATCGTCCATCATATTATCA CCAG F_2: CTGGTGATAATATGATGGA CGATG R_2: CTGGTGATAATATGATGGA CGATG	pENTR_D Topo_gRCD1_allA

Table 2-19: List of expression vectors obtained via Gateway® cloning

Entry clone	Destination vector	Expression vector
pENTR_DTopo_gRCD1_ND	pK7FWG2	pK7FWG-_gRCD1_ND_GFP
pENTR_DTopo_gRCD1_CD	pK7FWG2	pK7FWG-_gRCD1_CD_GFP
pENTR_DTopo_gRCD1_NA	pK7FWG2	pK7FWG-_gRCD1_NA_GFP
pENTR_DTopo_gRCD1_CA	pK7FWG2	pK7FWG-_gRCD1_CA_GFP
pENTR_DTopo_gRCD1_allD	pK7FWG2	pK7FWG-_gRCD1_allD_GFP
pENTR_DTopo_gRCD1_allA	pK7FWG2	pK7FWG-_gRCD1_allA_GFP
pENTR_DTopo_gRCD1_CA.2	pK7FWG2	pK7FWG-_gRCD1_CA.2_GFP
pENTR_DTopo_gRCD1_ND	pGWB414	pGWB414_gRCD1_ND_HA
pENTR_DTopo_gRCD1_CD	pGWB414	pGWB414_gRCD1_CD_HA
pENTR_DTopo_gRCD1_NA	pGWB414	pGWB414_gRCD1_NA_HA
pENTR_DTopo_gRCD1_CA	pGWB414	pGWB414_gRCD1_CA_HA
pENTR_DTopo_gRCD1_allD	pGWB414	pGWB414_gRCD1_allD_HA
pENTR_DTopo_gRCD1_allA	pGWB414	pGWB414_gRCD1_allA_HA
pENTR_DTopo_gRCD1_CA.2	pGWB414	pGWB414_gRCD1_CA.2_HA
pENTR4_gRCD1_Δ-Nter	pXCSG-GW-mYFP-NLS	pXCSG-GW_gRCD1_Δ-Nter:YFP:NLS
pENTR4_gSRO1_Δ-Nter	pXCSG-GW-mYFP-NLS	pXCSG-GW_gSRO1_Δ-Nter:YFP:NLS
pENTR_DTopo_gRCD1	pH7RWG2	pH7RWG2-_gRCD1_RFP
pENTR_DTopo_gSRO1	pH7RWG2	pH7RWG2-_gSRO1_RFP

Continues on the next page

Table 2 19: List of expression vectors obtained via Gateway® cloning

Entry clone	Destination vector	Expression vector
pENTR_DTopo_cMLK4	pH7WGR2	pH7WGR2_PPK1(MLK4)-RFP
pENTR_DTopo_cMLK2	pH7WGR2	pH7WGR2_PPK3(MLK2)-RFP
pENTR_DTopo_cMLK3	pH7WGR2	pH7WGR2_PPK4(MLK3)-RFP
pENTR_DTopo_RCD1_265	pH7WGR2	pH7WGR2_RCD1_265-RFP
pENTR4_TaSRO1_CDS	pK7FWG2	pK7FWG-_TaSRO1-GFP
pENTR4_RNF146_WWE_CDS	pH7RWG2	pH7RWG2_RNF146_WWE-RFP

Table 2-20: List of vectors obtained via restriction cloning

Target sequence	Vector	Oligonucleotides F: Forward primer R: Reverse primer	Restriction enzymes	Entry clone
rcd1_CD	pENTR D Topo	F: CCGCGGCCGCCCCCTTCACC ATGGAAGCCAAGATCG R: ATGGATCCCAACACCATAG ATGGACTTTCT	*NotI* *BamHI*	pENTR_D Topo_gRCD1_ CD
rcd1_NA	pENTR D Topo	F: CCGCGGCCGCCCCCTTCACCA TGGAAGCCAAGATCG R: ATGGATCCCAACACCATAGAT GGACTTTCT	*NotI* *BamHI*	pENTR_D Topo_gRCD1_ NA
rcd1_CA	pENTR D Topo	F: CCGCGGCCGCCCCCTTCACCA TGGAAGCCAAGATCG R: ATGGATCCCAACACCATAGAT GGACTTTCT	*NotI* *BamHI*	pENTR_D Topo_gRCD1_ CA

2.4.14 Restriction digestion of plasmids

The digestion of the plasmid DNA was performed using restriction endonucleases of type II. The FastDigest enzymes (Thermo Scientific, USA) were resuspended in the corresponding buffer, according to the manufacturer's instructions. 0.5-2 µg of plasmid

DNA and 1 µl of each enzyme (FastDigest) were added to a 20 µl reaction mix, that was incubated at 37 °C for one hour. The digested DNA fragments were analyzed by gel electrophoresis (section 2.4.8) and purified (section 2.4.9).

2.4.15 Ligation

A 10 µl ligation mixture containing 1 µl of 10x ligase buffer, 5 U of T4 DNA ligase (Thermo Scientific, USA) and 50 ng of restriction-digested vector DNA was added with the restriction-digested insert DNA in a molar ratio between 1:3 and 1:5 to the vector DNA. The incubation was carried out either for one hour at 22 °C or at 4 °C overnight.

2.4.16 DNA sequencing

To sequence the plasmids generated *via* the different cloning methods described above, 500 µg of plasmid DNA were sent to sequencing with appropriate primer, according to Macrogen Europe (Amsterdam) EZseq user guide.

2.5 Protein biochemistry methods

2.5.1 Transient expression of heterologous proteins in *N. benthamiana*

For transient protein expression and localization assays in *N. benthamiana, A. tumefaciens* cells of strain GV3101 and cells of *A. tumefaciens* strain C58C1:pCH32 (for the expression of silencing inhibitor p19) were plated on YEB solid medium with the appropriate antibiotics and incubated at 28 °C for 48 hours. The culture yield was scraped from the plates and resuspended in 10 ml infiltration buffer (10 mM MES pH 5.6, 10 mM $MgCl_2$). The OD_{600} of each suspension was measured and diluted to 0.8, with the exception of the suspension containing *A. tumefaciens* p19 strain, whose final OD_{600} was set at 8. The bacterial suspensions were incubated for two hours at room temperature, then added with 150 µM acetosyringone and incubated for one more hour at room temperature. The bacterial suspensions were injected using needleless syringes, from the leaf underside, into the intercellular space of 4 to 5 weeks old *N. benthamiana* plants. For heterologous protein expression, the plants were let grown for 3 days in a phytochamber under long-day conditions (16 hours of light/day).

2.5.2 Protein extraction after transient expression in *N. benthamiana*

One gram of frozen *N. benthamiana* leaf material was ground in liquid nitrogen using mortar and pestle to a fine powder. The powder was then thoroughly mixed with 2ml

of YS Protein Extraction Buffer (100 mM Tris-HCl pH 8.0, 5 mM EDTA, 150 mM NaCl, 20 mM DTT, 1:200 plant Protease Inhibitor Cocktail (P9599, Sigma, Steinheim), 10 mM NaF, 10 mM Na_3VO_4, 0.5% (v/v) TritonX-100). After complete thawing, the samples were transferred into 2 ml tubes and centrifuged at 20000 x *g* for 20 minutes at 4 °C to separate soluble and insoluble components. The supernatant (crude extract) was transferred to a new 2 ml reaction tube and centrifuged again at 20000 x *g*, at 4 °C, for 5 minutes. All further steps were carried out on ice. Extracted proteins were used to perform Western Blot assay (section 2.5.11), time-course assays and GFP-tagged proteins were used for co-immunoprecipitation assays as described in section 2.5.4

2.5.3 Preparation of αGFP magnetic beads

To manufacture αGFP magnetic beads, αGFP:Halo:His6 fusion protein was expressed in large-scale culture in Shuffle *E.coli* cells. Two liters of cell culture were incubated at 37 °C, shaking at 200 rpm, until the culture reached an OD_{600} around 1. The culture was incubated at 18 °C overnight, after inducing the expression of the heterologous protein with 0.5 mM IPTG. The protein of interest was extracted from cell pellet as described below (section 2.5.6) and purified with a combined approach of IMAC and gel filtration (section 2.5.8). The purified protein was then concentrated to 1 mg/ml, aliquoted in 2 ml tubes and snap-frozen in liquid nitrogen and stored at -80°C. 250 µl of Promega Magne® Halo Tag® beads were washed in 1 ml A4 buffer (20 mM HEPES, 150 mM NaCl, pH7.5) at 4 °C, using a magnetic rack to collect the beads. One aliquot of αGFP:Halo:His6 protein was added with the washed magnetic beads and incubated on a rotator, spinning at 12 rpm, for 2 hours a 4 °C. After the incubation time, the beads were washed, adding 2 ml of A4 buffer and incubating on a rotator at 4 °C for three times, 15 minutes each time. The beads were resuspended in 250 µl of beads storage buffer (50 mM HEPES, 150 mM NaCl, 15% Glycerol, 0.05% NaN_3, pH7.5) and stored at 4 °C until use, up to 5 weeks after the day of production. 15 µl of αGFP magnetic beads were used for each sample of co-immunoprecipitation assays.

2.5.4 Protein Co-Immunoprecipitation Assay

The co-immunoprecipitation assay was performed to assess whether two proteins, heterologously expressed in *N. benthamiana* leaf tissues, interacted *in vivo*. 15 µl of Magne® HaloTag® Beads (Promega, USA), coupled with Halo-αGFP nanobody (produced and purified *via* FLPC in AG Romeis Laboratory, FU Berlin), were added to 1.5 ml of soluble fraction of protein extract (section 2.5.2) and incubated at 4 °C, on a rotator mixer, spinning at 12 rpm, for 5 to 15 minutes, depending on the proteins of interest. After the incubation time, the magnetic beads were collected on the wall of the tubes with a magnetic rack and washed three times, for 5 minutes each time, with 1 ml of the same protein extraction buffer described in section 2.5.2, with half the

concentration of plant Protease Inhibitor Cocktail. The beads were resuspended in 60 µl of A4 buffer (20 mM HEPES, 150 mM NaCl, pH7.5), added with 20 µl of 4x SDS sample buffer (200 mM Tris-Cl (pH 6.8), 400 mM DTT, 8% SDS, 0.4% bromophenol blue, 40% glycerol) and boiled at 96 °C for 5 minutes. As control of the input, for each sample 90 µl of the initial protein extract were added with 30 µl of 4x SDS loading buffer and boiled, as control.

2.5.5 Small-scale protein expression in *E. coli* and protein extraction

An overnight culture of each *E. coli* strain needed for experimental purposes was incubated at 37 °C, shaking at 200 rpm. The next day, new cultures were started using 0.02% (v/v) of the overnight cultures with the appropriate antibiotics: samples were incubated at 37 °C, shaking at 200 rpm, until they reached an OD_{600} around 1. At this point, heterologous protein production was induced by adding IPTG at the final concentration of 0.5 mM, after transferring the cultures at 18 °C, shaking at 200 rpm, overnight. The next day, the cultures were centrifuged in 2 ml tubes at 7000 x *g*, and the pellet was resuspended in 1 ml of lysis buffer (see Table 2-21). After incubation at room temperature for 10 minutes, 200 µl of the lysate were transferred into 1.5 ml tubes and sonicated twice in a sonicating bath for 10 minutes. After vortexing, 90 µl of the lysate were transferred to new 1.5 ml tubes and labelled as total fractions. The remaining part of the lysate was centrifuged at 20000 x *g* for 5 minutes, and, afterwards, 90 µl of the supernatant were transferred to new 1.5 ml tubes and labelled as soluble fractions. 30 µl of 4x SDS sample buffer (200 mM Tris-Cl (pH 6.8), 400 mM DTT, 8% SDS, 0.4% bromophenol blue, 40% glycerol) were added to each sample and boiled at 96 °C for 5 minutes. The total and soluble fractions of each sample were analyzed via either SDS-gel electrophoresis (section 2.5.9) or using the Western blot assay (section 2.5.11).

Table 2-21: Composition of *E. coli* lysis buffer

Component	Quantity
EDTA-free protease inhibitor cocktail (Sigma-Aldrich, now Merck, Steinheim)	1 tablet
DNAse I (Applichem, Darmstadt)	0.05 mg/ml
Lysozyme Sigma-Aldrich, now Merck (Steinheim))	0.5 mg/ml

Continues on the next page

Table 2-21: Composition of *E. coli* lysis buffer

Component	Quantity
Protease Inhibitor Cocktail for *E. coli* (Sigma-Aldrich, now Merck (Steinheim))	10 % (v/v)
Triton X 100 (Applichem, Darmstadt)	0.1 % (v/v)
A1 buffer (50 mM Tris-HCl, 0.3 M NaCl, 20 mM imidazole, 5% glycerol, 50 mM glycine, pH 8.0	Up to 50 ml

2.5.6 Large-scale culture, expression and extraction of HIS-tagged protein in *E. coli*

After induction via IPTG, according to the purpose of the experiment, either 4 or 8 liters of overnight cell culture of the transformed *E. coli* strain were transferred in plastic containers suitable for centrifuging after weighing and were centrifuged at 5000 x *g*, for 15 minutes at 4 °C. The cell pellet was resuspended in 2% of the initial volume of the culture, using A1 buffer (50mM Tris-HCl, 0.3M NaCl, 20mM imidazole, 5% glycerol, 50 mM glycine, pH8.0) supplemented with 1 tablet of EDTA-free protease inhibitor cocktail (Sigma-Aldrich, now Merc, Steinheim) per 2 liters of original culture and 0.1% (v/v) of polyethylenimine detergent. 0.25 grams of lysozyme were added to the pellet per each litre of original culture and the suspension was let stirring at room temperature for 20 minutes. Next, the cell suspension was sonicated in ice bath while stirring three times, for 2 minutes each. The cell extract was centrifuged at 30000 x *g* for 20 minutes at 4 °C, to remove cell debris and insoluble proteins. The supernatant was further processed to purify the protein of interest (Section 2.5.8)

2.5.7 *E. coli* large-scale culture for production of recombinant protein, labelled with Seleno-Methionine

The *E. coli* large-scale culture for production of recombinant protein, labelled with Seleno-Methionine, was carried out in M9 minimal medium (Table 2-22). First, 10 ml of an overnight culture of the *E. coli* strain of interest were added per each liter of M9 minimal medium and incubated at 37 °C, shaking at 200 rpm, until reaching an OD_{600} of 1.2. At this point, a mixture of amino acids (0.5 mg per liter, of which 10% lysine, threonine, phenylalanine, 5% of leucine, isoleucine, valine and Seleno-methionine) were added to induce a feedback inhibition. After 15 minutes, IPTG was added to the final concentration of 0.5 mM. The culture was incubated at 18 °C, shaking at 200 rpm overnight. The culture was then processed as described in section 2.5.6 to extract the protein content.

Table 2-22: Composition of M9 minimal medium per liter

Component	Final concentration
$MgSO_4$	2 mM
Glucose	0.4 % (w/v)
Vitamin mix solution	0.001% (v/v)
Trace elements solution	0.01% (v/v)

2.5.8 Protein purification using Immobilized Metal Affinity Chromatography (IMAC) combined with Size Exclusion Chromatography (SEC)

The supernatant obtained as described in section 2.5.6 was transferred to a sterile glass bottle and loaded onto a 5 mL HisTrap HP Immobilized Metal Affinity Chromatography (IMAC) column (Cytiva, USA). The column was washed with buffer A1 (Table 2-23) until the absorbance at 280 nm (A_{280}) reached 25 mAU; the proteins were then eluted with buffer B1 (Table 2-23). The obtained elution was injected onto a pre-equilibrated HiLoad Superdex 75 pg column (GE healthcare, USA) for a size exclusion chromatography (SEC) using a NGC™ Medium-Pressure Liquid Chromatography System (Biorad Laboratories, Munich). The fractions of the flow-through were collected in 24-well plates, and the ones containing the protein of interest were transferred to a 50 ml tube. The concentration of protein was measured using the Nanodrop ND-100 (PEQLAB, Erlangen) at a wavelength of 280 nm and normalized on the base of the theoretical extinction coefficient of the protein, previously calculated on the base of the protein sequence using the online software ProtParam (ExPASy, Swiss Institute of Bioinformatic). The volume of the collected fractions was reduced to less than 20 ml via centrifugation in Vivaspin 2 columns (Sartorius GmbH, Goettingen) at 4 °C, 7500 x *g*, for 15 minutes until reaching the appropriate volume. Then, dithiothreitol (DTT) was added to the final concentration of 1 mM. For enzymatic assays, the purified protein was concentrated up to 1 µg/µl, split into 200 µl aliquots and stored at -80 °C, right after snap-freezing. For crystal screening, the purified protein was further processed. In order to remove the HIS(6X) tag, for each milligram of protein purified 20 µg of human rhinovirus (HRV) 3C protease were added and the solution was incubated overnight at 4 °C. The next day, the solution was manually loaded onto a HisTrap IMAC 5 ml column (Cytiva, USA). Using an Äkta Purifier (GE healthcare, USA), the loaded protein was eluted into fractions, and those containing the protein were collected and the volume was reduced to less than 10 ml, as described above. The solution was manually loaded onto the sample pump of NGC™ Medium-Pressure Liquid Chromatography System (Biorad Laboratories, Munich), and another SEC was performed using an HiLoad Superdex 75pg column (GE healthcare, USA). Finally, the flow-through was collected

in fractions and those containing the protein of interest were transferred to a 50 ml tube. After determining the protein concentration as above described, the protein solution was concentrated up to ~30 µg/µl, aliquoted into 100 µl aliquots, snap-frozen in liquid nitrogen and stored at -80°C. At each step, 5 µg ca. of protein were transferred to a 1.5 ml tube and the samples were then boiled in SDS loading buffer and ran on an SDS-denaturing gel to check that the protein did not denature during the purification procedure.

Table 2-23: List of buffers for Protein purification using Immobilized Metal Affinity Chromatography (IMAC) combined with Size Exclusion Chromatography (SEC)

Buffer	Composition
A1	50 mM Tris-HCl pH 8.0, 0.3 M NaCl, 20 mM imidazole, 5% glycerol, 50 mM glycine
A4	20 mM HEPES, 150 mM NaCl, pH 7.5
Recharging solution	0.1 M $NiCl_2$
IMAC stripping buffer	20 mM sodium phosphate, 0.5 M NaCl, 50 mM EDTA, pH 7.4
B1	50 mM Tris-HCl pH 8.0, 0.3 M NaCl, 0.5 M imidazole, 5% glycerol, 50 mM glycine

2.5.9 Denaturing SDS-polyacrylamide gel electrophoresis (SDS-PAGE)

SDS-PAGE assay was performed according to Laemmli (1970) as discontinuous electrophoresis with 9% or 12% separating gel and 5% stacking gel (Table 2-24) with the Mini-SDS gel system from Bio-Rad (Munich). The protein extracts were resuspended with 4x SDS sample buffer (300 mM Tris-HCl pH 6.8, 50% glycine, 10% (w / v) SDS, 500 mM DTT, 0.02% (w/v) bromophenol blue) and then incubated for 5 minutes at 95 °C. Electrophoresis running buffer (50 mM Tris-HCl pH 6.8, 0.1% (w/v) SDS, 0.192 M glycine) was used to run the samples, and the PageRuler Plus Prestained Protein Ladder (Thermo Scientific, USA) served as a size standard. The separation of the proteins was carried out at a voltage of 90 V in the stacking gel and at 120 V in the separating gel. Proteins on SDS-polyacrylamide gels were either visualized by gel staining or transferred by protein transfer to a PVDF membrane through Western Blot assay (section 2.5.11).

Table 2-24: Composition of polyacrylamide gels

Stacking gel	Running gel
5% (v/v) Acrylamide-Bis	9% or 12% (v/v) Acrylamide-Bis
125mM Tris-HCl (pH 6.8)	375 mM Tris-HCl (pH 8.8)
0.1 % (v/v) TEMED	0.04 % (v/v) TEMED
0.1% (w/v) APS	0.1% (w/v) APS
0.1% (w/v) SDS	0.1% (w/v) SDS

2.5.10Polyacrylamide Gel staining

Proteins in polyacrylamide gels were visualized by placing each gel in a square plate with 35 ml of InstantBlue staining solution (Sigma-Aldrich, now Merck, Steinheim) and incubating for one hour under gentle shaking at room temperature.

2.5.11Western Blot assay

Protein transfer to a polyvinylidene difluoride membrane (PVDF, Amersham Hybond P 0.45, VWR International, Darmstadt) was performed with the Mini-PROTEAN system (Bio-Rad, Munich). First, the PVDF membrane was activated with 100% methanol for 20 seconds and consequently washed in the transfer buffer (48 mM Tris pH 9.2, 39 mM Glycine, 0.43 mM SDS, 20% (v / v) methanol). Before starting with the protein transfer, the stacked polyacrylamide gel and the membrane were coated on both sides with two pieces of Whatman Paper and enclosed between two sponges in a plastic grid. It was always ensured the lack of air bubbles between the polyacrylamide gel and the PVDF membrane to allow a complete transfer of the proteins. The transfer was carried out for 1 hour at 100 V under ice-cooling in transfer buffer (48 mM Tris pH 9.2, 39 mM Glycine, 0.43 mM SDS, 20% (v / v) methanol).

2.5.12Immunodetection

After transfer of the proteins from polyacrylamide gel to the PVDF membrane by Western Blot assay, the PVDF membrane was incubated under gentle shaking for one hour in 20 ml blocking solution (5% milk powder in 1x TBS-T buffer (20 mM Tris-HCl pH 7.6, 150 mM NaCl, 0.1% (v / v) Tween 20)). Then, the PVDF membrane was washed for five minutes with 20 ml of TBS-T buffer. The detection of diversely tagged proteins was carried out in three steps: first, the membrane was incubated in 20 ml TBS-T added with 2.5 % (w/v) of milk powder and the appropriate primary antibody (diluted according to the manufacturer's instruction) overnight at 4 °C. After washing three times for 5 minutes with 20 ml of TBS-T, the membrane was incubated in 20 ml

TBS-T added with 2.5 % (w/v) of milk powder and the appropriate secondary antibody (diluted according to the manufacturer's instruction) conjugated to Horse Radish Peroxidase (HRP) for three hours at room temperature, under gentle shaking. Finally, after washing three times for 5 minutes with 20 ml of TBS-T, the detection of the enzymatic reaction of the HRP conjugate was carried out via a luminol-based reaction of Enhanced Chemo Luminescence (ECL). SuperSignal West Femto Chemiluminescent Substrate (Thermo Scientific, USA) or Western Blot Ultra Substrate (TaKaRa, France) were used as substrate and the ImageQuant LAS 400 MINI (GE Healthcare, USA) as imaging station.

2.5.13PVDF membrane staining with either Coomassie or Ponceau S staining

The staining of PVDF membranes after protein transfer and immunodetection assays was carried out by incubation for 15 minutes of the membrane in a 5:1 solution of Coomassie staining solution (0.1% (w / v) Coomassie Brilliant Blue R-250, 45% (v / v) methanol, 10% acetic acid) and de-staining solution (5% (v / v) methanol, 9% acetic acid) under gentle shaking. Alternatively, 35 ml of Ponceau S staining solution (0.1% (w/v) Ponceau S in 5% acetic acid) were added to the membrane and let shake for 30 minutes. In either case, the membranes were then washed three times for five minutes in water and left to dry at room temperature. Afterwards, pictures were acquired via scanning.

2.5.14Plate setting for protein crystals growth

The solution containing the purified protein was concentrated up to 30 µg/µl and aliquoted. One aliquot of 100 µl was used for crystal growth per each plate setting. 1 µl of protein solution was added with 1 µl of buffer. After setting the entire plate with droplets of protein and buffer, the plates were sealed and stored at 20 °C. After seven to ten days, the plate wells were checked for crystal growth using an optical microscope.

2.5.15Thermal stability assay

According to Lo *et al.* (2004), the thermal stability assay was performed with the thermo-fluorescent dye SYPRO Orange (Thermo Scientifics, USA) to assess changes in denaturation temperature of the proteins of interest in solution with putative ligands. After the protein purification described in section 2.5.8, the purified proteins were added to several solutions with increasing amounts (25 mM to 25 nM, with a 10-fold difference) of putative ligands, such as NAD^+, 6-(5H)-phenanthridinone (6(5H)-PHE) and 3-amino benzamide (3AB). The components of each solution and the relative concentrations are listed in Table 2-25. 25 µl of each solution were used for the assay, with three technical replicates for each dilution of the ligand. The samples were pipetted into 96-wells qPCR plates, including two negative controls with the relative replicates, without either the protein or the ligand. The fluorescence values were recorded for each

0.5° C increment of temperature using the thermocycler CFX 96 (Bio-Rad, Munich) and the means value for each sample were plotted on a graphic using Microsoft Excel. As a positive control, the catalytic domain (CAT) of HsPARP1, carrying a mutation (L713F) in the regulatory Helical Domain (HD), was expressed in *E. coli* large-scale cultures, extracted and purified as described before.

Table 2-25: Composition of samples for Thermal Stability Assay

Component	Quantity per well (25µl)
Purified protein	0.01 mg/ml
SYPRO Orange (diluted 1:10 in A4 buffer)	0.33 µl
HEPES 1 M pH 7.5	1 µl
NaCl 5 M	0.75 µl
Ligand at the appropriate concentration	2 µl
ddH_2O	Up to 25 µl

2.6 Confocal microscopy on leaf discs of *N. benthamiana*

Two days post-infection, leaf discs of 4 to 5-week-old *N. benthamiana* plants were expunged and placed between two microscopy glass slides, with approximately 100 µl filtered and sterilized water. The Leica DMI6000 CS microscope was used with the Leica TCS SP5 confocal unit as attachment, to study the subcellular localization of the fluorescent-tagged proteins of interest. Green- and Yellow-Fluorescent Protein (GFP and YFP), as well as Venus fluorescent protein were excited at a wavelength of 488 nm and the fluorescent signals were collected at a wavelength of 500-525 nm for the GFP, and 525-540 nm for the YFP and Venus protein. Red-Fluorescent-Protein (RFP) was excited at a wavelength of 561 nm and the emission signal was collected at 590-640 nm. According to the specific purpose of each assay, the confocal imaging procedure was either performed using an HCX PL APO lambda blue 63.0x1.20 objective or an HCX PL APO lambda blue 20.0x0.70. For each image, the gain setting of the confocal unit was set well below the threshold of signal saturation to avoid possibly misleading background signal. The acquisition and analysis of the images were carried out using LAS AF software (Leica Microsystems CMS GmbH) and Leica X (Leica Microsystems CMS GmbH). Sequential scanning was used to avoid fluorescent signal crosstalk, due to the presence of multiple fluorescent proteins.

3 Results

3.1 The role of *A. thaliana* RCD1 N-terminus in respect to the molecular function of RCD1

Arabidopsis thaliana RADICAL-INDUCED CELL DEATH1 (RCD1) has been found to play a main role in the regulation of plant stress responses, as well as in plant development (Jaspers *et al.,* 2009; Teotia and Lamb, 2009). Due to the pleiotropic phenotype of the corresponding knockout mutant, Col-0 *rcd1-1* (Overmyer *et al.*, 2000; Jaspers *et al.*, 2009; Teotia & Lamb, 2009), RCD1 has been raising a particular interest over the years. By now, both the RST and the PARP domain of RCD1 have been structurally and functionally characterized (Tossavainen *et al.*, 2017; Bugge *et al.,* 2018; Wirthmüller *et al.,* 2018).

The least well-characterized domain of RCD1 is the WWE domain. This domain is located at the N-terminal portion of RCD1, and it was shown to be involved in protein-protein interaction with an oomycete effector and MUT9-LIKE KINASES (MLKs), later renamed PPKs, (Wirthmüller *et al.,* 2018), via mass spectrometry and Yeast-two-Hybrid assays. In this work, a biochemical characterization of the N-terminal portion of RCD1, consisting of the WWE domain and the linker region between the WWE and the PARP domains, was carried out in order to uncover its role in RCD1 activity and regulation in plants.

3.1.1 The RCD1 N-terminal domains affect localization in nuclear speckles

In order to gain further knowledge in this respect, localization studies were performed via transient expression of fluorescently tagged RCD1-GFP or a YFP-tagged mutant variant of this protein, lacking the N-terminus, including both the WWE domain and the linker region (1-265 aa), in *Nicotiana benthamiana* leaves, using confocal microscopy. As shown in **Figure 3.1**, upon transient expression in *N. benthamiana* leaves (Methods 2.5.1) of *A. thaliana* RCD1-GFP via *A. tumefaciens* infiltration, the GFP-tagged protein localized in cell nuclei in interspersed nuclear speckles. The appearance and the number of the speckles varied from nucleus to nucleus, but the compartmentalized sub-localization of RCD1 was consistent.

The same experiment was performed transiently expressing a YFP-tagged RCD1 construct lacking the N-terminus of RCD1, but presenting an additional Nuclear Localization Sequence (NLS) to ensure the protein translocation to the nucleus. In this case, the subnuclear localization in speckles was lost. Instead, RCD1-NLS-ΔNter-YFP was homogeneously distributed throughout the sampled nuclei.

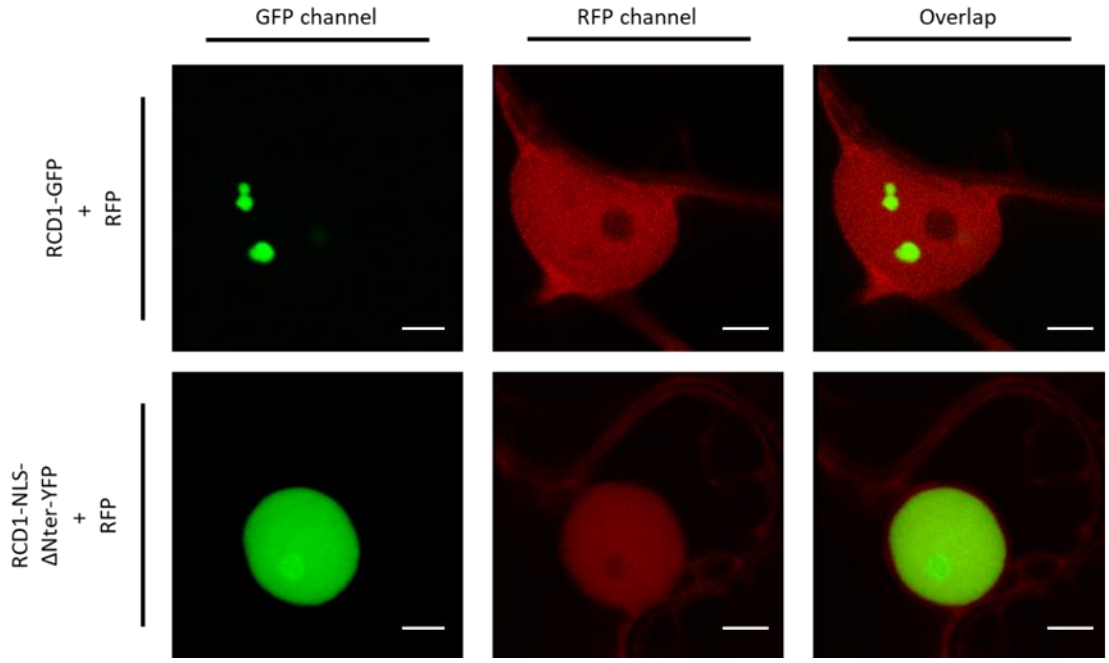

Figure 3.1: Nuclear localization of *A. thaliana* RCD1 in *N. benthamiana* leaf tissues. Two days post infiltration (dpi) with *A. tumefaciens* suspensions, leaf discs of *N. benthamiana* co-expressing under CaMV 35S promoter either AtRCD1-GFP or AtRCD1-NLSΔNter-YFP together with Red Fluorescent Protein (RFP) were excised and used for confocal microscopy assay to assess the subnuclear localization of the transiently expressed proteins. The experiment was repeated three times with similar results (20x or 63x magnification, number of imaged nuclei (n)> 10. Scale bar = 5μm).

However, RCD1-NLS-ΔNter-YFP construct lacks both the WWE (50-180 aa) domain and the linker region between the WWE and the PARP domain (180-265 aa). Hence, in order to narrow down the exact region or domain needed for RCD1 subnuclear localization in speckles, different mutated constructs of RCD1, tagged with a triple Venus tag (-3V), were tested for their localization. These constructs were created by Professor Dr. Jaakko Kangasjärvi and his team (University of Helsinki), with whom a collaboration was established. Each construct either lacks the WWE domain (RCD1-ΔWWE-3V) or the PARP domain (RCD1-ΔPARP-3V). As a positive control, the full-length version of RCD1 tagged with the same fluorescent tag (RCD1-3V) was used for the confocal microscopy assay.

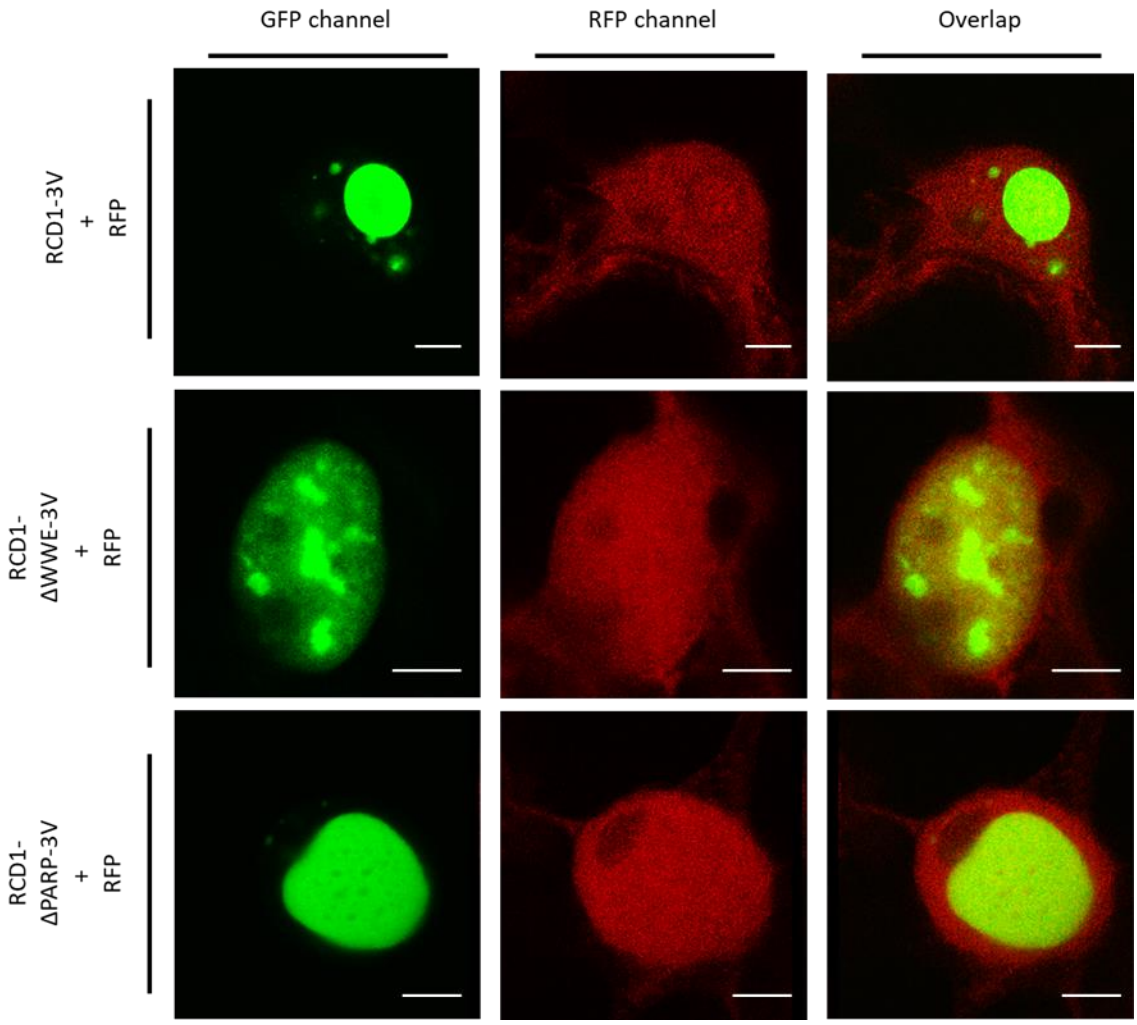

Figure 3.2: Nuclear localization of *A. thaliana* RCD1 constructs with a triple Venus tag (3V) in *N. benthamiana* leaf tissues. Two days post infiltration (dpi) with *A. tumefaciens* suspensions, leaf discs of *N. benthamiana* co-expressing under CaMV 35S promoter either AtRCD1-3V, AtRCD1-ΔWWE-3V or AtRCD1-ΔPARP-3V together with Red Fluorescent Protein (RFP) were excised and used for confocal microscopy assay to assess the subnuclear localization of the transiently expressed proteins. The expression vectors pBm43GW-cRCD1-3V, pBm43GW-cRCD1ΔWWE-3V and pBm43GW- cRCD1ΔPARP-3V are courtesy of Prof. Dr. Kangasjärvi and his team. The experiment was repeated three times with similar results (63x magnification, (n)> 7. Scale bar = 5µm).

As shown in **Figure 3.2** the localization in nuclear speckles of wild type RCD1 remains unchanged, despite the different and bulkier fluorescent tag. In the nuclei where RCD1-ΔWWE-3V was transiently expressed, the 3V fluorescent signal was interspersed throughout the nucleus. However, the presence of protein conglomerates was not totally abolished, although those did not present a defined shape in comparison with the typical nuclear speckles in which RCD1 localizes. The results of the confocal microscopy

analysis of *N. benthamiana* nuclei transiently expressing the RCD1-ΔPARP-3V construct were more heterogeneous. In the sampled nuclei, the tagged protein localized in one or two conspicuous agglomerates inside the nuclei, with occasionally peripherical punctiform speckles, much less noticeable.

3.1.2 Role of WWE domain of RCD1 as a protein-protein interaction domain

The WWE domain of RCD1 was first identified in 2001 when its sequence and putative structure were analysed through a bioinformatics study by Aravind (Arvind, 2001) and its role in protein-protein interaction was proposed by Ahlfors *et al.*, in 2004. However, only recently its protein-binding activity was tested in Yeast-two-Hybrid assay, as well as in co-immunoprecipitation assay (Co-IP) coupled to mass spectrometry (MS), both in *N. benthamiana* and in *A. thaliana*, to identify its possible interactors (Wirthmüller *et al.,* 2018). Amongst these identified interactors, other than RCD1 itself and its closest homologue, AtSRO1, the PHOTOREGULATORY PROTEIN KINASES (PPKs) were identified, formerly named MUT9-LIKE KINASES (MLKs).

The interaction between RCD1 and the above-mentioned kinases was further studied in this work. First of all, the *in vivo* localization of PPK1, PPK3 and PPK4, tagged with Red Fluorescent Protein (RFP), in transient expression in *N. benthamiana* leaves was tested using confocal microscopy. As shown in **Figure 3.3,** all the three kinases are mostly interspersed in the nuclei in an even manner.

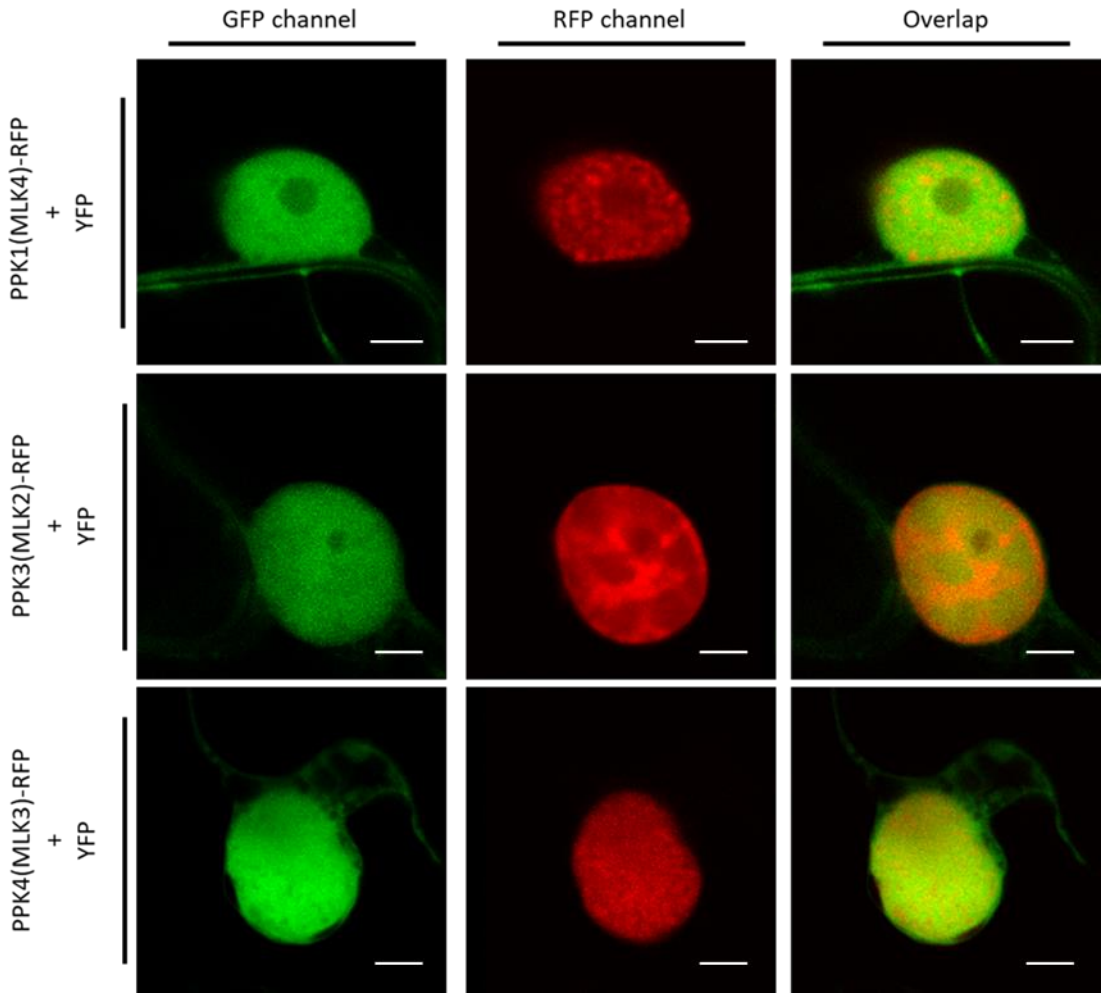

Figure 3.3: Nuclear localization of *A. thaliana* PPK1 (MLK4), PPK3 (MLK2) and PPK4(MLK3) in *N. benthamiana* leaf tissues. Two days post infiltration (dpi) with *A. tumefaciens* suspensions, leaf discs of *N. benthamiana* co-expressing under CaMV 35S promoter either AtPPK1-RFP, AtPPK3-RFP or AtPPK4-RFP together with Yellow Fluorescent Protein (YFP) were excised and used for confocal microscopy assay to assess the subnuclear localization of the transiently expressed proteins. The experiment was repeated three times with similar results (63x magnification, (n)> 7. Scale bar = 5µm).

In contrast, when RCD1-GFP was transiently co-expressed together with either PPK1-RFP, PPK3-RFP or PPK4-RFP, the fluorescent signal coming from the PPK kinases concentrated in the same subnuclear speckles where the RCD1-GFP was localized, as shown in **Figure 3.4**.

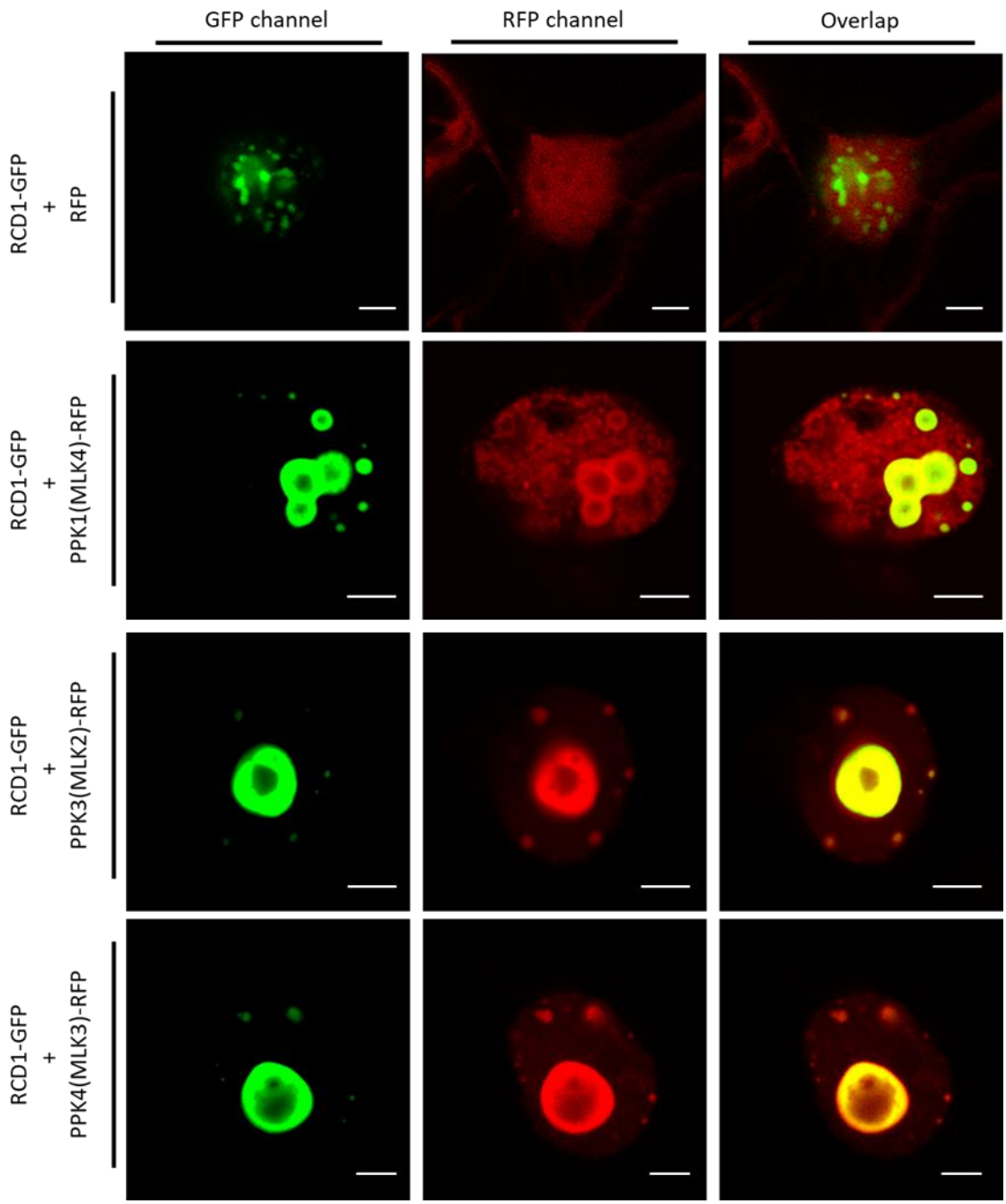

Figure 3.4: Nuclear co-localization of *A. thaliana* RCD1 and PPK1, PPK3 and PPK4 in *N. benthamiana* leaf tissues. Two days post infiltration (dpi) with *A. tumefaciens* suspensions, leaf discs of *N. benthamiana* co-expressing under CaMV 35S promoter *A. thaliana* RCD1-GFP together with either AtPPK1-RFP, AtPPK3-RFP or AtPPK4-RFP were excised and used for confocal microscopy assay to assess the subnuclear localization of the transiently expressed proteins. As a control, the subnuclear localization of AtRCD1-GFP and RFP was tested. The experiment was repeated three times with similar results (63x magnification, n> 7. Scale bar = 5µm).

To gather additional supporting evidence of the interaction between RCD1 and the above mentioned PPKs, transient co-expression of RCD1-GFP with each of the three PPK (PPK1, PPK3 and PPK4), carrying a triple HA- tag, was induced upon infiltration of *N. benthamiana* leaves with *A. tumefaciens* transformed strains, carrying the constructs of interest. After protein extraction and co-immunoprecipitation assay, the results of the immunoblotting clearly confirmed the *in vivo* interaction between RCD1 and PPK1, PPK3 and PPK4 (**Figure 3.5**).

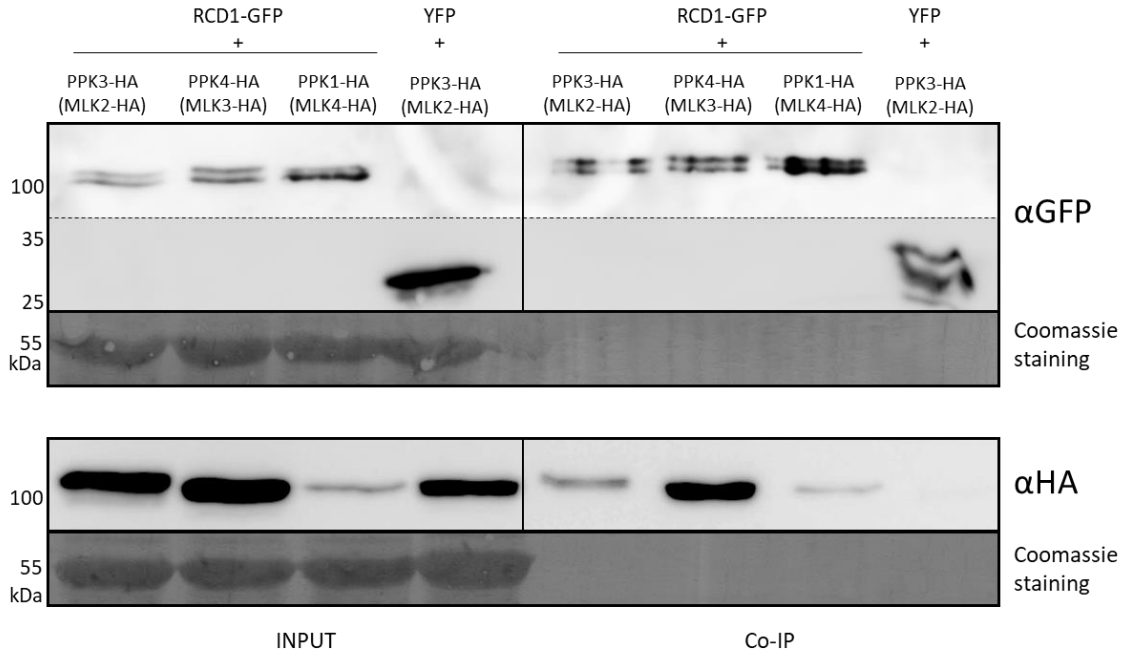

Figure 3.5: Co-immunoprecipitation of *A. thaliana* PPK1, PPK3 and PPK4 with RCD1. Two days post infiltration (dpi) with *A. tumefaciens* suspensions, leaf samples of *N.benthamiana* transiently co-expressing under CaMV 35S promoter *A. thaliana* RCD1-GFP together with either AtPPK1-HA, AtPPK3-HA or AtPPK4-HA were collected, and a protein extraction assay was performed on the samples. αGFP-nanobody-tagged magnetic beads were added to half of each protein extract to perform a Co-Immunoprecipitation (CoIP) of GFP-tagged RCD1 and its interactors. Immunoprecipitated and co-purified proteins were detected *via* Immunoblotting with αGFP and αHA antibodies. A leaf sample co-expressing YFP and AtPPK3-3HA was processed in the same way and used as a negative control. Coomassie staining of the membranes served as the loading control. This experiment was repeated three times.

The same experiment was performed using a GFP-tagged truncated version of RCD1, consisting of the RCD1 N-terminus (1-265 aa), as bait for the αGFP nanobodies-tagged beads, which pulled down the GFP-tagged protein together with its interactors. In **Figure 3.6**, the results of the immunoblot assay on CoIP-ed samples show how the N-terminus of RCD1 is sufficient for the interaction between RCD1 and PPK1, PPK3 and PPK4.

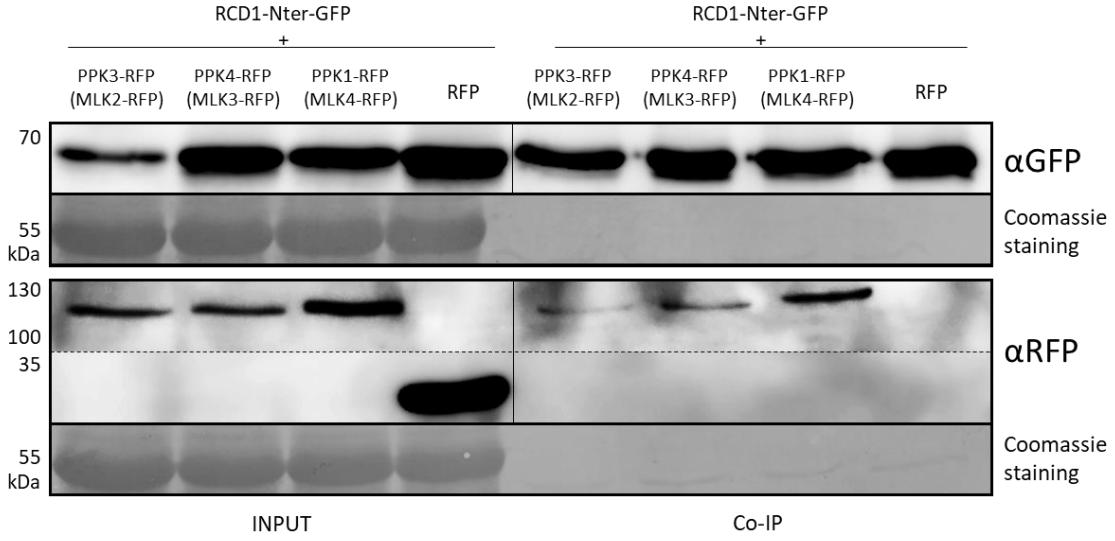

Figure 3.6: Co-immunoprecipitation of *A. thaliana* PPK1, PPK3 and PPK4 with RCD1 N-terminus (1-265 aa). Two days post infiltration (dpi) with *A. tumefaciens* suspensions, leaf samples of *N. benthamiana* transiently co-expressing under CaMV 35S promoter *A. thaliana* RCD1-Nter-GFP together with either AtPPK1-RFP, AtPPK3-RFP or AtPPK4-RFP, were collected, and a protein extraction assay was performed on the samples. αGFP-nanobody-tagged magnetic beads were added to half of each protein extract to perform a Co-Immunoprecipitation (CoIP) of GFP-tagged RCD1-Nter and its interactors. Immunoprecipitated and co-purified proteins were detected *via* Immunoblotting with αGFP and αRFP antibodies. A leaf sample co-expressing AtRCD1-Nter-GFP and Red Fluorescent Protein (RFP) was processed in the same way and used as a negative control. Coomassie staining of the membranes served as loading control. This experiment was repeated three times.

3.1.3 The role of WWE domain in subnuclear co-localization of RCD1 with PPK1, PPK3 and PPK4

Being the N-terminus of *A. thaliana* RCD1, including the WWE domain and the linker region, sufficient to ensure the interaction between RCD1 and the abovementioned PPK kinases, it was sensible also to test whether and how the absence of the N-terminal region of RCD1 would affect the subnuclear localization of PPK1, PPK3 and PPK4.

In **Figure 3.7**, it is shown that PPK1-, PPK3- and PPK4-RFP, transiently co-expressed with YFP-tagged RCD1-NLS-ΔN-terminus in *N. benthamiana* leaf tissues appear to be evenly interspersed in the imaged nuclei, in a similar way as when they were co-expressed with free YFP (**Figure 3.3**).

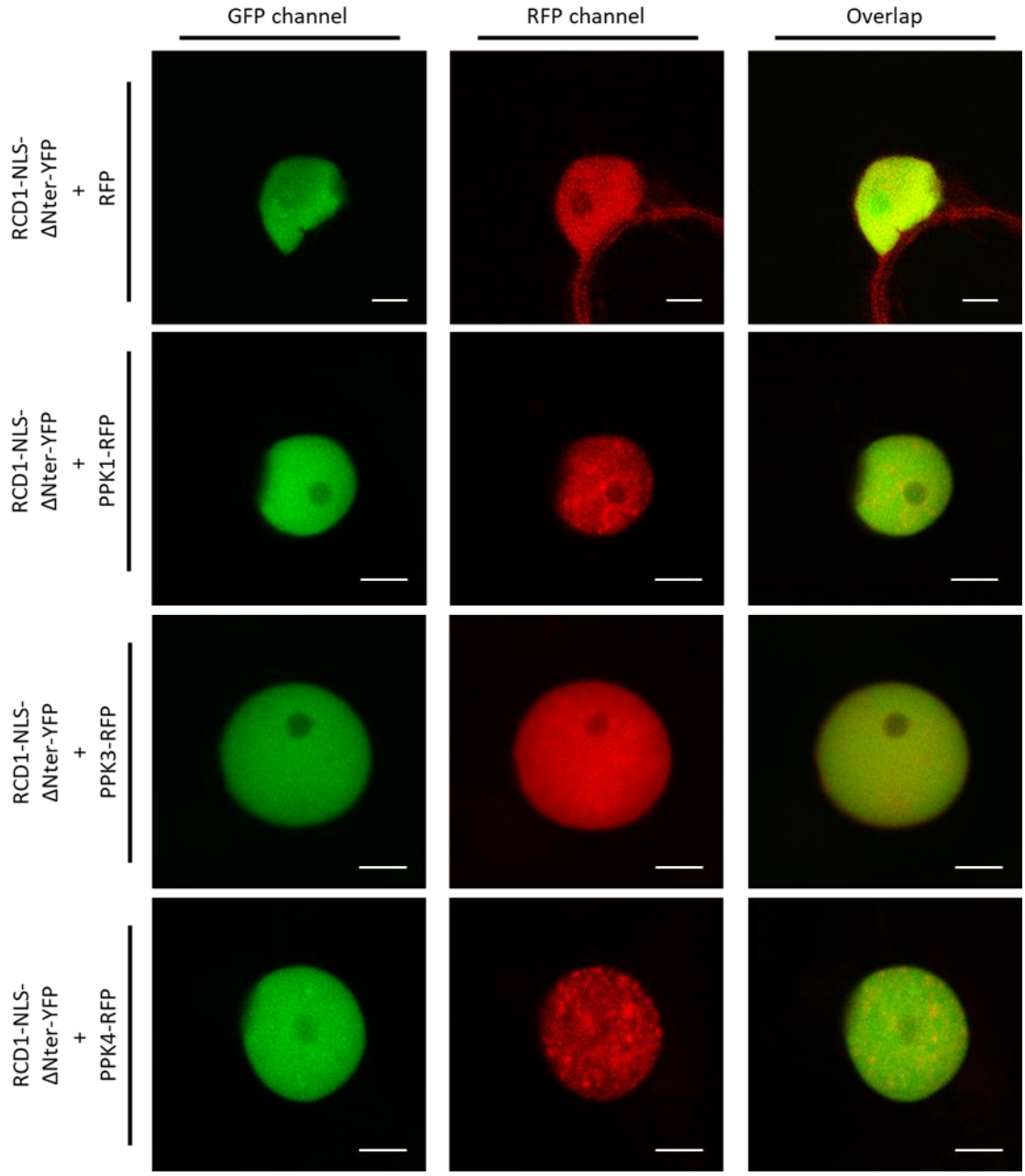

Figure 3.7: Nuclear co-localization of *A. thaliana* RCD1ΔNter-YFP and PPK1-RFP, PPK3-RFP and PPK4-RFP in *N. benthamiana* leaf tissues. Two days post infiltration (dpi) with *A. tumefaciens* suspensions, leaf discs of *N. benthamiana* co-expressing under CaMV 35S promoter *A. thaliana* RCD1-NLS-ΔNter-YFP together with either AtPPK1-RFP, AtPPK3-RFP or AtPPK4-RFP were excised and used for confocal microscopy assay to assess the subnuclear localization of the transiently expressed proteins. As a control, the subnuclear localization of AtRCD1-NLS-ΔNter-YFP and RFP was tested. The experiment was repeated three times with similar results (63x magnification, n> 7. Scale bar = 5µm).

These findings led to wonder whether it was the lack of WWE domain rather than the lack of the entire N-terminus of RCD1 to produce a differential sub-nuclear co-localization of the PPKs kinases with the RCD1-NLS-ΔN-terminus construct. To test this hypothesis, the co-localization assay via confocal microscopy was repeated, transiently expressing RFP-tagged PPK-1, PPK3 and PPK4 together with two different RCD1-3V constructs, either lacking the WWE domain (90-151 aa) or the PARP domain (304-442 aa).

In **Figure 3.8,** it is shown that while PPK1-RFP co-localizes with wild type RCD1-3V in the aforementioned subnuclear speckles, this co-localization was lost when either the WWE domain or the PARP domain were lacking. Hence, the signal from PPK1-RFP was found to be evenly distributed throughout the nucleus, although the localization of RCD1ΔWWE-3V and RCD1ΔPARP-3V appear to be differentially localized in the sampled nuclei.

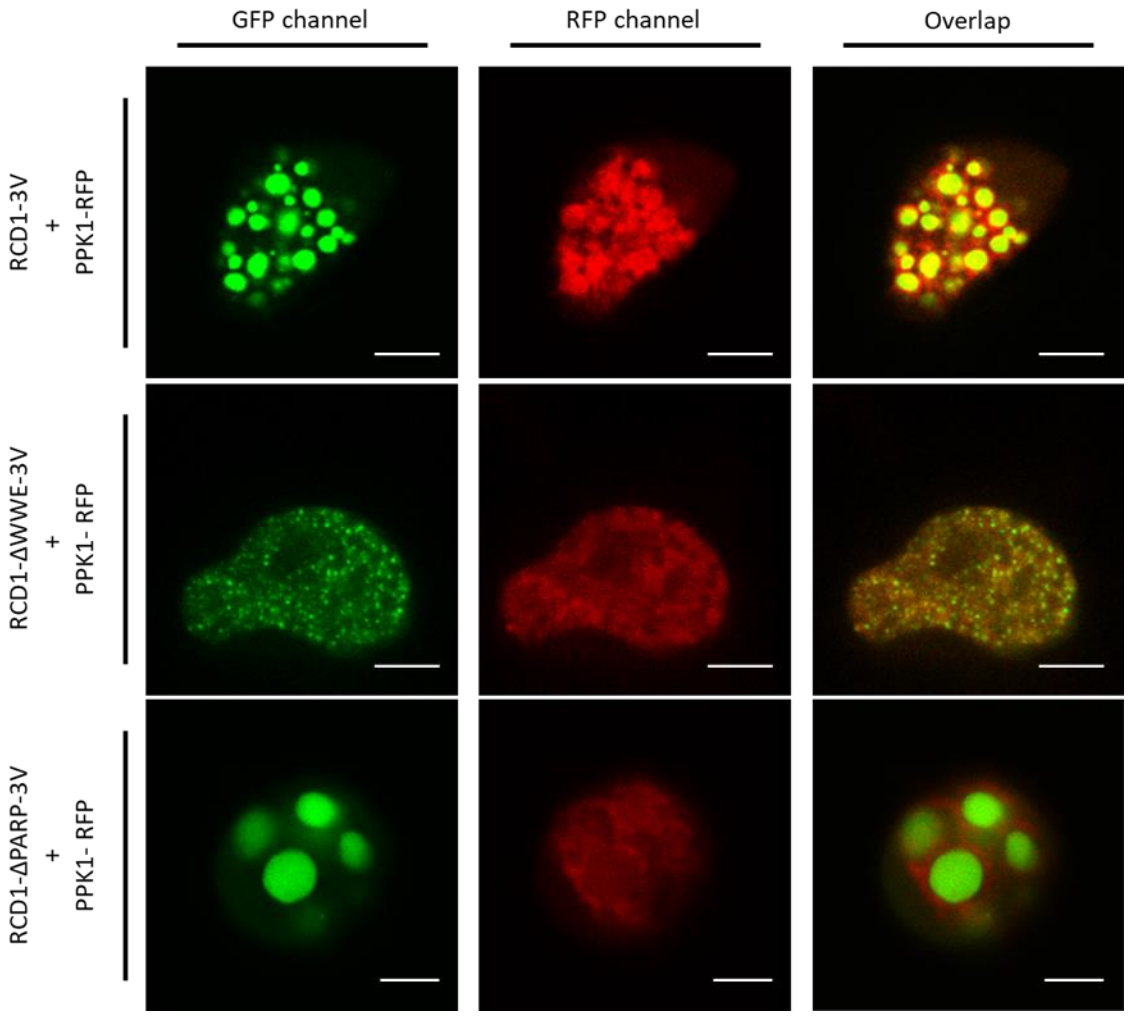

Figure 3.8: Nuclear co-localization of *A. thaliana* PPK1-RFP with RCD1-3V, RCD1-ΔWWE-3V and RCD1-ΔPARP-3V in *N. benthamiana* leaf tissues. Two days post infiltration (dpi) with *A. tumefaciens* suspensions, leaf discs of *N. benthamiana* co-expressing under CaMV 35S promoter *A. thaliana* PPK1-RFP together with either AtRCD1-3V, AtRCD1ΔWWE-3V or AtRCD1ΔPARP-3V were excised and used for confocal microscopy assay to assess the subnuclear localization of the transiently expressed proteins. The expression vectors pBm43GW-cRCD1-3V, pBm43GW-cRCD1ΔWWE-3V and pBm43GW- cRCD1ΔPARP-3V are courtesy of Prof. Dr. Kangasjärvi and his team. The experiment was repeated three times with similar results (63x magnification, n> 7. Scale bar = 5µm).

The same assay was performed using PPK3-RFP and PPK4-RFP in order to assess whether the variations in the subnuclear localization of PPK1 when co-expressed with RCD1-ΔWWE-3V and RCD1-ΔPARP-3V were observable also with these other two PPKs. Interestingly, neither the lack of the WWE domain (90-151 aa) nor the PARP domain (304-442 aa) disrupted the co-localization of fluorescent signal deriving from PPK3-RFP. As shown in **Figure 3.9**, although the truncated RCD1 constructs differed

from the full-length protein in the subnuclear localization, which appear less structured, causing the diffusion of signal deriving from the triple Venus tag throughout the nuclei and not in the characteristic speckles, the co-localization together with PPK3 was not abolished.

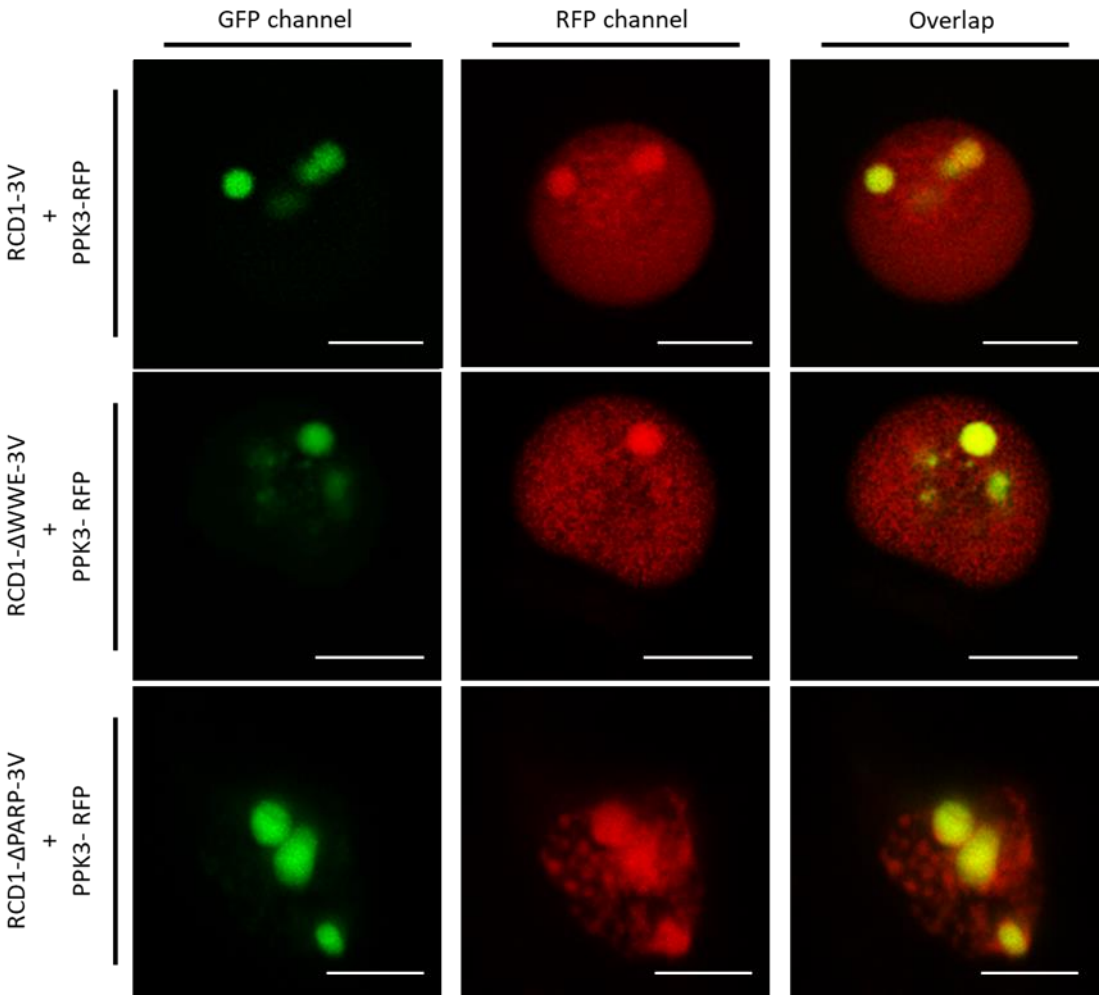

Figure 3.9: Nuclear co-localization of *A. thaliana* PPK3-RFP with RCD1-3V, RCD1ΔWWE-3V and RCD1ΔPARP-3V in *N. benthamiana* leaf tissues. Two days post infiltration (dpi) with *A. tumefaciens* suspensions, leaf discs of *N. benthamiana* co-expressing under CaMV 35S promoter *A. thaliana* PPK3-RFP together with either AtRCD1-3V, AtRCD1ΔWWE-3V or AtRCD1ΔPARP-3V were excised and used for confocal microscopy assay to assess the subnuclear localization of the transiently expressed proteins. The expression vectors pBm43GW-cRCD1-3V, pBm43GW-cRCD1ΔWWE-3V, and pBm43GW- cRCD1ΔPARP-3V are courtesy of Prof. Dr. Kangasjärvi and his team. The experiment was repeated three times with similar results (63x magnification, n> 7. Scale bar = 5µm).

Figure 3.10 shows the exemplifying results obtained by performing the same assay to test possible variation of subnuclear localization of PPK4, as a consequence of the abovementioned deletions along RCD1 sequence (ΔWWE and ΔPARP). In this case, the co-localization of PPK4 with RCD1 appeared to be affected by the deletion of the WWE domain, whereas it was overall unaltered when the PARP domain was missing.

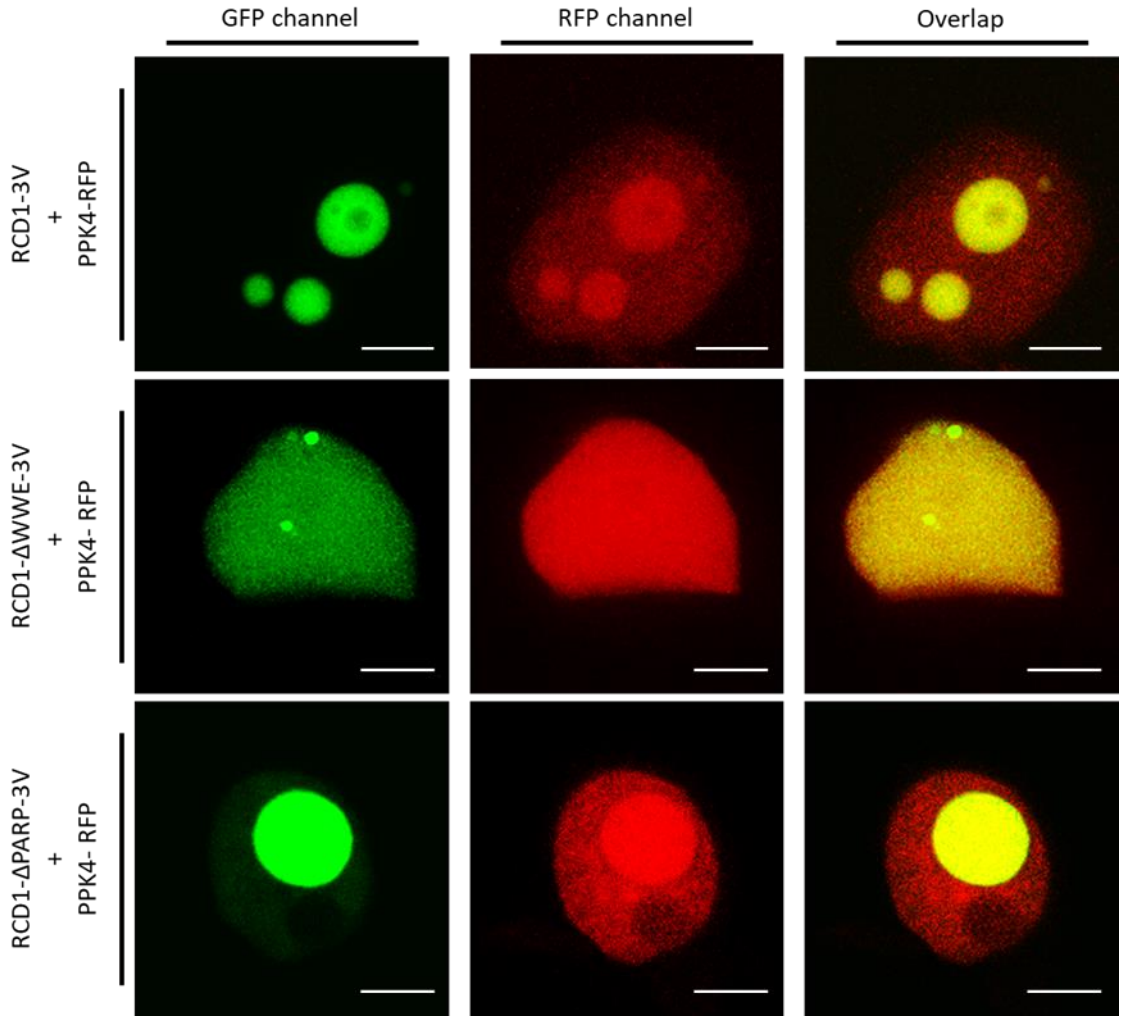

Figure 3.10: Nuclear co-localization of *A. thaliana* PPK4-RFP with RCD1-3V, RCD1ΔWWE-3V and RCD1ΔPARP-3V in *N. benthamiana* leaf tissues. Two days post infiltration (dpi) with *A. tumefaciens* suspensions, leaf discs of *N. benthamiana* co-expressing under CaMV 35S promoter *A. thaliana* PPK4-RFP together with either AtRCD1-3V, AtRCD1ΔWWE-3V or AtRCD1ΔPARP-3V were excised and used for confocal microscopy assay to assess the subnuclear localization of the transiently expressed proteins. The expression vectors pBm43GW-cRCD1-3V, pBm43GW-cRCD1ΔWWE-3V, and pBm43GW- cRCD1ΔPARP-3V are courtesy of Prof. Dr. Kangasjärvi and his team. The experiment was repeated three times with similar results (63x magnification, n> 7. Scale bar = 5µm).

3.1.4 The WWE domain is involved in the oligomerization process of RCD1 and its closest homologue AtSRO1

The involvement of WWE domain in RCD1 as a domain mediating the protein-protein interaction has been hypothesized (Aravind, 2001) and tested in Yeast-two-Hybrid (Y2H) and with LC-MS assay (Wirthmüller *et al.*, 2018). In this work, these results were tested and confirmed in plant *ex vivo* with Co-ImmunoPrecipitation (CoIP) assay (see Methods 2.5.4)**.** Furthermore, some of the results presented in Wirthmüller *et al*. (2018) suggested that the N-terminus of RCD1 and of its closest homologue in *A. thaliana*, SRO1, both consisting of a WWE domain and a linker region, were involved in the hetero-oligomerization of RCD1 and SRO1. This oligomerization, previously tested with Yeast-two-Hybrid (Y2H) and mass spectrometry (MS) assays, was tested and confirmed in this work, using a co-immunoprecipitation (Co-IP) assay on protein extract of *N. benthamiana* leaves transiently expressing the constructs of interest. As shown in **Figure 3.11**, HA-tagged RCD1 co-immunoprecipitated both with the GFP-tagged version of the full-length RCD1 as well as with its GFP-tagged truncated version, consisting of the N-terminus. However, RCD1-HA did not co-immunoprecipitate with the free YFP nor with the truncated construct of RCD1, lacking the N-terminus. Although at high exposure with ultra-sensitive reagent, a faint band seldom would also appear in the anti-HA immunoblot for the immuno-precipitate fraction of this last RCD1 truncated construct, this could have been due to a marginal spill-over of the sample in the adjacent well. The same samples were loaded in the same order on two different 9% polyacrylamide gels and transferred via Western Blot to different PVDF membranes, in order to avoid cross-contamination of signals during detection, being the proteins of interest in a tight range of molecular weight.

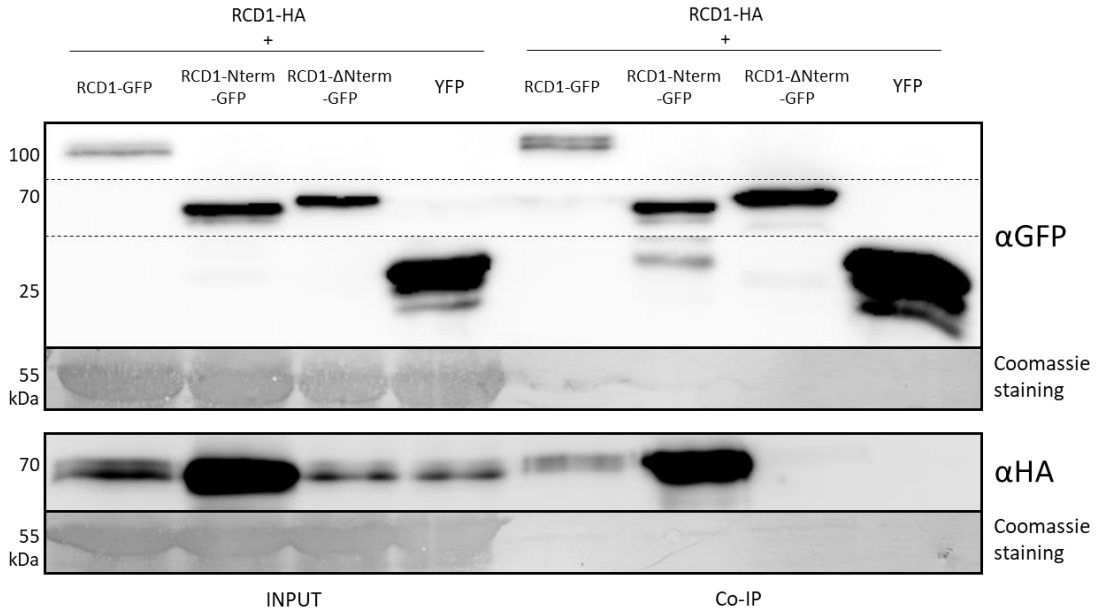

Figure 3.11: Oligomerization of *A. thaliana* RCD1 is mediated by its N-terminal region (1-265 aa).Two days post infiltration (dpi) with *A. tumefaciens* suspensions, leaf samples of *N. benthamiana* transiently co-expressing under CaMV 35S promoter *A. thaliana* RCD1-HA together with either AtRCD1-GFP, AtRCD1-Nterm-GFP or AtRCD1-NLS-ΔNter-YFP, were collected and a protein extraction assay was performed on the samples. αGFP-nanobody-tagged magnetic beads were added to half of each protein extract to perform a Co-Immunoprecipitation (Co-IP) of GFP- or YFP-tagged RCD1variants and their interactors. Immunoprecipitated and co-purified proteins were detected *via* Immunoblotting with αGFP and αHA antibodies. A leaf sample co-expressing AtRCD1-HA and Yellow Fluorescent Protein (YFP) was processed in the same way and used as a negative control. Coomassie staining of the membranes served as the loading control. This experiment was repeated three times.

Performing the same assay with the respective full-length and truncated versions of SRO1 showed that the primary importance of the N-terminus of SRO1 in the process of its oligomerization was analogous to the aforementioned findings on RCD1 N-terminus. In fact, as shown in **Figure 3.12**, the N-terminal region (1-262 aa) of SRO1 is sufficient to ensure the interaction with the full-length protein and, hence, to allow the protein to oligomerize with itself.

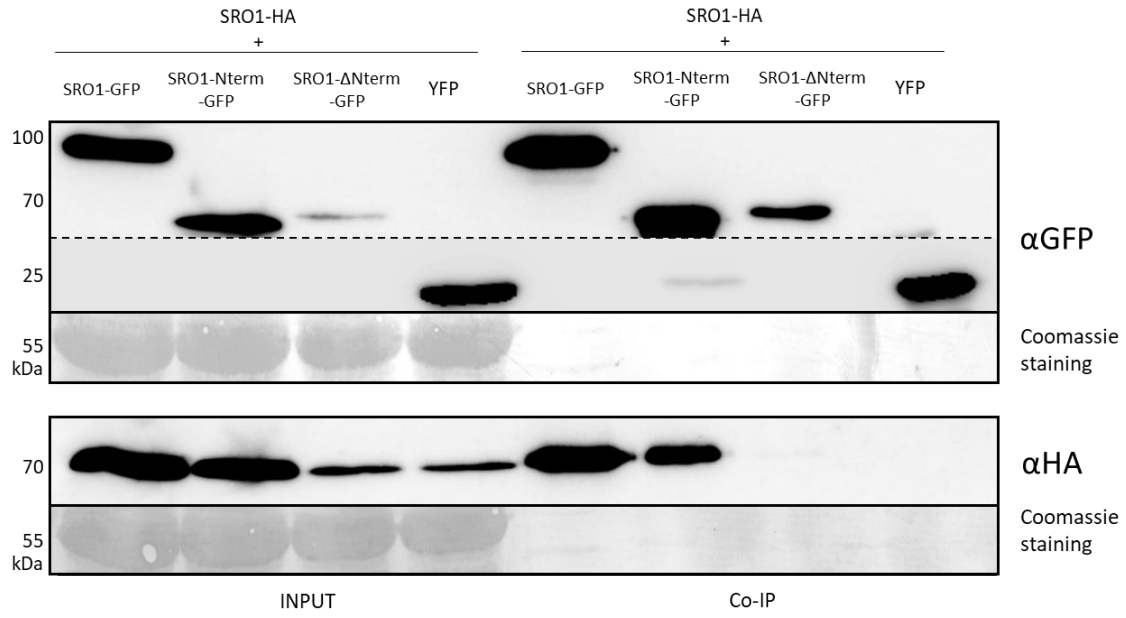

Figure 3.12: Oligomerization of *A. thaliana* SRO1 is mediated by its N-terminal region (1-262 aa). Two days post infiltration (dpi) with *A. tumefaciens* suspensions, leaf samples of *N. benthamiana* transiently co-expressing under CaMV 35S promoter *A. thaliana* SRO1-HA together with either AtSRO1-GFP, AtSRO1-Nterm-GFP or AtSRO1-NLS-ΔNter-YFP, were collected, and a protein extraction assay was performed on the samples. αGFP-nanobody-tagged magnetic beads were added to half of each protein extract to perform a Co-Immunoprecipitation (Co-IP) of GFP- or YFP-tagged SRO1 variants and their interactors. Immunoprecipitated and co-purified proteins were detected *via* Immunoblotting with αGFP and αHA antibodies. A leaf sample co-expressing AtSRO1-HA and Yellow Fluorescent Protein (YFP) was processed in the same way and used as a negative control. Coomassie staining of the membranes served as loading control. This experiment was repeated three times.

3.1.5 The role of WWE domain in PAR chain binding *in vivo*

When first described by Aravind in 2001, the WWE domain in eukaryotes was hypothesized to function as a protein "reader", amongst its other possible features. This "reader" function of the WWE domain would determine the recognition of specific sequences on target proteins and consequently the addition of post-translational modifications, e.g. PARylation or ubiquitination, to be attached to the recognized proteins (Aravind, 2001). Another function of the WWE domain that has been demonstrated in *H. sapiens* (Zhou *et al.,* 2011; Wang *et al.,* 2012) is its role in the binding of iso-Poly-(ADP-ribose) (iso-PAR) moieties. However, in plants, there was no evidence that such function of the WWE domain is conserved. To test this hypothesis, two different RFP-tagged constructs of the RCD1 N-terminus, both including the WWE domain, but differing for the presence of the linker region, were transiently co-express in *N. benthamiana* leaf tissue together with *A. thaliana* PARP2, a poly(ADP-ribosyl)polymerase, that in the presence of NAD^+ is able to catalyse a reaction producing PAR chains attached to itself (auto-PARylation)(Feng *et al.*, 2015). In this work, it was tested whether one or both of the RCD1 N-terminal constructs comprising the WWE domain were able to bind PAR chains produced by GFP-tagged PARP2 *in vivo*. This would have determined the co-immunoprecipitation of the PAR-binding RCD1 constructs together with auto-PARylated PARP2, using αGFP-nanobodies attached to magnetic beads. The production of PAR chains was promoted in half of the samples through the addition of NAD^+ (0.3 mM), and, as a control, the PAR-binding WWE domain of HsRNF146 was used.

Interestingly, as shown in **Figure 3.13,** the shorter truncated version of RCD1 N-terminus (1-203 aa) was co-immunoprecipitated together with PARP2-GFP independently of the addition of NAD^+ and, hence, of the presence of PAR-chains, whereas the longer version of RCD1 N-terminus (1-265 aa) did not. As a control, the RFP-tagged version of the WWE domain of HsRNF146 co-immunoprecipitated together with PARP2-GFP only in the presence of PAR chains attached to the latter. It is worth noting that in one of the replicates, the longer version of the RCD1 N-terminus (1-265aa) was CoIP-ed along with PARP2. This result was not considered contrasting the previously stated findings due to the fact that the linker region (around 200^{th} to 265^{th} aa) does not present a well-defined secondary structure. Hence, it could be hypothesized that this region, in different spatial dispositions and maybe due to different post-translational modifications, could possibly represent an obstacle to the binding of PARP2 by the WWE region (1-203 aa).

Altogether, the result of this assay seems to suggest that the first two-hundred and three amino acids at the N-terminus of RCD1, including the WWE domain, are involved in the binding of PARP2, hence confirming the protein-protein interaction feature of this

region of RCD1, but without providing a clear indication of whether the PAR chain binding function is conserved in the WWE domain of RCD1.

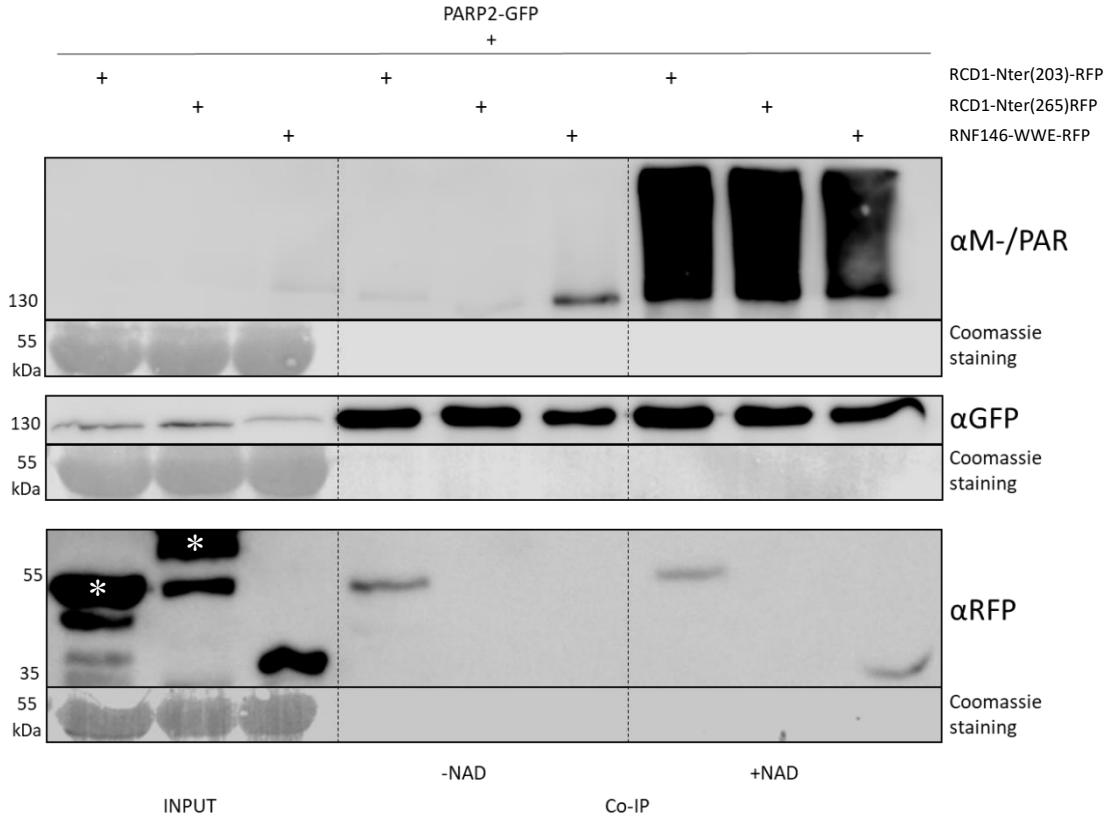

Figure 3.13: *A. thaliana* RCD1 binds to PARP2 irrespectively of the presence of Poly-(ADP-ribose) (PAR) chains. Two days post infiltration (dpi) with *A. tumefaciens* suspensions, leaf samples of *N. benthamiana* transiently co-expressing under CaMV 35S promoter *A. thaliana* PARP2-GFP together with either AtRCD1-Nter(203)-RFP, AtRCD1-Nter(265)-RFP or HsRNF146-WWE-RFP were collected, and a protein extraction assay was performed. Co-Immunoprecipitation (Co-IP) of GFP -tagged PARP2 and its interactors was performed by adding αGFP-nanobody-tagged magnetic beads. Each sample used for the Co-IP assay was split into two reaction tubes, and one half of each sample was added with NAD^+ to a concentration of 0.3 mM to allow PAR chain polymerization by PARP2 auto-PARylation. Immunoprecipitated and co-purified proteins were detected *via* Immunoblotting with αGFP and αRFP antibodies, while PAR chain formation was assessed using antibodies against Mono- and Poly(ADP-ribose) moieties (αM-/PAR). All the samples were loaded on three different gels and transferred to three membranes in the same order to avoid cross-contamination of signals during Immunoblotting detection. Coomassie staining of the membranes was used to assess the even loading of the samples. The asterisks on the bands distinguish the specific signal of proteins of interest from unspecific bands in the same lane (n=3 biological replicates).

3.1.6 The role of phosphorylation of the RCD1 N-terminus in respect to its molecular function

Due to the evidence displayed in the previous paragraphs of this work and in Wirthmüller *et al.* (2018), the role of the N-terminal region of RCD1in respect to the functioning of this protein became even more evident, and for this reason, it was further investigated. In pursuit of understanding the functioning and activating mechanisms of RCD1, the attention was focused on several phospho-peptides of RCD1 that were identified in previous mass spectroscopy screenings (Wirthmüller *et al.,* 2018) (**Figure 3.14**).

MVSKGEELFTGVVPILVELDGDVNGHKFSVSGEGEGDATYGKLTLKFICTTGKLPVPWPTLVTTLTYGVQCFSRYP
DHMKQHDFFKSAMPEGYVQERTIFFKDDGNYKTRAEVKFEGDTLVNRIELKGIDFKEDGNILGHKLEYNYNSHN
VYIMADKQKNGIKVNFKIRHNIEDGSVQLADHYQQNTPIGDGPVLLPDNHYLSTQSALSKDPNEKRDHMVLLE
FVTAAGITLGMDELYKDITSLYKKAGSAAAPFTMEAKIVKVLDSSRCEDGFGKKRKRAASYAAYVTGVSCAKLQNV
PPPNGQCQIPDKRRRLEGENKLSAYENRSGKALVRYYTYFKKTGIAKRVMMYENGEWNDLPEHVICAIQNELEE
KSAAIEFKLCGHSFILDFLHMQRLDMETGAKTPLAWIDNAGKCFFPEIYESDERTNYCHHKCVEDPKQNAPHDIK
LRLEIDVNGGETPRLNLEECSDESGDNMMDDVPLAQRSSNEHYDEATEDSCSRKLEAAVSKWDETDAIVVSGA

Figure 3.14: Phospho-peptides identified in the *A. thaliana* RCD1 GFP:WWE-linker fusion protein. The sequence of AtRCD1 WWE-linker truncated protein is indicated in yellow and phospho-peptides are shown in red (adapted from Wirthmüller *et al.,* 2018).

These phospho-peptides were analysed in this work and some potentially interesting phospho-sites were identified throughout the N-terminus of RCD1 (1-265 aa). In particular, eleven residues, either Serines (Ser) or Threonines (Thr), were taken into account: S27, T33, S36, T204, S230, S231, T239, S242, S244, T257, S263. In order to investigate whether these potentially phosphorylated residues played a role in the *in vivo* functioning mechanism of RCD1, the selected Serine and Threonine amino acids were mutated into either Aspartate (Asp) or Alanine (Ala), hence mimicking the presence (Asp) or the lack (Ala) of post-translational phosphorylation. To further narrow down the functionally relevant sites, or at least the portion of the N-terminus of RCD1, possibly carrying these modifications, four different constructs were synthetized by BioCat GmbH (Heidelberg, Germany), encoding four different mutated versions of the N-terminal portion of RCD1 (1-265 aa). In detail, two of these constructs carried four mutated residues towards the N-terminus (S27, T33, S36, T204); these residues were substituted either with Aspartate (Asp) or with Alanine (Ala) amino acids. Hence, these two constructs were named RCD1_N-ter_ND, because of the position of the residues along RCD1 N-terminus (N) mutated to Aspartate (D), and RCD1_N-ter_NA,

because of the position of the residues along RCD1 N-terminus (N) mutated to Alanine (A) (**Figure 3.15**).

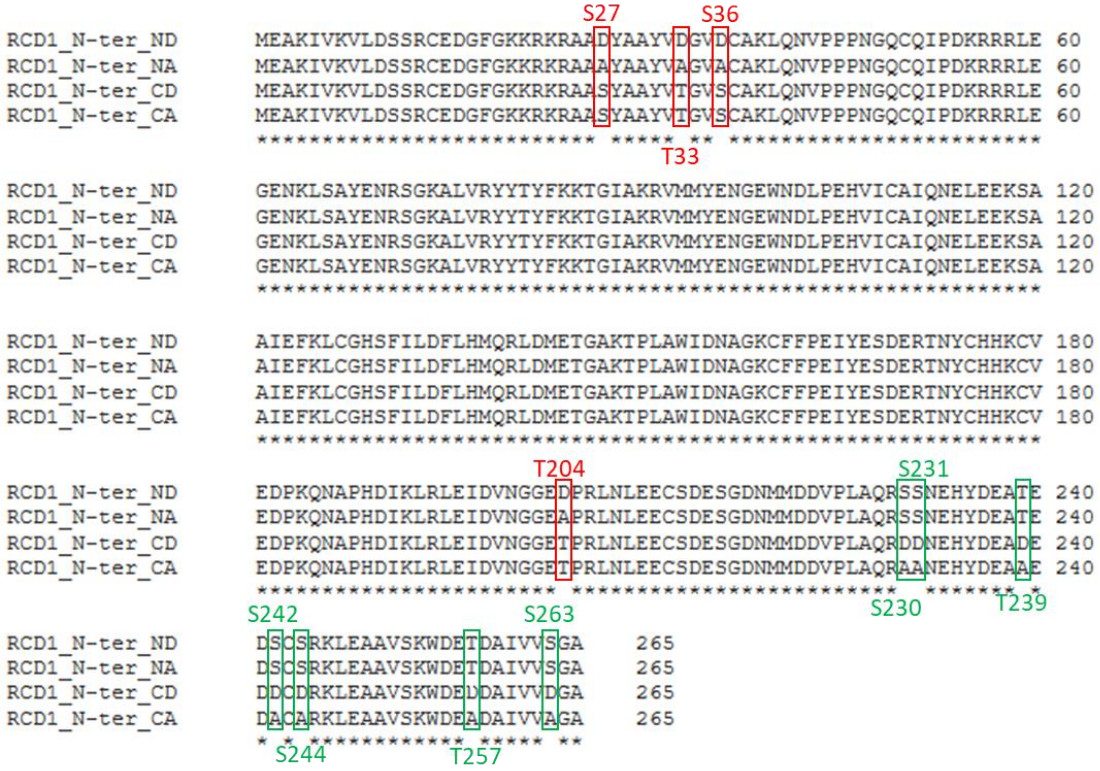

Figure 3.15: Multiple alignment of the sequences of four mutated constructs of *A. thaliana* RCD1 N-terminus (1-265 aa). The sequence alignment was performed using Clustal Omega (EMBL-EBI) (Sievers *et al.*, 2011). The squared frames indicate the mutated residues, either at the N-terminus of the constructs (in red) or at the C-terminus (in green). The position of each mutated amino acid in the sequences is displayed above or beneath it, using the same colour scheme.

The other two constructs presented seven mutated residues (S230, S231, T239, S242, S244, T257, S263) towards their C-terminus of the considered portion of RCD1. These residues as well were substituted either with Aspartate (Asp) or with Alanine (Ala). Hence, the resulting constructs were named RCD1_N-ter_CD, because of position of the residues along RCD1 N-terminus mutated to Aspartate (D), and RCD1_N-ter_CA, because of the position of the residues along RCD1 N-terminus mutated to Alanine (A) (**Figure 3.15**).

Three of the synthetized constructs, RCD1_N-ter_NA, RCD1_N-ter_CA and RCD1_N-ter_CD, were cloned into pENTRD_Topo_gRCD1 using restriction enzyme digestion and ligation (Methods 2.4.14 and 2.4.15). The same cloning strategy was initially used to clone also the RCD1_N-ter_ND construct, but after some unsuccessful

attempts and the finding of an additional BamHI restriction site, due to one of the nucleotides mutated in this construct, a two-step cloning strategy was necessary. The entry vectors pENTRD_Topo_gRCD1_NA, pENTRD_Topo_gRCD1_CA, pENTRD_Topo_gRCD1_CD and, later on, pENTRD_Topo_gRCD1_ND, after being sequenced (Macrogen EZ-Seq, Amsterdam), were used to set up LR reactions for Gateway™ cloning system, together with the destination vectors pK7FWG2 and pGWB414. These cloning reactions led to the creation of the binary expression vectors pK7FWG2_gRCD1_NA-GFP, pK7FWG2_gRCD1_CA-GFP, pK7FWG2_ gRCD1_CD-GFP, pK7FWG2_gRCD1_ND-GFP and of pGWB414_gRCD1_NA-3HA, pGWB414_gRCD1_CA-3HA, pGWB414_gRCD1_CD-3HA, pGWB414_ gRCD1_ND-3HA. All of the aforementioned binary expression vectors, after being sequenced (Macrogen EZ-Seq, Amsterdam) were transformed into electrocompetent *Agrobacterium tumefaciens* GV3101 cells. After selecting one transformed colony per each construct, the resulting transgenic *A. tumefaciens* strains carrying the pGWB414 vectors encoding one mutated construct under Cauliflower Mosaic Virus (CaMV) 35S promoter, were used to create steadily transformed overexpressing *A. thaliana* lines, via Agrobacterium-mediated transformation, using *A. thaliana rcd1-1* knockout mutant plants (Overmyer *et al.*, 2000), in Col-0 ecotype, courtesy of Professor Dr. Kangasjärvi (University of Helsinki).

The transformed seeds were selected in plates on ½ MS solid medium added with Kanamycin; the resistant seedlings for each line were transferred to soil and let grow under long-day conditions. After collecting the seeds, forty-five seeds for each plant were again screened on plates containing ½ MS solid medium, plus Kanamycin, to check that the transgenic DNA was inserted in the genomic DNA only one time, and hence, showing a segregation of the gene coding for the Kanamycin resistance with a 3 to 1 ratio. Then, twenty of the resistant seeds were again transferred to soil and let grow. Forty-five of the collected seeds of each T2 plant were grown in plates on ½ MS solid medium added with Kanamycin to identify homozygous lines. Therefore, two homozygous lines for *A. thaliana rcd1-1* KO mutant expressing RCD1_NA-3HA were selected (*rcd1-1* RCD1_NA #2.4 and #2.16), two homozygous lines for *A. thaliana rcd1-1* KO mutant expressing RCD1_CA-3HA (*rcd1-1* RCD1_CA # 3.2 and #12.11) and three homozygous lines for *A. thaliana rcd1-1* KO mutant expressing RCD1_CD-3HA (*rcd1-1* RCD1_CD #3.1, #3.6 and #4.8). Due to the initial difficulties found in cloning RCD1_ N-ter_ND construct into the entry vector and the subsequent delay in the generation of stable transgenic lines, T3 homozygous lines of *A. thaliana rcd1-1* KO mutant expressing RCD1_ND-3HA were not obtained for further experiments.

3.1.7 Characterization of RCD1 phospho-mutant lines

The EMS mutant line *rcd1-1*, characterized by Overmyer *et al*. (2000), presented a pleiotropic phenotype. For example, rosette size was reduced compared to Col-0 wild type plants of the same age; leaves shape was altered and curled, pointing upwards, and it showed early flowering, always in comparison to Col-0 wild type plants of the same age. Hence, in the first instance, the phenotype of the abovementioned homozygous lines, carrying the phospho-mutated constructs of RCD1, from now on referred to as "phospho-mutant lines", was analysed, both under long-day (LD, 16 hours of light/day) (**Figure 3.16**) and under short-day growth conditions (SD, 10 hours of light/day) (**Figure 3.17**).

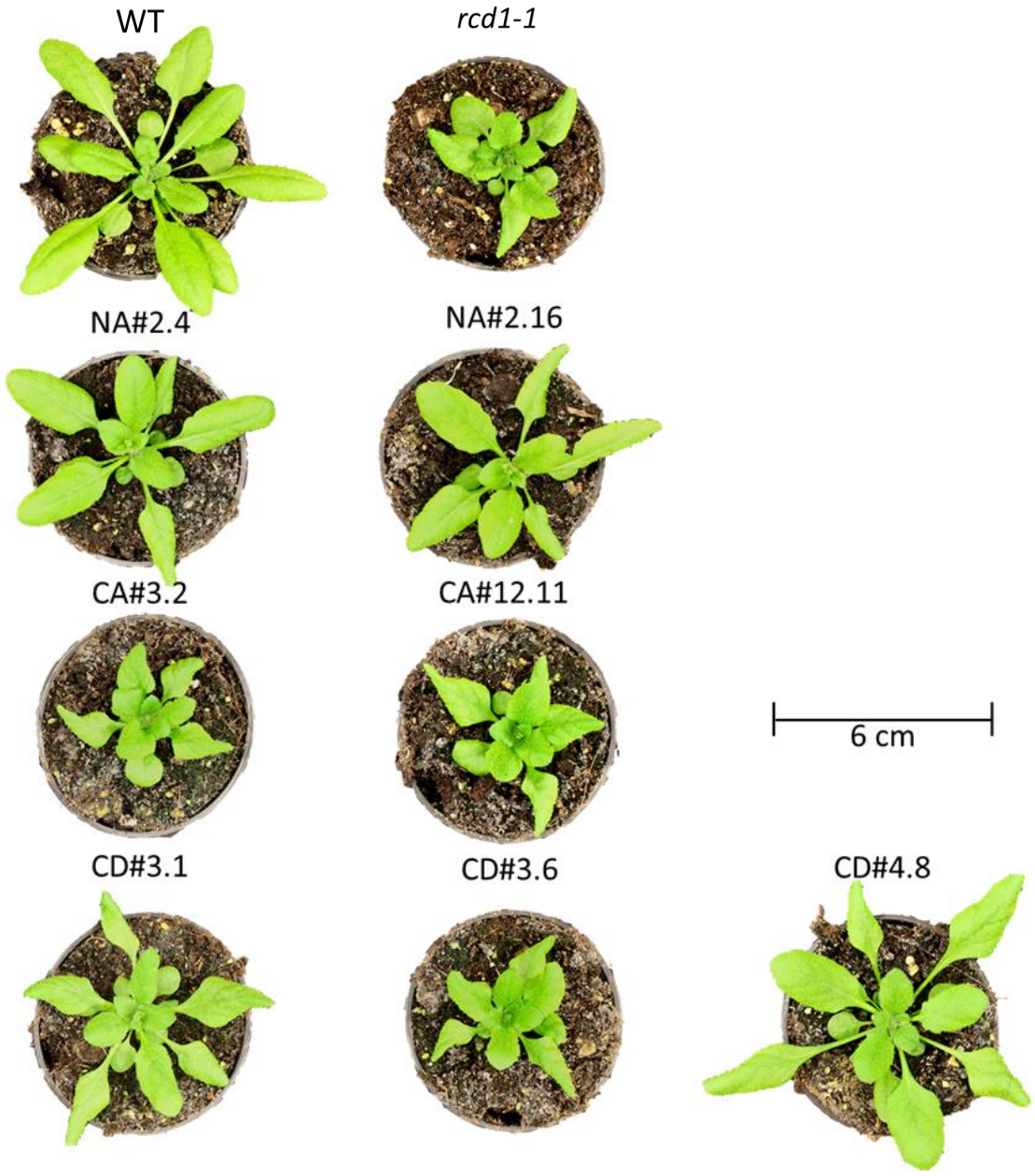

Figure 3.16: Phenotype of *A. thaliana rcd1-1* KO lines overexpressing RCD1 phospho-mutants grown under long-day conditions. The figure shows representative examples of the characteristic phenotype of six-week-old *A. thaliana* transgenic lines *rcd1-1* RCD1_NA #2.4 and #2.16, *rcd1-1* RCD1_CA #3.2 and #12.11, *rcd1-1* RCD1_CD # 3.1, #3.6 and #4.8 grown under long-day (LD) conditions (16 hours light/day, 22 °C, 55% humidity, light intensity of 150 µmol/(m^2s)) after six weeks from sowing, in comparison to Col-0 wild type (WT) and *rcd1-1* knockout mutant.

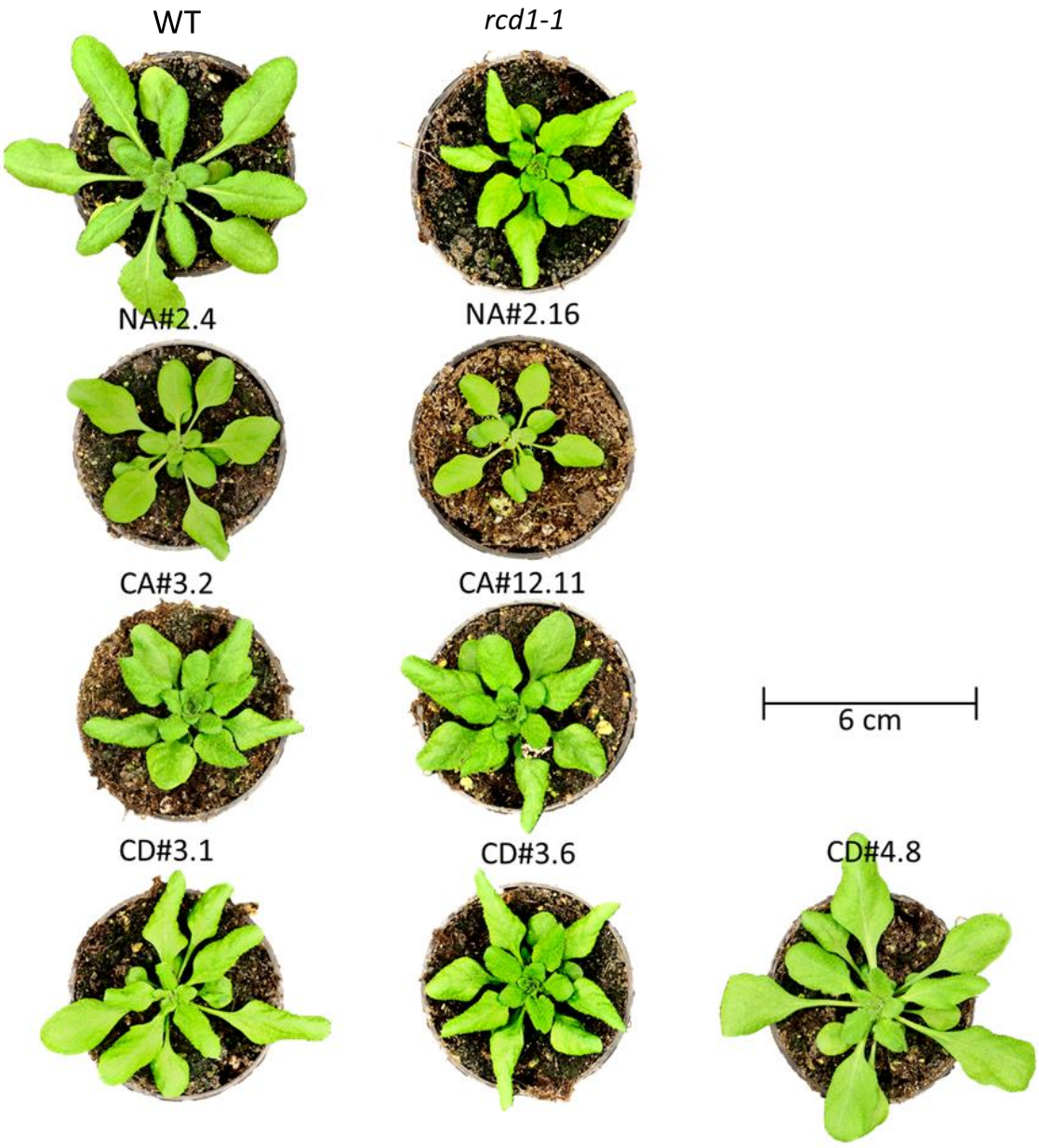

Figure 3.17: Phenotype of *A. thaliana rcd1-1* KO lines overexpressing RCD1 phospho-mutants grown under short-day conditions. The figure shows representative examples of the characteristic phenotype of six-week-old *A. thaliana* transgenic lines *rcd1-1* RCD1_ NA #2.4 and #2.16, *rcd1-1* RCD1_CA #3.2 #12.11, *rcd1-1* RCD1_CD # 3.1, #3.6 and #4.8 grown under short day (SD) conditions (10 hours light/day, 20 °C, 55% humidity, light intensity of 100 µmol/(m^2s)), in comparison to Col-0 wild type (WT) and *rcd1-1* knockout.

As shown in **Figure 3.16** and **Figure 3.17**, Col-0 *rcd1-1* showed the characteristic reduced size of the rosette, as well as downwards curved leaves in comparison with the Col-0 wild type. Under both growth conditions, the phospho-mutant lines overexpressing RCD1_NA #2.4 and # 2.16 showed a slightly reduced rosette size in comparison to the wild type, but the rounder and flatter shape of the leaves was rather similar to the Col-0 wild type than the one characterizing Col-0 *rcd1-1* mutant line. On the contrary, the transgenic lines overexpressing RCD1_CA #3.2 and #12.11, grown either under long-day or short-day conditions, presented a phenotype very much resembling the one of the knockout line *rcd1-1*, with smaller rosette size and downwards curved leaves.

Interestingly, the *rcd1-1* mutant lines overexpressing RCD1_CD #3.1, #3.6 and #4.8 presented relevant phenotypical differences amongst themselves, even though each was transformed with the same construct. In fact, the line *rcd1-1* RCD1_CD #3.6 showed a strong mutant phenotype, overall similar to the one distinctive of Col-0 *rcd1-1* line, whereas the lines *rcd1-1* RCD1_CD #3.1 and, even more, *rcd1-1* RCD1_CD #4.8 presented a rosette size comparable to the Col-0 wild type line, although developing at the same time leaves flat and wide, typical of wild type phenotype, or bent downwards, like in *rcd1-1* mutant, especially under long-day growth conditions.

The analysis of transcript levels of *RCD1* was performed via quantitative Real-Time PCR (qRT-PCR) (Methods 2.4.11), to assess whether the partially uncomplemented phenotype observed in *rcd1-1* RCD1_CA and *rcd1-1* RCD1_CD overexpressing lines might have been due to the lack of expression of the transgenes *rcd1_CA* and *rcd1_CD*. For this assay, it was used cDNA synthesized from RNA extracted from eight-week-old leaves. The *RCD1* gene is well expressed in this tissue at this stage, as reported by Klepikova *et al.* (2016). A region of *RCD1* gene transcript of approximately of 150 base-pairs at the 3' end of the mature mRNA was used to test the expression levels of the gene of interest. This particular region was chosen in order to make sure that the entire gene was being transcribed *in vivo*, as well as for the absence of any designed mutation. In this work, all the results of the qRT-PCR assays were normalized to the expression levels of the housekeeping gene *NBLACK* (AT4G34270) as described in Czechowski *et al.* (2005) and the experiment was performed three times for each growth condition, for three biological replicates. As shown in **Figure 3.18**, the overall trend of *RCD1* transcriptional levels is conserved both under long- and short-day conditions in each tested line. However, the values for the relative expression of the gene of interest were slightly higher for the samples grown under long-day conditions.

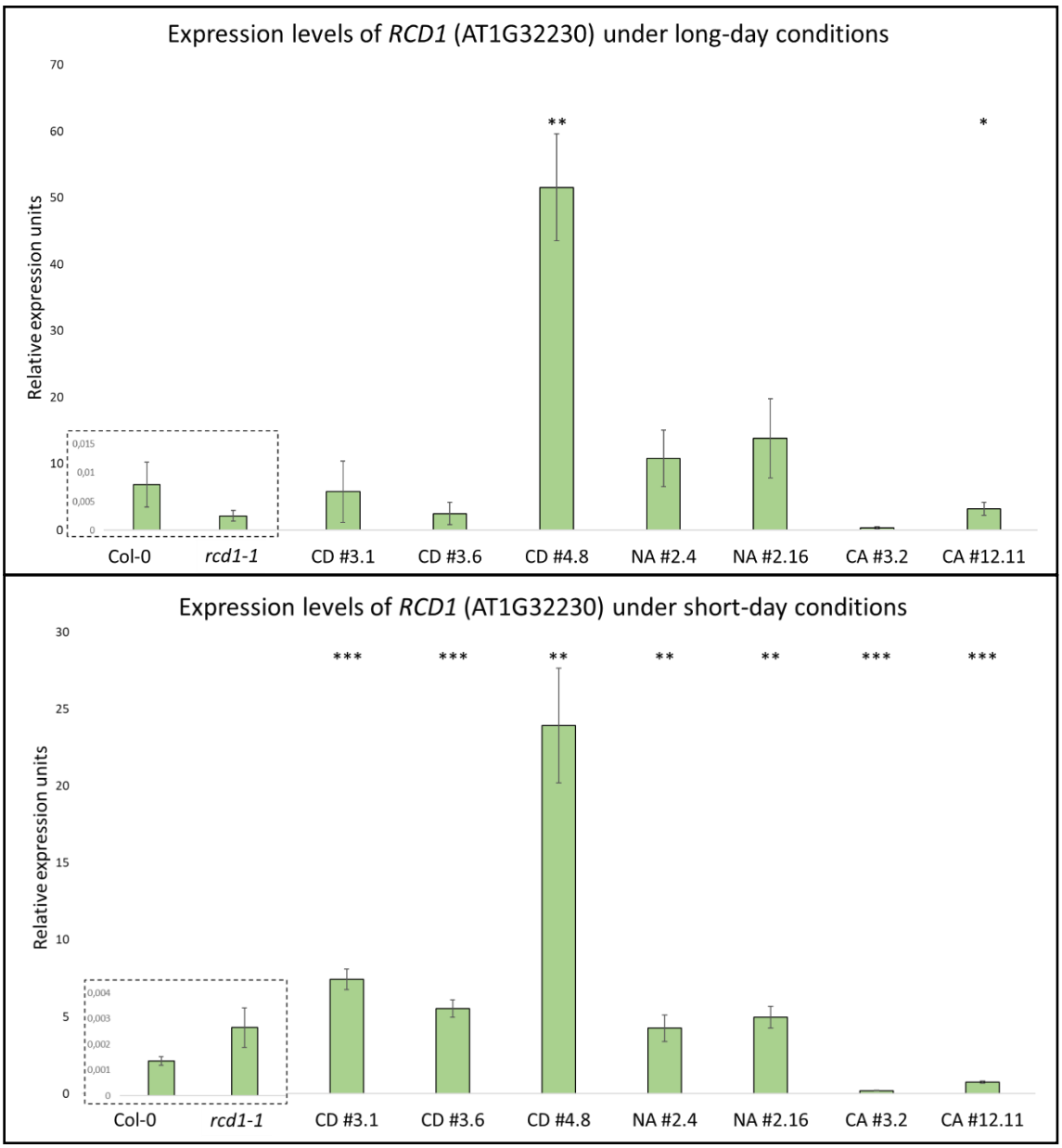

Figure 3.18: Analysis of expression levels of *RCD1* (AT1G32230) in *A. thaliana* adult leaves of *rcd1-1* lines overexpressing phospho-mutant versions of RCD1. Per each line, about 200 mg of leaf tissue were used to extract RNA from adult leaves of eight-week-old plants. Mean values of the relative expression, calculated in each replicate per each genotype, are presented in the graphs. The dotted panel on the left bottom of each graph show the relative expression levels of the *RCD1* gene in Col-0 WT and *rcd1-1* lines, whose values were too small to be displayed without an enlargement. Error bars show the standard error. Asterisks indicate significant differences in expression levels of the gene of interest between the Col-0 wild type and the other tested *A. thaliana* lines, according to Student's *t*-test. * = P-value< 0.05; **= P-value< 0.01; *** = P-value< 0.001; **** = P-value <0.0001 (n=3 biological replicates).

Although the analysis of expression level of *RCD1*confirmed that all the generated transgenic lines were overexpressing the gene of interest, to a different extent, in comparison to the Col-0 wild type and the *rcd1-1* knockout mutant, it was yet to be assessed whether the transcriptional levels were proportional to the level of protein synthetized *in vivo*. Hence, a protein extraction procedure was performed to test the presence of the 3HA-tagged protein via immunoblotting. As shown in **Figure 3.19**, the presence of the tagged protein was detectable only in protein fractions extracted from overexpressing lines *rcd1-1* RCD1_CD #3.6 and *rcd1-1* RCD1_CD #4.8.

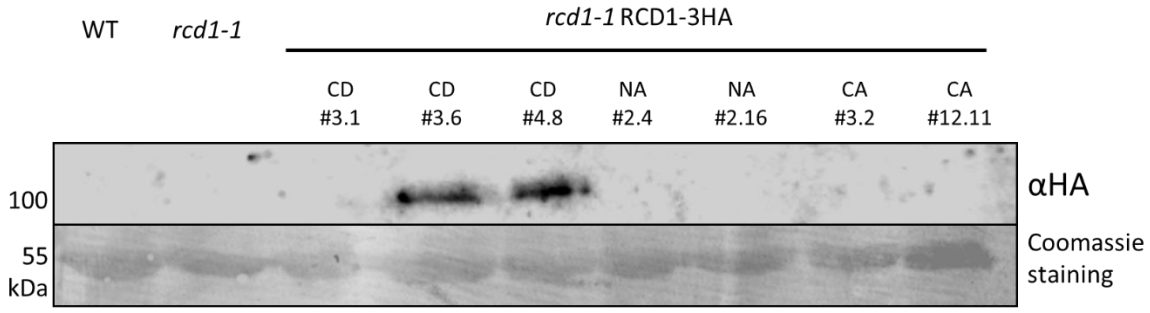

Figure 3.19: Detection of the presence of 3HA-tagged RCD1 protein in *A. thaliana* overexpressing phospho-mutant lines. Protein extract of one adult leave, of approximately the same size (~200 mg), from eight-week-old rosettes for each overexpressing line was used to assess the presence of the proteins of interest via immunoblotting. In order to verify the specificity of the detected signal, Col-0 wild type and *rcd1-1* knockout line protein extracts were loaded as negative control. The Coomassie staining of the membrane was used to assess the even loading of the samples. (n=2 biological replicates)

Despite the absence of detectable signal in most of the samples, which might be due to the limited intrinsic sensitivity of the detection method or of the detecting apparatus itself, the phenotypic characterization and the transcript analysis provided convincing proof of the expression of the mutated versions of *RCD1*. Hence, the characterization of these stable overexpressing lines was taken further by analysing transcript levels of genes, whose transcription was previously reported to be altered in the Col-0 *rcd1-1* knockout mutant line. In particular, the levels of expression of the genes *NUDX6* (AT2G04450), encoding an NADH pyrophosphatase involved in NADH metabolism, and *RAP2.6* (AT1G43160), encoding a member of the ERF (ethylene response factor) transcription factor family (RAP2.6), were previously described to be decreased in *rcd1* knockout mutant, in comparison with the Col-0 wild type (Broschè *et al.*, 2014). On the other hand, *AOX1A* (AT3G22370), encoding the most abundant isoform of

mitochondrial alternative oxidases in *A. thaliana*, was found to be increasingly expressed in the *rcd1-1* mutant (Shapiguzov *et al.*, 2019).

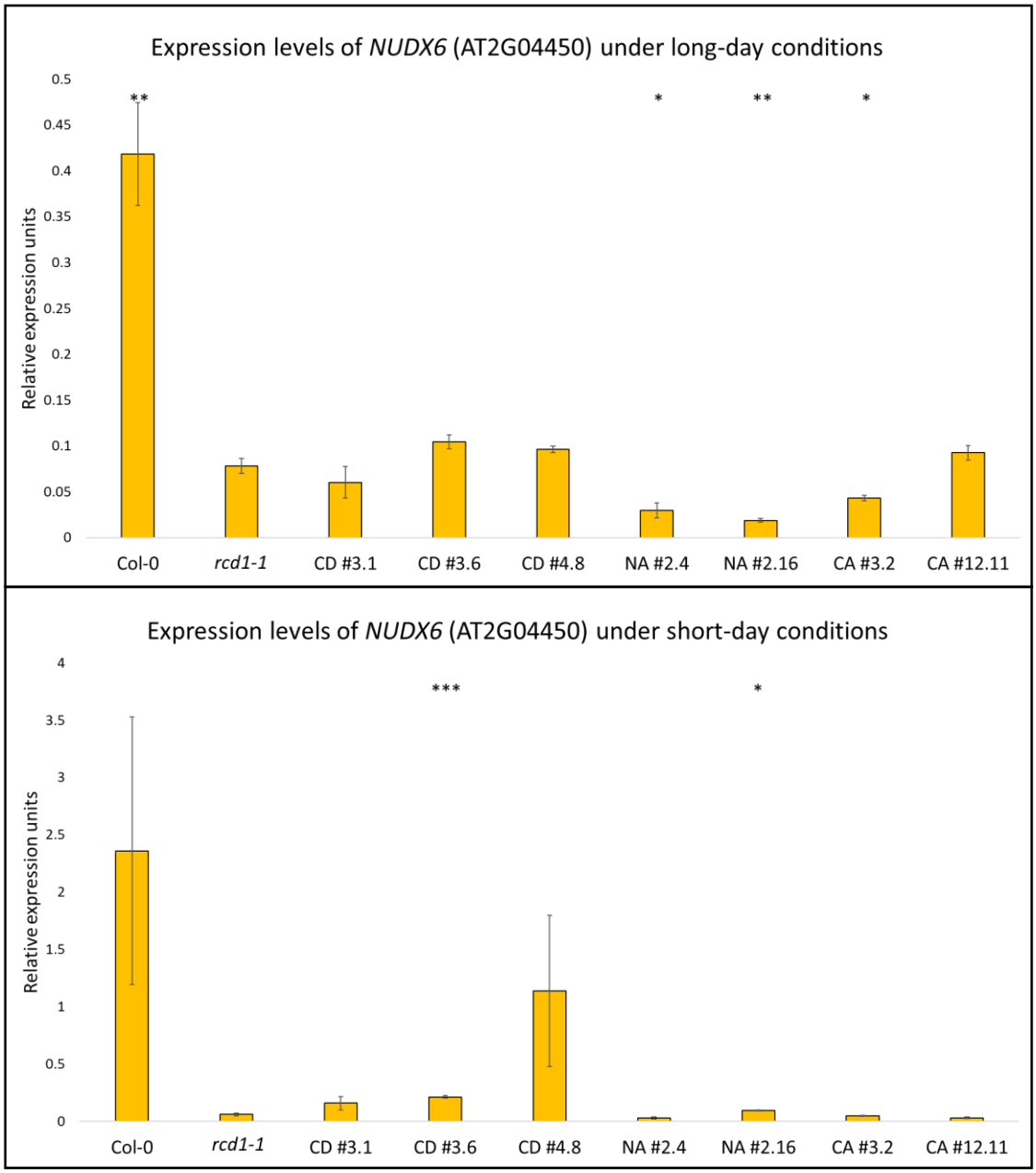

Figure 3.20: Analysis of expression levels of *NUDX6* (AT2G04450) in *A. thaliana* adult leaves of *rcd1-1* lines overexpressing phospho-mutant versions of RCD1. Per each line, about 200 mg of leaf tissue were used to extract RNA from adult leaves of eight-week-old plants. Mean values of the relative expression, calculated in each replicate per each genotype, are presented in the graphs. Error bars show the standard error. Asterisks indicate significant differences in expression levels of the gene of interest between *rcd1*-1 knockout mutant and the other tested *A. thaliana* lines, according to Student's *t*-test. * = P-value< 0.05; **= P-value< 0.01; *** = P-value< 0.001; **** = P-value <0.0001 (n=3 biological replicates).

The analysis of the expression levels of *NUDX6* confirmed the lower abundance of transcript for this gene in the *rcd1-1* knockout line, compared with the Col-0 wild type, both under long- and in short-day growth conditions. Interestingly, although, on the graphics, the expression levels of *NUDX6* in the phosphomutant lines under long-day conditions appeared to be comparable with those shown by *rcd1-1* knockout, after the statistical analysis some values showed significant differences. On the contrary, under short-day conditions, the wild type and the *rcd1-1* RCD1_CD #4.8 lines (**Figure 3.20,** lower panel), showed increased levels of expression of the tested gene. However, under long-day conditions, an overall reduced level of expression of the *NUDX6* gene was observed in comparison with the short-day conditions.

When the same analysis of expression levels was performed for *RAP2.6*, the reduction of expression of *RAP2.6* in Col-0 *rcd1-1*, in comparison to Col-0 wild type, as described by Brioschè *et al.* (2014), was confirmed only in samples from plants grown under short-day conditions. In this case, all the phospho-mutant lines presented intermediate values of *RAP2.6* expression level, but the *rcd1-1* RCD1_CA #12.11, whose transcript analysis showed a significant increase in the level of expression of the tested gene both in comparison with *rcd1-1* knockout and the wild type lines. On the other hand, the analysed samples grown under long-day conditions showed very low expression levels of *RAP2.6*. However, the variations in the expression levels in the different lines, compared to *rcd1-1* knockout, once analysed, resulted in few statistically significant differences, showing a reduction in the expression of *RAP2.6*.

As reported by Shapiguzov *et al.* (2019), the increased expression of *AOX1A* in the *rcd1-1* knockout mutant, in comparison to the Col-0 wild type, was due to the transcriptional activation of the abovementioned gene in the absence of RCD1. In the wild type, RCD1 binds to the transcription factor that initiates the transcription of *AOX1A,* hence preventing the transcriptional activation of the abovementioned gene. This finding was confirmed by the data gathered in this work, as shown in **Figure 3.22**. Both under long- and short-day conditions, not only *rcd1-1*, but all the phospho-mutant lines, except for *rcd1-1* RCD1_CD #4.8, presented an increased level of expression of *AOX1A*, in comparison to the Col-0 wild type. However, under short-day conditions, also the *rcd1-1* RCD1_CD #3.1 and 3.6, showed significantly reduced level of expression of the tested gene, in comparison to the *rcd1-1* knockout mutant and the *rcd1-1* RCD1_CA lines.

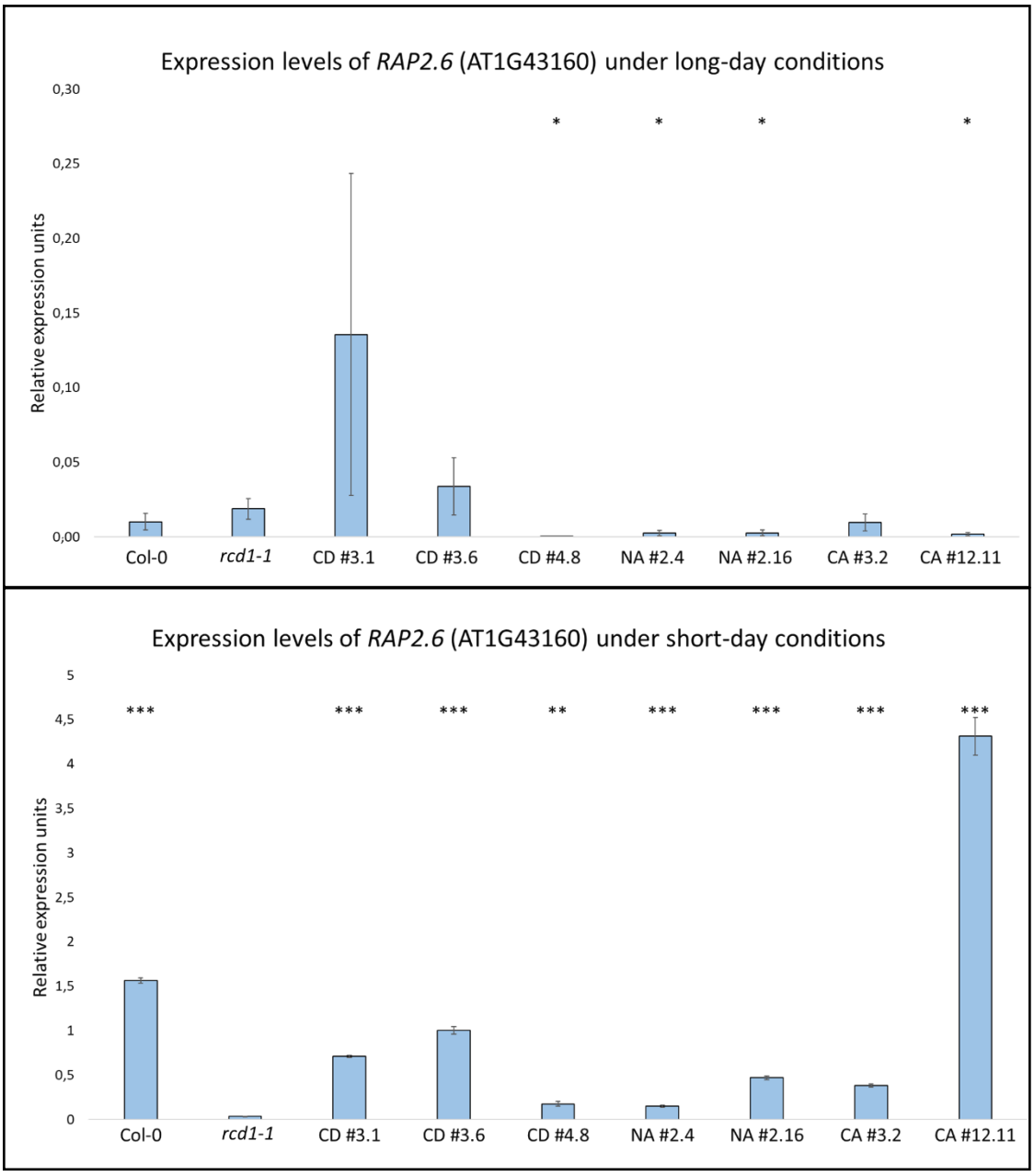

Figure 3.21: Analysis of expression levels of *RAP2.6* (AT1G43160) in *A. thaliana* adult leaves of *rcd1-1* lines overexpressing phospho-mutant versions of RCD1. Per each line, about 200 mg of leaf tissue were used to extract RNA from adult leaves of eight-week-old plants. Mean values of the relative expression, calculated in each replicate per each genotype, are presented in the graphs. Error bars show the standard error. Asterisks indicate significant differences in expression levels of the gene of interest between *rcd1*-1 knockout mutant and the other tested *A. thaliana* lines, according to Student's *t*-test. * = P-value< 0.05; **= P-value< 0.01; *** = P-value< 0.001; **** = P-value <0.0001 (n=3 biological replicates).

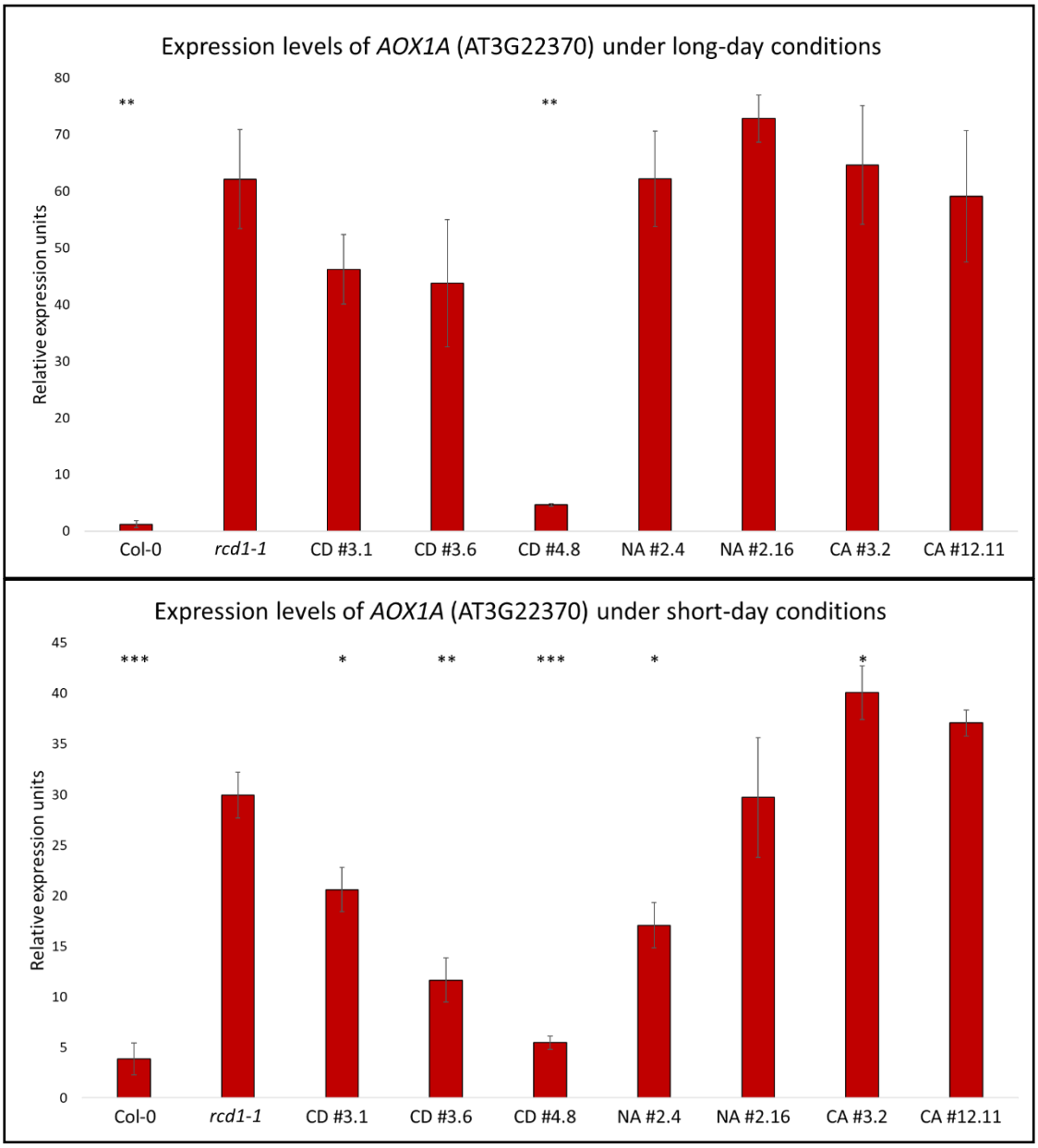

Figure 3.22: Analysis of expression levels of *AOX1A* (AT3G22370) in *A. thaliana* adult leaves of *rcd1-1* lines overexpressing phospho-mutant versions of RCD1. Per each line, about 200 mg of leaf tissue were used to extract RNA from adult leaves of eight-week-old plants. Mean values of the relative expression, calculated in each replicate per each genotype, are presented in the graphs. Error bars show the standard error. Asterisks indicate significant differences in expression levels of the gene of interest between *rcd1*-1 knockout mutant and the other tested *A. thaliana* lines, according to Student's *t*-test. * = P-value< 0.05; **= P-value< 0.01; *** = P-value< 0.001; **** = P-value <0.0001 (n=3 biological replicates).

3.1.8 Analysis of tolerance to chloroplastic Reactive Oxygen Species (ROS) in phospho-mutant lines

The *rcd1-1* knockout line was first identified by Overmyer *et al.* in 2000 in a screening for mutants with enhanced sensitivity to apoplastic Reactive Oxygen Species (ROS) upon exposure to ozone (O_3). Interestingly, when the same line was tested for its tolerance to ROS generated in the chloroplast (Ahlfors *et al.,* 2004) upon exposure to the oxidizing agent methyl-viologen (MV, also known as paraquat), Col-0 *rcd1-1* seedlings showed enhanced tolerance to this oxidative stress, in comparison to Col-0 wild type. This resistant phenotype to chloroplastic oxidative stress was found to be due to the role of RCD1 as a transcription factor binding protein. As explained in Shapiguzov *et al.* (2019), the RST domain of RCD1 binds to the transcription factors ANAC013 and ANAC017, which are necessary for the initialization of mitochondrial dysfunction stimulon (MDS) genes transcription, including the one encoding the aforementioned oxidase AOX1A. Therefore, it was hypothesized that, in the absence of RCD1, the transcription of the MDS genes would be constantly active, leading to an increment of the AOX1A level. It was proposed that this isoform of AOX would take part in a multi-organellar pathway, the malate shuttle pathway, which is involved in the reduction of chloroplast-generated ROS via electron transportation to the mitochondria.

In this work, a tolerance assay was performed, in order to test whether the mutated residues of the generated RCD1 constructs, either mimicking the presence (D constructs) or the absence (A constructs) of phosphorylation, could affect the function of RCD1 as a transcription factor binding protein and, hence, its role in chloroplastic oxidative stress regulation, as described in Methods 2.2.3**.** The oxidative compound methyl viologen was added to the growth medium ½ Murashige&Skoog (MS) to different final concentrations in order to remain in a range that would affect the development of true leaves while still allowing the seeds to germinate. The assay was performed both under short-day and under long-day growth conditions, with final concentrations of methyl viologen of 0.5 and 1 µM. Additionally, under long-day growth conditions, the effects of 1.5 µM methyl viologen in the growth medium were tested to assess whether this experimental condition would represent the upper limit to the tolerance, hence producing a lethal effect on the seedlings.

Fifty 20-day-old seedlings, sown in plates on ½ MS solid medium added with oxidizing agent methyl viologen and grown under short-day condition, were examined to detect the presence of true leaves, which are defined as the leaves developed after the emergence of the two cotyledons (**Figure 3.23**). The Col-0 wild type was not able to generate true leaves even at the lower concentration of methyl viologen (0.5 µM), whereas Col-0 *rcd1-1* and phospho-mutant lines seedlings showed tolerance to chloroplastic oxidative stress caused by methyl viologen at both tested concentrations,

to different extents. Furthermore, the *rcd1-1* RCD1_CA and *rcd1-1* RCD1_NA transgenic lines presented a better fitness to the induced stress: the size of the seedling was discernibly bigger, in comparison to the other genotypes, and the leaves, both cotyledons and true leaves, present barely any trace of chlorosis due to the stressful growth conditions. On the contrary, symptoms of chlorosis were extensively present in the seedlings of wild type under the same growth conditions. At the highest concentration of methyl viologen (1 µM), a drastic reduction in seedling size was observed, as well as diffuse signs of chlorosis. Nevertheless, all the phospho-mutant lines as well as *rcd1-1* knockout seedlings showed a significant increase in tolerance in comparison to the Col-0 wild type (**Figure 3.25**).

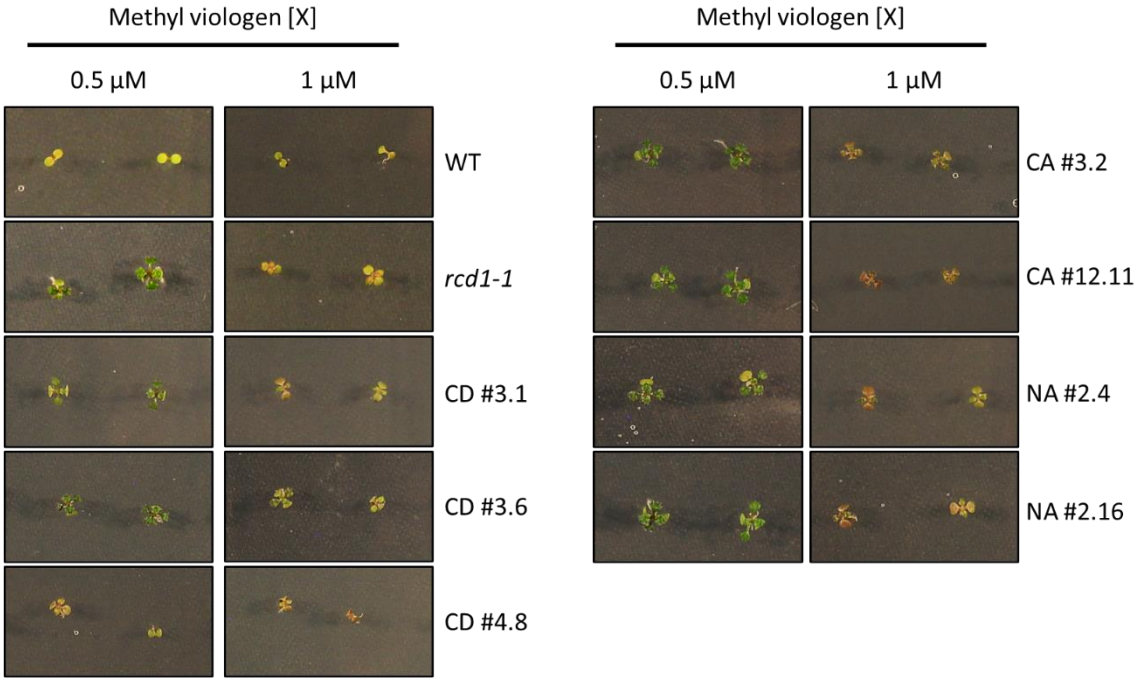

Figure 3.23 Effects of oxidative stress in chloroplasts of *A. thaliana* seedlings of Col-0 wild type, *rcd1-1* and the phospho-mutant lines grown under short-day (SD) conditions upon exposure to methyl viologen. Fifty seeds per line were sown in plates on ½ MS solid medium added with oxidizing agent methyl viologen (final concentration of 0.5 and 1 µM) and grown under short-day conditions (10h light/day, 55% humidity). Pictures show representative examples of seedlings for each tested line twenty days after sowing.

The same experiment, carried out under long-day conditions, gave results partially similar to those described above, with some interesting differences. The overall increased tolerance of the transgenic lines to chloroplastic ROS in comparison to the Col-0 wild type was confirmed. However, a remarkable difference in the phenotype of seedlings of different lines was observed. As shown in **Figure 3.24**, the darkening of leaves in seedlings grown under long-day conditions upon chloroplastic oxidative stress occurred already at the lowest concentration of methyl viologen, and it was likely due to the increased amount of anthocyanins. The higher levels of anthocyanins in seedlings grown under long-day conditions might have been due to these molecules' protective function against photooxidative stress (Polle, 1997). Furthermore, the average size of the seedlings grown under long-day conditions appeared reduced compared to the size of seedlings grown under short-day conditions at the same concentration of the oxidizing compound. This decrease in seedlings size is particularly evident for *rcd1-1* RCD1_NA lines seedlings (**Figure 3.23** and **3.24**) and could be an effect of the well-known trade-off between plant growth and responses to stresses (Bechtold & Field, 2018).

The tolerance to chloroplastic ROS upon methyl viologen treatment of the tested lines was quantified by counting the number of seedlings that developed true leaves. As shown in **Figure 3.25**, a significant difference was found between the wild type and the *rcd1-1* knockout line (as reported in Ahlfors *et al.,* 2004), as well as between the wild type and the phospho-mutant lines generated in this work. This result was confirmed for all the tested concentrations of methyl viologen and the two different photoperiods in which the seedlings were grown. Interestingly, in the short-day growth conditions, the number of seedlings developing true leaves was significantly different also between the *rcd1-1* knockout mutant and the *rcd1-1* RCD1_CD #4.8 line, with the latter showing an intermediate level of tolerance to the chloroplastic oxidative stress under short-day condition. However, when the same experiment was performed with a long-day photoperiod, *rcd1-1* and *rcd1-1* RCD1_CD #4.8 line presented a similar trend in the tolerance assay, with the number of seedlings developing true leaves reduced, in comparison to the other phospho-mutant lines, but still significantly higher that the Col-0 wild type.

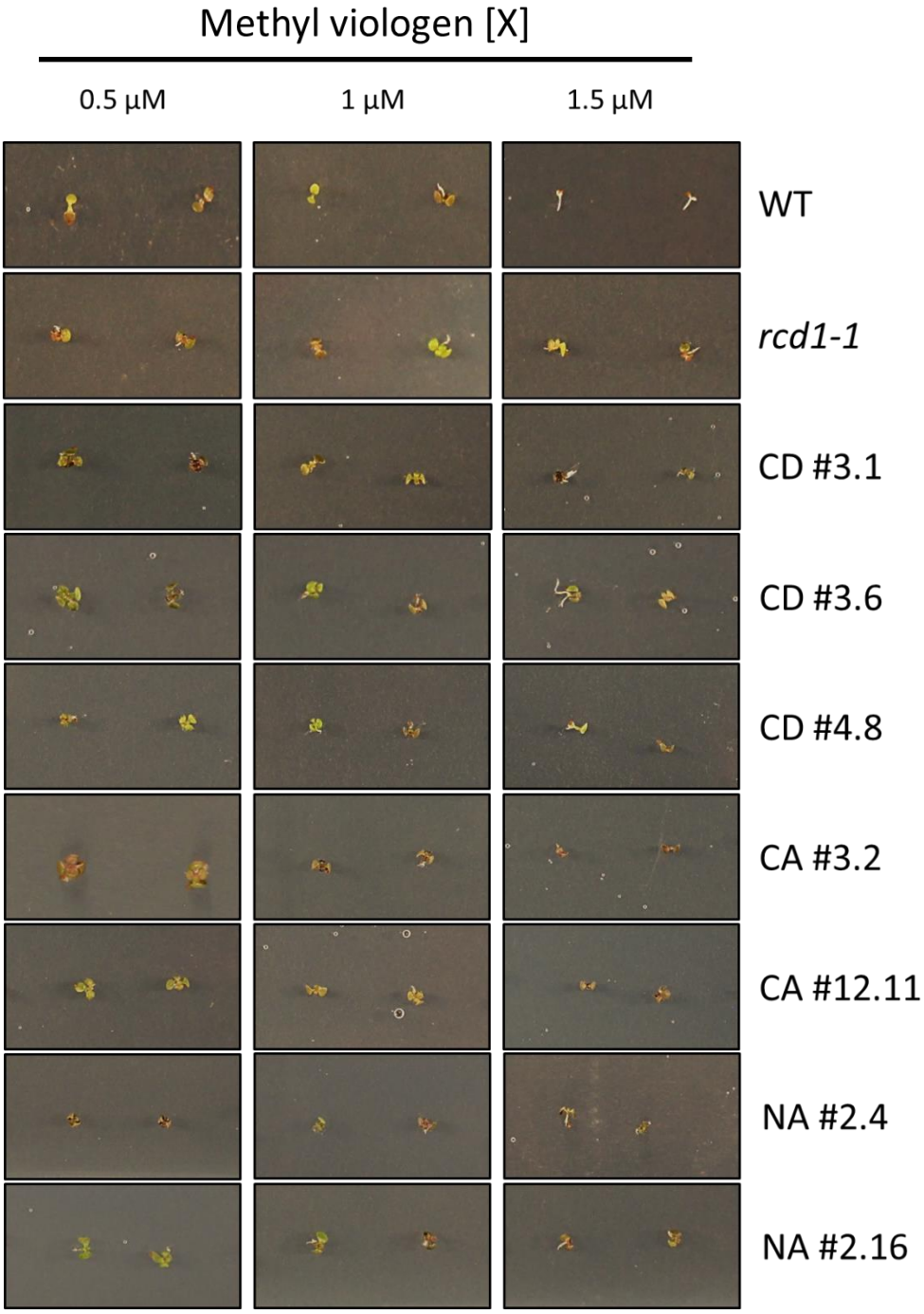

Figure 3.24: Effects of oxidative stress in chloroplasts of *A. thaliana* seedlings of Col-0 wild type, *rcd1-1* and the phospho-mutant lines grown under long-day (LD) conditions upon exposure to methyl viologen. Fifty seeds per genotype were sown in plates on ½ MS solid medium added with oxidizing agent methyl viologen (final concentration of 0.5, 1 and 1.5 µM) and grown under long-day conditions (16h light/day, 55% humidity). Pictures show representative examples of seedlings for each tested line twenty days after sowing.

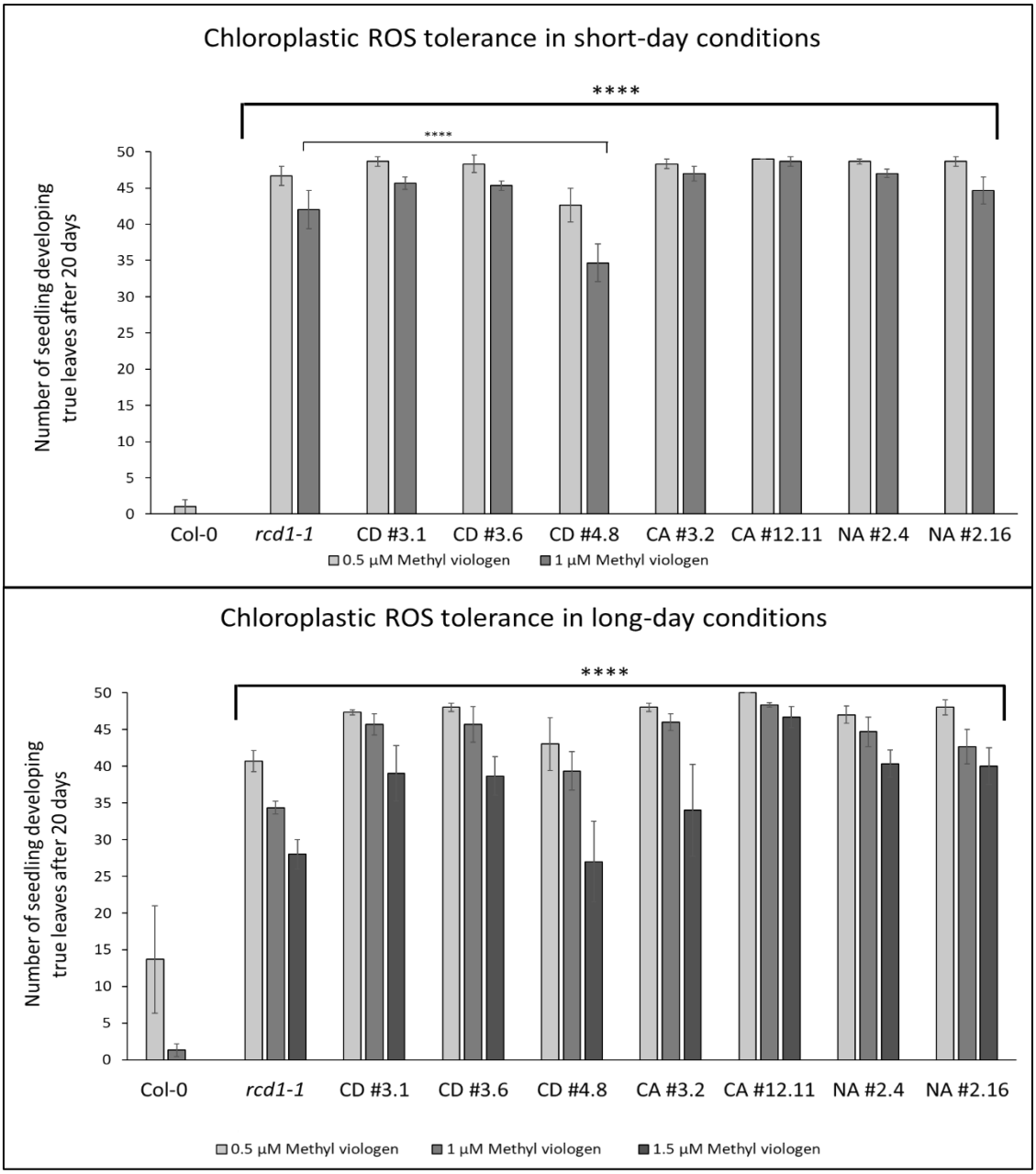

Figure 3.25: Variable levels of tolerance to chloroplastic reactive oxygen species (ROS) in *A. thaliana* seedlings of Col-0 wild type, *rcd1-1* and the phospho-mutant lines grown under short-day (SD) and long-day (LD) conditions upon exposure to methyl viologen. Fifty seeds per genotype were sown on plates containing ½ MS solid medium added with methyl viologen (final concentration either 0.5, 1 or 1.5 µM). After 20 days post sowing, the number of seedlings presenting true leaves was scored per each tested line. Each panel shows the mean values of three independent assays. Statistic evaluation of the results was performed with TWO-WAY ANOVA test (****= P-value < 0.0001). Error bars show the standard error values.

3.1.9 Mutations of phosphorylatable residues of RCD1 resulted in variation of its subnuclear localization

As a post-translational modification (PTM), protein phosphorylation is a reversible and flexible signalling mechanism, involved in a series of different cellular processes, amongst which activation or deactivation of enzymes (Budde and Chollet, 1988), conformational alterations, changes in subcellular localization as well as in protein-protein interactions (Muslin *et al.*, 1996). In this work, the investigation on the possible effects of the alterations at phosphorylation sites on RCD1 was started. First, the potential impact of modified residues mimicking the presence or the absence of phosphorylation on the subnuclear localization of RCD1 were considered. In addition to the RCD1_ND, RCD1_NA, RCD1_CD and RCD1_CA constructs, three more constructs were synthetized and tested, RCD1_allD, RCD1_allA and RCD1_CA.2. The first presented all the considered phosphosites, S27, T33, S36, T204S230, S231, T239, S242, S244, T257, S263 (**Figure 3.15**), mutated to Aspartate (D); the second presented all the considered phosphosites mutated to Alanine (A); the third one RCD1_CA.2 corresponded to the RCD1_CA construct plus an additional amino acid (T204) mutated to alanine. The RCD1_allD and RCD1_allA constructs were cloned via Gibson assembly (Methods 2.4.12.1) into pENTR_DTopo, after proceeding with overlap-extension polymerase chain reaction (OE-PCR) respectively performed on the *rcd1_ND* and *rcd1_CD* or on the *rcd1_NA* and *rcd1_CA* fragments using appropriate overlapping primers. Subsequently, the complete constructs were cloned into the Gateway plant expression vectors pK7FWG2 and pGWB414 via LR reaction (Methods 2.4.12.2). The pENTR_DTopo_RCD1_CA.2 clone was obtained by site-direct mutagenesis by PCR (Methods 2.4.7), using pENTR_DTopo_RCD1_CA as a template. The resulting construct was, hence, cloned into Gateway plant expression vectors pK7FWG2 and pGWB414 via LR reaction. The abovementioned constructs cloned in the expression vectors were then transformed into *A. tumefaciens* GV3101 electrocompetent cells. Out of one transformed colony per each construct, permanent glycerol stocks were obtained, in order to perform further experiments, e. g. transient expression in *N. benthamiana* leaf tissues.

The localization of GFP-tagged phospho-mutant versions of RCD1 was assessed using confocal microscopy upon transient expression in *N. benthamiana* leaf tissues via infiltration with suspensions of *A. tumefaciens* strains, each carrying one of the constructs of interest. As shown in **Figures 3.26** and **3.27**, RCD1-GFP presented the typical subnuclear localization, already described, in nuclear bodies, in variable numbers, and interspersed throughout the examined nuclei. RCD1_ND-GFP (**Figure 3.26**) and RCD1_NA-GFP (**Figure 3.27**), in general, both displayed a similar localization to the wild type protein. On the other hand, RCD1_CD-GFP and RCD1_allD-GFP mainly localized in wider and less numerous bodies located in the centre of the nuclei.

Interestingly, the mimicked absence of phosphorylation on the mutated residues in RCD1_CA-, RCD1_CA.2- and RCD1_allA-GFP, along the linker region between WWE and PARP domain, seemed to overall reduce the aggregation of these RCD1 constructs in separate nuclear bodies, in favour of a more interspersed localization of the protein of interest towards the nuclear periphery (RCD1_CA-GFP and RCD1_allA-GFP, **Figure 3.27**).

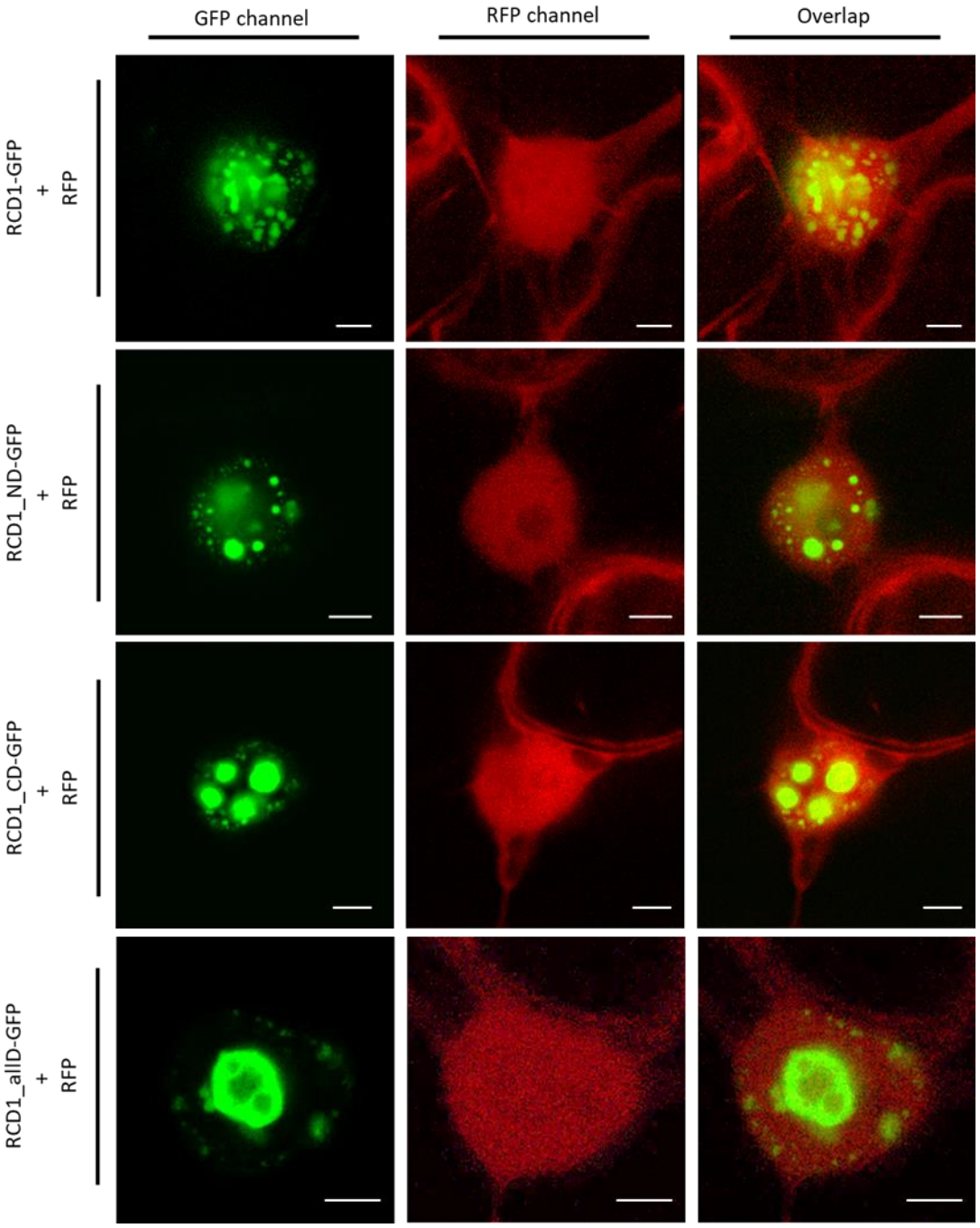

Figure 3.26: Nuclear localization of GFP-tagged *A. thaliana* RCD1 phospho-mutants in *N. benthamiana* leaf tissues. Two days post infiltration (dpi) with *A. tumefaciens* suspensions, leaf discs of *N. benthamiana* co-expressing under CaMV 35S promoter either AtRCD1-GFP, AtRCD1_ND-GFP, AtRCD1_CD-GFP or AtRCD1_allD-GFP, together with Red Fluorescent Protein (RFP) were excised and used for confocal microscopy assay to assess the subnuclear localization of the transiently expressed proteins. The experiment was repeated three times with similar results (63x magnification, n> 7. Scale bar = 5µm).

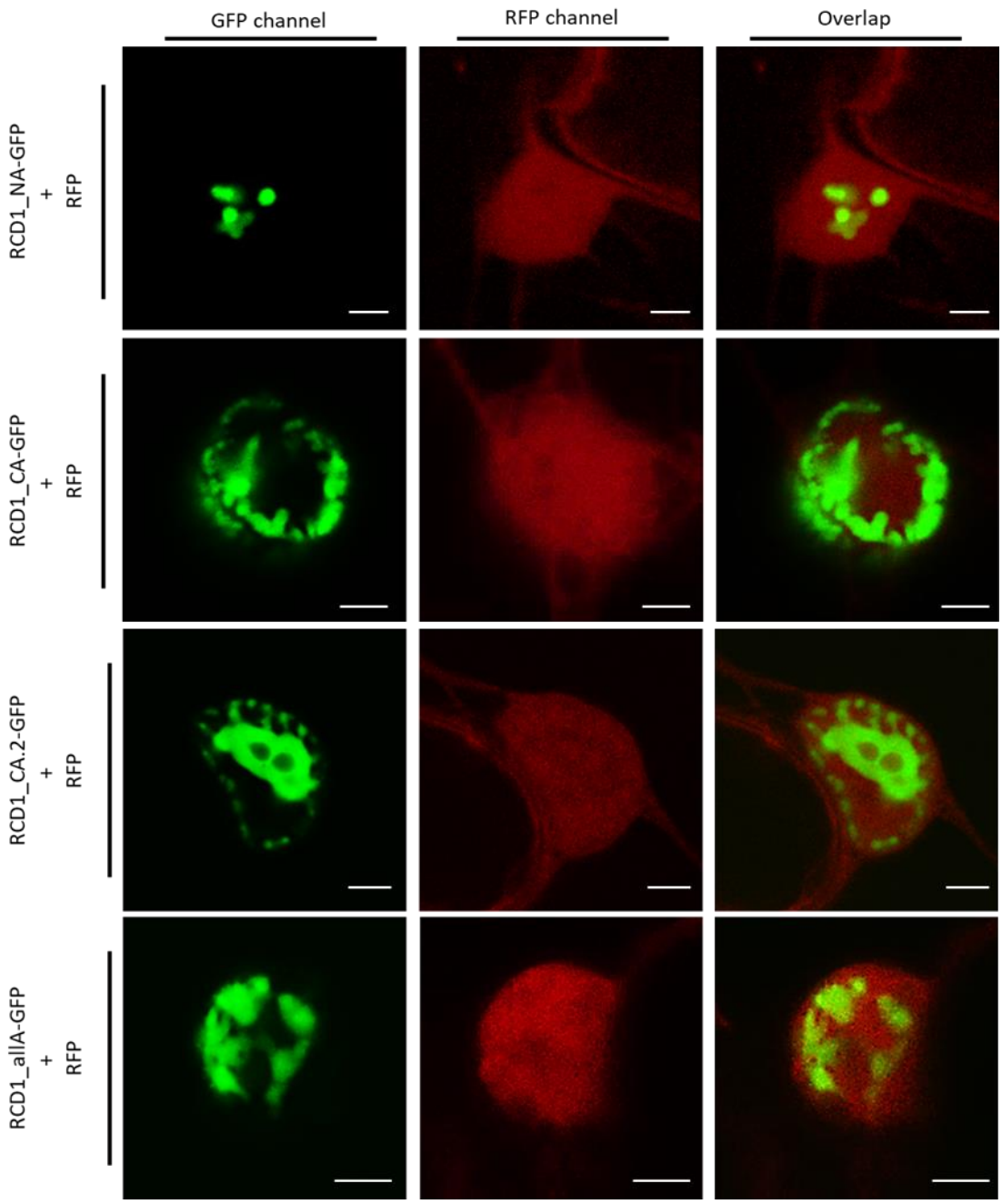

Figure 3.27: Nuclear localization of GFP-tagged *A. thaliana* RCD1 phospho-mutants in *N. benthamiana* leaf tissues. Two days post infiltration (dpi) with *A. tumefaciens* suspensions, leaf discs of *N. benthamiana* co-expressing under CaMV 35S promoter either AtRCD1_NA-GFP, AtRCD1_CA-GFP, AtRCD1_CA.2-GFP or AtRCD1_allA-GFP together with Red Fluorescent Protein (RFP) were excised and used for confocal microscopy assay to assess the subnuclear localization of the transiently expressed proteins. The experiment was repeated three times with similar results (63x magnification, n> 7. Scale bar = 5µm).

3.1.10 Mutations at phosphorylatable sites of RCD1 influenced subnuclear co-localization with PPK1 and PPK 4, but not with PPK3

As described in the previous paragraph, the mutations at the mentioned phosphorylatable residues of RCD1 affected the protein subnuclear localization in a relevant way. Therefore, the question of whether these mutations could affect the co-localization of the different RCD1 constructs with the kinases PPK1, PPK3 and PPK4 arose. The co-localization studies were performed using confocal microscopy on *N. benthamiana* leaf tissues, previously infiltrated with a suspension of two *A. tumefaciens* strains, carrying respectively an expression vector encoding a GFP-tagged version of one of the RCD1 mutant constructs and one of the RFP-tagged PPK. All the combinations were tested in three independent experiments, with a minimum number of sampled nuclei of seven per combination. The images shown below are representative of the localization most frequently observed per each of the tested proteins, although slight variations were also observed and could be attributed to different factors, such as different cellular stages of the analysed nuclei or variable expression levels of the same heterologous proteins.

Figures 3.28 and **3.29** show representative images of the nuclei tested for the variation of subnuclear co-localization of RCD1 phospho-mutant constructs and PPK1. It was observed that the GFP-tagged RCD1_ND and RCD1_NA constructs both maintained the co-localization with PPK1, as the RCD1-GFP. The observation that the size and number of the nuclear bodies, in which the tested proteins co-localized, varied from nucleus to nucleus was consistent with the findings gathered on the localization of RCD1 wild type expressed both with free RFP or PPK1-RFP (**Figure 3.1** and **3.4**).

The other tested RCD1 constructs presented conspicuous alteration in localization compared to wild type. First, the distribution of PPK1 throughout the nuclei appeared to be even, as it was when the kinase was tested for its nuclear localization in the absence of RCD1 (**Figure 3.3**). RCD1_CD and RCD1_allD located in bulkier nuclear bodies, presenting an undefined shape. Although the co-localization with PPK1 did not seem to be abolished entirely, it was strongly reduced. The same results were found for the RCD1-allA construct, which was not totally lacking co-localization with PPK1, but whose subnuclear localization presented evident alterations in comparison to the wild type. In fact, RCD1_allA appeared to be mainly localized in the nuclear periphery and did not present distinguishable nuclear speckles. The same peripheric localization was shared by the RCD1_CA and RCD1_CA.2 constructs and, in both cases, the proteins were interspersed below the nuclear surface, and the co-localization with PPK1 appeared strongly affected, if not lost.

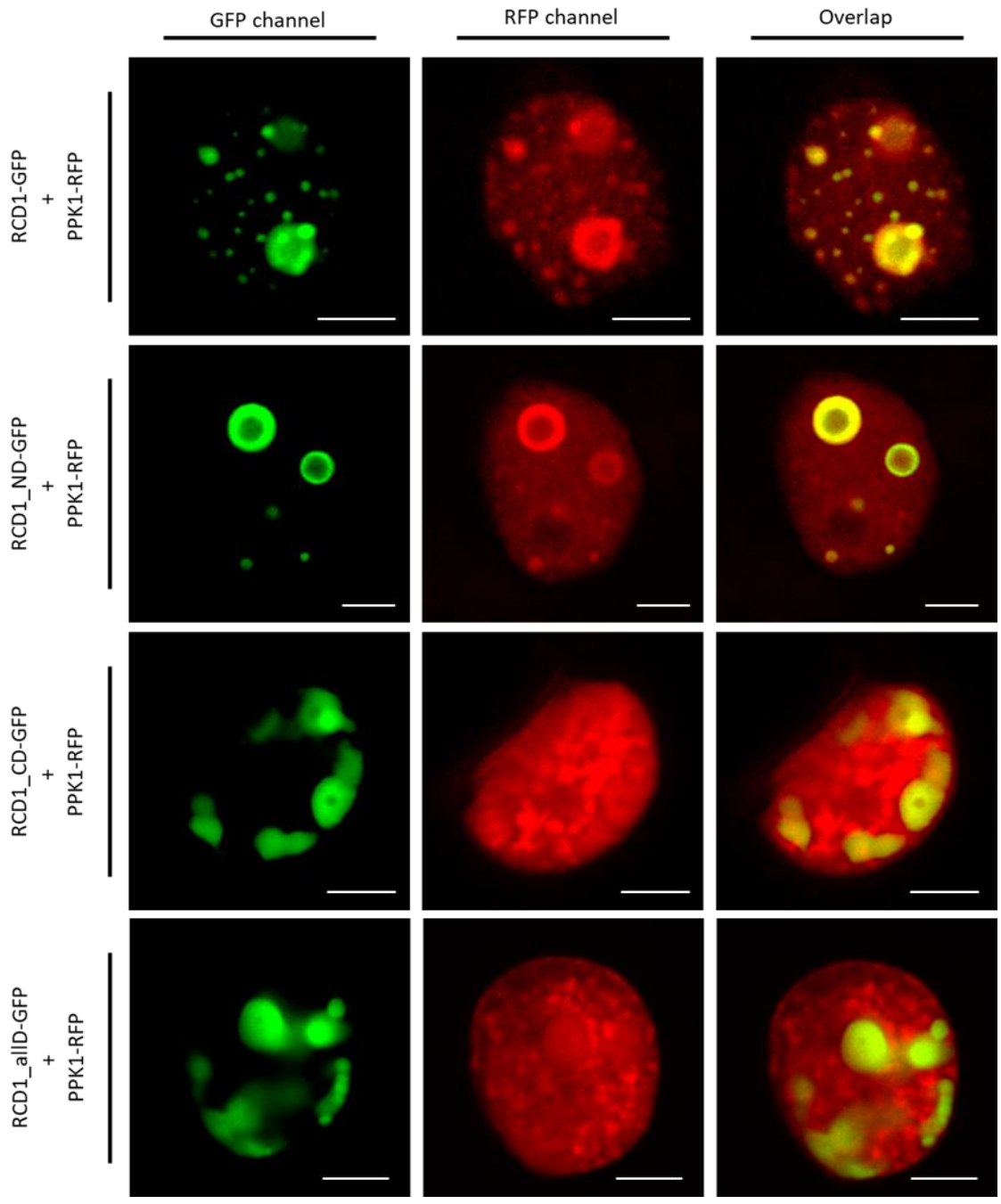

Figure 3.28: Nuclear localization of GFP-tagged *A. thaliana* RCD1 phospho-mutants and PPK1-RFP in *N. benthamiana* leaf tissues. Two days post infiltration (dpi) with *A. tumefaciens* suspensions, leaf discs of *N. benthamiana* co-expressing under CaMV 35S promoter AtPPK1_RFP together with either AtRCD1_GFP, AtRCD1_ND-GFP, AtRCD1_CD-GFP or AtRCD1_allD-GFP were excised and used for confocal microscopy assay to assess possible variations in the subnuclear colocalization of the transiently expressed proteins. The experiment was repeated three times with similar results (63x magnification, n> 7. Scale bar = 5µm).

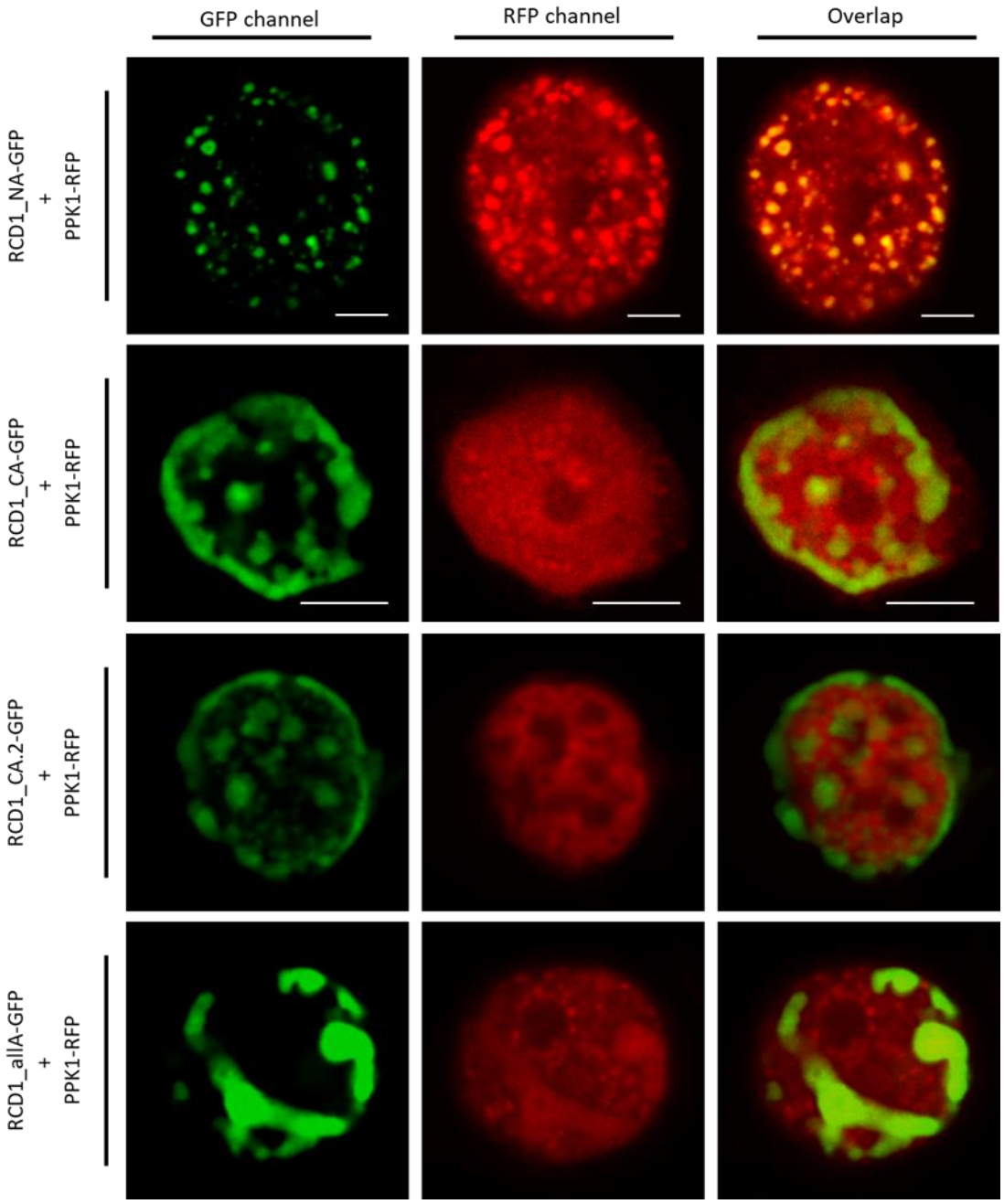

Figure 3.29 Nuclear localization of GFP-tagged *A. thaliana* RCD1 phospho-mutants and PPK1-RFP in *N. benthamiana* leaf tissues. Two days post infiltration (dpi) with *A. tumefaciens* suspensions, leaf discs of *N. benthamiana* co-expressing under CaMV 35S promoter AtPPK1_RFP together with either AtRCD1_NA-GFP, AtRCD1_CA-GFP, AtRCD1_CA.2-GFP or AtRCD1_allA-GFP were excised and used for confocal microscopy assay to assess possible variations in the subnuclear localization of the transiently expressed proteins. The experiment was repeated three times with similar results (63x magnification, n> 7. Scale bar = 5μm).

Altogether, the findings presented above seemed to suggest that the generated mutations at the phosphorylation sites T204, S230, S231, T239, S242, S244, T257, S263 determined a shift in the localization of RCD1 in shape-defined nuclear bodies. Furthermore, these modifications influenced the co-localization of RCD1 with PPK1, especially when the lack of phosphorylation was mimicked by the substituted alanine residues (RCD1_CA, RCD1_CA.2 and RCD1_allA).

The same experimental procedure was used to test whether the RCD1 phospho-mutant constructs presented any modification in the previously assessed co-localization of the wild type protein with PPK3 (see **Figure 3.4** and **Figure 3.30**, **3.31**). In this case, all of the different constructs, transiently expressed in *N. benthamiana*, maintained the co-localization with PPK3, although the subnuclear distribution of the mutant proteins differed. In particular, while RCD1_ND (**Figure 3.30**) and RCD1_NA (**Figure 3.31**) presented a subnuclear localization in all respects similar to the one of the wild type protein, the other constructs displayed a less homogeneous and more aggregated distribution. While RCD1_CD and RCD1_allD (**Figure 3.30**) localized in one massive nuclear body, RCD1_CA and RCD1_CA.2 (**Figure 3.31**) localized in more interspersed nuclear bodies, which nevertheless were present in the number of one or few distinct entities. RCD1_allA (**Figure 3.30**) presented a more various localization in the examined nuclei: however, from the analysis of the collected images, it seemed reasonable to conclude that the subnuclear localization of this construct presented an intermediate phenotype between the one of RCD1_NA, with regular round-shaped bodies, and the one of RCD1_CA and RCD1_CA.2 (**Figure 3.31**) construct, presenting a polarized localization in bodies with a less defined shape.

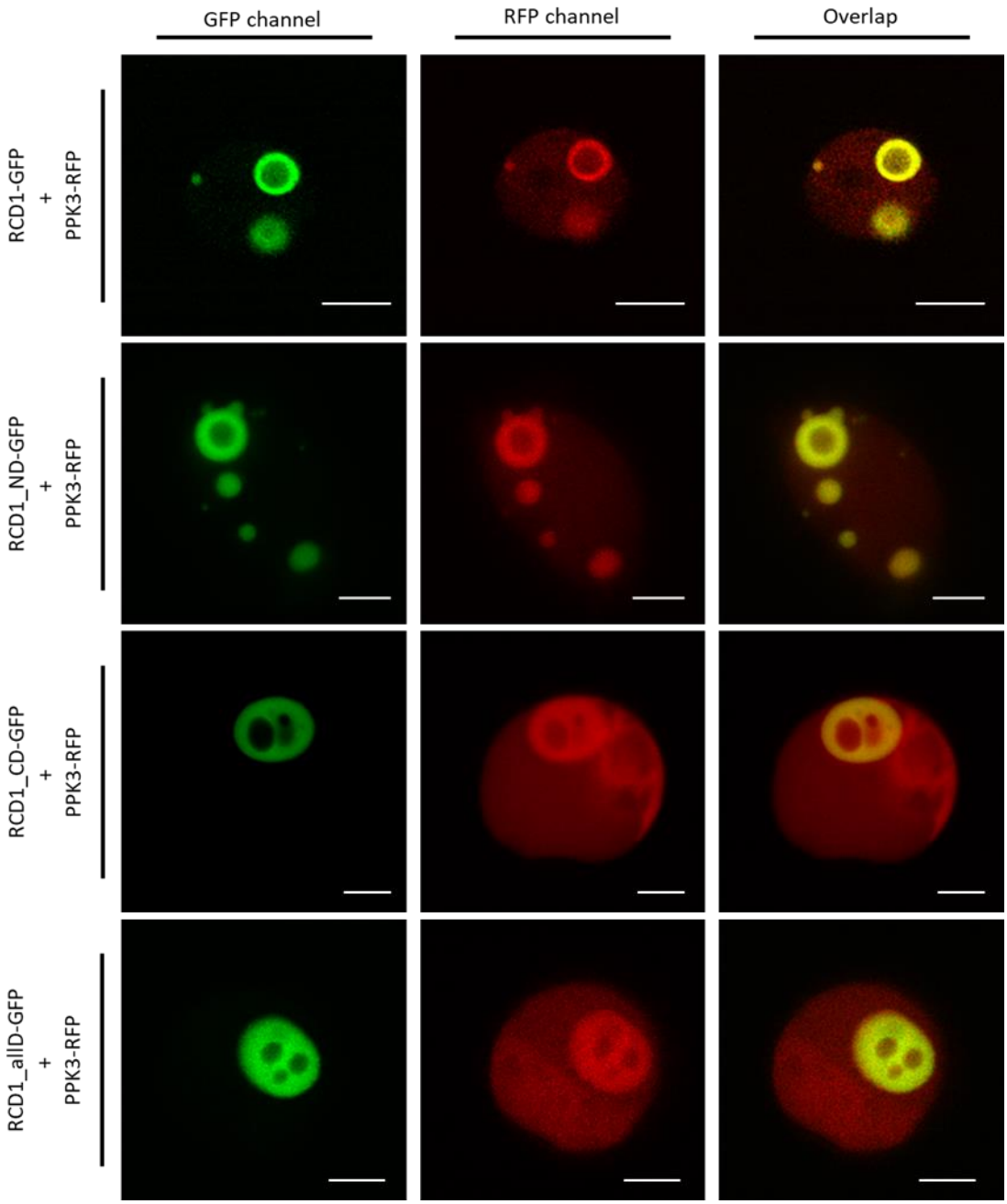

Figure 3.30: Nuclear localization of GFP-tagged *A. thaliana* RCD1 phospho-mutants and PPK3-RFP in *N. benthamiana* leaf tissues. Two days post infiltration (dpi) with *A. tumefaciens* suspensions, leaf discs of *N. benthamiana* co-expressing under CaMV 35S promoter AtPPK3_RFP together with either AtRCD1_GFP, AtRCD1_ND-GFP, AtRCD1_CD-GFP or AtRCD1_allD-GFP were excised and used for confocal microscopy assay to assess possible variations in the subnuclear colocalization of the transiently expressed proteins. The experiment was repeated three times with similar results (63x magnification, n> 7. Scale bar = 5µm).

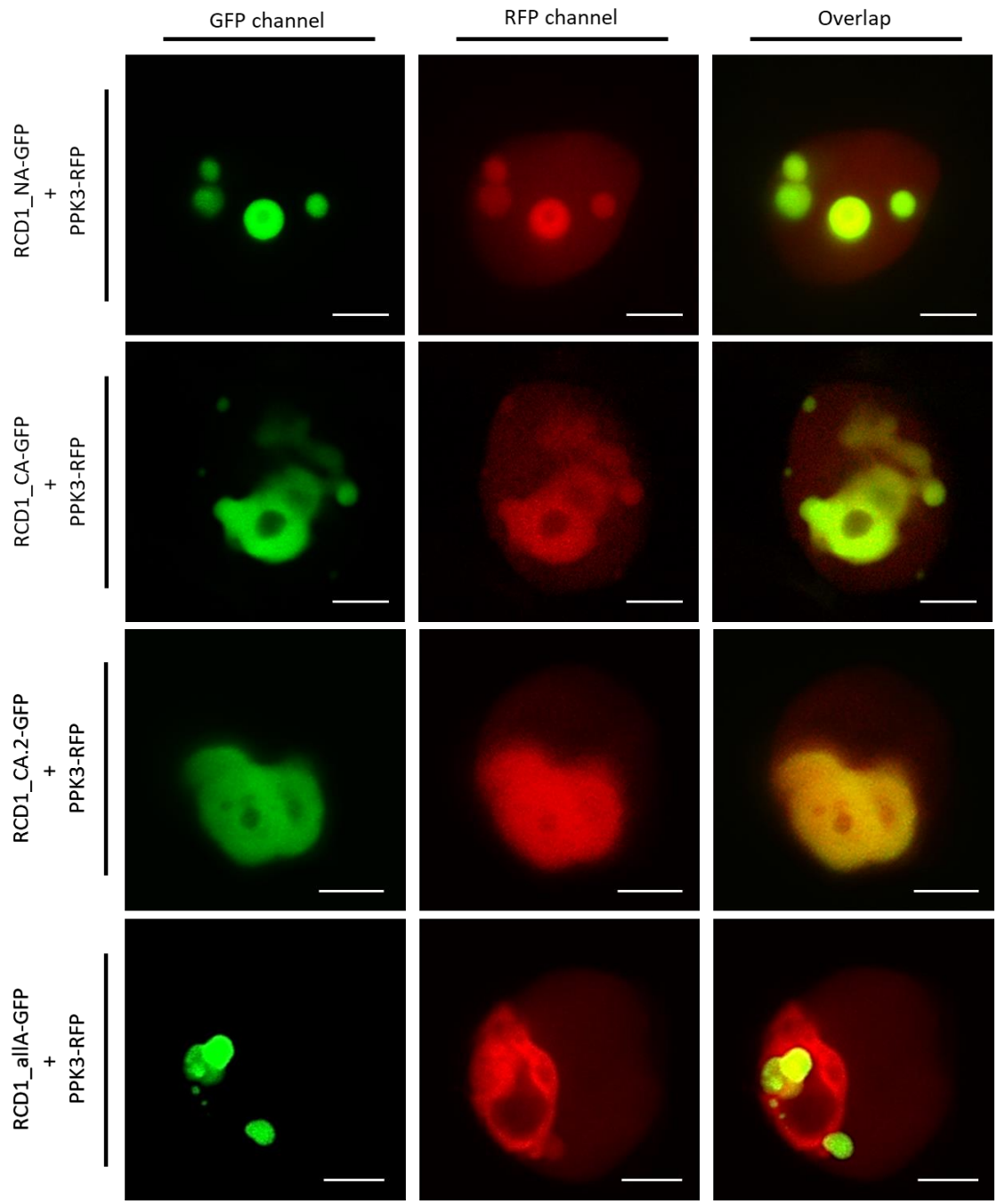

Figure 3.31 Nuclear localization of GFP-tagged *A. thaliana* RCD1 phospho-mutants and PPK3-RFP in *N. benthamiana* leaf tissues. Two days post infiltration (dpi) with *A. tumefaciens* suspensions, leaf discs of *N. benthamiana* co-expressing under CaMV 35S promoter AtPPK3(MLK2)-RFP together with AtRCD1_NA-GFP, AtRCD1_CA-GFP, AtRCD1_CA.2-GFP or AtRCD1_allA-GFP were excised and used for confocal microscopy assay to assess possible variations in the subnuclear colocalization of the transiently expressed proteins. The experiment was repeated three times with similar results (63x magnification, n> 7. Scale bar = 5µm).

When the co-localization between RCD1 phospho-mutant constructs and PPK4 was analysed, it was found that RCD1_ND and RCD1_NA were again localized in round and distinct nuclear bodies, as the wild type, albeit varying for number and size.

On the contrary, PPK4 did not appear to co-localize neither with RCD1_CD, RCD1_allD, nor RCD1_CA, all of which were clustered in one or few bulky bodies in the nucleoplasm.

Finally, RCD1_CA.2 and RCD1_allA presented intermediate localization features: in fact, as shown in **Fig 3.33,** a faint overlapping of GFP- and RFP-signal was still present, indicating that the co-localization is not entirely lost, although the overall appearance of distinct subnuclear bodies was missing, in favour of a series of conglomerated small speckles.

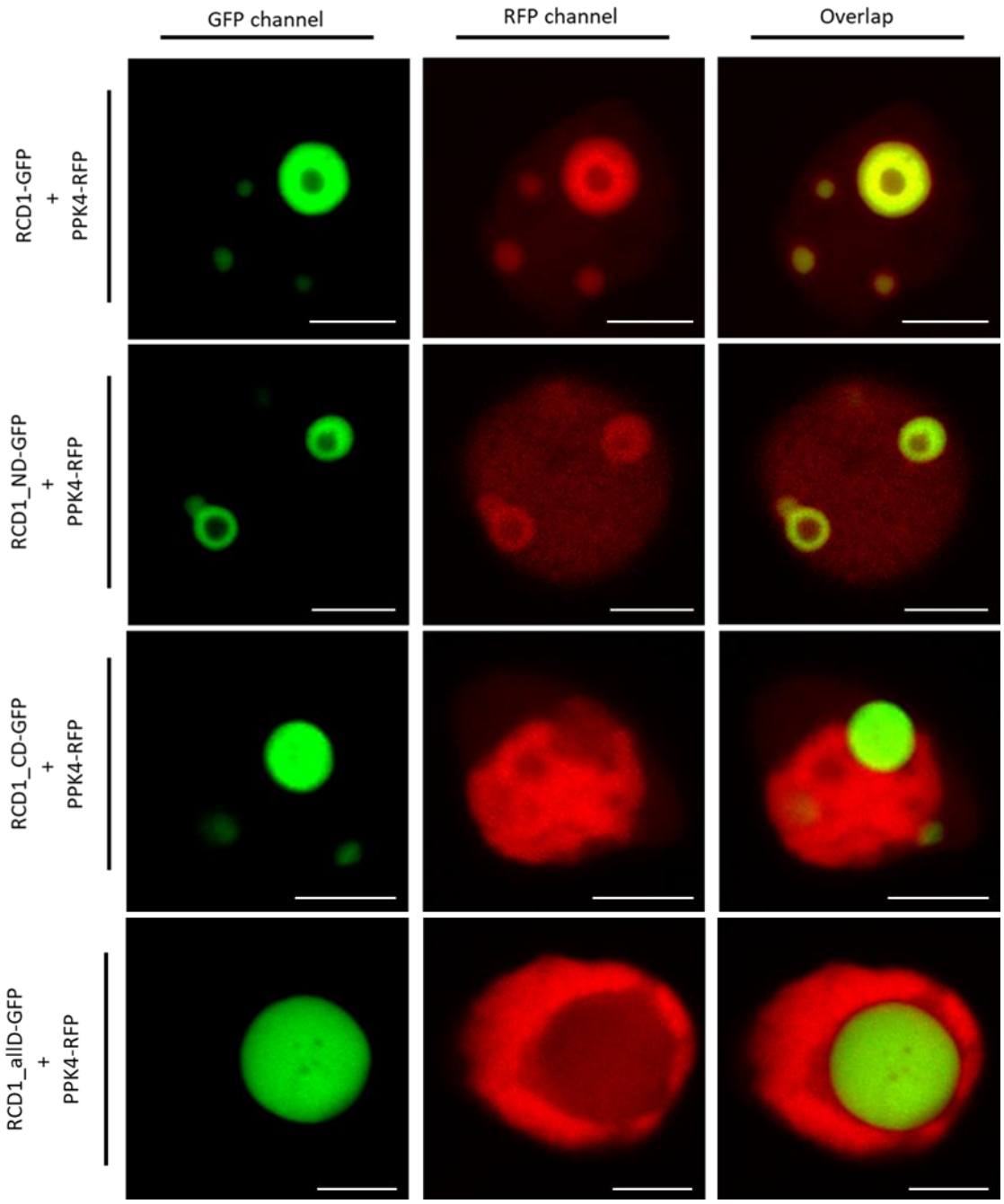

Figure 3.32: Nuclear localization of GFP-tagged *A. thaliana* RCD1 phospho-mutants and PPK4-RFP in *N. benthamiana* leaf tissues. Two days post infiltration (dpi) with *A. tumefaciens* suspensions, leaf discs of *N. benthamiana* co-expressing under CaMV 35S promoter AtPPK4(MLK3)-RFP together with either AtRCD1_GFP, AtRCD1_ND-GFP, AtRCD1_CD-GFP or AtRCD1_allD-GFP were excised and used for confocal microscopy assay to assess possible variations in the subnuclear colocalization of the transiently expressed proteins. The experiment was repeated three times with similar results (63x magnification, n> 7. Scale bar = 5µm).

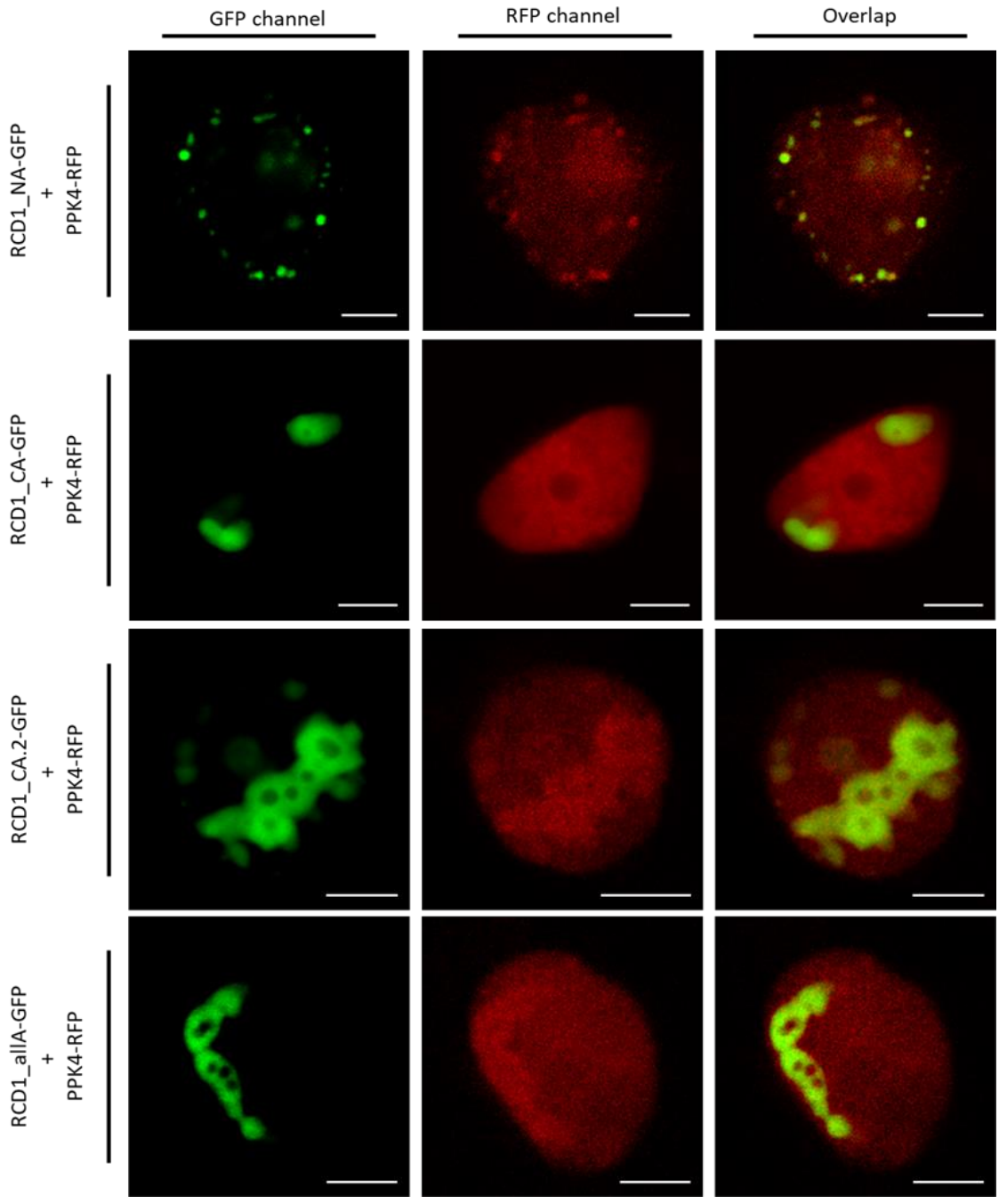

Figure 3.33 Nuclear localization of GFP-tagged *A. thaliana* RCD1 phospho-mutants and PPK4-RFP in *N. benthamiana* leaf tissues. Two days post infiltration (dpi) with *A. tumefaciens* suspensions, leaf discs of *N. benthamiana* co-expressing under CaMV 35S promoter AtPPK4(MLK3)-RFP together with either AtRCD1_NA-GFP, AtRCD1_CA-GFP, AtRCD1_CA.2-GFP or AtRCD1_allA-GFP were excised and used for confocal microscopy assay to assess possible variations in the subnuclear colocalization of the transiently expressed proteins. The experiment was repeated three times with similar results (63x magnification, n> 7. Scale bar = 5µm).

3.1.11 Modifications of phosphorylatable residues on RCD1 do not influence the protein-protein interaction with PPK3 kinase

The confocal microscopy assays to assess the localization of the diverse phospho-mutant constructs of RCD1 with PPK3 showed that this kinase, on the contrary of the other member of its family (PPK1 and PPK4) considered in this work, showed the preservation of the subnuclear co-localization with the RCD1 mutant constructs. However, the co-localization of two proteins did not provide evidence of their interaction, which was tested separately in a co-immunoprecipitation assay (**Figure 3.34**).

In spite of the slight variation of signal amongst the replicates, likely due to the variation of the efficiency during protein transfer, the overall results suggested that the interaction of PPK3 kinase with RCD1 phospho-mutants mainly was preserved, but for the RCD1_CA construct. In fact, this version of RCD1 seemed only to bind weakly the considered PPK3.

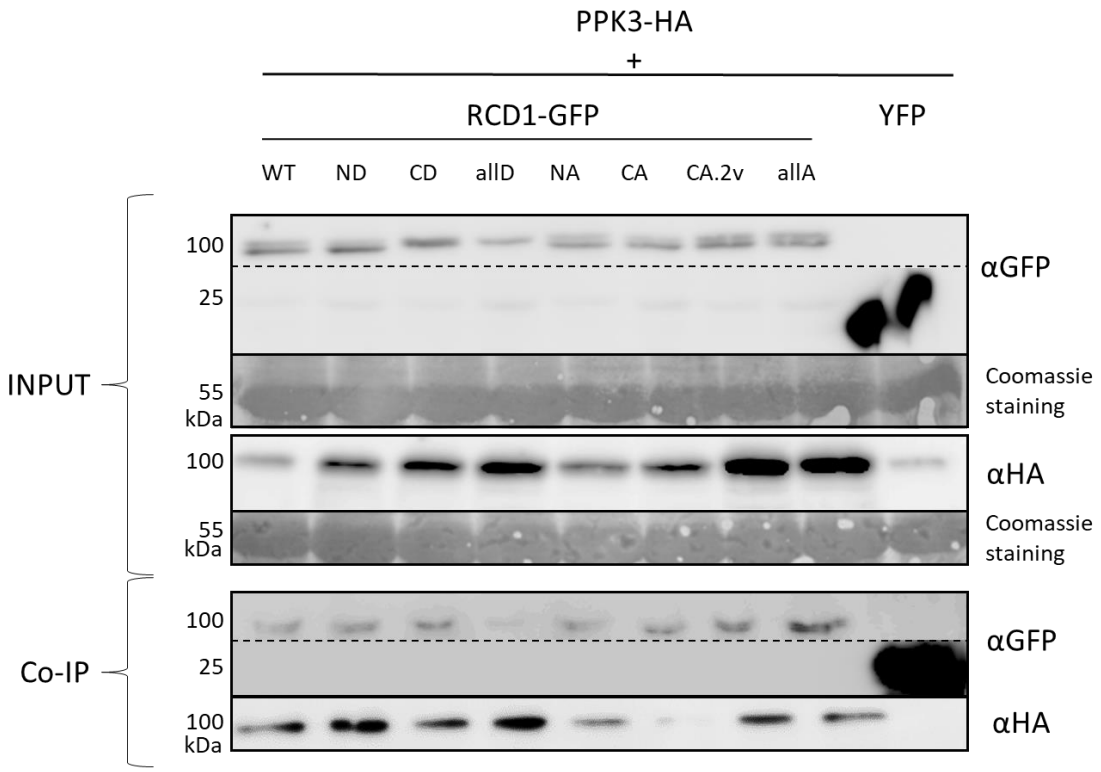

Figure 3.34: Variation in protein-protein binding between *A. thaliana* PPK3 and RCD1 phospho-mutants. Two days post infiltration (dpi) with *A. tumefaciens* suspensions, leaf samples of *N. benthamiana* co-expressing under CaMV 35S promoter AtPPK3-HA together with either AtRCD1-GFP, AtRCD1_ND-GFP, AtRCD1_CD-GFP, AtRCD1_allD-GFP, AtRCD1_NA-GFP, AtRCD1_CA-GFP, AtRCD1_CA.2-GFP or AtRCD1_allA-GFP were collected, and a protein extraction assay was performed on the samples. αGFP-nanobody-tagged magnetic beads were added to half of each protein extract to perform a Co-Immunoprecipitation (Co-IP) of GFP-tagged RCD1 variants and their interactors. Immunoprecipitated and co-purified proteins were detected *via* Immunoblotting with αGFP and αHA antibodies. A leaf sample co-expressing AtPPK3-HA and Yellow Fluorescent Protein (YFP) was processed in the same way and used as a negative control. Coomassie staining of the membranes served as a loading control. This experiment was repeated two times.

3.2 Analysis of a unique RCD1 homologue in *Triticum aestivum* presenting poly-ADP-ribose polymerizing activity

As mentioned in the Introduction section of this work, the family of proteins containing PARP-like domain, known as SIMILAR TO RCD1 (SRO) family, is specific to higher plants (Vainonen *et al.,* 2016). The lack of mono- or poly-(ADP-ribosyl) polymerizing (MAR- or PARP) activity amongst the members of this family has been confirmed in *A. thaliana* (Wang *et al.*, 2011; Jasper *et al.,* 2010). However, in 2014 Liu *et al*. described a homologue of RCD1, TaSRO1 (**Figure 3.35**), found in *Triticum aestivum* cultivar JN177, presenting PARP activity. It was also described that the introgression line of *Triticum aestivum* SR3 presented an allelic variant of *TaSRO1*(*TaSRO1_SR3*), encoding a variant of the protein (TaSRO1_SR3) that displayed an even higher level of PARP activity *in vitro* compared to the wild type.

Upon analysis of three-dimensional modelling results, the enzymatic activity of TaSRO1 was attributed to the catalytic triad Leu^{312}-His^{344}-His^{407}, which resided in a negatively charged pocket, similar to the catalytic site of HsPARP1, AtPARP1 and AtPARP2 (Liu *et al.,* 2014). The increased PARP activity of the protein TaSRO1_SR3 was attributed to two allelic variations that encoded two amino acid mutations (G250V and A343T), allowing a better DNA binding and, consequently, a higher PARP activity.

In contrast, the lack of PARP activity of AtRCD1 was imputed to the positive charge of the correspondent pocket, constituted by the unorthodox triad Leu^{333}-His^{365}-Asn^{428}. The observation that TaSRO1, similarly to PARP-inactive AtRCD1, did not conserve in the catalytic triad the tyrosine residue, that, together with the histidine, is necessary to bind NAD^+ in all canonical ADP-ribosyl-transferases (Vyas *et al.,* 2015), led to further investigating the reported PARP enzymatic activity of TaSRO1.

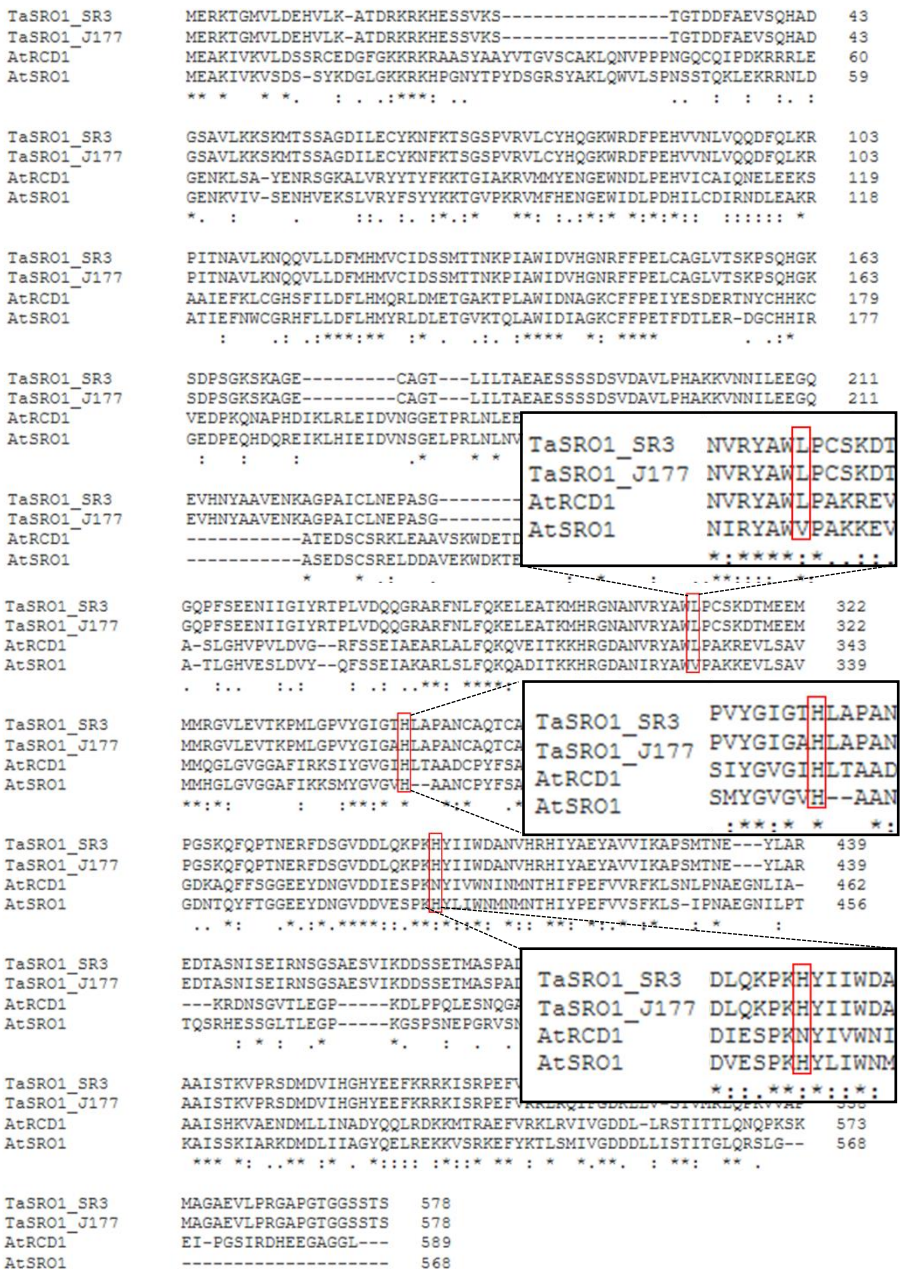

Figure 3.35: Multiple alignment of amino acid sequences of *Triticum aestivum* TaSRO1_JN177, *Thinopyrum ponticum* x *Triticum aestivum* TaSRO1_SR3 and their homologues in *A. thaliana*, AtRCD1 and AtSRO1. The alignment was performed using Clustal Omega (EMBL-EBI) (Sievers *et al.*, 2011). Two panels in the foreground display the magnification of three regions of the alignment where are present the amino acids composing the catalytic triads in TaSRO1_JN177 and TaSRO1_SR3, as well as the corresponding amino acids of AtRCD1 and its closest homologue, AtSRO1 (in red squared frames).

First, the PARP activity of GFP-tagged TaSRO1 was tested *in vivo* and compared to the enzymatic activity of AtPARP2-GFP. The coding DNA sequence (CDS) of TaSRO1 was cloned via Gibson assembly from the pET24a_TaSRO-His, courtesy of Dr. Guangmin Xia (Shandong University, Jinan, China) and published in Liu *et al.* (2014), into a pENTRD_Topo vector. After sequencing, the assembled plasmid was used as an entry vector in an LR reaction with the Gateway compatible destination vector pK7FWG. The resulting pK7FWG_TaSRO1_GFP expression vector was transformed into *A. tumefaciens* strain GV3101 and used to induce transient expression of the protein of interest in *N. benthamiana* leaf tissues.

The protein extract of the infiltrated leaves expressing TaSRO1_GFP was split into two fractions, added with 15µL of magnetic beads coupled with αGFP-nanobody, for co-immunoprecipitation purposes. NAD^+ at the final concentration of 0.3 mM was added to one of the two fractions. All the samples were incubated at room temperature on a rotating wheel to allow the polymerization of poly-ADP-ribose (PAR) chains.

The same procedure was performed on *N. benthamiana* leaves transiently expressing either AtPARP2-GFP, free YFP or a non-infiltrated sample, the last two as positive and negative controls, respectively. All the samples were loaded onto two polyacrylamide gels (9%) and, after the SDS-PAGE assay, an immunoblot was performed, using αMAR/PAR and αGFP antibodies to detect the presence of the proteins of interest and the ADP-ribosyl moieties.

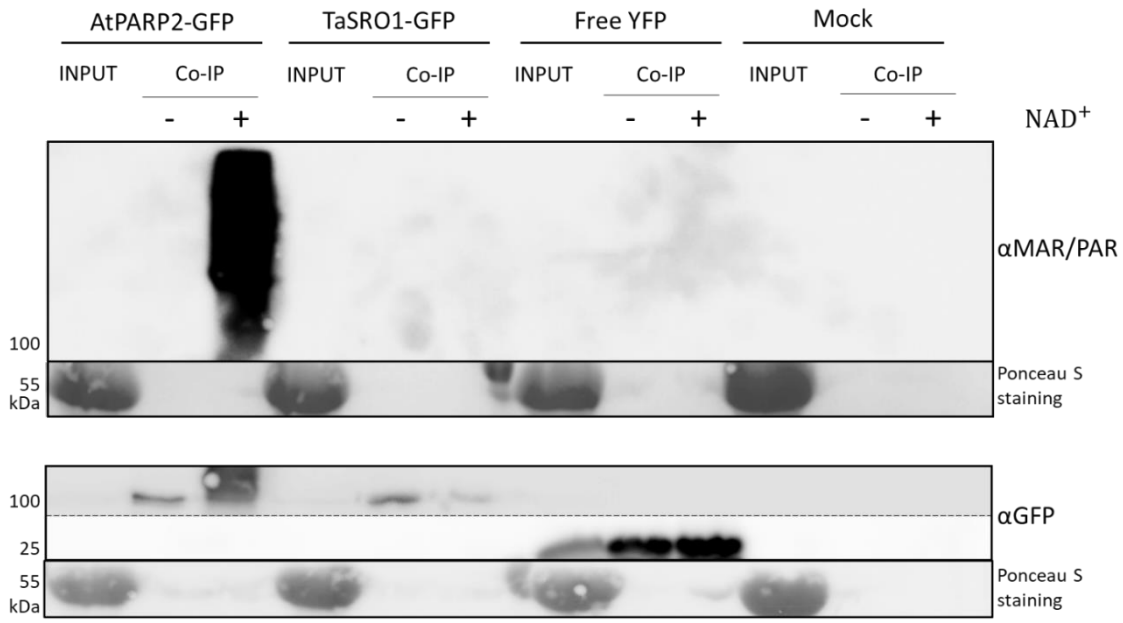

Figure 3.36 Polymerization of MAR and PAR occurs upon the addition of NAD^+ in the presence of AtPARP2, but not TaSRO1. Two days post infiltration (dpi) with *A. tumefaciens* suspensions, leaf samples of *N. benthamiana* transiently co-expressing under CaMV 35S promoter *A. thaliana* PARP2-GFP, *Triticum aestivum* TaSRO1-GFP, free YFP or untreated leaf were collected, and a protein extraction was performed. αGFPnanobody-tagged beads were added to half of each sample and used to perform the immunoprecipitation assay. Each IP sample was further split into two reaction tubes, one of whose was added with NAD^+ to a concentration of 0.3 mM. The results of the IP assay were assessed *via* Immunoblotting with αMono- and αPoly-ADP-ribose moieties (αMAR/PAR) and αGFP. All the samples were loaded on two different membranes in the same order to avoid cross-contamination of signals during detection. Ponceau S staining of the membranes was used to assess the even loading of the samples. Non infiltrated leaves samples were used as an additional negative control to check for possible aspecific signals from secondary antibody cross-reactivity. (n=3 biological replicates).

As shown in **Figure 3.36**, the presence of mono-(ADP-ribosyl) moieties and poly-(ADP-ribosyl) chains (MAR and PAR) was retrieved only in the immunoprecipitated fraction containing AtPARP2-GFP added with NAD^+, which performed a reaction of auto-PARylation on itself. The auto-modification of specific glutamate residues is a common feature of PARP enzymes, both in plants and in mammals (Rissel and Peiter, 2019). In contrast, none of the fractions containing TaSRO1-GFP displayed signs of the presence of MAR or PAR modifications.

In order to test *in vitro* the PARP enzymatic activity of TaSRO1, the inducible vector pET24a_TaSRO1-His was transformed into three different *E. coli* strains (BL21, SoluBL21 and Shuffle). Several tests were performed for obtaining small-scale expression of TaSRO1-His (65.1 kDa ca.), upon Isopropyl-β-D-thiogalactoside (IPTG) induction. However, it was not possible to detect a corresponding protein band on the polyacrilamide gels after SDS-PAGE assay, using the protein extracts and Instant Blue gel staining, nor was TaSRO1-His detectable via immunoblotting using the αHis antibody (**Figure 3.37**). As a positive control, an *E. coli* Shuffle strain expressing the PARP domain of TaSRO1 (I246 to G453, 24.6 kDa, provided by Dr. Wirthmüller) was used. Upon small-scale culture and IPTG induction, this strain was able to synthesize the protein of interest, His-tagged, in a soluble form (**Figure 3.37**), necessary for further *in vitro* experiments. This result was attested both via polyacrylamide gel staining with Instant Blue solution and via immunoblot with αHis antibody after performing a Western Blot assay.

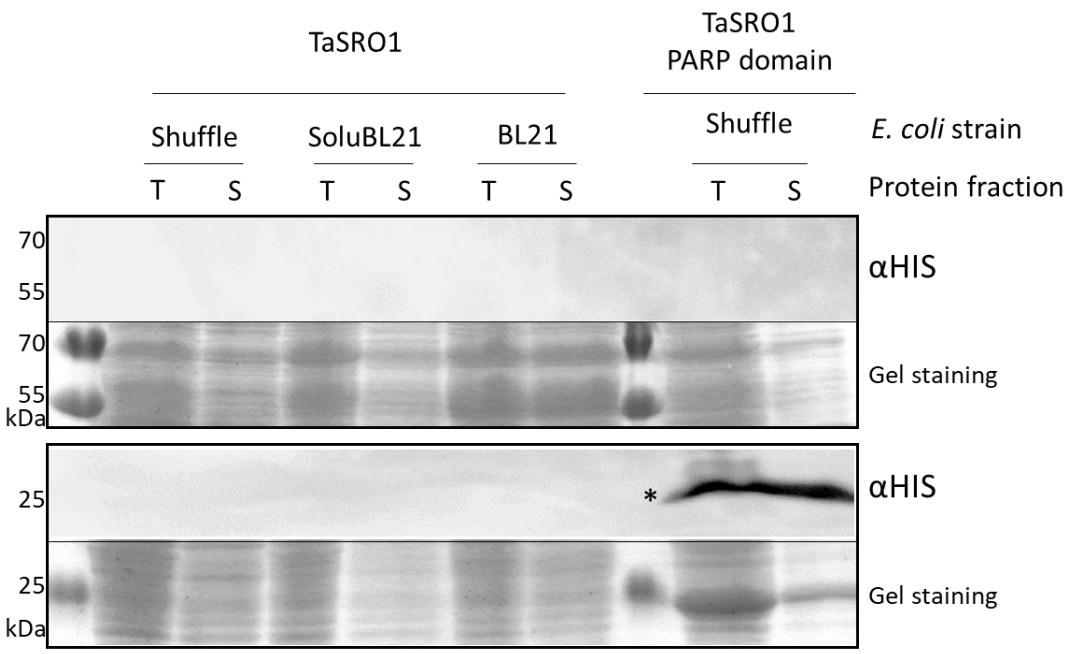

Figure 3.37: Inducible expression on small-scale in different *E. coli* strains of TaSRO1-His and of TaSRO1_PARP-His in *E. coli* Shuffle. After 16h from the expression induction of the protein of interest by adding of 0.5Mm IPTG, the cell suspensions were centrifuged, and the cell pellet of each strain was used to extract total (T) and soluble (S) protein fractions. After boiling with SDS loading buffer, all the samples were loaded in the same order on two polyacrylamide gels (9%) for SDS-PAGE. One of the gels was stained with Instant blue staining solution, and the other was used for Western Blot assay and immunodetection of His-tagged proteins. (n=3 independent replicates; T= total protein fraction; S= soluble protein fraction; asterisk (*) indicates TaSRO1 PARP domain signal upon immunoblot detection).

The *E. coli* Shuffle::pOPIN-F_TaSRO1_PARP-His was, hence, used to produce on a large-scale the PARP domain (246-453 aa) of TaSRO1, which was subsequently purified and used to perform Thermal stability assay (Methods 2.6.1). The thermal stability assay allowed to assess the ability of the TaSRO1 PARP domain to bind the PARP inhibiting compound 6-(5H)-phenanthridinone (6(5H)-PHE, Wahlberg *et al.*, 2012). Upon binding to this chemical compound, the protein of interest was expected to be stabilized against the unfolding process due to constant temperature increases. As a positive control, it was used the PARP domain of *H. sapiens* PARP1 (HsPARP1, 661-1014 aa), with a mutated residue (L713F), which allowed the domain to be constitutively active. The clone pET28_HsPARP1_PARP(L713F), used for large-scale protein expression, was courtesy of Dr. Langelier (University of Montréal, Montréal, Canada). The purified PARP domains of TaSRO1 and HsPARP1 were tested at increasing concentrations of 6(5H)-PHE, starting from 25 nM to 2.5 mM. It was expected that, upon increasing the

amount of available 6(5H)-PHE, its stabilizing effect on a binding protein would have led to an increased melting temperature, which was assessed via the measurement of the emissions of the fluorescent dye, SYPRO Orange. This dye unspecifically binds hydrophobic regions of proteins: because of this feature, the binding of the dye to the protein and the consequent fluorescent emission were only expected upon protein unfolding, which causes the exposure of the hydrophobic and, typically, inner portions of proteins. The variations in the detected fluorescent signal along with the increase of the temperature constituted the melting curves of the protein, and the peak of each curve represents the maximum of fluorescence, corresponding to the melting temperature of the protein for each concentration of the binding molecule.

As shown in **Figure 3.38**, the expected increase in melting temperature upon increased concentrations of the 6(5H)-PHE compound was observed when testing the PARP domain of HsPARP1, but not for the PARP domain of TaSRO1. In fact, curve peaks of the TaSRO1 PARP domain corresponded to a melting temperature of ca. 42 °C, without any noticeable shift due to the increasing stabilization effect at higher concentrations of the binding molecule. This result gave a further indication that the incapability of TaSRO1_PARP to bind the PARP inhibitor 6(5H)-PHE could result in overall inability of binding NAD^+ itself, hence determining the domain to be catalytically inactive.

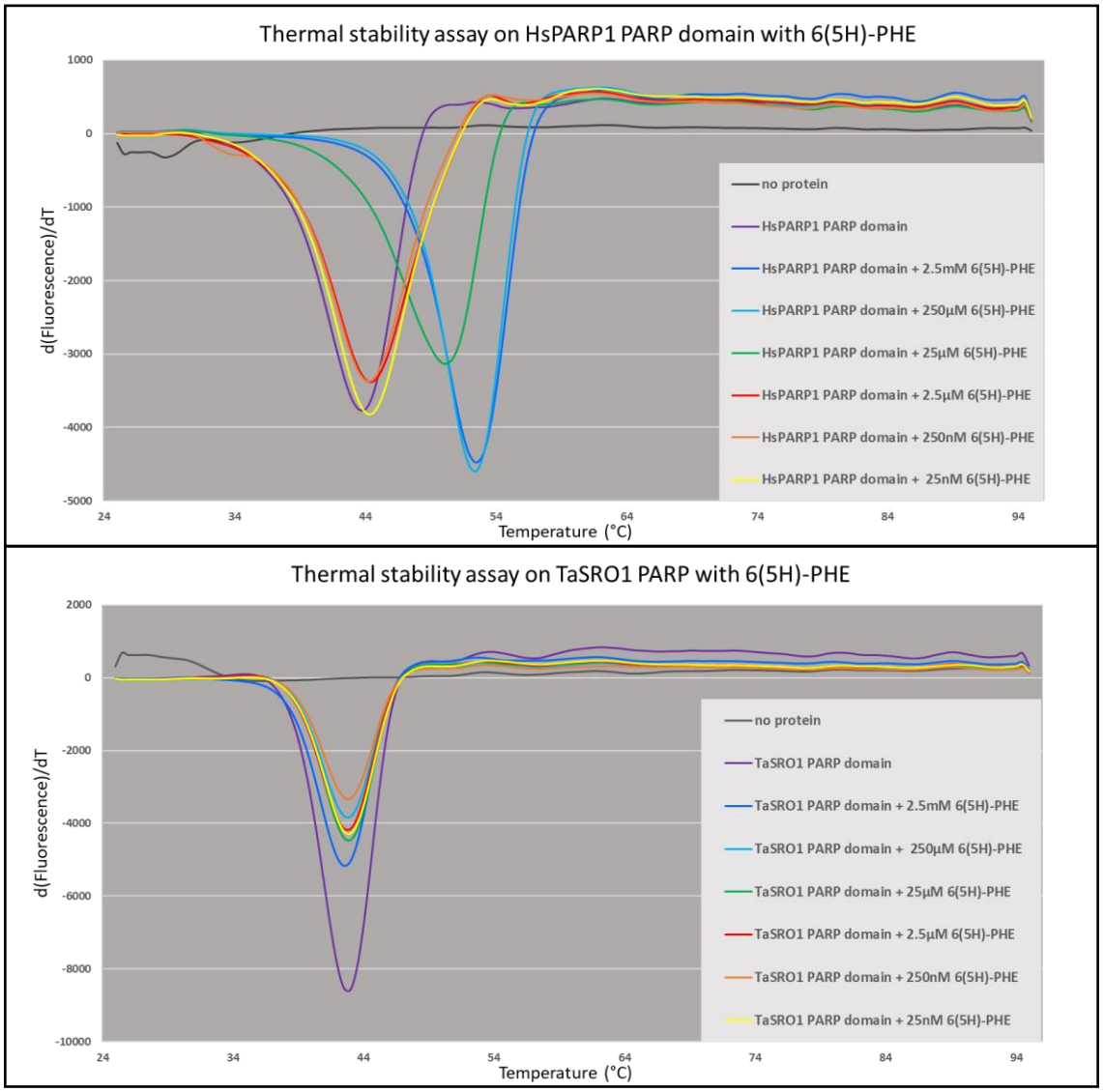

Figure 3.38 Thermal stability assay on PARP domain of HsPARP1 and TaSRO1 in the presence of PARP inhibitor 6-(5H)-phenanthridinone (6(5H)-PHE). After large-scale expression, extraction and purification, the proteins of interest were placed in separate multi-well plates, at the final concentration of 0.01 µg/µL per well. Increasing concentrations of 6(5H)-PHE were added between 25 nM and 2.5 mM, as well as equal amounts of SYPRO Orange, buffer and water up to 25 µL per well. Three technical replicates were set per each condition, and mean values were used for the curves on the graphics (n=3 independent replicates).

The aforementioned thermal shift assay and the same experimental procedures were used to assess the interaction of TaSRO1 PARP domain with both 3-aminobenzamide, a PARP inhibitor sharing steric similarities to the NAD^+ molecule (Purnell and Whish, 1980), as well as the PARP enzymatic substrate nicotinamide adenine dinucleotide

(NAD^+) itself, in order to gain further insight into the ability of the protein domain of interest to bind this class of compounds.

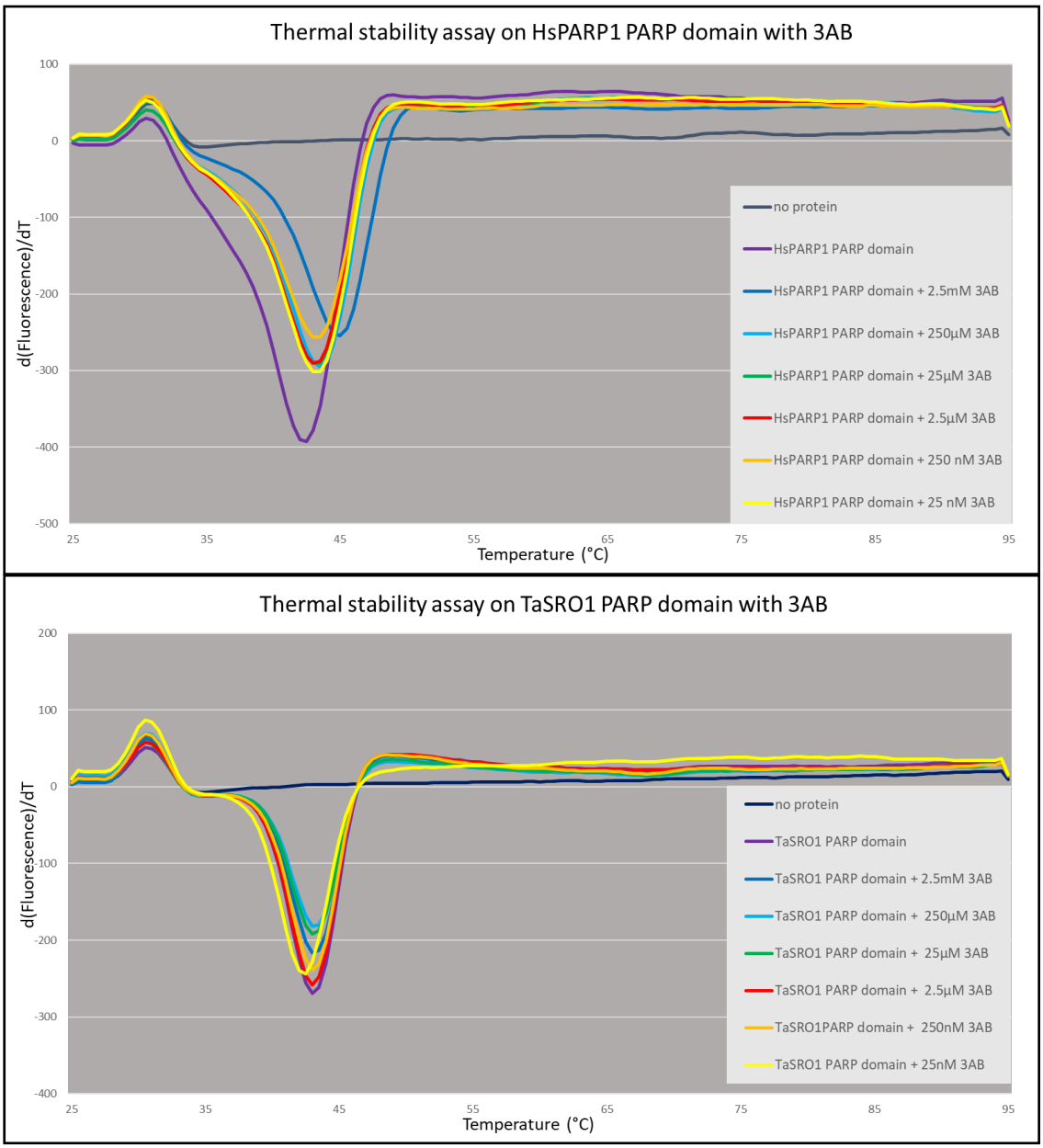

Figure 3.39: Thermal stability assay on PARP domain of HsPARP1 and TaSRO1 in the presence of PARP inhibitor 3-aminobenzamide (3AB). After large-scale expression, extraction and purification, the proteins of interest were placed in separate multi-well plates, at the final concentration of 0.01 µg/µL per well. Increasing concentrations of 3-aminobenzamide (3AB) were added between 25 nM and 2.5 mM, as well as equal amounts of SYPRO Orange, buffer and water up to 25 µL per well. Three technical replicates were set per each condition, and mean values were used for the curves on the graphics (n=2 independent replicates).

In the upper panel of **Figure 3.39**, is displayed how the PARP inhibitor 3AB, upon binding with the PARP domain of HsPARP1 and especially at the highest concentration of the inhibiting compound tested, influenced the melting temperature (T_m) of the protein, while stabilizing the tertiary structure and hence the overall unfolding process, in comparison to the T_m displayed by the protein in the absence of the inhibitor.

In contrast with the results obtained for HsPARP1, the PARP domain of TaSRO1 (**Figure 3.39,** lower panel) was not affected by the presence of the PARP binding molecule 3AB, even at the highest concentration, hence presenting a constant T_m (around 42.5 °C). The lack of shifting in the peaks of the melting curves for the PARP domain of TaSRO1 in the presence of the NAD^+ (**Figure 3.40**) gave the further indication that this region of TaSRO1 might not be able to bind NAD^+ molecules and, hence, might lack MAR- and PARylating activity. Since NAD^+ is the natural substrate for PARP enzymes, binding this molecule is an indispensable feature for enzymatically active PARP proteins in order to catalyze the mono- or poly-ADP-ribosylation reaction. In turn, the PARP domain of Hs PARP1 presented a shift in the peak of the melting curves, as expected, although only at higher initial concentrations of NAD^+. However, this result was not at all surprising due to the fact that the L713E mutation determined the tested protein to be constitutively active. Hence, it was expectable that, for the lower concentrations of substrate, the enzymatic reaction would have consumed all the available NAD^+ before the beginning of the assay. In this case, the binding compound could not stabilize the tertiary structure of the protein and produce a shift in the melting curves. For this reason, in this assay, an additional higher concentration of substrate was taken into account (25mM), due to the expected high rate of catalytic activity of the PARP domain, so to make sure that at least for the higher [NAD^+], the shifts of the melting curve peaks would still be appreciable.

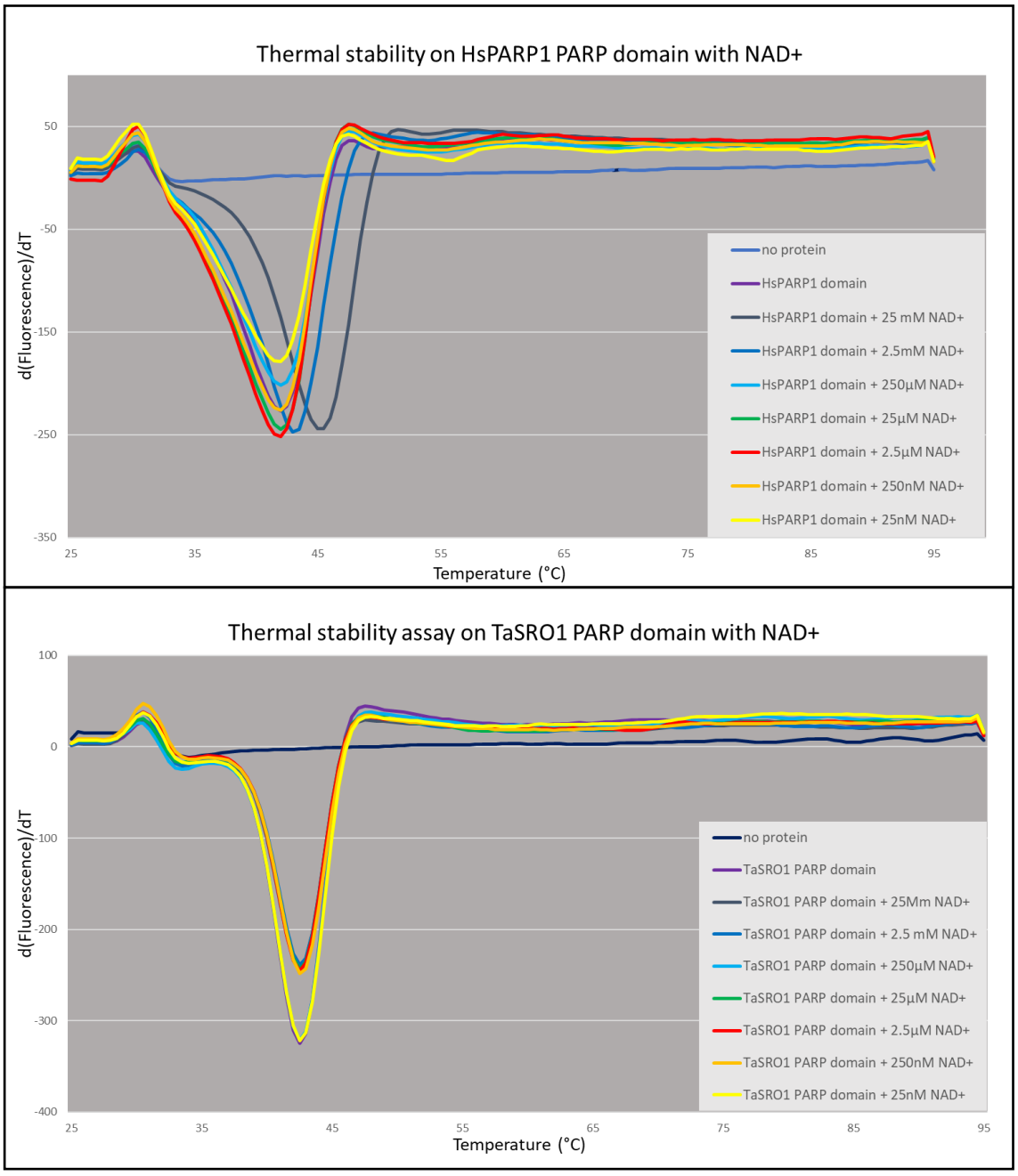

Figure 3.40: Thermal stability assay on PARP domain of HsPARP1 and TaSRO1 in the presence of PARP substrate nicotinamide adenine dinucleotide (NAD^+). After large-scale expression, extraction and purification, the proteins of interest were placed in separate multi-well plates, at the final concentration of 0.01 µg/µL per well. Increasing concentrations of nicotinamide adenine dinucleotide (NAD+) were added between 25 nM and 25 mM, as well as equal amounts of SYPRO Orange, buffer and water up to 25 µL per well. Three technical replicates were set per each condition and mean values were used for the curves on the graphics (n=2 independent replicates).

3.2.1 TaSRO1 PARP domain purification and crystal plating for structural studies

The chemical features and the three-dimensional disposition of the amino acids in a peptide are essential to determine the functionality of the resulting protein. Hence, the structural study of residues of a possible catalytic site is a valuable tool to determine whether the protein of interest has enzymatic activity. The NAD^+ binding pocket, which is conserved in all the catalytically active human PARP, presents a well-characterized catalytic triad: Histidine-Tyrosine-Glutamate (H-Y-E). Histidine residue binds to the 2′-OH of NAD^+ adenine-ribose and substitutions that interfere with the binding of NAD+ were found in catalytically inactive HsPARP9 and HsPARP13 (Vyas *et al.*, 2015). Tyrosine residue stacks with the nicotinamide ring (Steffen *et al.*, 2013), while Glutamate forms a hydrogen bond with the 2′-OH of the nicotinamide ribose, hence polarizing the donor molecule NAD^+ for nucleophilic attack (Ruf *et* al.,1998). In nature, replacements of Glutamate residue by Leucine, Isoleucine, Tyrosine, Valine or Threonine have been observed in HsPARPs, although these variations determined these enzymes to be only mono(ADP-ribose) transferases in vitro (Barkauskaite *et al.,* 2015).

Due to the substantial differences observed in the chemical features of the catalytic triad of TaSRO1 identified by Liu *et al.* (2014), in comparison to the classic triad (H-Y-E) present in the most well-known human PARP enzymes, it seemed reasonable to attempt to determine the three-dimensional structure of TaSRO1 PARP domain via X-ray crystallography, to gain further insight on its enzymatic activity. The objective was to obtain data on the 3D model of the domain and to assess whether the resulting tertiary structure would be compatible with the binding of the NAD^+ molecule in the catalytic pocket, possibly via a non-canonical catalytic triad, that, in spite of the variations in the chemical nature of the residues, could still allow the formation of the specific non-covalent bonds necessary for the interaction with the substrate.

In order to produce the crystals suitable to be subjected to X-ray diffraction, chemo-competent cells of *E. coli* Shuffle strain were transformed with pOPIN-F_TaSRO1_PARP-His_sv vector for bacterial expression, encoding a 20 amino acid shorter version of the PARP domain of TaSRO1 used in the previously described thermal stability assay, under IPTG inducible promotor. The need for cloning a slightly shorter version of the construct of interest was due to the fact that the coiled conformation of this portion of the protein could represent an obstacle to the crystallization process. The resulting strain was used to start a large-scale bacterial culture and, after inducing the expression of the protein of interest, the extraction of the total protein fraction was performed, followed by the purification, using

Immobilized Metal Affinity Chromatography (IMAC) combined with Size Exclusion Chromatography (SEC) (Methods 2.5.8). A second purification step was performed after removing the His-tag of TaSRO1_PARP_sv upon 3C protease treatment. The initial step of condition screening was conducted by Dr. Wirthmüller, at Professor Wahl Laboratory (FU Berlin). After analysing the results, it was chosen to use 1M MES (2-(N-morpholino) ethanesulfonic acid) buffer (pH 5.8), added with 0.2 M ammonium sulfate and variable percentages of polyethylene glycol 3350 (PEG3350, 14, 16, or 18%), in order to recreate the optimal condition for the formation of crystals, via sitting-drop vapor-diffusion method (McPherson & Gavira, 2013). After manual setting of several plates and after the nucleation phase, protein crystals began to form (**Figure 3.41**), but none was stable enough to be removed, while still intact, with nylon loops from the crystallization drops and used for diffraction pattern testing.

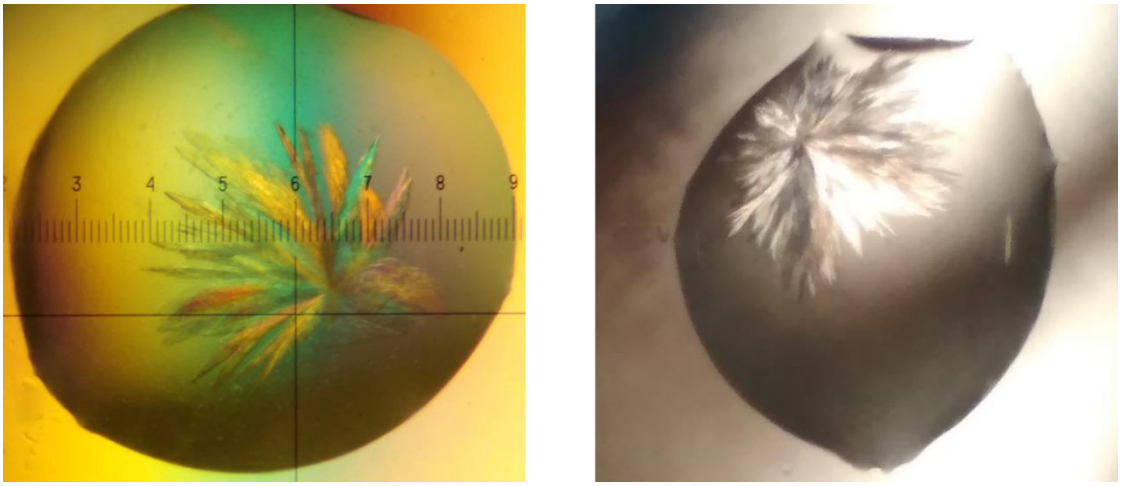

Figure 3.41: Protein crystals of TaSRO1 PARP-sv domain. The pictures display the variety of crystals that can be obtained in protein crystal growth assay. Pictures were taken with a digital camera coupled to an optical microscope (20x magnification).

At the same time, a different approach to the resolution of the three-dimensional structure of TaSRO1 PARP domain was pursued. The induction and the expression of the protein of interest were carried out in *E. coli* culture on M9 minimal medium, supplemented with Seleno-Methionine (SeMet) (Methods 2.5.7), a naturally occurring amino acid carrying a Selenium atom on its side chain. The crystals resulting from plating the SeMet labelled protein were intended to be used for X-ray crystallography via single-wavelength anomalous diffraction (SAD) (Hendrickson *et al.*, 1990) in order to obtain diffraction data that could be more easily interpretable. However, it was decided in favour of the shortened version of TaSRO1 PARP domain, labelled with Seleno-Methionine, to proceed with the subsequent steps in the study of its structural features.

4 Discussion

In this work, two members of the plant-specific SRO protein family, AtRCD1 and TaSRO1, were characterized using a biochemical approach. On the one hand, the role of the N-terminus of AtRCD1, including the WWE and the linker region between the latter and the PARP domain, was studied in relation to its protein-interacting feature, as well as to the possible functions of the identified phosphorylation sites. On the other hand, the study of the PARP domain of TaSRO1, previously reported to be catalytically active (Liu *et al.*, 2014), did not confirm the published findings.

4.1 The subnuclear localization and oligomerization of AtRCD1 rely on the integrity of its N-terminus

AtRCD1 has been previously studied for its involvement in several molecular mechanisms in the plant cell, such as the vegetative development (Teotia & Lamb, 2009) or transcription of ethylene- (ET-) and abscisic acid- (ABA-) regulated genes (Alhfors *et al.*, 2004). The diversified implications of the findings regarding the function of RCD1 have not allowed, yet, to hypothesize a coherent model that includes all the aspects of the molecular pathways in which this protein is involved.

First of all, in respect to RCD1 localization, data provided in different publications suggest a bivalent localization of the abovementioned protein, depending on the osmotic conditions applied to the systems taken into account. Initially, Katiyar-Agarwal *et al.* (2006) identified RCD1 as an interactor of Na^+/H^+ antiporter SOS1, via a yeast-two-hybrid screening: evidence was shown of translocation of RCD1 from the nucleus, where two out of its three supposed Nuclear Localization Signals (NLSs) initially direct the protein, to the plant cell periphery, upon salt and oxidative stress treatment, where RCD1 interacted with SOS1, independently of the WWE domain. Whilst this shift in RCD1 localization was tested both in transient expression in protoplast and in stable-line transformed seedlings, the following study of Jaspers *et al.* (2009) showed that transiently expressed RCD1 and its closest homologue, SIMILAR TO RCD1 (AtSRO1), were exclusively localized in nuclei of onion epidermal cells. In 2021, Vainonen *et al.* showed that the RCD1*nls*-HA line did not complement the development- and stress-related phenotypes of the *rcd1* knockout.

In this work, the subnuclear localization of RCD1 was further investigated. Upon transient expression of GFP-tagged RCD1, the fluorescent signal was only evident in the nucleus of the transformed cells in the examined leaf tissue of *Nicotiana benthamiana*.

The expression of RCD1 under transcriptional control of the constitutively active CaMV 35S promotor was chosen due to the low level of expression of the *RCD1* gene under its native promotor in untreated *A. thaliana* Col-0 wild type plants (**Figure 3.18**) to ensure detectable levels of fluorescent signal. Furthermore, the study of the subnuclear localization of transiently expressed RCD1-GFP revealed the presence of peculiar round-shaped bodies, henceforth named "speckles". Whilst it might be argued that the formation of these aggregates inside the nuclei could be an artefact due to the high levels of the heterologous protein, it is worth stressing that the concomitant overexpression of RFP did not produce the same effect. Hence, it seems licit to infer that the formation of the speckles is specific to RCD1.

However, the subnuclear localization of RCD1 in speckles was lost when expressing a mutant version of the protein, lacking the N-terminal end (1–265 aa) of RCD1 (**Figure 3.1**). This mutated version of RCD1 showed an even distribution throughout the nucleus, in which it was still localizing due to an additional heterologous NLS. The deleted region in the RCD1-NLS-ΔNter-YFP protein consisted of the initial portion containing the endogenous NLSs (1–49 aa), the WWE domain (50-151 aa) and the linker region between the WWE domain and the PARP domain (151-265 aa). In order to further narrow down the exact portion of RCD1 responsible for the formation of the speckles, three RCD1 clones, the full-length version and two mutated constructs, lacking either the WWE domain or the PARP domain (304–442 aa), were transiently expressed in *N. benthamiana* leaf tissue. Whilst the full-length protein was still located in speckles of varying number and size, the other two mutant variants differed in their subnuclear localization (**Figure 3.2**). On the one hand, the RCD1-ΔWWE construct failed to form shape-defined speckles, and the fluorescent signal was interspersed throughout the nucleus. On the other hand, while RCD1-ΔPARP still localized in round speckles, the size and the number of these bodies differed clearly from the full-length construct, presenting less numerous nuclear bodies and of a higher surface, occupying the majority of the imaged nuclei sections. This finding might suggest that the PARP domain acts as a regulative domain of the WWE domain function of protein-protein interaction and aggregation. Testing this hypothesis could provide an insight into the function of the RCD1 PARP domain, which, until now, has only been ascertained not to have PARylating activity (Wirthmüller *et al.*, 2018).

Altogether, these results show that the WWE domain at the N-terminus of RCD1 plays a role in mediating protein-protein interaction (Jaspers *et al.*, 2009), as predicted by Aravind (2001) and partially confirmed by Wirthmüller *et al.* (2018), in this specific case amongst RCD1 proteins themselves. The construct lacking this domain almost abolished the formation of aggregates in the nuclei, and the few aggregated bodies

present, although shapeless, might be due to the presence of the linker region between the WWE domain and the PARP domain.

Furthermore, the aforementioned linker region, which together with the WWE domain constitutes the N-terminus of RCD1, has been previously shown to be necessary for the interaction of RCD1 with the oomycete effector HaRxL106 (Wirthmüller *et al.*, 2018). This previous finding supports the hypothesis that the linker region could also play a role in the formation of the speckles, especially if the latter relied on the protein-protein interaction amongst several RCD1 moieties to aggregate. Wirthmüller *et al.* also described that the WWE domain of RCD1 and its closest homologue, AtSRO1, were involved in oligomerization and could interact amongst themselves in yeast-two-hybrid screenings and MS analysis. In this work, the oligomerization of RCD1 and SRO1 was tested and confirmed via Co-IP assays upon transient expression of these proteins in *N. benthamiana* leaf tissues (**Figure 3.11 and 3.12**). It was also shown that the N-terminus of both the aforementioned proteins, including the WWE domain and the linker region, is sufficient for allowing the homo-oligomerization of RCD1 and SRO1, which was lost when this region was missing.

Furthermore, the WWE domain and the linker region of RCD1 interact with *A. thaliana* PHOTOREGULATORY PROTEIN KINASES (AtPPKs) (Wirthmüller *et al.*, 2018). The PPK family members are serine/threonine kinases localized in the nucleus, where they were shown to phosphorylate several target proteins, such as the CRYPTOCHROME 2 PHOTORECEPTOR (CRY2) and PHYTOCHROME INTERACTING FACTOR (PIF3) (Liu *et al.*, 2017; Ni *et al.*, 2017).

In this work, the subnuclear localization of the Arabidopsis PPK1, PPK3 and PPK4 was studied in regard to the peculiar subnuclear localization of RCD1 itself. Interestingly, when the abovementioned PPKs were transiently expressed together with free YFP, the kinases appeared to be interspersed throughout the nuclei (**Figure 3.3**), but when co-expressed together with RCD1-GFP, the kinases preferentially co-localized with the latter in nuclear speckles (**Figure 3.4**). In addition, when PPK1, PPK3 or PPK4 were transiently co-expressed with the mutated version of RCD1, lacking the N-terminus containing the WWE domain and the linker region, the fluorescent signals from both RCD1 and the PPKs were evenly distributed throughout the nuclei (**Figure 3.7**).

Hence, it was further investigated if specific portions of RCD1 were directly involved in the subnuclear co-localization with the three PPKs. Interestingly, PPK1-RFP, when co-expressed with the RCD1-3V constructs lacking either the WWE domain (80-151 aa) or the PARP domain (304–442 aa), clearly lost the co-localization (**Figure 3.8**), which was conserved when co-expressed with full-length RCD1-3V.

On the contrary, the co-localization between RCD1 and PPK3 was not lost in the absence of either the WWE domain or of the PARP domain (**Figure 3.9**), whereas PPK4 did not show sign of co-localization with RCD1 when co-expressed with the mutant variant lacking the WWE domain (**Figure 3.10**).

Altogether, these results suggest that there could be several residues, distributed both in the WWE and the PARP domain, which are involved in the stabilization of the co-localization of RCD1 and PPKs.

The absence of just one of the two domains, altering the subnuclear localization of RCD1, could also disrupt the spatial distribution of residues needed for the co-localization with PPK1. Hence, it could be hypothesized that the co-localization of PPK1 and RCD1 might rely on the formation of a peculiar tertiary structure in RCD1 in order to happen. In contrast, the co-localization of PPK3 and PPK4 seems to require only the presence of specific sites along the RCD1 sequence but not a specific spatial conformation of the protein itself.

In order to further narrow down the specific sites needed for the co-localization of RCD1 and the abovementioned protein kinases, it could be useful to design additional clones of RCD1, each lacking smaller regions of the WWE and PARP domain and test via confocal microscopy in transiently expressing tissues whether the co-localization with each of the considered kinases was lost or maintained.

Additional supporting evidence was gained from the results of Co-immunoprecipitation (Co-IP) assays of the mentioned PPKs with RCD1 upon *A. tumefaciens*-mediated transient co-expression assay in *N. benthamiana* leaf tissues. As shown in **Figure 3.5**, PPK1, PPK3 and PPK4 co-precipitated together with RCD1-GFP. The same experiment repeated, this time co-expressing only the YFP-tagged N-terminus of RCD1 with the PPKs (**Figure 3.6**), gave the same results. Altogether, these findings confirm that the N-terminal portion of RCD1, including the WWE domain and the linker region (1-265 aa), is sufficient for the interaction of RCD1 with the abovementioned kinases.

The results illustrated in this paragraph seem to support, with localization study and *ex vivo* assays, the hypothesis of the involvement of the N-terminal domain of RCD1 in the subnuclear localization as well as in protein-protein interaction. In fact, further proof was gathered that the N-terminal portion of RCD1 is linked to the homo-oligomerization, as well as the formation of nuclear speckles by RCD1 itself. Furthermore, it was also confirmed that the previously described protein-protein interaction of RCD1 with PPK1, PPK3 and PPK4 is mediated by RCD1 N-terminus.

However, although it was shown that the WWE domain has a primary role in the localization of RCD1 in nuclear speckles, it was not possible to reach the same conclusion in respect to protein-protein interaction or the oligomerization feature of RCD1. Hence, to gain further insight on the mechanism of protein-binding, the Co-IP assay could be repeated using mutated versions of RCD1, either lacking the WWE domain or the linker region, in order to verify whether both of these regions are required for it or, in case only one is needed, which one of two has a prevalent role.

4.2 The N-terminus of AtRCD1 interacts with AtPARP2 independently of the presence of PAR chains

The function of the WWE domain as Poly(ADP)-Ribose (PAR) chains binding domain has been described in animals for the first time (Zhang *et al.*, 2011): in fact, HsRNF146 was reported to bind iso-ADP moieties in PAR chains via its WWE domain. The binding of HsRNF146 WWE domain to iso-ADP moieties was found to be supported by the RING domain present in the same protein, which, while binding together with the WWE the PAR chains, would undergo conformational changes, resulting in catalytic activation of the RING domain itself.

In this work, a first attempt was made to test the hypothesis that the WWE domain of AtRCD1 could act as a binding domain that recognizes the PAR chains (**Figure 3.13**). Using the auto-PARylating AtPARP2 to produce PAR chains (Feng *et al.*, 2015), upon addition of NAD^+, two different constructs of AtRCD1 N-terminus, differing for the presence of the linker region, were tested. Whereas the results of the experimental procedure did not give a clear indication that the PAR binding described for human WWE in HsRNF146 was conserved in RCD1, the results showed that the shorter RCD1 construct, including the N-terminal portion of the protein with the NLS sequence and the WWE domain (1–203 aa), binds to PARP2 irrespectively of the presence of PAR chains. As addressed in the corresponding paragraph of Results section, in only one out of three biological replicates, the longer RCD1 construct, including both the WWE domain and the linker region (1–265 aa), co-immunoprecipitated along with PARP2. This finding did not appear to conflict with the abovementioned data, mainly because of the high degradation rate of RCD1, which has been extensively observed during the experimental procedures presented in this work and that in Vainonen *et al.* (2021) was inferred to be primarily linked to the phosphorylation of several residues identified in this linker region of RCD1, also referred to as Intrinsically Disordered Region 2 (IDR2). Furthermore, in the same article, Vainonen *et al.* (2021) showed via Surface Plasmon

Resonance that the full-length RCD1, unlike the truncated protein lacking the WWE domain, binds PAR chains, whilst did not show to interact with monomeric or cyclic ADP-ribose moieties.

Nevertheless, the finding presented here that RCD1 might interact via its N-terminal portion with PARP2, irrespectively of the presence of PAR chains, does not come along totally unexpected. In 2015, Darosa *et al.*, described that HsRNF146 binds directly to the poly [ADP-ribose] polymerase tankyrase HsTNKS. Hence, it could be argued that the direct interaction between protein presenting a WWE domain and PAR polymerizing enzymes could be conserved both in *H. sapiens* and plants. Indeed, this hypothesis has to be further tested. A localization study *in vivo* via fluorescent tags could provide an indication of whether RCD1 and PARP2 localize in the same nuclear districts. This interaction could also be tested via yeast-two-hybrid (Y2H) assay or *in planta* via Bimolecular Fluorescent Complementation (BiFC) assay performed transiently expressing the proteins of interest in *N. benthamiana*. Additionally, it would be interesting to test whether the N-terminus of RCD1 closest homologue, AtSRO1, showed specific interaction with PARP2, as well. The results of this assay would possibly help to clarify the different functions of the two homologous proteins, or to which extent their role in the plant cell is overlapping, especially considering the high degree of sequence homology that RCD1 and SRO1 present. The specific function of SRO1 in Arabidopsis has not been fully characterized, yet, partially due to the fact that the knockout mutant line of *SRO1* does not share the same strongly impaired phenotype that has been previously observed and thoroughly studied in the *rcd1-1* knockout mutant.

4.3 Alteration of phosphorylation sites affects AtRCD1 function in development and abiotic stress responses

The analysis of the phospho-peptides previously identified by Wirthmüller *et al.* (2018) (**Figure 3.14**) led to the identification of eleven possible phosphorylatable residues on the N-terminal region of RCD1 (1–265 aa) (**Figure 3.15**). In this work, the function of these phosphorylation sites was studied in the generated *A. thaliana* stable lines overexpressing different mutant versions of RCD1. The mutated residues on the RCD1 variants mimicked the presence or the absence of post-translational phosphorylation at the abovementioned phospho-sites respectively through the substitution with Aspartate (D) or Alanine (A), in order to test whether the phosphorylation state of RCD1 influenced its *in vivo* function.

As shown in **Figure 3.16** and **Figure 3.17**, the RCD1 phospho-mutant lines presented a variety of intermediate phenotypes in between the Col-0 wild type and the knockout *rcd1-1* mutant. Six-week-old *rcd1-1* RCD1_NA lines #2.4 and #2.16, carrying four Serine/Threonine to Alanine mutations (S27A, T33A, S36A and T204A), presented comparable leaf shape and size to the wild type, with a slight reduction of the latter, whereas the other examined lines, carrying seven mutated residues (S230, S231, T239, S242, S244, T257, S263 either to Alanine or to Aspartate) exhibited, to different extents, the typical phenotypic features of the *rcd1-1* knockout mutant (Ahlfors *et al.*, 2004). Reduced size of the rosette, downwards curved and discoloured leaves were evident, particularly under long-day growth conditions, in the lines *rcd1-1* RCD1_CA #3.2 and #12.11, *rcd1-1* RCD1_CD #3.1 and #3.6 (**Figure 3.16**). An exception was constituted by the *rcd1-1* RCD1_CD #4.8 line, which, in contrast to the other lines expressing the same mutated variant of RCD1, presented a rosette size and leaf shape comparable to the wild type, both under long- and short-day growth conditions. Furthermore, this line also presented the most abundant transcript level for the *RCD1* gene amongst the tested lines (**Figure 3.18**). It can be argued that the higher transcription level of the transgene in *rcd1-1* RCD1_CD #4.8, corresponding to a higher level of protein in the plant cells, determined the different phenotype that this line exhibited in comparison to *rcd1-1* RCD1_CD #3.1 and #3.6 lines. If we hypothesized that the phosphorylation of the mutated residues influenced the turnover rate of RCD1, the higher level of protein in line *rcd1-1* RCD1_CD #4.8 might effectively restore the wild type phenotype only based on higher protein abundance. The role of phosphorylation in respect to RCD1 *in vivo* function has also been addressed in Vainonen *et al.* (2021): here, the authors proposed that the post-translational modification of the multiple phosphorylation sites on RCD1, located in the linker region, not only affects its functionality but also determines its degradation, possibly via a progressive increase in the phosphorylation levels. This hypothesis, if proven correct, would also explain why the *rcd1-1* RCD1_CA lines, although overexpressing the transgene *rcd1_CA* that prevents any phosphorylation of RCD1 at the mentioned phosphosites, does not restore the wild type phenotype.

It could be argued that the lack of reverted phenotype in the *rcd1-1* RCD1_CA and *rcd1-1* RCD1_CD lines could be due to the absence of translation of the mRNA into the protein of interest or the possibility that the lack of correct protein folding prevents the proteins from being active *in vivo*. To ascertain whether the HA-tagged RCD1 mutant versions were indeed translated, the protein extract from *A. thaliana* leaves of transformed lines was tested via immunoblotting: the signal for RCD1-HA mutant variants was retrieved only in the sample of lines *rcd1-1* RCD1_CD #3.6 and #4.8.

This finding could suggest that the RCD1 mutants in *rcd1-1* RCD1_NA and *rcd1-1* RCD1_CA lines, due to the absence of phosphorylation on the identified phospho-sites, had lower protein stability or, more likely, that the sensitivity of the immunoblotting assay was not sufficient to detect the chemiluminescent signal. Especially in regard to the *rcd1-1* RCD1_NA lines, the reverted phenotype of the plant leaves together with the transcription level analysis for the *RCD1* gene left no doubt that the transgene was expressed and that its product was translated and active inside the plant cells of these lines. Nevertheless, the amount of the transcript level and the actual protein level might still differ grandly, and hence, due to sensitivity limits of the technique, the presence of the protein could not be detected, but its *in vivo* effects were still observable.

In future, to further assess the amount of mutated protein accumulated *in vivo* in the transgenic lines in comparison with the wild type and the knockout mutant, a customized antibody anti-RCD1 could be used to verify the presence and the variation of protein levels directly, although the limit of the sensitivity of immuno-blotting assay would still represent a possible issue. A more long-term goal to visualize the presence of the products of transgene variants *in vivo* would involve the generation of stable lines transformed with the same constructs but with a fluorescent tag. Although this option was put aside in the first attempts to generate mutant lines expressing RCD1 variants, due to the possibility that the fluorescent tag might interfere with the *in vivo* functionality of the protein itself, it could still be a valuable tool to assess not only the presence of the proteins of interest but also the possible variation in the subnuclear localization of the different constructs.

However, in this study, the *in vivo* synthesis of the constructs of interest was confirmed during the localization study performed via transient expression in *N. benthamiana*. As mentioned in the Introduction section, post-translational phosphorylation represents a molecular tool that regulates several aspects of protein functionality. Hence, hypothesizing that phosphorylation is involved in the regulation of RCD1 activity, it could also affect its localization as part of a dynamic regulatory system. In this work, preliminary tests were carried out to assess whether the phosphorylation state of the identified phosphorylatable residues played a role in the subnuclear localization of RCD1.

The findings described in the Results section showed that the alteration of phosphorylation sites S27, T33, S36 and T204, mutated in the RCD1_ND and RCD1_NA constructs, did not prevent the localization of the protein in evenly distributed nuclear speckles (**Figure 3.26** and **3.27**), as seen for the native protein. This might indicate that the abovementioned residues are not directly involved in the

localization of RCD1 or require post-translational modifications at additional sites to affect the subnuclear localization of the protein of interest visibly.

When the localization of the RCD1_CD-GFP, RCD1_CA-GFP, RCD1_CA.2-GFP, RCD1_allD-GFP and RCD1_allA-GFP constructs was tested, the spatial disposition of the tagged proteins transiently expressed underwent substantial remodelling. The RCD1_CD-GFP and RCD1_allD-GFP showed a more central localization, in fewer but bigger speckles for the first, and often in one main speckle, in the centre of the nucleus, for the latter construct (**Figure 3.26**). The opposite situation was found for the RCD1_CA-GFP, RCD1_CA.2-GFP and RCD1_allA-GFP constructs: the first and the last presented the loss of localization in speckles, with an interspersed fluorescent signal being located in the nuclear periphery (**Figure 3.27**). The localization of the RCD1_CA.2-GFP construct exhibited an intermediate distribution since its fluorescent signal was retrieved both in one central cluster as well as interspersed in the nuclear periphery, often concomitantly. It seems licit to ascribe the difference in the subnuclear localization of RCD1_CA.2, in comparison to RCD1_CA, to the additional mutation on the Threonine 204 residue, which could play a pivotal role in the regulatory mechanism of RCD1. Interestingly, it has been shown by Vainonen *et al.* (2021) that T204 is predicted to be a target for protein kinases that are proline-direct, such as the GSK3/SHAGGY-LIKE PROTEIN KINASES (AtSKs), and that the mutation of the T204 to Alanine reduced the phosphorylation level of RCD1. Hence, it could be argued that the phosphorylation, or the lack thereof, on T204 affects the *in vivo* function of RCD1, possibly also by altering its subnuclear localization. To further test this hypothesis, it might be helpful to clone and express an RCD1_CD.2 construct, additionally replacing the Threonine 204 with Aspartate, to test if and to which extent the mimicking of phosphorylation on this residue affects RCD1 activity and localization.

From an overall analysis of the presented data, it is possible to claim that the modifications of the phosphorylatable residues located in the linker region (T204, S230, S231, T239, S242, S244, T257, S263) influenced the subnuclear localization of the protein of interest. The localization of RCD1variants in the nuclear centre, as well as their delocalization in the nuclear periphery, could be determined either by partial disruption of the native tertiary structure of the protein or, more interestingly, by a dynamic regulatory mechanism, which determines the subnuclear localization of the protein of interest by modifying its phosphorylation state, hence, possibly regulating its function at different times and developmental stages in the plant cell via the phosphorylation-dependent degradation pathway. The concomitant presence *in vivo* of phosphorylated and non-phosphorylated RCD1 in the plant cell is supported by the presence of a double band for HA- or GFP-tagged RCD1 transiently expressed when

analysing the results of the immunoblotting assay (**Figure 3.5**). The *in vivo* phosphorylation of RCD1 was confirmed by Vainonen *et al.* (2021): in addition, the phosphorylation of the linker region of RCD1 was hypothesized to regulate different protein-protein interactions and was shown to play a pivotal role (Wirthmüller *et al.*, 2018). In conclusion, the findings described in this work, together with those presented in the abovementioned articles, agree in pointing at the linker region of RCD1 as a possible regulatory domain of the protein activity. This hypothesis could be further investigated in future to assess the molecular mechanisms by which the phosphorylation state of RCD1 is linked to the fine-tuning of the different roles that this protein has been described to play.

4.4 Co-localization of AtRCD1 with PPK1 and PPK4 is affected by mutations at phospho-sites.

After observing the shift in localization of some of the phospho-mutant variants of AtRCD1 tested in this work, the question of whether the change in localization would also affect the co-localization with the previously mentioned PPK1, PPK3 and PPK4 followed. The co-localization with PPK3 (**Figure 3.30** and **3.31**) appeared not to be drastically altered, in spite of the different subnuclear localization of the RCD1 mutants tested and although the localization signal of PPK3 was more evenly interspersed in the nucleus, especially when co-expressed with the RCD1_allD-GFP and RCD1__allA-GFP variants.

The analysis of the data resulting from the transient co-expression and localization study of RCD1 variants and PPK1 and PPK4 showed that the co-localization was not preserved with all the mutated constructs. When co-expressed with RCD1_CD-GFP, RCD1_CA-GFP, RCD1_CA.2-GFP, RCD1_allA-GFP and RCD1_allD-GFP, PPK1 presented an evenly interspersed localization throughout the nucleus, whereas the localization in speckles was generally unaltered when co-expressed with RCD1_ND-GFP and RCD1_NA-GFP (**Figure 3.28** and **3.29**).

A comparable result was obtained for the co-expression of PPK4-RFP with the GFP-tagged RCD1 variants (**Figure 3.32** and **3.33**). Also in this case, the fluorescent signal of PPK4 mainly co-localized with the signal of RCD1_ND-GFP and _NA-GFP, in small speckles, whereas the localization signal was interspersed throughout the nucleus and lacking any overlapping with the fluorescent signal of RCD1_CD-GFP, RCD1_allD-GFP, RCD1_CA-GFP and RCD1_CA.2-GFP. This finding seems to indicate that the alterations at the sites S230, S231, T239, S242, S244, T257 and S263 prevented the co-

localization of RCD1 with PPK1 and PPK4, and it could lead to hypothesize that these modifications could also affect the interaction with PPK1 and PPK4. The lack of co-localization, together with the hypothesized consequent lack of interaction, could derive from a modification in the tertiary structure of RCD1 itself, which would constitute a steric impediment to the interaction. Furthermore, the modification of these sites could prevent the enzymatic activities of PPK1 and PPK4 from targeting RCD1, hence implying that the mentioned kinases might act directly on RCD1 by phosphorylating one or more of the modified residues. This hypothesis was confirmed by Vainonen *et al.* (2021), who showed that PPK4 and PPK2 directly phosphorylate RCD1 at multiple sites in the linker region, where the seven mutated residues of RCD1_CA and RCD1_CD are located. In this work, PPK2, the fourth member of the PPK family in *A. thaliana,* was not tested due to the fact that it was not possible to confirm its interaction with RCD1 using the Co-IP assay.

It is also worth emphasizing that the co-expression of RCD1 variants and PPK1, PPK3 or PPK4 seemed to have an effect on the subnuclear localization of the RCD1 mutated versions. On the one hand, as discussed above, the co-expression of wild type RCD1 with the three PPK kinases modified the subnuclear localization of the kinases themselves, going from evenly interspersed in the nucleus to mainly localizing in speckles, together with RCD1. On the other hand, there seems to be a mutual influence of RCD1 and PPKs on reciprocal subnuclear localization. For example, when PPK1 was co-expressed with RCD1_CD-GFP and RCD1_allD-GFP, the localization of these proteins was shifted from the centre of the nucleus to its periphery (**Figure 3.28**), in comparison to the localization of the same two proteins when co-expressed with free RFP (**Figure 3.26**). However, this observation seemed to be limited to PPK1 and RCD1_CD and RCD1_allD, which could suggest a different way of interaction of PPK1 in respect to RCD1, compared to the other two kinases. PPK3 and PPK4 transiently co-expressed with the same two constructs, RCD1_CD and RCD1_allD, showed an overall more centred localization in one or few bulkier bodies, amongst which distinct speckles were not possible to distinguish. This could be a further indication that the three PPK kinases taken into account in this work might not only have different ways of sterically interacting with RCD1, but also that these enzymes could affect in opposite manner the subnuclear localization of RCD1, and possibly its *in vivo* activity.

Finally, it is also worth noticing that the co-localization of PPK3 and the phospho-variants of RCD1 was never disrupted, oppositely to the findings gathered for the co-localization with PPK1 and PPK4. This result led to the question of whether the interaction, previously tested and discussed, between RCD1 and PPK3 would also be conserved when the phosphorylatable residues considered in this work were mutated.

The outcome of the co-immuno-precipitation (Co-IP) assay, although preliminary, showed that the interaction as well was never totally lost (**Figure 3.34**), but just slightly reduced with RCD1_NA and _CA. Nevertheless, due to the limit of this assay in respect to binding efficiency quantification, the relevant data that this assay provided was the confirmation that the interaction with PPK3 was not disrupted by the mutations on RCD1 phosphosites, consistently with the co-localization assay data reported above both when using the mutant versions of RCD1 lacking either the WWE or the PARP domain, as well as the phosphomutant variants. Altogether, the analysis of these results might suggest that the interaction and the co-localization of PPK3 with RCD1 do not depend on a particular tertiary structure which would have been disrupted in the absence of the WWE or PARP domain, nor on the phosphorylatable residues studied in this work, whose mutation should have sorted a considerable effect on the co-localization or the interaction with RCD1, or on both of the two. It is worth mentioning that, as reported by Vainonen *et* al. (2021), other potential phosphorylation sites were identified both at the N- and C-terminus of RCD1, as well as in the linker region between the PARP and the RST domains. Hence, a mutated version of RCD1 presenting specific mutations at these additional phospho-sites could be used both for localization study and Co-IP together with PPK3 to assess possible alterations in their interaction.

In future, it would be interesting to perform a Co-IP assay to test the possible variations in the interaction between PPK1 and PPK4 with RCD1 phosphomutants to assess whether the lack of co-localization in the typical speckles also correlated with the absence of binding for some of the RCD1 variants. As an alternative, Bimolecular Fluorescent Complementation (BiFC) assay could be carried out in order to gain *in vivo* proof of interaction or of its disruption, performing transient expression of the conveniently tagged protein of interest in *N. benthamiana* leaf tissues.

4.5 The phosphorylation state of RCD1 influences transcript levels of marker genes in phospho-mutant lines

As previously mentioned in the Introduction section of this work, it is well-known that the phosphorylation state of proteins regulates their *in vivo* function under different aspects, e.g., through the alteration of the tertiary structure, the subcellular localization or the enzymatic activity. Hence, it was only reasonable to look further into the possible effects of the modification of the aforementioned phosphorylatable residues on RCD1, in respect to the expression levels of marker genes that have been previously reported

to be altered in the *rcd1-1* knockout mutant (Broschè *et al.*,2014; Shapiguzov *et al.*, 2019). In this work, it was described that the phospho-mimicking and phospho-ablating mutations on the abovementioned phospho-sites on RCD1 influenced the expression of marker genes *AtNUDX6, AtAOX1A* and *AtRAP2.6*.

In regard to the variation of expression levels of the gene *AtNUDX6*, that encodes an ADP-ribose/NADH pyrophosphohydrolase, the decrease in the expression level of the tested gene transcript in the *rcd1-1* knockout mutant, in comparison to the wild type (Broschè *et al.*, 2014), was confirmed and the same was found for all the phospho-mutant lines tested, although to a different extent (**Figure 3.20**). The relative abundance of *NUDX6* transcript presented a low level of expression in the samples from plants grown under long-day conditions. Instead, under short-day growth conditions, the *rcd1-1* RCD1_CD #4.8 transgenic line exhibited an intermediate level of expression of the *NUDX6* gene: this finding, together with the high level of expression of the transgene in this line, seems to suggest that a high amount of the mutated protein with residues mimicking the presence of phosphorylation partially reinstates the wild type transcription levels of this marker gene in the knockout mutant.

A similar scenario was observed when analysing the transcript levels of the *AtRAP2.6* gene that encodes the ethylene-responsive factor (ERF) RELATED TO AP2.6 (RAP2.6) (**Figure 3.21**). Under short-day growth conditions, the expression levels of *RAP2.6* in the *rcd1-1* mutant were sensibly reduced, in comparison to the wild type, as previously described by Broschè *et al.* (2014). All the transgenic lines tested presented an intermediate level of *RAP2.6* expression, but the *rcd1-1* RCD1_CA #12.11 line, which, in turn, exhibited an increased transcript abundance, compared to the wild type. It could be hypothesized that this increase might be due to the position of the insertion of the transgene along the genome in this line, which might have randomly affected the transcriptional regulation of the tested gene. On the other hand, under long-day growth conditions, the outcome of the experiments was difficult to interpret, since the overall levels of expression of the tested gene were found to be very low. However, some of the tested lines resulted to have a statistically significative reduction in the expression levels of *RAP2.6*. It should be noticed that the one outlier line, *rcd1-1* RCD1_CD #3.1, that shows an increase of the transcript abundance of the tested gene, was found no to represent a statistically significant difference in comparison with the *rcd1-1* knockout mutant, due to the variability of the data gathered from the biological replicates.

Interestingly, when analysing the transcript level of *AtAOX1A* (**Figure 3.22**), the expression level of this gene in the leaf tissues of transgenic line *rcd1-1* RCD1_CD #4.8 was comparable to the one exhibited by the wild type, whereas all the other phospho-

mutant lines showed a noticeable increase in the level of expression under long-day growth conditions, similarly to the *rcd1-1* knockout. As demonstrated by Shapiguzov *et al*. (2019), RCD1 inhibits the transcription of *AOX1A* by binding, via its RST domain, the transcription factors ANAC017 and ANAC013, both of which are involved in the transcriptional activation of mitochondrial dysfunction stimulon (*MDS*) genes, including the *AtAOX* gene family. Additionally, under short-day growth conditions, also *rcd1-1* RCD1_CD #3.1 and #3.6 showed a significantly reduced level of *AtAOX1A* transcript. It could be hypothesized that the higher light intensity, as well as prolonged photoperiod under long-day growth conditions, might have enhanced the degradation rate of the phospho-mimicking RCD1_CD constructs, hence determining an increase in *AOX1A* in these two lines. The phosphorylation state of RCD1 by PPKs might influence its activity, as well as its degradation rate, similarly as it was described by Liu *et al.* (2017) for another interactor of the PPKs, AtCRYPTOCHROME2 (CRY2). The phosphorylation of CRY2 by PPKs was shown to be light-dependent and to correlate with an increase both in CRY2 *in vivo* activity and in its degradation rate. The above-discussed reduction of the *AOX1A* transcript levels in all the *rcd1-1* RCD1_CD lines in comparison to the *rcd1-1* knockout seems to suggest that the mimicked phosphorylation state of the residues S230, S231, T239, S242, S244, T257, S263 plays a role in the protein-binding activity of RCD1 towards the transcription factors ANAC013 and ANAC017, hence interfering with the transcriptional activation of *AOX* genes.

This hypothesis was tested *in vivo*, by testing seedlings of each phospho-mutant line, together with *rcd1-1* knockout and the wild type, for tolerance to chloroplastic ROS oxidizing agent Methyl Viologen (or Paraquat). As for the transcript level analysis of the marker genes, the chloroplastic ROS tolerance of the considered lines was tested under two different growth conditions: this experimental setup was designed on the ground of the consideration that the different light intensity and the duration of exposure to different light intensities affect the state of chloroplasts to different extents, hence contributing differently to chloroplastic ROS formation. Surprisingly, all the mutant lines showed a high level of tolerance to chloroplastic ROS, comparable or even higher than the *rcd1-1* knockout mutant. The only exception to this finding was represented by the line *rcd1-1* RCD1_CD #4.8, which, under short-day conditions, displayed a significant reduction of tolerance in comparison to the knockout mutant, and hence representing an intermediate level of ROS tolerance between the wild type and the other mutant lines.

From the analysis of the aforementioned data, it seems possible to infer that the modification of the identified phosphorylation sites modulates the functionality of RCD1 itself. It still remains to be unravelled whether the modification of the considered

residues, and which of those, affects the RCD1 role in the plant cell and whether the mimicking of presence or absence of phosphorylation acts as a switch.

Overall, the increased tolerance to chloroplastic ROS formation, upon exposure of seeds to oxidizing agent Methyl Viologen, seems to suggest that the modifications of phosphorylation sites along RCD1 impaired its functions, independently of whether the mutated residues mimicked the presence or the absence of phosphorylation. Interestingly, the observation that the *rcd1-1* RCD1_CD #4.8 line displayed an intermediate level of tolerance to methyl viologen, significantly under short-day growth conditions, seems to correlate with the previous findings in regard to the abundance of the transcript and transgenic protein level in this line, as well as the marker genes expression levels. It could be argued that the abundance of the mutated protein, more than the presence of residues mimicking the phosphorylation, has an impact on the functionality of the protein itself in the plant cell, at least for what concerned the modification of the mutated phospho-sites in the *rcd1-1* RCD1_CD and *rcd1-1* RCD1_CA lines (S230, S231, T239, S242, S244, T257, S263). However, as mentioned before and also discussed by Vainonen *et al*. (2021), it could also be argued that the modification of these residues might affect the stability of the protein itself. On the one hand, the mimicked phosphorylation of the residues in the *rcd1-1* RCD1_CD lines could impact the protein stability of RCD1 itself, accelerating its turnover via redirecting the activated protein towards a phosphorylation-dependent degradation pathway. On the other hand, the absence of phosphorylation in the *rcd1-1* RCD1_CA and *rcd1-1* RCD1_NA lines might determine a perduring state of inactivation of RCD1 variants. In this scenario, the partially reverted phenotype described for the *rcd1-1* RCD1_CD #4.8 line, as well as its lowered tolerance to chloroplastic ROS and lower expression level of *AOX1A* in comparison to the *rcd1*-1 knockout under short-light growth conditions, could be linked to the higher protein abundance in an active state. Hence, it can be hypothesized a model for the regulation of RCD1 activity in which the phosphorylation state of RCD1 by PPKs, and possibly other kinases, determine the activation and, subsequently, the degradation of this protein, as a molecular mechanism to fine-tuning the diverse functions that RCD1 has been shown to play in the plant cell, in a similar way as previously described for CRY2 by Liu *et al.* (2017).

The results discussed until here in this paragraph and the hypothesized model on RCD1 activity only pertain to the phospho-sites in the linker region between the WWE and the PARP domain of RCD1. In order to gain further insight into the function of the phosphorylatable residues mutated in the *rcd1-1* RCD1_NA lines, it will be necessary to select at least two homozygous *rcd1-1* lines expressing RCD1_ND and repeat the experiments performed in this work. Furthermore, it would be advisable to add also

two homozygous lines overexpressing the 3xHA-tagged wild type RCD1 construct as a positive control. It could be argued that the results obtained in this work, especially in regard to the lack of complementation of chloroplastic ROS tolerance, could be due to the functional inactivation of the RCD1 constructs caused by the presence of the 3xHA tag. Although in theory possible, such an inhibiting effect of the triple HA tag does not seem likely, in part due to the low molecular weight of the tag (ca. 3.3kDa), which should not represent a steric interference to the transcription factor binding by the RST domain in RCD1. Furthermore, the presence of the 3xHA tag did not impede the partial complementation for the phenotype in *rcd1-1* RCD1_NA and *rcd1-1* RCD1_CD lines (**Figure 3.16, 3.17;** Appendix **Figure A.2** and **A.3**), hence it seems licit to infer that the tag did not interfere at least in respect to some of the functions of RCD1. Finally, in Vainonen *et al*. (2021), the complementation line *rcd1-1* RCD1-3xHA presented a fully restored phenotype as well as loss of enhanced chloroplastic ROS tolerance, typical of the knockout mutant.

Furthermore, how the transgene in the *rcd1-1* RCD1_NA lines complemented the *rcd1-1* knockout phenotype and, at the same time, presented the increased chloroplastic ROS tolerance typical of the aforementioned knockout mutant line is still under investigation. It could be argued that the mutations at the residues S27, T33, S36 and T204 could interfere with the ROS tolerance function of RCD1 but do not impair its role in the correct phenotypic development of the plant, although the molecular mechanism by which these two functions of RCD1 are split and regulated in the plant cell, remains to be uncovered. It is worth noticing that, while the residues Serine 27, Threonine 33 and Serine 36 are located at the N-terminus of RCD1, the residue Threonine 204 is located in the linker region between the WWE domain and the PARP domain. Hence, it could be hypothesized that the phospho-ablating modification at this site could result in the impossibility to fully activate RCD1 via phosphorylation by the PPKs, or other kinases, hence determining the lack of complementation of the enhanced chloroplastic ROS tolerance. The results gathered in regard to the *rcd1-1* RCD1_NA lines seem to hint at the possibility that the several cellular pathways in which RCD1 is involved require different regulation mechanisms of RCD1 activity.

4.6 Biochemical analysis of TaSRO1 could not confirm its previously published PARP catalytic activity

As described in the Introduction section of this work, so far, only one member of the SRO protein family in plants, *Triticum aestivum* SRO1, together with its allelic variant

SR3, was described to show PARP catalytic activity (Liu *et al.*, 2014). Due to the singularity of this finding and the high similarity in sequence with the PARP catalytically inactive AtRCD1, which was the main research topic in this work, it seemed opportune to try to understand the molecular features that provided TaSRO1 with its enzymatic activity. As a first step, it was necessary to verify, using the methodological means at disposal, the published findings regarding the PARP activity of TaSRO1. The results of the transient expression of the full-length GFP-tagged version of TaSRO1 in *N. benthamiana* leaf tissues and the consequent protein extraction and incubation with NAD^+ did not result in the formation of mono- or poly-ADP-ribose chains, via auto-PARylating activity, which was assessed in AtPARP2, used as the positive control. Although not conclusive, the data gained by performing this experiment gave a clear indication of the lack of auto-PARylating activity of the protein of interest, a feature that is common in active PARP enzymes (Rissel and Peiter, 2019).

In order to reproduce the evidence of the PARP activity of TaSRO1, the small-scale expression of TaSRO1-His, whose clone was kindly provided by Dr. Guangmin Xia (Shandong University, Jinan, China), correspondent author of the published paper abovementioned, was repeatedly attempted in the same *E.coli* strain used in Liu *et al.* (2014), BL21, as well in other two strains optimized for heterologous protein expression, Shuffle and Solub21. As shown in the Result section of this work, the full-length His-tagged protein never succeeded to be produced in this work. On the other hand, the PARP domain of TaSRO1 was expressed, purified and used for further analysis. The purified PARP domain of TaSRO1 was used for Thermal Stability assay, in order to determine the effect of NAD^+ molecules, as the natural substrate of PARP enzymatic activity, as well as of 6-(5H)-phenanthridinone (6(5H)-PHE) and 3-aminobenzamide (3AB), respectively a PARP enzyme inhibitor (Wahlberg *et al.*, 2012) and a steric homologue of the natural substrate NAD^+ (Purnell and Whish, 1980), in respect to their stabilizing effect on the TaSRO1 PARP domain upon increasing temperature. Whereas the positive control, constitutively active HsPARP1 PARP domain, showed an increased melting temperature, congruently with the increase in the concentrations of the tested compounds, although to different extents, the PARP domain of TaSRO1 did not show to be stabilized by any of these molecules. This experiment provided clear evidence that the PARP domain of TaSRO1 did not bind to the tested molecules, all well-known interactors of PARP enzymes, hence leading to reconsidering the molecular mechanism behind the reported PARP enzymatic activity of TaSRO1.

In order to gain further insight into the three-dimensional structure of the TaSRO1 PARP domain, protein crystallization of this domain was attempted. The rationale

behind this experiment was that the possibility to compare the TaSRO1 PARP domain with the correspondent domain of catalytically active HsPARP1 and of AtRCD1, which lacks PARP enzymatic activity (Wirthmüller *et al.*, 2018), would have helped to clarify the PARP catalytic mechanism of TaSRO1. The remarkable similarity between the catalytic triad of TaSRO1, identified by Liu *et al.* (2014) (Leu^{312}-His^{344}-His^{407}) and the triad of AtRCD1 (Leu^{333}-His^{365}-Asn^{428}), forming a positively charged pocket which does not allow NAD^+ binding, led to the hypothesis that the published PARP catalytic activity of TaSRO1 might not involve the aforementioned residues, whose biochemical features do not fit with those of the residues involved in NAD^+ binding in the canonical PARP enzymes, Histidine-Tyrosine-Glutamate. Additionally, the lack of the Tyrosine residue that is involved in stabilizing the bond via stacking with the nicotinamide ring (Steffen *et al.*, 2013), in the supposed triad of TaSRO1 PARP domain raised further questions on its catalytic mechanism.

In conclusion, the results of the experiments conducted in this work regarding the PARP activity of TaSRO1, as the only member of the SRO plant-specific protein family to display this enzymatic feature, do not allow to confirm the previous finding on this subject. On the contrary, the lack of auto-PARylating activity in *ex vivo* co-immunoprecipitation experiments, together with the results obtained via *in vitro* Thermal Stability assay, in respect to the lack of binding to NAD^+, nor with its structural homologue 3AB or the PARP inhibitor 6(5H)-PHE, seems to indicate the absence of a canonical PARP enzymatic activity of the PARP domain of TaSRO1. Although the mere PARP domain of HsPARP1 was sufficient to bind *in vitro* the aforementioned tested molecules, nonetheless, it could be argued that the corresponding domain of TaSRO1 might not be sufficient, and that the integrity of the protein structure could be necessary for the enzymatic activity of its catalytic domain. The fact that, in this work, it was not possible to express and isolate the His-tagged full-length protein could depend on an erroneous protein folding, possibly due to the abundance of random coil regions interspersed throughout the sequence of TaSRO1, according to the secondary structure of TaSRO1, calculated using PSIPRED secondary structure prediction method (Jones, D.T., 1999) shown in **Figure 4.1**.

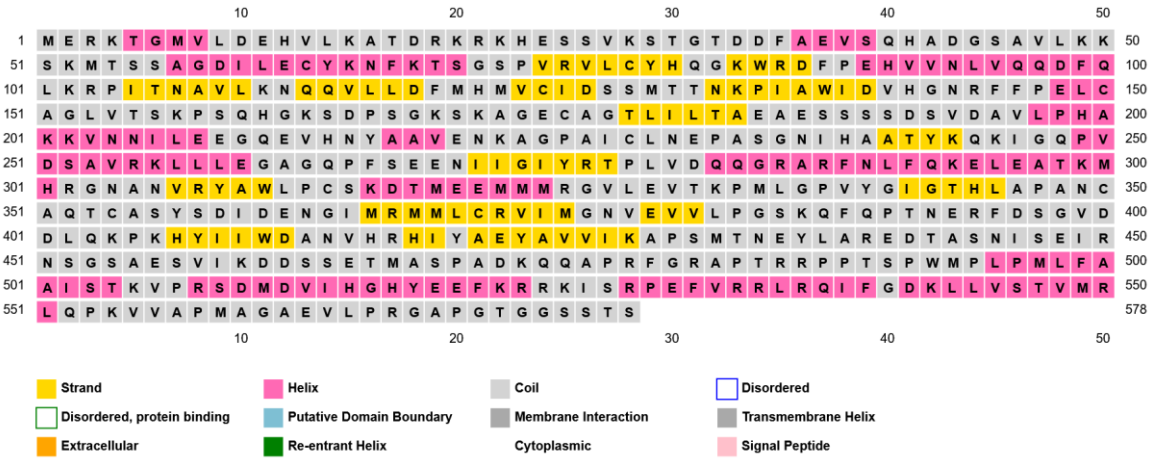

Figure 4.1: Predicted secondary structure of TaSRO1 using position-specific scoring matrices by PSIPRED (Jones, D.T., 1999).

The incorrect folding of TaSRO1 in *E. coli* under the tested conditions could be prevented by the addition of a different tag, such as the Glutathione S-transferase (GST). In fact, the addition of a GST-tag is renowned for its chaperone feature on fusion protein, as well as for increasing the solubility of the fusion protein, thus avoiding its localization in inclusion bodies (Harper and Speicher, 2013). In this regard, a full-length GST-tagged version of the protein of interest was cloned and a preliminary test in small-scale expression assay, performed using multiple *E. coli* strains, showed the detectable presence of the tagged product via immuno-blotting. In the future, the optimization of heterologous GST-tagged protein expression and extraction, together with the analysis of the three-dimensional structure of the PARP domain of TaSRO1, will offer two new valid tools for further study of the catalytic activity of this protein. Whether the next set of experiments will provide proof of catalytic activity of TaSRO1 or its lack, the results will undoubtfully strengthen the current body of knowledge in regard to the molecular mechanism and structural feature of TaSRO1, thus allowing us to gain further insight on the role of SIMILAR TO RCD1 (SRO) protein family in higher plants.

4.7 Diverse yet critical functions of catalytically inactive PARP-like proteins in eukaryotes

The pivotal role of PARP-like proteins, such as the members of the SRO family in plants, has been studied at length. These proteins are known for their role in abiotic stress response and plant development, as well as being involved in different hormonal signalling pathways, such as auxin, jasmonate and ethylene (Blomster *et al.,* 2011; Overmyer *et al.*, 2000). However, also in mammals, few PARP-like proteins, e.g. HsPARP9 and HsPARP13, have been described to play a role in responding to cellular stress, albeit of a different kind, such as antiviral activity via viral RNA-binding or transgene activation suppression, and none of these has been reported for PARP-like proteins in plants.

HsPARP13, also known as Zinc-finger Antiviral Protein (ZAP), is present in human cells in two isoforms, HsPARP13.1 and HsPARP13.2 (Kerns *et al.*, 2008), the latter lacking the PARP-like domain. This domain in HsPARP13.1 was described to be inactive (Vyas *et al.*, 2014) due to the Y-Y-V catalytic motif, which substantially diverges from the H-Y-E motif present in canonical active PARP proteins. Both isoforms localize in the cytoplasm and bind untranslated mRNA (Leung *et al.*, 2011) and, although both variants were found to have antiviral activity. Upon viral infection, HsPARP13 localizes in cytoplasmic stress granules (SGs) and inhibits the translation of viral RNA *via* RNA binding through its four N-terminal CCCH type zinc fingers leading to the degradation of the viral RNA (Law *et al.*, 2019; Chen *et al.*, 2012). Aside from its key role in antiviral responses, the RNA binding function of HsPARP13 has also been described to be involved in inhibition of retrotransposition of endogenous elements, such as Long Interspersed Nuclear Elements (LINEs) (Goodier *et al.*, 2015) as well as targeting cellular RNAs to degradation (Todorova et al., 2014). Interestingly, the study of the function of PARP-like domain in the isoform 1 showed that the non-catalytic motif (V-Y-Y-) was essential for its antiviral activity, which was abolished when either the third or all of the three residues were mutated to Alanine (Gläsker *et al.*, 2014). These findings led to hypothesize that the PARP domain of HsPARP13.1 is involved in conformational changes that might regulate or influence the ability of the CCCH type zinc fingers to bind repetitive sequences of viral RNA.

Recently, another PARP-like domain, lacking PARylating activity, has been identified in a human protein, HsTASOR, which constitutes the core of the Human Silencing Hub (HUSH) complex. This complex was described as the homologue of yeast RNA-induced transcriptional silencing (RITS) complex and recruits H3K9 methyltransferase SETDB1

(Tchasovnikarova *et al.*, 2015) in order to compact chromatin and hence silence transcription in regions of the genome where endogenous retrotransposons, e.g. LINE-1s elements (Liu *et al.*, 2018), and retroviruses (Robbez-*Masson et* al., 2018) are inserted. In 2020, Douse *et al.* identified and characterized the HsTASOR DUF3715 domain as a PARP domain, lacking NAD^+ binding site and presenting an L-Y-Q motif in the catalytic site, which hence makes the protein inactive with respect to canonical ADP-ribosyl-transferase activity. It was also shown that the PARP-like domain of HsTASOR weakly binds ssRNA and that the fourteen residues (Tyr^{303}-His^{316}) constituting the loop connecting the ß8 and ß9 strands were necessary for both the deposition of H3K9me3 along the whole genome and the repression of LINE-1 elements by HUSH complex. It was, hence, hypothesized that this region is involved in conformational changes within the HUSH complex already bound to the chromatin, which is pivotal for the transcription repression mediated by this complex. This hypothesis seems to point towards a similarity between the functioning mechanisms of PARP-like domains in HsPARP13.1 and HsTASOR.

However, the identification and functional characterization of PARP-like proteins and their PARP-like domains have proved to be a difficult task to achieve. It is the case of HsPARP9, also known as HsBAL or HsBAL1, that was at first described to lack PARylating activity (Vyas *et al.*, 2014), but later described to show such an enzymatic activity when heterodimerizing with HsDTX3L (Yang *et al.*, 2017), with whom HsPARP9 shares a bidirectional promoter (Juszczynski *et al.*, 2006). In 2020, Chatrin *et al.* showed how the ADP-ribosylating activity was to be ascribed to HsDTX3L rather than to HsPARP9. These different findings on the catalytic activity of HsPARP9 were attributed to the fact that Yang *et al.*, (2017) tested the activity of both the heterodimer and the PARP9 alone, which did not show to be catalytically active, without testing DTX3L alone. However, it remains interesting how deletions and mutations in the PARP-like domain of PARP9 could affect the PARylating activity of the heterodimer. This might hint towards a regulatory function of the PARP9 PARP-like domain, possibly related to conformational changes, instead of it being the active catalysing component (Yang *et al.*, 2017; Chatrin *et al.*, 2020).

The characterization of PARP-like domain in plants has been less extensive, but in 2018 Wirthmüller *et* al. tested whether the PARP-inactive site of AtRCD1 might have evolved to bind other smaller compounds and whether this might be an essential feature for RCD1 correct function. It was shown that three single point mutations in *A. thaliana* RCD1 PARP-like domain on residues corresponding to the catalytic centre of active PARPs did not affect the protein function *in vivo* in respect to its involvement in development and chroloplastic ROS tolerance, hence leading towards the hypothesis

that this PARP-like domain might have a function in protein scaffolding rather than in interactors binding. This latter hypothesis could be tested via *in vivo* expression of mutated versions lacking different portions of the pseudo-PARP domain and, hence, studying the possible effects of the mutation in the complementation lines.

Overall, a series of factors have influenced the study of PARP-like protein: their pleiotropic effects, which made it challenging to identify and dissect the different molecular pathways in which these proteins are involved. Their structural features, especially the high-disorder regions, on the one hand, allow the PARP-like proteins to bind to several interactors, but on the other, reduce the extent of the results of structure-based approaches to functional studies. Furthermore, their association with other cellular components, not all yet identified, complicates the correct understanding and attribution of functions to PARP-like proteins and to their PARP-like domains.

4.8 Perspectives

The preservation of the plant-specific SIMILAR TO RCD1 (SRO) protein family throughout evolution in higher plants (Vainonen *et al.*, 2016) suggests its relevant role in plant physiology, together with the pleiotropic effect that the absence of its most representative member, RCD1, has in *A. thaliana* (Alhfors *et al.*, 2004; Jasper *et al.*, 2009). Several members of the SRO family have been described to play a role in abiotic stress responses, especially to chloroplastic ROS, salt and drought stress and, yet, a comprehensive model to explain the functions of SRO proteins and the molecular mechanisms through which they perform their role in plant cells has not been proposed. The absence of a cohesive model for the role of SRO proteins is mainly due to the scarce knowledge gathered in the past two decades, which in turn is to be ascribed to the high level of homology amongst the SRO family in the plant model organism, *A. thaliana*: this factor determined an evident difficulty in assessing the function of each member. An exception is represented by RCD1, whose absence in the knockout mutant results in a characteristic pleiotropic phenotype, impaired in the development and susceptible to apoplastic oxidative stress, but more resistant to oxidative stress in the chloroplasts (Overmayer *et al.,* 2000; Alhfors *et al.*, 2004). Although by now, it has been ascertained that RCD1 lacks PARP enzymatic activity despite presenting a PARP domain (Wirthmüller *et al.*, 2018), hence being described as a pseudo-PARP protein, it is well-characterized for its role of transcription factor interacting protein, via the RST domain. Nonetheless, the regulatory pathway that determines RCD1 function *in vivo* has not been uncovered yet. The hypothesis that the N-terminal portion of this protein, including the WWE domain and the linker region, could be involved in its regulatory mechanism has

been tested in this work, especially in regard to the role of the several phosphorylatable sites identified in the linker region. As shown and discussed above, the considered mutations at some of the phosphorylatable residues resulted in the alteration of the functionality of the protein itself, thus inviting to a further investigation on the effects of phosphorylation changes in RCD1. According to the data gathered in this work and in agreement with the results published by Vainonen *et al*. (2021), a molecular model of the regulation of RCD1 activity can be hypothesized, in which the level of phosphorylation of the phosphosites present on the linker region between the WWE and the PARP domains proportionally increase the activation of RCD1 and, concurrently, its degradation rate. However, remains to be characterized the exact role of each of the phosphorylation sites in the abovementioned linker region. Furthermore, it is worth mentioning that additional phosphosites have been identified by Vainonen *et al*. (2021) at the C-terminus of RCD1: hence, the study of these phosphorylatable residues could help gain a deeper insight into the complex regulatory mechanism of RCD1 activity and to theorize a cohesive model.

The aim of this work was to widen the knowledge on the functioning mechanisms of the SRO proteins through the biochemical characterization of AtRCD1, the first protein member of this family to be identified, as well as of TaSRO1, the first SRO protein described to present PARP catalytic activity. The results gathered and presented in this work offer new insight into the possible way of functioning of AtRCD1 while raising new questions regarding the enzymatic activity of TaSRO1, which was not possible to confirm in this case. Altogether, the newly gained insights provided future research on SRO proteins with some valuable data and observations from which to continue the quest for understanding the intricate universe enclosed in the plant cell.

Bibliography

ABRAMOVITCH, R. B., ANDERSON, J. C., & MARTIN, G. B. (2006). Bacterial elicitation and evasion of plant innate immunity. *Nature Reviews. Molecular Cell Biology*, *7*(8), 601–611. https://doi.org/10.1038/nrm1984

ACHARD, P., GONG, F., CHEMINANT, S., ALIOUA, M., HEDDEN, P., & GENSCHIK, P. (2008). The cold-inducible CBF1 factor-dependent signalling pathway modulates the accumulation of the growth-repressing DELLA proteins via its effect on gibberellin metabolism. *The Plant Cell*, *20*(8), 2117–2129. https://doi.org/10.1105/tpc.108.058941

AGARWAL, M., HAO, Y., KAPOOR, A., DONG, C. H., FUJII, H., ZHENG, X., & ZHU, J. K. (2006). A R2R3 type MYB transcription factor is involved in the cold regulation of CBF genes and in acquired freezing tolerance. *The Journal of Biological Chemistry*, *281*(49), 37636–37645. https://doi.org/10.1074/jbc.M605895200

ARAVIND L. (2001). The WWE domain: a common interaction module in protein ubiquitination and ADP ribosylation. *Trends in Biochemical Sciences*, *26*(5), 273–275. https://doi.org/10.1016/s0968-0004(01)01787-x

BAIER, M., STRÖHER, E., & DIETZ, K. J. (2004). The acceptor availability at photosystem I and ABA control nuclear expression of 2-Cys peroxiredoxin-A in Arabidopsis thaliana. *Plant & Cell Physiology*, *45*(8), 997–1006. https://doi.org/10.1093/pcp/pch114

BANIWAL, S. K., CHAN, K. Y., SCHARF, K. D., & NOVER, L. (2007). Role of heat stress transcription factor HsfA5 as specific repressor of HsfA4. *The Journal of Biological Chemistry*, *282*(6), 3605–3613. https://doi.org/10.1074/jbc.M609545200

BARKAUSKAITE, E., JANKEVICIUS, G., & AHEL, I. (2015). Structures and Mechanisms of Enzymes Employed in the Synthesis and Degradation of PARP-Dependent Protein ADP-Ribosylation. *Molecular Cell*, *58*(6), 935–946. https://doi.org/10.1016/j.molcel.2015.05.007

BECHTOLD, U., & FIELD, B. (2018). Molecular mechanisms controlling plant growth during abiotic stress. *Journal of Experimental Botany*, *69*(11), 2753–2758. https://doi.org/10.1093/jxb/ery157

BERROW, N. S., ALDERTON, D., SAINSBURY, S., NETTLESHIP, J., ASSENBERG, R., RAHMAN, N., STUART, D. I., & OWENS, R. J. (2007). A versatile ligation-independent cloning method suitable for high-throughput expression screening applications. *Nucleic Acids Research*, *35*(6), e45. https://doi.org/10.1093/nar/gkm047

BESANT, P. G., & ATTWOOD, P. V. (2009). Detection and analysis of protein histidine phosphorylation. *Molecular and Cellular Biochemistry*, *329*(1-2), 93–106. https://doi.org/10.1007/s11010-009-0117-2

BLOMSTER, T., SALOJÄRVI, J., SIPARI, N., BROSCHÉ, M., AHLFORS, R., KEINÄNEN, M., OVERMYER, K., & KANGASJÄRVI, J. (2011). Apoplastic reactive oxygen species transiently decrease auxin signaling and cause stress-induced morphogenic response in Arabidopsis. *Plant Physiology*, *157*(4), 1866–1883. https://doi.org/10.1104/pp.111.181883

BLUMWALD, E., & POOLE, R. J. (1985). Na/H Antiport in Isolated Tonoplast Vesicles from Storage Tissue of Beta vulgaris. *Plant Physiology*, *78*(1), 163–167. https://doi.org/10.1104/pp.78.1.163

BUDDE, R.J.A. AND CHOLLET, R. (1988), Regulation of enzyme activity in plants by reversible phosphorylation. *Physiologia Plantarum*, 72: 435-439. https://doi.org/10.1111/j.1399-3054.1988.tb05857.x

BUGGE, K., STABY, L., KEMPLEN, K. R., O'SHEA, C., BENDSEN, S. K., JENSEN, M. K., OLSEN, J. G., SKRIVER, K., & KRAGELUND, B. B. (2018). Structure of Radical-Induced Cell Death1 Hub Domain Reveals a Common αα-Scaffold for Disorder in Transcriptional Networks. *Structure* (London, England: 1993), 26(5), 734–746.e7. https://doi.org/10.1016/j.str.2018.03.013

CANONNE, J., & RIVAS, S. (2012). Bacterial effectors target the plant cell nucleus to subvert host transcription. *Plant Signaling & Behavior*, *7*(2), 217–221. https://doi.org/10.4161/psb.18885

CASAL, J. J., & BALASUBRAMANIAN, S. (2019). Thermomorphogenesis. *Annual Review of Plant Biology*, *70*, 321-346. https://doi.org/10.1146/annurev-arplant-050718-095919

CHANG, P., COUGHLIN, M., & MITCHISON, T. J. (2009). Interaction between Poly(ADP-ribose) and NuMA contributes to mitotic spindle pole assembly. *Molecular Biology of the Cell*, *20*(21), 4575–4585. https://doi.org/10.1091/mbc.e09-06-0477

CHATRIN, C., GABRIELSEN, M., BUETOW, L., NAKASONE, M. A., AHMED, S. F., SUMPTON, D., SIBBET, G. J., SMITH, B. O., & HUANG, D. T. (2020). Structural insights into ADP-ribosylation of ubiquitin by Deltex family E3 ubiquitin ligases. *Science Advances*, *6*(38), eabc0418. https://doi.org/10.1126/sciadv.abc0418

CHEN, S., XU, Y., ZHANG, K., WANG, X., SUN, J., GAO, G., & LIU, Y. (2012). Structure of N-terminal domain of ZAP indicates how a zinc-finger protein recognizes complex RNA. *Nature Structural & Molecular Biology*, *19*(4), 430–435. https://doi.org/10.1038/nsmb.2243

CHINNUSAMY, V., OHTA, M., KANRAR, S., LEE, B. H., HONG, X., AGARWAL, M., & ZHU, J. K. (2003). ICE1: a regulator of cold-induced transcriptome and

freezing tolerance in Arabidopsis. *Genes & Development*, *17*(8), 1043–1054. https://doi.org/10.1101/gad.1077503

CHRISTIAN, J. O., BRAGINETS, R., SCHULZE, W. X., & WALTHER, D. (2012). Characterization and Prediction of Protein Phosphorylation Hotspots in Arabidopsis thaliana. *Frontiers in Plant Science*, *3*, 207. https://doi.org/10.3389/fpls.2012.00207

CITARELLI, M., TEOTIA, S., & LAMB, R. S. (2010). Evolutionary history of the poly(ADP-ribose) polymerase gene family in eukaryotes. *BMC Evolutionary Biology*, *10*, 308. https://doi.org/10.1186/1471-2148-10-308

CUTLER, S. R., RODRIGUEZ, P. L., FINKELSTEIN, R. R., & ABRAMS, S. R. (2010). Abscisic acid: emergence of a core signaling network. *Annual Review of Plant Biology*, *61*, 651–679. https://doi.org/10.1146/annurev-arplant-042809-112122

CZECHOWSKI, T., STITT, M., ALTMANN, T., UDVARDI, M. K., & SCHEIBLE, W. R. (2005). Genome-wide identification and testing of superior reference genes for transcript normalization in Arabidopsis. *Plant Physiology*, *139*(1), 5–17. https://doi.org/10.1104/pp.105.063743

DAROSA, P. A., WANG, Z., JIANG, X., PRUNEDA, J. N., CONG, F., KLEVIT, R. E., & XU, W. (2015). Allosteric activation of the RNF146 ubiquitin ligase by a poly(ADP-ribosyl)ation signal. *Nature*, *517*(7533), 223–226. https://doi.org/10.1038/nature13826

DELKER, C., SONNTAG, L., JAMES, G. V., JANITZA, P., IBAÑEZ, C., ZIERMANN, H., PETERSON, T., DENK, K., MULL, S., ZIEGLER, J., DAVIS, S. J., SCHNEEBERGER, K., & QUINT, M. (2014). The DET1-COP1-HY5 pathway constitutes a multipurpose signaling module regulating plant photomorphogenesis and thermomorphogenesis. *Cell Reports*, *9*(6), 1983–1989. https://doi.org/10.1016/j.celrep.2014.11.043

DESPRÉS, C., DELONG, C., GLAZE, S., LIU, E., & FOBERT, P. R. (2000). The Arabidopsis NPR1/NIM1 protein enhances the DNA binding activity of a subgroup of the TGA family of bZIP transcription factors. *The Plant Cell*, *12*(2), 279–290.

DING, Y., JIA, Y., SHI, Y., ZHANG, X., SONG, C., GONG, Z., & YANG, S. (2018). OST1-mediated BTF3L phosphorylation positively regulates CBFs during plant cold responses. *The EMBO Journal*, *37*(8), e98228. https://doi.org/10.15252/embj.201798228

DING, Y., LI, H., ZHANG, X., XIE, Q., GONG, Z., & YANG, S. (2015). OST1 kinase modulates freezing tolerance by enhancing ICE1 stability in Arabidopsis. *Developmental Cell*, *32*(3), 278–289. https://doi.org/10.1016/j.devcel.2014.12.023

DING, Y., LV, J., SHI, Y., GAO, J., HUA, J., SONG, C., GONG, Z., & YANG, S. (2019). EGR2 phosphatase regulates OST1 kinase activity and freezing tolerance in

Arabidopsis. *The EMBO Journal*, *38*(1), e99819. https://doi.org/10.15252/embj.201899819

DOHERTY, C. J., VAN BUSKIRK, H. A., MYERS, S. J., & THOMASHOW, M. F. (2009). Roles for Arabidopsis CAMTA transcription factors in cold-regulated gene expression and freezing tolerance. *The Plant Cell*, *21*(3), 972–984. https://doi.org/10.1105/tpc.108.063958

DOUSE, C.H., TCHASOVNIKAROVA, I.A., TIMMS, R.T. *et al.* TASOR is a pseudo-PARP that directs HUSH complex assembly and epigenetic transposon control. *Nat Commun* **11,** 4940 (2020). https://doi.org/10.1038/s41467-020-18761-6

EREMINA, M., UNTERHOLZNER, S. J., RATHNAYAKE, A. I., CASTELLANOS, M., KHAN, M., KUGLER, K. G., MAY, S. T., MAYER, K. F., ROZHON, W., & POPPENBERGER, B. (2016). Brassinosteroids participate in the control of basal and acquired freezing tolerance of plants. *Proceedings of the National Academy of Sciences of the United States of America*, *113*(40), E5982–E5991. https://doi.org/10.1073/pnas.1611477113

FAROOQ M., HUSSAIN M., WAHID A., SIDDIQUE K. H. M. (2012). "Drought stress in plants: an overview," in *Plant Responses to Drought Stress*, ed. Aroca R. (Berlin: Springer-Verlag), 1–33.

FENG, B., LIU, C., DE OLIVEIRA, M. V., INTORNE, A. C., LI, B., BABILONIA, K., DE SOUZA FILHO, G. A., SHAN, L., & HE, P. (2015). Protein poly(ADP-ribosyl)ation regulates Arabidopsis immune gene expression and defense responses. *PLoS Genetics*, *11*(1), e1004936. https://doi.org/10.1371/journal.pgen.1004936

FINKELSTEIN, R. R., GAMPALA, S. S., & ROCK, C. D. (2002). Abscisic acid signaling in seeds and seedlings. *The Plant Cell*, *14 Suppl*(Suppl), S15–S45. https://doi.org/10.1105/tpc.010441

FUCHS, J., DEMIDOV, D., HOUBEN, A., & SCHUBERT, I. (2006). Chromosomal histone modification patterns--from conservation to diversity. *Trends in Plant Science*, *11*(4), 199–208. https://doi.org/10.1016/j.tplants.2006.02.008

FUGLSANG, A. T., BORCH, J., BYCH, K., JAHN, T. P., ROEPSTORFF, P., & PALMGREN, M. G. (2003). The binding site for regulatory 14-3-3 protein in plant plasma membrane H+-ATPase: involvement of a region promoting phosphorylation-independent interaction in addition to the phosphorylation-dependent C-terminal end. *The Journal of Biological Chemistry*, *278*(43), 42266–42272. https://doi.org/10.1074/jbc.M306707200

FUGLSANG, A. T., GUO, Y., CUIN, T. A., QIU, Q., SONG, C., KRISTIANSEN, K. A., BYCH, K., SCHULZ, A., SHABALA, S., SCHUMAKER, K. S., PALMGREN, M. G., & ZHU, J. K. (2007). Arabidopsis protein kinase PKS5 inhibits the plasma membrane H+ -ATPase by preventing interaction with 14-3-3 protein. *The Plant Cell*, *19*(5), 1617–1634. https://doi.org/10.1105/tpc.105.035626

GAO, W. R., WANG, X. S., LIU, Q. Y., PENG, H., CHEN, C., LI, J. G., ZHANG, J. S., HU, S. N., & MA, H. (2008). Comparative analysis of ESTs in response to drought stress in chickpea (C. arietinum L.). *Biochemical and Biophysical Research Communications*, *376*(3), 578–583. https://doi.org/10.1016/j.bbrc.2008.09.030

GAO, S., GAO, J., ZHU, X., SONG, Y., LI, Z., REN, G., ZHOU, X., & KUAI, B. (2016). ABF2, ABF3, and ABF4 Promote ABA-Mediated Chlorophyll Degradation and Leaf Senescence by Transcriptional Activation of Chlorophyll Catabolic Genes and Senescence-Associated Genes in Arabidopsis. *Molecular Plant*, *9*(9), 1272–1285. https://doi.org/10.1016/j.molp.2016.06.006

GLÄSKER, S., TÖLLER, M., & KÜMMERER, B. M. (2014). The alternate triad motif of the poly(ADP-ribose) polymerase-like domain of the human zinc finger antiviral protein is essential for its antiviral activity. *The Journal of General Virology*, *95*(Pt 4), 816–822. https://doi.org/10.1099/vir.0.060988-0

GONZÁLEZ-GUZMÁN, M., APOSTOLOVA, N., BELLÉS, J. M., BARRERO, J. M., PIQUERAS, P., PONCE, M. R., MICOL, J. L., SERRANO, R., & RODRÍGUEZ, P. L. (2002). The short-chain alcohol dehydrogenase ABA2 catalyzes the conversion of xanthoxin to abscisic aldehyde. *The Plant Cell*, *14*(8), 1833–1846. https://doi.org/10.1105/tpc.002477

GOODIER, J. L., PEREIRA, G. C., CHEUNG, L. E., ROSE, R. J., & KAZAZIAN, H. H., JR (2015). The Broad-Spectrum Antiviral Protein ZAP Restricts Human Retrotransposition. *PLoS Genetics*, *11*(5), e1005252. https://doi.org/10.1371/journal.pgen.1005252

GUO, X., LIU, D., & CHONG, K. (2018). Cold signaling in plants: Insights into mechanisms and regulation. *Journal of Integrative Plant Biology*, *60*(9), 745–756. https://doi.org/10.1111/jipb.12706

HAHN, A., BUBLAK, D., SCHLEIFF, E., & SCHARF, K. D. (2011). Crosstalk between Hsp90 and Hsp70 chaperones and heat stress transcription factors in tomato. *The Plant Cell*, *23*(2), 741–755. https://doi.org/10.1105/tpc.110.076018

HARPER, S., & SPEICHER, D. W. (2011). Purification of proteins fused to glutathione S-transferase. *Methods in Molecular Biology (Clifton, N.J.)*, *681*, 259–280. https://doi.org/10.1007/978-1-60761-913-0_14

HENDRICKSON, W. A., HORTON, J. R., & LEMASTER, D. M. (1990). Selenomethionyl proteins produced for analysis by multiwavelength anomalous diffraction (MAD): a vehicle for direct determination of three-dimensional structure. *The EMBO Journal*, *9*(5), 1665–1672.

HIGUCHI, R., KRUMMEL, B., & SAIKI, R. K. (1988). A general method of in vitro preparation and specific mutagenesis of DNA fragments: study of protein and DNA interactions. *Nucleic Acids Research*, *16*(15), 7351–7367. https://doi.org/10.1093/nar/16.15.7351

HILTSCHER, H., RUDNIK, R., SHAIKHALI, J., HEIBER, I., MELLENTHIN, M., MEIRELLES DUARTE, I., SCHUSTER, G., KAHMANN, U., & BAIER, M. (2014). The radical induced cell death protein 1 (RCD1) supports transcriptional activation of genes for chloroplast antioxidant enzymes. *Frontiers in Plant Science*, *5*, 475. https://doi.org/10.3389/fpls.2014.00475

HONG, J. H., SAVINA, M., DU, J., DEVENDRAN, A., KANNIVADI RAMAKANTH, K., TIAN, X., SIM, W. S., MIRONOVA, V. V., & XU, J. (2017). A Sacrifice-for-Survival Mechanism Protects Root Stem Cell Niche from Chilling Stress. *Cell*, *170*(1), 102–113.e14. https://doi.org/10.1016/j.cell.2017.06.002

IAKOUCHEVA, L. M., RADIVOJAC, P., BROWN, C. J., O'CONNOR, T. R., SIKES, J. G., OBRADOVIC, Z., & DUNKER, A. K. (2004). The importance of intrinsic disorder for protein phosphorylation. *Nucleic Acids Research*, *32*(3), 1037–1049. https://doi.org/10.1093/nar/gkh253

ISHIKAWA, K., YOSHIMURA, K., HARADA, K., FUKUSAKI, E., OGAWA, T., TAMOI, M., & SHIGEOKA, S. (2010). AtNUDX6, an ADP-ribose/NADH pyrophosphohydrolase in Arabidopsis, positively regulates NPR1-dependent salicylic acid signaling. *Plant Physiology*, *152*(4), 2000–2012. https://doi.org/10.1104/pp.110.153569

ISMAIL, A. M., & HORIE, T. (2017). Genomics, Physiology, and Molecular Breeding Approaches for Improving Salt Tolerance. *Annual Review of Plant Biology*, *68*, 405–434. https://doi.org/10.1146/annurev-arplant-042916-040936

JAFFÉ, F. W., FRESCHET, G. E., VALDES, B. M., RUNIONS, J., TERRY, M. J., & WILLIAMS, L. E. (2012). G protein-coupled receptor-type G proteins are required for light-dependent seedling growth and fertility in Arabidopsis. *The Plant Cell*, *24*(9), 3649–3668. https://doi.org/10.1105/tpc.112.098681

JASPERS, P., BLOMSTER, T., BROSCHÉ, M., SALOJÄRVI, J., AHLFORS, R., VAINONEN, J.P., REDDY, R.A., IMMINK, R., ANGENENT, G., TURCK, F., OVERMYER, K. AND KANGASJÄRVI, J. (2009), Unequally redundant RCD1 and SRO1 mediate stress and developmental responses and interact with transcription factors. *The Plant Journal*, 60: 268-279. doi:10.1111/j.1365-313X.2009.03951.x

JIA, Y., DING, Y., SHI, Y., ZHANG, X., GONG, Z. AND YANG, S. (2016), The *cbfs* triple mutants reveal the essential functions of *CBFs* in cold acclimation and allow the definition of CBF regulons in *Arabidopsis*. *New Phytol*, 212: 345-353. doi:10.1111/nph.14088

JIANG, Z., ZHOU, X., TAO, M., YUAN, F., LIU, L., WU, F., WU, X., XIANG, Y., NIU, Y., LIU, F., LI, C., YE, R., BYEON, B., XUE, Y., ZHAO, H., WANG, H. N., CRAWFORD, B. M., JOHNSON, D. M., HU, C., PEI, C., … PEI, Z. M. (2019). Plant cell-surface GIPC sphingolipids sense salt to trigger Ca^{2+} influx. *Nature*, *572*(7769), 341–346. https://doi.org/10.1038/s41586-019-1449-z

JONES, D. T. (1999). Protein secondary structure prediction based on position-specific scoring matrices. *Journal of Molecular Biology*, *292*(2), 195–202. https://doi.org/10.1006/jmbi.1999.3091

JONES, J. D., & DANGL, J. L. (2006). The plant immune system. *Nature*, *444*(7117), 323–329. https://doi.org/10.1038/nature05286

JULKOWSKA, M. M., & TESTERINK, C. (2015). Tuning plant signaling and growth to survive salt. *Trends in Plant Science*, *20*(9), 586–594. https://doi.org/10.1016/j.tplants.2015.06.008

JUNG, J. H., DOMIJAN, M., KLOSE, C., BISWAS, S., EZER, D., GAO, M., KHATTAK, A. K., BOX, M. S., CHAROENSAWAN, V., CORTIJO, S., KUMAR, M., GRANT, A., LOCKE, J. C., SCHÄFER, E., JAEGER, K. E., & WIGGE, P. A. (2016). Phytochromes function as thermosensors in Arabidopsis. *Science (New York, N.Y.)*, *354*(6314), 886–889. https://doi.org/10.1126/science.aaf6005

JUSZCZYNSKI, P., KUTOK, J. L., LI, C., MITRA, J., AGUIAR, R. C., & SHIPP, M. A. (2006). BAL1 and BBAP are regulated by a gamma interferon-responsive bidirectional promoter and are overexpressed in diffuse large B-cell lymphomas with a prominent inflammatory infiltrate. *Molecular and Cellular Biology*, *26*(14), 5348–5359. https://doi.org/10.1128/MCB.02351-05

KATIYAR-AGARWAL, S., ZHU, J., KIM, K., AGARWAL, M., FU, X., HUANG, A., & ZHU, J. K. (2006). The plasma membrane Na+/H+ antiporter SOS1 interacts with RCD1 and functions in oxidative stress tolerance in Arabidopsis. *Proceedings of the National Academy of Sciences of the United States of America*, *103*(49), 18816–18821. https://doi.org/10.1073/pnas.0604711103

KERNS, J. A., EMERMAN, M., & MALIK, H. S. (2008). Positive selection and increased antiviral activity associated with the PARP-containing isoform of human zinc-finger antiviral protein. *PLoS Genetics*, *4*(1), e21. https://doi.org/10.1371/journal.pgen.0040021

KIM, H. J., HYUN, Y., PARK, J. Y., PARK, M. J., PARK, M. K., KIM, M. D., KIM, H. J., LEE, M. H., MOON, J., LEE, I., & KIM, J. (2004). A genetic link between cold responses and flowering time through FVE in Arabidopsis thaliana. *Nature Genetics*, *36*(2), 167–171. https://doi.org/10.1038/ng1298

KIM, J. M., SASAKI, T., UEDA, M., SAKO, K., & SEKI, M. (2015). Chromatin changes in response to drought, salinity, heat, and cold stresses in plants. *Frontiers in Plant Science*, *6*, 114. https://doi.org/10.3389/fpls.2015.00114

KLEPIKOVA, A. V., KASIANOV, A. S., GERASIMOV, E. S., LOGACHEVA, M. D., & PENIN, A. A. (2016). A high-resolution map of the Arabidopsis thaliana developmental transcriptome based on RNA-seq profiling. *The Plant Journal : for Cell and Molecular Biology*, *88*(6), 1058–1070. https://doi.org/10.1111/tpj.13312

KONG, L., LIU, Y., WANG, X., & CHANG, C. (2020). Insight into the Role of Epigenetic Processes in Abiotic and Biotic Stress Response in Wheat and Barley. *International Journal of Molecular Sciences*, *21*(4), 1480. https://doi.org/10.3390/ijms21041480

KOTAK, S., VIERLING, E., BÄUMLEIN, H., & VON KOSKULL-DÖRING, P. (2007). A novel transcriptional cascade regulating expression of heat stress proteins during seed development of Arabidopsis. *The Plant Cell*, *19*(1), 182–195. https://doi.org/10.1105/tpc.106.048165

KRAGELUND, B. B., JENSEN, M. K., & SKRIVER, K. (2012). Order by disorder in plant signaling. *Trends in Plant Science*, *17*(11), 625–632. https://doi.org/10.1016/j.tplants.2012.06.010

LAW, L., RAZOOKY, B. S., LI, M., YOU, S., JURADO, A., RICE, C. M., & MACDONALD, M. R. (2019). ZAP's stress granule localization is correlated with its antiviral activity and induced by virus replication. *PLoS Pathogens*, *15*(5), e1007798. https://doi.org/10.1371/journal.ppat.1007798

LEE, H. G., LEE, K., & SEO, P. J. (2015). The Arabidopsis MYB96 transcription factor plays a role in seed dormancy. *Plant Molecular Biology*, *87*(4-5), 371–381. https://doi.org/10.1007/s11103-015-0283-4

LEE, H. J., PARK, Y. J., SEO, P. J., KIM, J. H., SIM, H. J., KIM, S. G., & PARK, C. M. (2015). Systemic Immunity Requires SnRK2.8-Mediated Nuclear Import of NPR1 in Arabidopsis. *The Plant Cell*, *27*(12), 3425–3438. https://doi.org/10.1105/tpc.15.00371

LEE, K. H., PIAO, H. L., KIM, H. Y., CHOI, S. M., JIANG, F., HARTUNG, W., HWANG, I., KWAK, J. M., LEE, I. J., & HWANG, I. (2006). Activation of glucosidase via stress-induced polymerization rapidly increases active pools of abscisic acid. *Cell*, *126*(6), 1109–1120. https://doi.org/10.1016/j.cell.2006.07.034

LEGRIS, M., KLOSE, C., BURGIE, E. S., ROJAS, C. C., NEME, M., HILTBRUNNER, A., WIGGE, P. A., SCHÄFER, E., VIERSTRA, R. D., & CASAL, J. J. (2016). Phytochrome B integrates light and temperature signals in Arabidopsis. *Science (New York, N.Y.)*, *354*(6314), 897–900. https://doi.org/10.1126/science.aaf5656

LAEMMLI U. K. (1970). Cleavage of structural proteins during the assembly of the head of bacteriophage T4. *Nature*, *227*(5259), 680–685. https://doi.org/10.1038/227680a0

LEUNG, A. K., VYAS, S., ROOD, J. E., BHUTKAR, A., SHARP, P. A., & CHANG, P. (2011). Poly(ADP-ribose) regulates stress responses and microRNA activity in the cytoplasm. *Molecular Cell*, *42*(4), 489–499. https://doi.org/10.1016/j.molcel.2011.04.015

LIN, H., YANG, Y., QUAN, R., MENDOZA, I., WU, Y., DU, W., ZHAO, S., SCHUMAKER, K. S., PARDO, J. M., & GUO, Y. (2009). Phosphorylation of SOS3-LIKE CALCIUM BINDING PROTEIN8 by SOS2 protein kinase stabilizes their protein complex and regulates salt tolerance in Arabidopsis. *The Plant Cell*, *21*(5), 1607–1619. https://doi.org/10.1105/tpc.109.066217

LIU, H.-C., LIAO, H.-T. and CHARNG, Y.-Y. (2011), The role of class A1 heat shock factors (HSFA1s) in response to heat and other stresses in *Arabidopsis*. *Plant, Cell & Environment*, 34: 738-751. https://doi.org/10.1111/j.1365-3040.2011.02278.x

LIU, J., & ZHU, J. K. (1997). An Arabidopsis mutant that requires increased calcium for potassium nutrition and salt tolerance. *Proceedings of the National Academy of Sciences of the United States of America*, *94*(26), 14960–14964. https://doi.org/10.1073/pnas.94.26.14960

LIU, J., ISHITANI, M., HALFTER, U., KIM, C. S., & ZHU, J. K. (2000). The Arabidopsis thaliana SOS2 gene encodes a protein kinase that is required for salt tolerance. *Proceedings of the National Academy of Sciences of the United States of America*, *97*(7), 3730–3734. https://doi.org/10.1073/pnas.060034197

LIU, N., LEE, C. H., SWIGUT, T., GROW, E., GU, B., BASSIK, M. C., & WYSOCKA, J. (2018). Selective silencing of euchromatic L1s revealed by genome-wide screens for L1 regulators. *Nature*, *553*(7687), 228–232. https://doi.org/10.1038/nature25179

LIU, Q., KASUGA, M., SAKUMA, Y., ABE, H., MIURA, S., YAMAGUCHI-SHINOZAKI, K., & SHINOZAKI, K. (1998). Two transcription factors, DREB1 and DREB2, with an EREBP/AP2 DNA binding domain separate two cellular signal transduction pathways in drought- and low-temperature-responsive gene expression, respectively, in Arabidopsis. *The Plant Cell*, *10*(8), 1391–1406. https://doi.org/10.1105/tpc.10.8.1391

LIU, Q., WANG, Q., DENG, W., WANG, X., PIAO, M., CAI, D., LI, Y., BARSHOP, W. D., YU, X., ZHOU, T., LIU, B., OKA, Y., WOHLSCHLEGEL, J., ZUO, Z., & LIN, C. (2017). Molecular basis for blue light-dependent phosphorylation of Arabidopsis cryptochrome 2. *Nature Communications*, *8*, 15234. https://doi.org/10.1038/ncomms15234

LIU, S., LIU, S., WANG, M., WEI, T., MENG, C., WANG, M., & XIA, G. (2014). A wheat SIMILAR TO RCD-ONE gene enhances seedling growth and abiotic stress resistance by modulating redox homeostasis and maintaining genomic integrity. *The Plant Cell*, *26*(1), 164–180. https://doi.org/10.1105/tpc.113.118687

LIU, X., HU, P., HUANG, M., TANG, Y., LI, Y., LI, L., & HOU, X. (2016). The NF-YC-RGL2 module integrates GA and ABA signalling to regulate seed germination in Arabidopsis. *Nature Communications*, *7*, 12768. https://doi.org/10.1038/ncomms12768

LIU, X., WANG, J., & SUN, L. (2018). Structure of the hyperosmolality-gated calcium-permeable channel OSCA1.2. *Nature Communications*, *9*(1), 5060. https://doi.org/10.1038/s41467-018-07564-5

LO, M. C., AULABAUGH, A., JIN, G., COWLING, R., BARD, J., MALAMAS, M., & ELLESTAD, G. (2004). Evaluation of fluorescence-based thermal shift assays for hit identification in drug discovery. *Analytical Biochemistry*, *332*(1), 153–159. https://doi.org/10.1016/j.ab.2004.04.031

LOGEMANN, E., BIRKENBIHL, R. P., ÜLKER, B., & SOMSSICH, I. E. (2006). An improved method for preparing Agrobacterium cells that simplifies the Arabidopsis transformation protocol. *Plant Methods*, *2*, 16. https://doi.org/10.1186/1746-4811-2-16

LOHRMANN, J., & HARTER, K. (2002). Plant two-component signaling systems and the role of response regulators. *Plant Physiology*, *128*(2), 363–369. https://doi.org/10.1104/pp.010907

LUO, F., WANG, M., LIU, Y., ZHAO, X. M., & LI, A. (2019). DeepPhos: prediction of protein phosphorylation sites with deep learning. *Bioinformatics (Oxford, England)*, *35*(16), 2766–2773. https://doi.org/10.1093/bioinformatics/bty1051

MA Y, DAI X, XU Y, LUO W, ZHENG X, ZENG D, PAN Y, LIN X, LIU H,ZHANG D, XIAO J, GUO X, XU S, NIU Y, JIN J, ZHANG H, XU X, LI L,WANG W, QIAN Q, GE S, CHONG K (2015) COLD1 confers chilling tolerance in rice. *Cell* 160: 1209–1221. https://doi.org/10.1016/j.cell.2015.02.037

MA, Y., SZOSTKIEWICZ, I., KORTE, A., MOES, D., YANG, Y., CHRISTMANN, A., & GRILL, E. (2009). Regulators of PP2C phosphatase activity function as abscisic acid sensors. *Science (New York, N.Y.)*, *324*(5930), 1064–1068. https://doi.org/10.1126/science.1172408

MCPHERSON, A., & GAVIRA, J. A. (2014). Introduction to protein crystallization. *Acta Crystallographica. Section F, Structural Biology Communications*, *70*(Pt 1), 2–20. https://doi.org/10.1107/S2053230X13033141

MARINO, D., FROIDURE, S., CANONNE, J., BEN KHALED, S., KHAFIF, M., POUZET, C., JAUNEAU, A., ROBY, D., & RIVAS, S. (2013). Arabidopsis ubiquitin ligase MIEL1 mediates degradation of the transcription factor MYB30 weakening plant defence. *Nature Communications*, *4*, 1476. https://doi.org/10.1038/ncomms2479

MARTÍNEZ-ATIENZA, J., JIANG, X., GARCIADEBLAS, B., MENDOZA, I., ZHU, J. K., PARDO, J. M., & QUINTERO, F. J. (2007). Conservation of the salt overly sensitive pathway in rice. *Plant Physiology*, *143*(2), 1001–1012. https://doi.org/10.1104/pp.106.092635

MARUYAMA, K., URANO, K., YOSHIWARA, K., MORISHITA, Y., SAKURAI, N., SUZUKI, H., KOJIMA, M., SAKAKIBARA, H., SHIBATA, D., SAITO, K., SHINOZAKI, K., & YAMAGUCHI-SHINOZAKI, K. (2014). Integrated analysis of

the effects of cold and dehydration on rice metabolites, phytohormones, and gene transcripts. *Plant Physiology*, *164*(4), 1759–1771. https://doi.org/10.1104/pp.113.231720

MESSNER, S., & HOTTIGER, M. O. (2011). Histone ADP-ribosylation in DNA repair, replication and transcription. *Trends in Cell Biology*, *21*(9), 534–542. https://doi.org/10.1016/j.tcb.2011.06.001

MILLAR, A. H., HEAZLEWOOD, J. L., GIGLIONE, C., HOLDSWORTH, M. J., BACHMAIR, A., & SCHULZE, W. X. (2019). The Scope, Functions, and Dynamics of Posttranslational Protein Modifications. *Annual Review of Plant Biology*, *70*, 119–151. https://doi.org/10.1146/annurev-arplant-050718-100211

MUNNS, R., & TESTER, M. (2008). Mechanisms of salinity tolerance. *Annual Review of Plant Biology*, *59*, 651–681. https://doi.org/10.1146/annurev.arplant.59.032607.092911

MUSLIN, A. J., TANNER, J. W., ALLEN, P. M., & SHAW, A. S. (1996). Interaction of 14-3-3 with signaling proteins is mediated by the recognition of phosphoserine. *Cell*, *84*(6), 889–897. https://doi.org/10.1016/s0092-8674(00)81067-3

MUSTILLI, A. C., MERLOT, S., VAVASSEUR, A., FENZI, F., & GIRAUDAT, J. (2002). Arabidopsis OST1 protein kinase mediates the regulation of stomatal aperture by abscisic acid and acts upstream of reactive oxygen species production. *The Plant Cell*, *14*(12), 3089–3099. https://doi.org/10.1105/tpc.007906

NI, W., XU, S. L., GONZÁLEZ-GRANDÍO, E., CHALKLEY, R. J., HUHMER, A., BURLINGAME, A. L., WANG, Z. Y., & QUAIL, P. H. (2017). PPKs mediate direct signal transfer from phytochrome photoreceptors to transcription factor PIF3. *Nature Communications*, *8*, 15236. https://doi.org/10.1038/ncomms15236

NISHIZAWA-YOKOI, A., NOSAKA, R., HAYASHI, H., TAINAKA, H., MARUTA, T., TAMOI, M., IKEDA, M., OHME-TAKAGI, M., YOSHIMURA, K., YABUTA, Y., & SHIGEOKA, S. (2011). HsfA1d and HsfA1e involved in the transcriptional regulation of HsfA2 function as key regulators for the Hsf signaling network in response to environmental stress. *Plant & Cell Physiology*, *52*(5), 933–945. https://doi.org/10.1093/pcp/pcr045

OHAMA, N., SATO, H., SHINOZAKI, K., & YAMAGUCHI-SHINOZAKI, K. (2017). Transcriptional Regulatory Network of Plant Heat Stress Response. *Trends in Plant Science*, *22*(1), 53–65. https://doi.org/10.1016/j.tplants.2016.08.015

OVERMYER, K., TUOMINEN, H., KETTUNEN, R., BETZ, C., LANGEBARTELS, C., SANDERMANN, H., JR, & KANGASJÄRVI, J. (2000). Ozone-sensitive arabidopsis rcd1 mutant reveals opposite roles for ethylene and jasmonate signaling pathways in regulating superoxide-dependent cell death. *The Plant Cell*, *12*(10), 1849–1862. https://doi.org/10.1105/tpc.12.10.1849

PARK, S. Y., FUNG, P., NISHIMURA, N., JENSEN, D. R., FUJII, H., ZHAO, Y., LUMBA, S., SANTIAGO, J., RODRIGUES, A., CHOW, T. F., ALFRED, S. E., BONETTA, D., FINKELSTEIN, R., PROVART, N. J., DESVEAUX, D., RODRIGUEZ, P. L., MCCOURT, P., ZHU, J. K., SCHROEDER, J. I., VOLKMAN, B. F., … CUTLER, S. R. (2009). Abscisic acid inhibits type 2C protein phosphatases via the PYR/PYL family of START proteins. *Science (New York, N.Y.)*, *324*(5930), 1068–1071. https://doi.org/10.1126/science.1173041

PARK, S., LEE, C. M., DOHERTY, C. J., GILMOUR, S. J., KIM, Y., & THOMASHOW, M. F. (2015). Regulation of the Arabidopsis CBF regulon by a complex low-temperature regulatory network. *The Plant Journal: for Cell and Molecular Biology*, *82*(2), 193–207. https://doi.org/10.1111/tpj.12796

POLLE, A. (1997). Defense against Photooxidative Damage in Plants. *Cold Spring Harbor Monograph Archive*, 34, 623-666. http://dx.doi.org/10.1101/0.623-666

PURNELL, M. R., & WHISH, W. J. (1980). Novel inhibitors of poly(ADP-ribose) synthetase. *The Biochemical Journal*, *185*(3), 775–777. https://doi.org/10.1042/bj1850775

QI, J., SONG, C. P., WANG, B., ZHOU, J., KANGASJÄRVI, J., ZHU, J. K., & GONG, Z. (2018). Reactive oxygen species signaling and stomatal movement in plant responses to drought stress and pathogen attack. *Journal of Integrative Plant Biology*, *60*(9), 805–826. https://doi.org/10.1111/jipb.12654

QUAN, R., LIN, H., MENDOZA, I., ZHANG, Y., CAO, W., YANG, Y., SHANG, M., CHEN, S., PARDO, J. M., & GUO, Y. (2007). SCABP8/CBL10, a putative calcium sensor, interacts with the protein kinase SOS2 to protect Arabidopsis shoots from salt stress. *The Plant Cell*, *19*(4), 1415–1431. https://doi.org/10.1105/tpc.106.042291

QUINTERO, F. J., OHTA, M., SHI, H., ZHU, J. K., & PARDO, J. M. (2002). Reconstitution in yeast of the Arabidopsis SOS signaling pathway for Na+ homeostasis. *Proceedings of the National Academy of Sciences of the United States of America*, *99*(13), 9061–9066. https://doi.org/10.1073/pnas.132092099

RAFFAELE, S., VAILLEAU, F., LÉGER, A., JOUBÈS, J., MIERSCH, O., HUARD, C., BLÉE, E., MONGRAND, S., DOMERGUE, F., & ROBY, D. (2008). A MYB transcription factor regulates very-long-chain fatty acid biosynthesis for activation of the hypersensitive cell death response in Arabidopsis. *The Plant Cell*, *20*(3), 752–767. https://doi.org/10.1105/tpc.107.054858

RAGHAVENDRA, A. S., GONUGUNTA, V. K., CHRISTMANN, A., & GRILL, E. (2010). ABA perception and signalling. *Trends in Plant Science*, *15*(7), 395–401. https://doi.org/10.1016/j.tplants.2010.04.006

RISSEL, D., & PEITER, E. (2019). Poly(ADP-Ribose) Polymerases in Plants and Their Human Counterparts: Parallels and Peculiarities. *International Journal of Molecular Sciences*, *20*(7), 1638. https://doi.org/10.3390/ijms20071638

ROBBEZ-MASSON, L., TIE, C., CONDE, L., TUNBAK, H., HUSOVSKY, C., TCHASOVNIKAROVA, I. A., TIMMS, R. T., HERRERO, J., LEHNER, P. J., & ROWE, H. M. (2018). The HUSH complex cooperates with TRIM28 to repress young retrotransposons and new genes. *Genome Research*, *28*(6), 836–845. https://doi.org/10.1101/gr.228171.117

Rochon, A., Boyle, P., Wignes, T., Fobert, P. R., & Després, C. (2006). The coactivator function of Arabidopsis NPR1 requires the core of its BTB/POZ domain and the oxidation of C-terminal cysteines. *The Plant Cell*, *18*(12), 3670–3685. https://doi.org/10.1105/tpc.106.046953

ROCHON, A., BOYLE, P., WIGNES, T., FOBERT, P. R., & DESPRÉS, C. (2006). The coactivator function of Arabidopsis NPR1 requires the core of its BTB/POZ domain and the oxidation of C-terminal cysteines. *The Plant Cell*, *18*(12), 3670–3685. https://doi.org/10.1105/tpc.106.046953

RUF, A., DE MURCIA, G., & SCHULZ, G. E. (1998). Inhibitor and NAD^+ binding to poly(ADP-ribose) polymerase as derived from crystal structures and homology modeling. *Biochemistry*, *37*(11), 3893–3900. https://doi.org/10.1021/bi972383s

RUIJTER, J. M., RAMAKERS, C., HOOGAARS, W. M., KARLEN, Y., BAKKER, O., VAN DEN HOFF, M. J., & MOORMAN, A. F. (2009). Amplification efficiency: linking baseline and bias in the analysis of quantitative PCR data. *Nucleic Acids Research*, *37*(6), e45. https://doi.org/10.1093/nar/gkp045

RUS, A., LEE, B. H., MUÑOZ-MAYOR, A., SHARKHUU, A., MIURA, K., ZHU, J. K., BRESSAN, R. A., & HASEGAWA, P. M. (2004). AtHKT1 facilitates Na+ homeostasis and K+ nutrition in planta. *Plant Physiology*, *136*(1), 2500–2511. https://doi.org/10.1104/pp.104.042234

RUS, A., YOKOI, S., SHARKHUU, A., REDDY, M., LEE, B. H., MATSUMOTO, T. K., KOIWA, H., ZHU, J. K., BRESSAN, R. A., & HASEGAWA, P. M. (2001). AtHKT1 is a salt tolerance determinant that controls Na^+ entry into plant roots. *Proceedings of the National Academy of Sciences of the United States of America*, *98*(24), 14150–14155. https://doi.org/10.1073/pnas.241501798

SAKUMA, Y., MARUYAMA, K., OSAKABE, Y., QIN, F., SEKI, M., SHINOZAKI, K., & YAMAGUCHI-SHINOZAKI, K. (2006). Functional analysis of an Arabidopsis transcription factor, DREB2A, involved in drought-responsive gene expression. *The Plant Cell*, *18*(5), 1292–1309. https://doi.org/10.1105/tpc.105.035881

SALAZAR, C. AND HÖFER, T. (2009), Multisite protein phosphorylation – from molecular mechanisms to kinetic models. *The FEBS Journal*, 276: 3177-3198. https://doi.org/10.1111/j.1742-4658.2009.07027.x

SALEH, A., WITHERS, J., MOHAN, R., MARQUÉS, J., GU, Y., YAN, S., ZAVALIEV, R., NOMOTO, M., TADA, Y., & DONG, X. (2015). Posttranslational Modifications of the Master Transcriptional Regulator NPR1 Enable Dynamic but

Tight Control of Plant Immune Responses. *Cell Host & Microbe*, *18*(2), 169–182. https://doi.org/10.1016/j.chom.2015.07.005

SCHARF, K. D., BERBERICH, T., EBERSBERGER, I., & NOVER, L. (2012). The plant heat stress transcription factor (Hsf) family: structure, function and evolution. *Biochimica et Biophysica Acta*, *1819*(2), 104–119. https://doi.org/10.1016/j.bbagrm.2011.10.002

SCHLESINGER M. J. (1990). Heat shock proteins. *The Journal of Biological Chemistry*, *265*(21), 12111–12114.

SCHREIBER, V., DANTZER, F., AME, J. C., & DE MURCIA, G. (2006). Poly(ADP-ribose): novel functions for an old molecule. *Nature Reviews. Molecular Cell Biology*, *7*(7), 517–528. https://doi.org/10.1038/nrm1963

SCHUBERT, D., PRIMAVESI, L., BISHOPP, A., ROBERTS, G., DOONAN, J., JENUWEIN, T., & GOODRICH, J. (2006). Silencing by plant Polycomb-group genes requires dispersed trimethylation of histone H3 at lysine 27. *The EMBO Journal*, *25*(19), 4638–4649. https://doi.org/10.1038/sj.emboj.7601311

SCHWENKE, K.D. (1997), *Protein Phosphorylation*. Edited by F. Marks. XXIII and 381 pages, numerous figures and tables. VCH, Weinheim, New York, Basel, Cambridge, Tokyo 1996. Price: 198,-DM.. Nahrung, 41: 321-322. https://doi.org/10.1002/food.19970410537

SHAPIGUZOV, A., VAINONEN, J. P., HUNTER, K., TOSSAVAINEN, H., TIWARI, A., JÄRVI, S., HELLMAN, M., AARABI, F., ALSEEKH, S., WYBOUW, B., VAN DER KELEN, K., NIKKANEN, L., KRASENSKY-WRZACZEK, J., SIPARI, N., KEINÄNEN, M., TYYSTJÄRVI, E., RINTAMÄKI, E., DE RYBEL, B., SALOJÄRVI, J., VAN BREUSEGEM, F., … KANGASJÄRVI, J. (2019). Arabidopsis RCD1 coordinates chloroplast and mitochondrial functions through interaction with ANAC transcription factors. *eLife*, *8*, e43284. https://doi.org/10.7554/eLife.43284

SHI Y., DING Y., YANG S., Cold Signal Transduction and its Interplay with Phytohormones During Cold Acclimation, *Plant and Cell Physiology*, Volume 56, Issue 1, January 2015, Pages 7–15, https://doi.org/10.1093/pcp/pcu115

SHI, H., ISHITANI, M., KIM, C., & ZHU, J. K. (2000). The Arabidopsis thaliana salt tolerance gene SOS1 encodes a putative Na+/H+ antiporter. *Proceedings of the National Academy of Sciences of the United States of America*, *97*(12), 6896–6901. https://doi.org/10.1073/pnas.120170197

SHI, H., LEE, B. H., WU, S. J., & ZHU, J. K. (2003). Overexpression of a plasma membrane Na+/H+ antiporter gene improves salt tolerance in Arabidopsis thaliana. *Nature Biotechnology*, *21*(1), 81–85. https://doi.org/10.1038/nbt766

SHI, H., QUINTERO, F. J., PARDO, J. M., & ZHU, J. K. (2002). The putative plasma membrane Na(+)/H(+) antiporter SOS1 controls long-distance Na(+) transport in plants. *The Plant Cell*, *14*(2), 465–477. https://doi.org/10.1105/tpc.010371

SHI, H., QUINTERO, F. J., PARDO, J. M., & ZHU, J. K. (2002). The putative plasma membrane Na(+)/H(+) antiporter SOS1 controls long-distance Na(+) transport in plants. *The Plant Cell*, *14*(2), 465–477. https://doi.org/10.1105/tpc.010371

SHKOLNIK, D., NURIEL, R., BONZA, M. C., COSTA, A., & FROMM, H. (2018). MIZ1 regulates ECA1 to generate a slow, long-distance phloem-transmitted Ca^{2+} signal essential for root water tracking in *Arabidopsis*. *Proceedings of the National Academy of Sciences of the United States of America*, *115*(31), 8031–8036. https://doi.org/10.1073/pnas.1804130115

SIEVERS, F., WILM, A., DINEEN, D., GIBSON, T. J., KARPLUS, K., LI, W., LOPEZ, R., MCWILLIAM, H., REMMERT, M., SÖDING, J., THOMPSON, J. D., & HIGGINS, D. G. (2011). Fast, scalable generation of high-quality protein multiple sequence alignments using Clustal Omega. *Molecular Systems Biology*, *7*, 539. https://doi.org/10.1038/msb.2011.75

STEFFEN, J. D., BRODY, J. R., ARMEN, R. S., & PASCAL, J. M. (2013). Structural Implications for Selective Targeting of PARPs. *Frontiers in Oncology*, *3*, 301. https://doi.org/10.3389/fonc.2013.00301

STOCKINGER, E. J., GILMOUR, S. J., & THOMASHOW, M. F. (1997). Arabidopsis thaliana CBF1 encodes an AP2 domain-containing transcriptional activator that binds to the C-repeat/DRE, a cis-acting DNA regulatory element that stimulates transcription in response to low temperature and water deficit. *Proceedings of the National Academy of Sciences of the United States of America*, *94*(3), 1035–1040. https://doi.org/10.1073/pnas.94.3.1035

TAKAHASHI, F., SUZUKI, T., OSAKABE, Y., BETSUYAKU, S., KONDO, Y., DOHMAE, N., FUKUDA, H., YAMAGUCHI-SHINOZAKI, K., & SHINOZAKI, K. (2018). A small peptide modulates stomatal control via abscisic acid in long-distance signalling. *Nature*, *556*(7700), 235–238. https://doi.org/10.1038/s41586-018-0009-2

TCHASOVNIKAROVA, I. A., TIMMS, R. T., MATHESON, N. J., WALS, K., ANTROBUS, R., GÖTTGENS, B., DOUGAN, G., DAWSON, M. A., & LEHNER, P. J. (2015). GENE SILENCING. Epigenetic silencing by the HUSH complex mediates position-effect variegation in human cells. *Science (New York, N.Y.)*, *348*(6242), 1481–1485. https://doi.org/10.1126/science.aaa7227

TENA, G., BOUDSOCQ, M., & SHEEN, J. (2011). Protein kinase signaling networks in plant innate immunity. *Current Opinion in Plant Biology*, *14*(5), 519–529. https://doi.org/10.1016/j.pbi.2011.05.006

TEOTIA, S., & LAMB, R. S. (2009). The paralogous genes RADICAL-INDUCED CELL DEATH1 and SIMILAR TO RCD ONE1 have partially redundant functions

during Arabidopsis development. *Plant Physiology*, *151*(1), 180–198. https://doi.org/10.1104/pp.109.142786

TO, T. K., KIM, J. M., MATSUI, A., KURIHARA, Y., MOROSAWA, T., ISHIDA, J., TANAKA, M., ENDO, T., KAKUTANI, T., TOYODA, T., KIMURA, H., YOKOYAMA, S., SHINOZAKI, K., & SEKI, M. (2011). Arabidopsis HDA6 regulates locus-directed heterochromatin silencing in cooperation with MET1. *PLoS Genetics*, *7*(4), e1002055. https://doi.org/10.1371/journal.pgen.1002055

TODOROVA, T., BOCK, F. J., & CHANG, P. (2014). PARP13 regulates cellular mRNA post-transcriptionally and functions as a pro-apoptotic factor by destabilizing TRAILR4 transcript. *Nature Communications*, *5*, 5362. https://doi.org/10.1038/ncomms6362

TOSSAVAINEN, H., HELLMAN, M., VAINONEN, J. P., KANGASJÄRVI, J., & PERMI, P. (2017). ^{1}H, ^{13}C and ^{15}N NMR chemical shift assignments of A. thaliana RCD1 RST. *Biomolecular NMR Assignments*, *11*(2), 207–210. https://doi.org/10.1007/s12104-017-9749-4

TRAN, L. S., NAKASHIMA, K., SAKUMA, Y., SIMPSON, S. D., FUJITA, Y., MARUYAMA, K., FUJITA, M., SEKI, M., SHINOZAKI, K., & YAMAGUCHI-SHINOZAKI, K. (2004). Isolation and functional analysis of Arabidopsis stress-inducible NAC transcription factors that bind to a drought-responsive cis-element in the early responsive to dehydration stress 1 promoter. *The Plant Cell*, *16*(9), 2481–2498. https://doi.org/10.1105/tpc.104.022699

TRENTINI, D. B., FUHRMANN, J., MECHTLER, K., & CLAUSEN, T. (2014). Chasing Phosphoarginine Proteins: Development of a Selective Enrichment Method Using a Phosphatase Trap. *Molecular & Cellular Proteomics: MCP*, *13*(8), 1953–1964. https://doi.org/10.1074/mcp.O113.035790

VAINONEN, J. P., JASPERS, P., WRZACZEK, M., LAMMINMÄKI, A., REDDY, R. A., VAAHTERA, L., BROSCHÉ, M., & KANGASJÄRVI, J. (2012). RCD1-DREB2A interaction in leaf senescence and stress responses in Arabidopsis thaliana. *The Biochemical Journal*, *442*(3), 573–581. https://doi.org/10.1042/BJ20111739

VAINONEN, J.P, SHAPIGUZOV, A., KRASENSKY-WRZACZEK, J., GOSSENS, R., DE MASI, R., DANCIU, I., BATTCHIKOVA, N., JONAK, C., WIRTHMUELLER. L, WRZACZEK, M., KANGASJÄRVI, J. "Arabidopsis Poly(ADP-ribose)-binding protein RCD1 interacts with Photoregulatory Protein Kinases in nuclear bodies". https://www.biorxiv.org/content/10.1101/2020.07.02.184937v2.full

VAINONEN, J. P., SHAPIGUZOV, A., VAATTOVAARA, A., & KANGASJÄRVI, J. (2016). Plant PARPs, PARGs and PARP-like Proteins. *Current Protein & Peptide Science*, *17*(7), 713–723. https://doi.org/10.2174/1389203717666160419144721

VOINNET, O., RIVAS, S., MESTRE, P., & BAULCOMBE, D. (2003). An enhanced transient expression system in plants based on suppression of gene silencing by the

p19 protein of tomato bushy stunt virus. *The Plant Journal: for Cell and Molecular Biology*, *33*(5), 949–956. https://doi.org/10.1046/j.1365-313x.2003.01676.x (Retraction published Plant J. 2015 Nov;84(4):846)

VON KOSKULL-DÖRING, P., SCHARF, K. D., & NOVER, L. (2007). The diversity of plant heat stress transcription factors. *Trends in Plant Science*, *12*(10), 452–457. https://doi.org/10.1016/j.tplants.2007.08.014

VYAS, S., MATIC, I., UCHIMA, L., ROOD, J., ZAJA, R., HAY, R. T., AHEL, I., & CHANG, P. (2014). Family-wide analysis of poly(ADP-ribose) polymerase activity. *Nature Communications*, *5*, 4426. https://doi.org/10.1038/ncomms5426

WAHLBERG, E., KARLBERG, T., KOUZNETSOVA, E., MARKOVA, N., MACCHIARULO, A., THORSELL, A. G., POL, E., FROSTELL, Å., EKBLAD, T., ÖNCÜ, D., KULL, B., ROBERTSON, G. M., PELLICCIARI, R., SCHÜLER, H., & WEIGELT, J. (2012). Family-wide chemical profiling and structural analysis of PARP and tankyrase inhibitors. *Nature Biotechnology*, *30*(3), 283–288. https://doi.org/10.1038/nbt.2121

WANG, H., LIANG, Q., CAO, K., & GE, X. (2011). Endogenous protein mono-ADP-ribosylation in *Arabidopsis thaliana*. *Planta*, 233(6), 1287–1292. https://doi.org/10.1007/s00425-011-1415-y

WANG, Z., MICHAUD, G. A., CHENG, Z., ZHANG, Y., HINDS, T. R., FAN, E., CONG, F., & XU, W. (2012). Recognition of the iso-ADP-ribose moiety in poly(ADP-ribose) by WWE domains suggests a general mechanism for poly(ADP-ribosyl)ation-dependent ubiquitination. *Genes & Development*, *26*(3), 235–240. https://doi.org/10.1101/gad.182618.111

WEINER, M. P., COSTA, G. L., SCHOETTLIN, W., CLINE, J., MATHUR, E., & BAUER, J. C. (1994). Site-directed mutagenesis of double-stranded DNA by the polymerase chain reaction. *Gene*, *151*(1-2), 119–123. https://doi.org/10.1016/0378-1119(94)90641-6

WIRTHMUELLER, L., ASAI, S., RALLAPALLI, G., SKLENAR, J., FABRO, G., KIM, D. S., LINTERMANN, R., JASPERS, P., WRZACZEK, M., KANGASJÄRVI, J., MACLEAN, D., MENKE, F., BANFIELD, M. J., & JONES, J. (2018). Arabidopsis downy mildew effector HaRxL106 suppresses plant immunity by binding to RADICAL-INDUCED CELL DEATH1. *The New Phytologist*, *220*(1), 232–248. https://doi.org/10.1111/nph.15277

XU, Z. Y., KIM, S. Y., HYEON, D., KIM, D. H., DONG, T., PARK, Y., JIN, J. B., JOO, S. H., KIM, S. K., HONG, J. C., HWANG, D., & HWANG, I. (2013). The Arabidopsis NAC transcription factor ANAC096 cooperates with bZIP-type transcription factors in dehydration and osmotic stress responses. *The Plant Cell*, *25*(11), 4708–4724. https://doi.org/10.1105/tpc.113.119099

YAMADA, K., FUKAO, Y., HAYASHI, M., FUKAZAWA, M., SUZUKI, I., & NISHIMURA, M. (2007). Cytosolic HSP90 regulates the heat shock response that is

responsible for heat acclimation in Arabidopsis thaliana. *The Journal of Biological Chemistry*, *282*(52), 37794–37804. https://doi.org/10.1074/jbc.M707168200

YANG, C. S., JIVIDEN, K., SPENCER, A., DWORAK, N., NI, L., OOSTDYK, L. T., CHATTERJEE, M., KUŚMIDER, B., REON, B., PARLAK, M., GORBUNOVA, V., ABBAS, T., JEFFERY, E., SHERMAN, N. E., & PASCHAL, B. M. (2017). Ubiquitin Modification by the E3 Ligase/ADP-Ribosyltransferase Dtx3L/Parp9. *Molecular Cell*, *66*(4), 503–516.e5. https://doi.org/10.1016/j.molcel.2017.04.028

YANG, Z., WANG, C., XUE, Y., LIU, X., CHEN, S., SONG, C., YANG, Y., & GUO, Y. (2019). Calcium-activated 14-3-3 proteins as a molecular switch in salt stress tolerance. *Nature Communications*, *10*(1), 1199. https://doi.org/10.1038/s41467-019-09181-2

YOSHIDA, T., FUJITA, Y., MARUYAMA, K., MOGAMI, J., TODAKA, D., SHINOZAKI, K., & YAMAGUCHI-SHINOZAKI, K. (2015). Four Arabidopsis AREB/ABF transcription factors function predominantly in gene expression downstream of SnRK2 kinases in abscisic acid signalling in response to osmotic stress. *Plant, Cell & Environment*, *38*(1), 35–49. https://doi.org/10.1111/pce.12351

YOSHIDA, T., FUJITA, Y., SAYAMA, H., KIDOKORO, S., MARUYAMA, K., MIZOI, J., SHINOZAKI, K., & YAMAGUCHI-SHINOZAKI, K. (2010). AREB1, AREB2, and ABF3 are master transcription factors that cooperatively regulate ABRE-dependent ABA signaling involved in drought stress tolerance and require ABA for full activation. *The Plant Journal: for Cell and Molecular Biology*, *61*(4), 672–685. https://doi.org/10.1111

YOSHIDA, T., OHAMA, N., NAKAJIMA, J., KIDOKORO, S., MIZOI, J., NAKASHIMA, K., MARUYAMA, K., KIM, J. M., SEKI, M., TODAKA, D., OSAKABE, Y., SAKUMA, Y., SCHÖFFL, F., SHINOZAKI, K., & YAMAGUCHI-SHINOZAKI, K. (2011). Arabidopsis HsfA1 transcription factors function as the main positive regulators in heat shock-responsive gene expression. *Molecular Genetics and Genomics: MGG*, *286*(5-6), 321–332. https://doi.org/10.1007/s00438-011-0647-7

YUAN, F., YANG, H., XUE, Y., KONG, D., YE, R., LI, C., ZHANG, J., THEPRUNGSIRIKUL, L., SHRIFT, T., KRICHILSKY, B., JOHNSON, D. M., SWIFT, G. B., HE, Y., SIEDOW, J. N., & PEI, Z. M. (2014). OSCA1 mediates osmotic-stress-evoked Ca2+ increases vital for osmosensing in Arabidopsis. *Nature*, *514*(7522), 367–371. https://doi.org/10.1038/nature13593

ZHANG, J. L., & SHI, H. (2013). Physiological and molecular mechanisms of plant salt tolerance. *Photosynthesis Research*, *115*(1), 1–22. https://doi.org/10.1007/s11120-013-9813-6

ZHANG, J., & ZHOU, J. M. (2010). Plant immunity triggered by microbial molecular signatures. *Molecular Plant*, *3*(5), 783–793. https://doi.org/10.1093/mp/ssq035

ZHANG, X., BERNATAVICHUTE, Y. V., COKUS, S., PELLEGRINI, M., & JACOBSEN, S. E. (2009). Genome-wide analysis of mono-, di- and trimethylation of histone H3 lysine 4 in Arabidopsis thaliana. *Genome Biology*, *10*(6), R62. https://doi.org/10.1186/gb-2009-10-6-r62

ZHANG, Y., LIU, S., MICKANIN, C. *et al.* RNF146 is a poly(ADP-ribose)-directed E3 ligase that regulates axin degradation and Wnt signalling. *Nat Cell Biol* **13,** 623–629 (2011). https://doi.org/10.1038/ncb2222

ZHAO, C., ZHANG, Z., XIE, S., SI, T., LI, Y., & ZHU, J. K. (2016). Mutational Evidence for the Critical Role of CBF Transcription Factors in Cold Acclimation in Arabidopsis. *Plant Physiology*, *171*(4), 2744–2759. https://doi.org/10.1104/pp.16.00533

ZHOU, Z. D., CHAN, C. H., XIAO, Z. C., & TAN, E. K. (2011). Ring finger protein 146/Iduna is a poly(ADP-ribose) polymer binding and PARsylation dependent E3 ubiquitin ligase. *Cell Adhesion & Migration*, *5*(6), 463–471. https://doi.org/10.4161/cam.5.6.18356

ZHOU, H., LIN, H., CHEN, S., BECKER, K., YANG, Y., ZHAO, J., KUDLA, J., SCHUMAKER, K. S., & GUO, Y. (2014). Inhibition of the Arabidopsis salt overly sensitive pathway by 14-3-3 proteins. *The Plant Cell*, *26*(3), 1166–1182. https://doi.org/10.1105/tpc.113.117069

ZHU J. K. (2016). Abiotic Stress Signaling and Responses in Plants. *Cell*, *167*(2), 313–324. https://doi.org/10.1016/j.cell.2016.08.029

ZHU J. K. (2002). Salt and drought stress signal transduction in plants. *Annual Review of Plant Biology*, *53*, 247–273. https://doi.org/10.1146/annurev.arplant.53.091401.143329

ZIPFEL C. (2014). Plant pattern-recognition receptors. *Trends in Immunology*, *35*(7), 345–351. https://doi.org/10.1016/j.it.2014.05.004

Curriculum Vitae

For reasons of data protection, the *curriculum vitae* is not published in the electronic version.

Publications

During the doctorate

CHEN C., DE MASI R., LINTERMANN R., WIRTHMÜLLER L. (2018): "Nuclear Import of Arabidopsis Poly(ADP-Ribose) Polymerase 2 Is Mediated by Importin-α and a Nuclear Localization Sequence Located Between the Predicted SAP Domains". Frontiers in Plant Science Vol.9 2018 https://www.frontiersin.org/article/10.3389/fpls.2018.01581

Manuscript pre-print

VAINONEN, J.P, SHAPIGUZOV, A., KRASENSKY-WRZACZEK, J., GOSSENS, R., DE MASI, R., DANCIU, I., BATTCHIKOVA, N., JONAK, C., WIRTHMUELLER. L, WRZACZEK, M., KANGASJÄRVI, J. "Arabidopsis Poly(ADP-ribose)-binding protein RCD1 interacts with Photoregulatory Protein Kinases in nuclear bodies". https://doi.org/10.1101/2020.07.02.184937

VOGT, S., FEIJS, K., HOSCH, S., DE MASI, R., LINTERMANN, R., LOLL, B., WIRTHMUELLER, L. "The superior salinity tolerance of wheat cultivar Shanrong No. 3 cannot be attributed to elevated Ta-sro1 poly(ADP-ribose) polymerase activity". Manuscript pre-print https://doi.org/10.1101/2021.10.20.465099

Acknowledgements

I would like to thank Dr. Wirthmüller for the scientific guidance and, together with all the members of this workgroup, for the goal-oriented discussions during my doctorate.

I would also like to thank Prof. Dr. Romeis and Prof. Dr. Schubert for their supervision and guidance as second supervisors, as well as Ruth Lintermann, Dr. Silke Schilling and Claudia Alings, for their scientific support.

I would like to thank all the current and former members of AG Wirthmüller, AG Romeis and AG Schubert: from each, I had the chance to learn something about science and research while sharing three years of our lives in the lab.

I would also like to thank my Mother and my Father, who always supported and encouraged me to pursue my goals.

Finally, I would like to thank Damiano, for Everything.

.

Appendix

Table A. 1: Oligonucleotides for restriction cloning

Oligonucleotide identification name	Oligonucleotide sequence (5'-3')	Annealing temperature
RCD1_NotI_FW	CCGCGGCCGCCCCCTTCACCATGGAAGC CAAGATCG	64 °C
RCD1_BamHI_RV	ATGGATCCCAACACCATAGATGGACTTTC T	

Table A. 2: Oligonucleotides for site-direct mutagenesis

Oligonucleotide identification name	Oligonucleotide sequence (5'-3')	Annealing temperature
AtRCD1_CA_T204A_FW	ATTATGTTAATGGTGGCGAGGCACCGAGGT	62 °C
AtRCD1_CA_T204A_RV	CACTCCTCCAAATTTAACCTCGGTGCCTCGC CACCAT	

Table A. 3: Oligonucleotides for qRT-PCR

Oligonucleotide identification name	Oligonucleotide sequence (5'-3')	Annealing temperature
RCD1_AT1G32230_qRT_FW	AAGAAGGTGCAGGTGGATTGAAG	60 °C
RCD1_AT1G32230_qRT_RV	CATAGTCAGGAACATCGTATGGGTA AAAG	
NUDX6_AT2G04450_qRT_FW	AAACTGCCTACCGGTGTTGT	
NUDX6_AT2G04450_qRT_RV	CAAGAATGCTTGGTGGCTTT	
RAP2.6_AT1G43160_qRT_FW	CGGGGAAATTAAGCTTTGCT	
RAP2.6_AT1G43160_qRT_RV	ACGTGTATGGCTTGGGACAT	

Table A. 3: Oligonucleotides for qRT-PCR

Oligonucleotide identification name	Oligonucleotide sequence (5'-3')	Annealing temperature
AOX1A_AT3G22370_qRT_FW	GCATCATGTTCCAACGACGTTTCT	60 °C
AOX1A_AT3G22370_qRT_RV	TTCAAGCATCATAGCTCGACATCCA	
nBLACK_AT4G34270_qRT_FW	GTGAAAACTGTTGGAGAGAAGCAA	
nBLACK_AT4G34270_qRT_RV	TCAACTGGATACCCTTTCGCA	

Figure A. 1: Example of the phenotype of twelve-week-old *A. thaliana* Col-0 wild type and *rcd1-1* knockout mutant line, grown under short-day conditions.

Figure A. 2: Example of the phenotype of twelve-week-old *A. thaliana rcd1-1* lines overexpressing RCD1_CD (#3.1, #3.6, #4.8), grown under short-day conditions.

Figure A. 3: Example of the phenotype of twelve-week-old *A. thaliana rcd1-1* lines overexpressing RCD1_NA (#2.4 and #2.16), grown under short-day conditions.

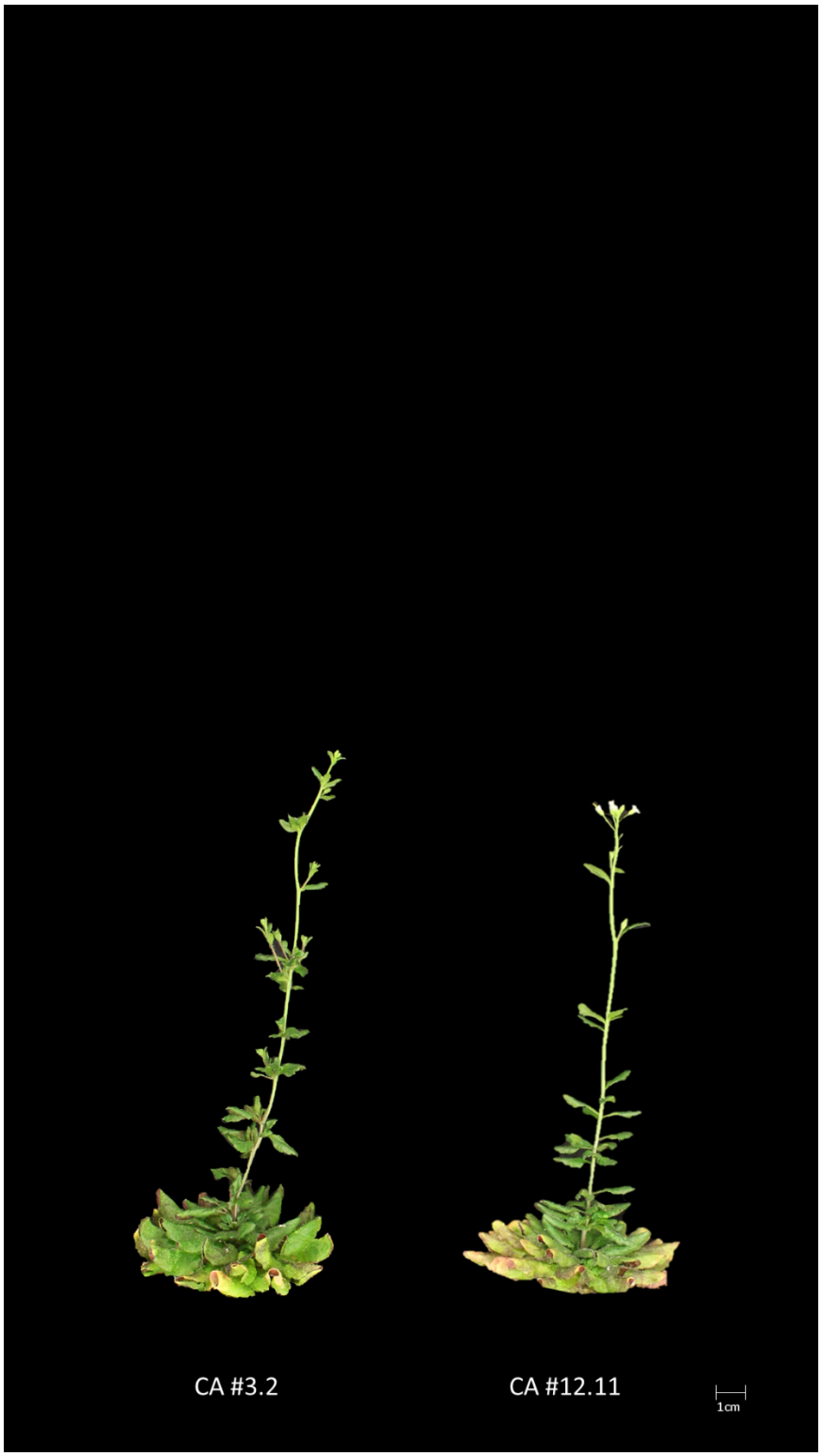

Figure A. 4: Example of the phenotype of twelve-week-old *A. thaliana rcd1-1* lines overexpressing RCD1_CA (#3.2 and #12.11), grown under short-day conditions.